

California State University, Northridge

Atropisomerism in Lutidine Systems

A thesis submitted in partial fulfillment of the requirements

For the degree of Master of Science in Chemistry

By

Parijat Sharma

December 2020

The thesis of Parijat Sharma is approved:

Professor Ravinder Abrol

Date

Professor Yann Schrodi

Date

Professor Taeboem Oh, Chair

Date

California State University Northridge

Acknowledgement

I would like to thank Dr. Oh for providing me the opportunity to learn and grow as a student in his laboratory. His dedication to ensuring my success as a student has helped me in large part to becoming who I am today. I also would like to thank Dr. Abrol and Dr. Schrodi for taking their time to be members on my committee and for making my thesis stronger overall. In addition, I would like to thank everyone that has supported and helped me grow during this program: Mike Kiser, Justice Mena, Ismail Hossain, Kevin Crossley, Thomas Minehan , Jheem Medh, Karin Crowhurst, Peiman Sobbi, Ravinder Abrol, Yann Schrodi, Heemal Dhanjee, Joseph Yoon, Gary Leonard, Nicolas Cena, Romny Sanchez, Simon J. Garrett, Satish Bal, Mohan Bal, Kellee Johnson, Vastuti Garuryar, Tamina Sabnani, Adam Mogul, Esteban Bautista, Mario Cardenas, Andy Gonzalez, Aarthi Vadhanam, Trevor Brewer, Rodney Gross, Jon Gates, Charlie Grigsby, Carter Richardson, Forrest Goodwin, Maria Hernandez, Yun Shi, Lianxiu Guan, Fang Wang, Jiemin Bao, Shrutee Tandon, Jennifer Lippens, Yong Xie, Heath Timmons, Brendan Dalbey, John Colyer, Michal Achmatowicz, Kyle Baucom, James Murray, Kyle Quasdorf, Hanh Nguyen, Tsang-lin Hwang, Maria Silva Elipe, Vasudha Murikipudi, Tawnya Flick, Jun Han, Mike Tang, Benjamin Woo, and the many more not listed on this page.

The two collaborators for this research are much appreciated. Dr. Joseph W. Ziller, Director, X-Ray Crystallography Facility, Department of Chemistry University of California, Irvine. Dr. Robert E. Taylor, NMR facilities, Department of Chemistry and Biochemistry
University of California, Los Angeles

Dedication

I'd like to dedicate this work to the two most wonderful and hardworking people I know: my parents Amit and Rashmi Sharma.

Table of contents

Signature page	ii
Acknowledgements	iii
Dedication	iv
List of Tables	vi
List of Figures	vii
Abstract	x
Introduction	1
Results	8
Syntheses	8
Ab-initio calculation	12
Single crystal X-ray structures	27
Dynamic ¹ HNMR investigations	32
Discussion	45
Experimental	52
References	61
Appendix A: Dynamic ¹ HNMR	64
Appendix B: X-ray diffraction data	103
Appendix C: ΔG^\ddagger calculations	176
Appendix D: Selected Spectral/spectrometry data	184

List of Tables

Table 1: Synthesis of 3,5-dimethyl-2,6-diarylpyridine	11
Table 2: Summary of the Calculated energies (kJ/mol)	26
Table 3: Crystal Structures Dihedral Angles Summary	31
Table 4: Summary of the Barrier to Rotations	44

List of Figures

Figure 1:	Example of a generic atropisomeric system	1
Figure 2	Guide on determining atropisomer classes	1
Figure 3	Chateoglobulin A and Vancomycin, examples of atropisomer pharmaceuticals	3
Figure 4	AMG 510 Atropisomer properties	4
Figure 5	Binaphthyl based asymmetric catalyst for hydrogenation	5
Figure 6	Depiction of the cisoid and transoid configurations	6
Figure 7	Two examples of non-binaphthyl asymmetric catalysts	6
Figure 8	Barrier to rotation for 2,6-diarylpyridine	7
Figure 9	Atropisomer conformations of 3,5-Dimethyl-2,6-di(2-methylphenyl)pyridine	7
Figure 10	Synthesis approach of 3,5-dimethyl-2,6-diarylpyridine	9
Figure 11	N-methylation of selected diarylated compounds	12
Figure 12	Minimized conformation of 3,5-dimethyl-2,6-di(2-methylphenyl)pyridine	13
Figure 13	Configuration of di(4-methylphenyl)-3,5-dimethylpyridine	14
Figure 14	Modeling of 3,5-dimethyl-2,6-di(4-methylphenyl)pyridine	15, 16
Figure 15	Modeling of 3,5-dimethyl-2,6-di(3-methylphenyl)pyridine	17, 18
Figure 16	Modeling of 3,5-dimethyl-2,6-di(2-methylphenyl)pyridine	19, 20
Figure 17	Modeling of 3,5-dimethyl-2,6-di(2-isopropylphenyl)pyridine	20, 21
Figure 18	Modeling of 3,5-dimethyl-2,6-di(4-methylnaphthyl-1-yl)pyridine	22
Figure 19	Modeling of isomers of 1,3,5-trimethyl-2,6-di(2-methylphenyl)pyridinium	23,24
Figure 20	Modeling of isomers of Diarylated N-methylated Pyridinium Iodide	25,26
Figure 21	<i>Trans-syn</i> -crystal structure of 3,5-dimethyl-2,6-di(3-methylphenyl)pyridine	28
Figure 22	Crystal structure of <i>cis-trans</i> -3,5-dimethyl-2,6-di(2-methylphenyl)pyridine	29

Figure 23	Crystal structure of 3,5-dimethyl-2,6-di(2-methylphenyl)pyridine	29
Figure 24	<i>Cis-syn-C</i> crystal structure of 3,5-dimethyl-2,6-di(2-isopropyl)pyridine	30
Figure 25	Crystal structure of 3,5-dimethyl-2,6-di(4-methylnaphthyl-1-yl)pyridine	30
Figure 26	Crystal structure of 2-bromo-3,5-dimethyl-6-(4-methylnaphthyl-1-yl)pyridine	31
Figure 27	Crystal structure of 1,3,5-trimethyl- <i>cis</i> -2,6-di(2-methylphenyl)pyridinium iodide	31
Figure 28	Low temperature D-NMR of 3,5-dimethyl-2,6-di(2-isopropylphenyl)pyridine	33
Figure 29	D-NMR of 3,5-dimethyl-2,6-di(2-isopropylphenyl)pyridine methyl region	35
Figure 30	High temperature D-NMR of 3,5-dimethyl-2,6-di(2-isopropylphenyl)pyridine	36
Figure 31	¹ H DNMR simulations of 3,5-dimethyl-2,6-di(2-isopropyl)pyridine	37
Figure 32	¹ H DNMR simulations of 3,5-dimethyl-2,6-di(2-isopropyl)pyridine (zoomed in)	37
Figure 33	Low temperature DNMR of 3,5-Dimethyl-2,6-di(2-methylphenyl)pyridine	38
Figure 34	DNMR of 3,5-Dimethyl-2,6-Di(4-methylnaphthyl-1-yl)pyridine	39
Figure 35	DNMR of 3,5-Dimethyl-2,6-Di(4-methylnaphthyl-1-yl)pyridine (zoomed in)	40
Figure 36	Simulation of 3,5-Dimethyl-2,6-Di(4-methylnaphthyl-1-yl)pyridine	41
Figure 37	Simulation of 3,5-Dimethyl-2,6-Di(4-methylnaphthyl-1-yl)pyridine	42
Figure 38	DNMR of 1,3,5-trimethyl-2,6-di-(2-methylphenyl)pyridinium iodide	43
Figure 39	Separation of <i>Cis</i> and <i>trans</i> isomers using GC	43
Figure 40	DNMR of 1,3,5-Dimethyl-2,6-Di(4-methylnaphthyl-1-yl)pyridinium Iodide	44
Figure 41	<i>Cis-trans</i> analogs of 1,3,5-trimethyl-2,6-di-(3-methylphenyl)pyridinium Iodide	44
Figure 42	Schematic of diarylated structure showing rotations preferences	46
Figure 43	Eyring equation and three pathways	47
Figure 44	Locations where atropisomeric occurs	48

Figure 45	Smaller substituent causing hinderance to rotation	48
Figure 46	Comparison of modeled/experimental mono and diarylated products	49, 50

Abstract

Atropisomerism in Lutidine Systems

By

Parijat Sharma

Master of Science in Chemistry

Starting with 3,5-dimethylpyridine, 2,6-diaryl compounds were prepared using the Suzuki-Miyaura cross coupling method. This approach uses palladium catalyzed coupling of 2,6-dibromopyridine with aryl-boronic acids giving 50-90% of the desired 2,6-diaryl-3,5-dimethylpyridine. The diarylated compounds were investigated to find the atropisomerism of the aryl-substituents on the pyridine ring system. Molecular modeling was initiated for insight on the expectations. Single-crystal X-ray structures gave the dihedral angles around the pyridyl-aromatic groups. Dynamic ¹H NMR provided the coalescence temperature and shifts to find the barriers of rotation in *trans-cis* conformational isomers. As expected, the rotational barriers of the 2-substituted aromatic groups gave similar values.

INTRODUCTION

Throughout the world of chemistry, there are a number of variables that can allow seemingly similar molecules to have vastly different reactive properties. One such variable, that is often overlooked, is the ability of a molecule to form atropisomers. The property of atropisomerism is brought about by hindered rotation about a bond axis due to steric clashes between bulky functional groups found within the same molecule. Unlike the classical chiral centers, which racemize based on differences in the bond forming mechanism, atropisomers racemize primarily due to thermodynamic stability around a bond axis that is prone to rotation (Fig. 1). It is due to this thermodynamic stability that interconversion between two conformers of an atropisomer is a slow process. Therefore, one of the main requirements to characterize an atropisomer, is a need for the interconversion process to have a half-life of >1000 s. As long as this condition is met, it is possible to observe and even isolate the conformers of an atropisomer. This same requirement can alternatively be stated in terms of the torsional angle rotational barrier energy. This barrier energy is a manifestation of the hindered rotation along a bond axis,

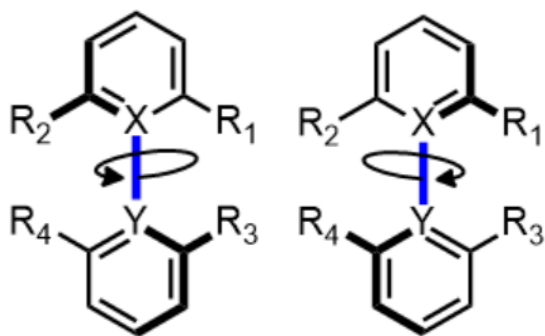


Figure 1: Example of a generic atropisomeric system. The R_1 - R_4 functional groups block the rotation of both rings with respect to each other due to steric hinderance.

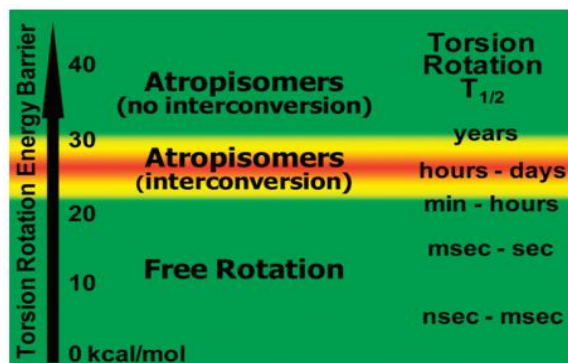


Figure 2: Guide on determining atropisomer classes.¹

due to steric or electronic constraints and atropisomers have the capability of being formed only if the barrier energy value is ≥ 20 kcal/mol.

As a consequence of these defining guidelines, atropisomers are divided into three different thermodynamic classes. As displayed in figure 2, class 1 atropisomers consist of compounds that have the ability to interconvert from one conformer to another within a timescale of nanoseconds to seconds. The rotational barrier energy that corresponds with this class of atropisomers ranges anywhere from 0 kJ/mole – 79.5 kJ/mole (0 kcal/mol - 19 kcal/mol)¹. In most cases, class 1 atropisomers aren't even considered to be atropisomers due to their ability to switch conformers in such a short period of time and are usually referred to as freely rotating. On the other hand, the class 2 atropisomers, have an approximate rotational barrier energy range of (84 kJ/mole – 125.5 kJ/mole (20 kcal/mol - 30 kcal/mol)) and have a half-life interconversion timescale of minutes to hours. In some extreme cases this timescale can even range up to months. Lastly, the class 3 atropisomers are the most stable of all. These compounds experience interconversion on the timescale of years. The relatively high rotational barrier energy allows for these compounds to exist in a stable conformation and ($\Delta E_{\text{rot}}^{\ddagger} \geq 125.5 \text{ kJ/mole}$ or 30 kcal/mol) is a result of significant steric and electronic hinderances. It is important to note that the classifications just described require the compound to be dissolved in solution. When the compound is in its crystalline state the ΔE_{rot} values may be higher than reported due to the presence of noncovalent interactions (London dispersion forces, hydrogen bonding, etc.).¹

The phenomenon of atropisomerism was first encountered when a bi-phenyl molecule consisting of no asymmetrically substituted carbons displayed properties of being optically active. This puzzling discovery wasn't fully described until 1922, when Christie and Kenner determined that the phenomenon was arising due to hindered rotation around the covalent bond, which connected the two phenyl rings.² At the time, this realization wasn't fully appreciated due to a lack of relevant applications. However, in the mid-20th century, a large number of

atropisomers were discovered in a number of the most common medicinal products used at the time and it was also determined that the atropisomeric moiety of the product is the key active pharmaceutical ingredient in a number of cases. Some examples of natural products with atropisomerism as part of the structural architect are shown in Figure 3.^{3,4}

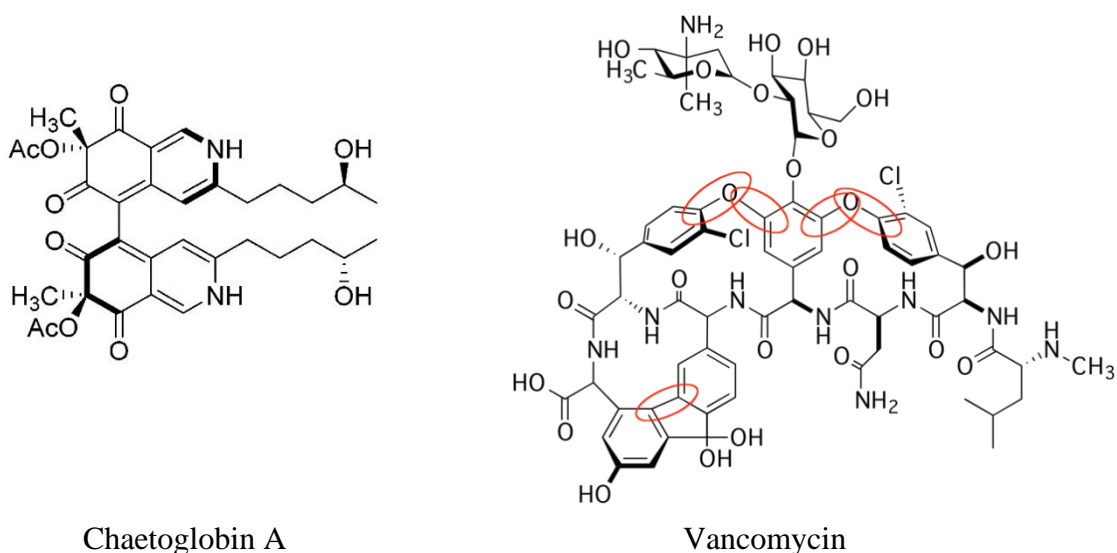


Figure 3. Chaetoglobobin A, exhibits anti-cancer activities in breast and colon cancer cell lining. Vancomycin is currently used as an antibiotic.

A more recent example of pharmaceuticals exhibiting atropisomeric activity is that of AMG 510, which makes use of nitrogen heterocycles (Figure 4).⁵ AMG 510 is known to be the first covalent inhibitor of the cancer causing KRAS protein. During pharmacokinetic studies, it was determined that atropisomer slow interconversion was taking place in the isopropylphenyl-quinazolinone biaryl bond (circled in red, Figure 4). Specifically, the interconversion occurred at room temperature with a half-life of 8 days and an interconversion free energy barrier (ΔG^\ddagger) of 26 kcal/mol. For a potential drug candidate, the occurrence of a slow interconversion between atropisomers is unacceptable since the structure of the drug is responsible for its pharmaceutical activity and the slow interconversion will eventually alter the structure. Consequently, a number

of structural modifications were attempted in the hopes of finding a structural substitution that would raise the free energy barrier and prevent slow interconversion while simultaneously leaving the activity and potency of the drug intact. Eventually, it was decided that a simple C-6 methyl substitution provided the desired results.

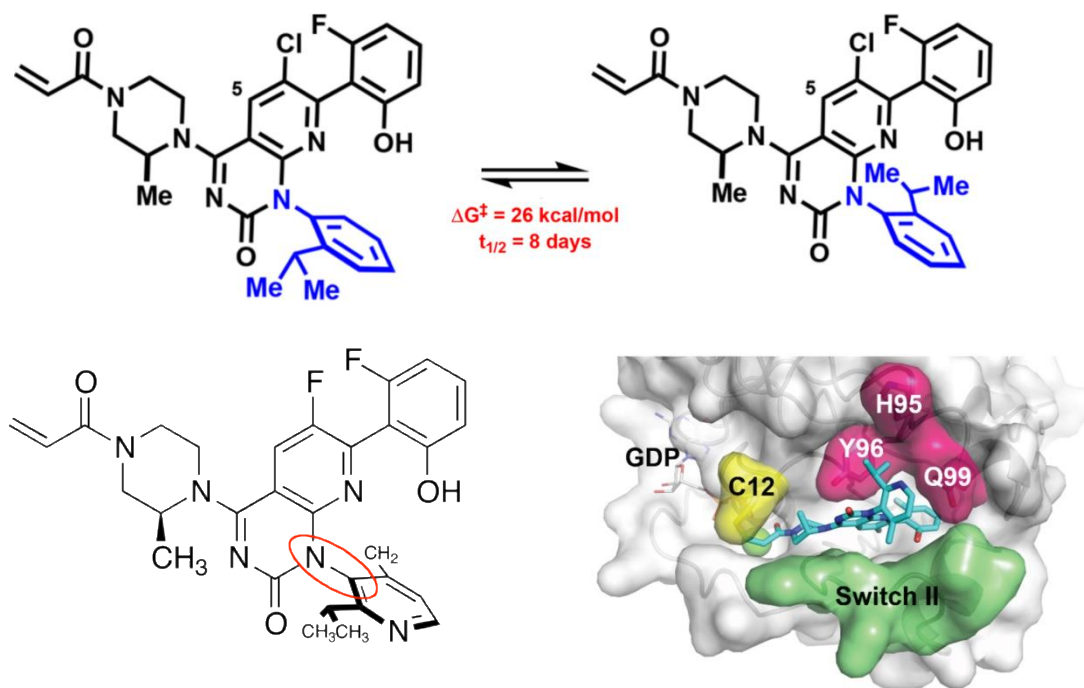


Figure 4: The interconversion taking place between atropisomers (top). The final structure of AMG 510 (bottom left) and the X-ray crystal structure of AMG 510 bound to GDP KRAS (bottom right).

Besides pharmaceuticals, atropisomers have also been designed into some catalyst for asymmetric synthesis methods. The majority of atropisomer catalysts make use of some form of a biaryl moiety. Two examples of structural features are binaphthyl based ligands and Lewis acids (Figure 5).^{6,7}

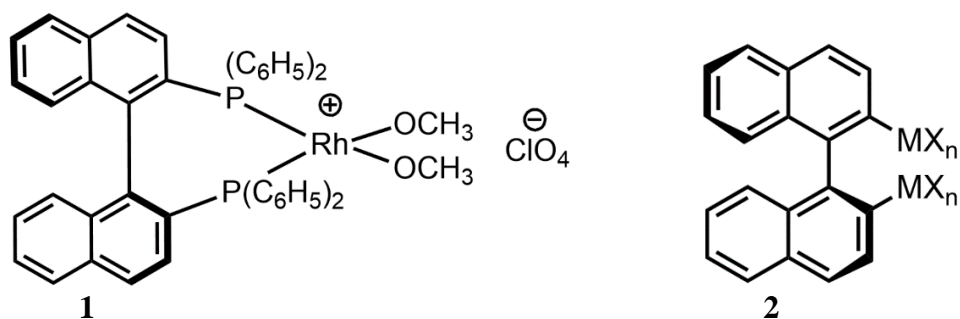


Figure 5. Binaphthyl based asymmetric catalyst for hydrogenation and bidentate Lewis acids.

The majority of biaryl atropisomer catalysts concerning enantioselective synthesis are binaphthyl based ligands and this is primarily due to the highly stable atropselective configurations that the base binaphthyl (**1**) structure provides. Furthermore, there are a number of positions on the molecule that allow for functionalization, which can then result in a variety of derivatives of compound **1**.⁸ It is important to note that in order to achieve stable atropisomer configurations, the functionalization at the 2,2 position is critical. Through a number of experiments, the Cooke group determined that as long as the 2,2 positions are functionalized, a stable atropisomer of only one configuration is attainable. If in the case that positions 8,8 were functionalized instead, the atropisomer stability was determined to be equal to that of the unfunctionalized **1** molecule. Furthermore, the size and electronic environment of the functionalized groups have an important effect on the preferred atropisomer configurations and consequently the preferred dihedral angle of the 2,2 functionalized **1**. Gottarelli and Solladie et. al. determined that if the functional groups are small and capable of intermolecular hydrogen bonding, the cisoid conformation was the preferred atropisomer. However, if the substituent is large, the transoid configuration is preferred instead (Figure 6).⁹

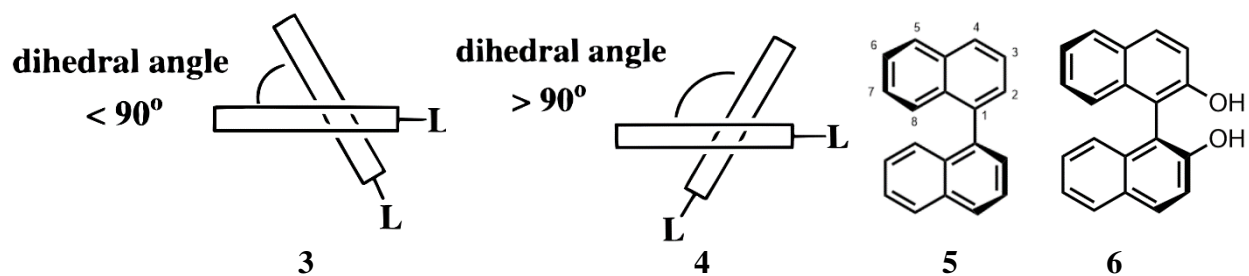


Figure 6: Depiction of the cisoid configuration, 2 and the Transoid configuration 3.

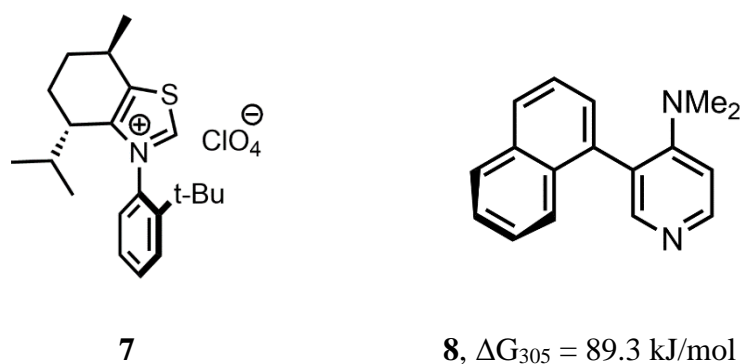
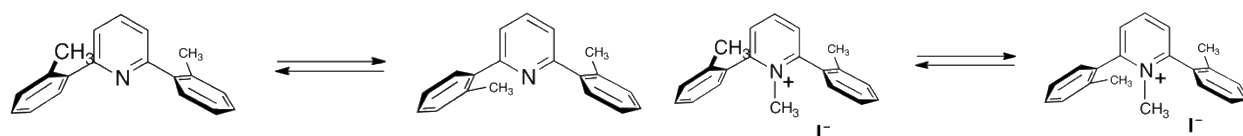


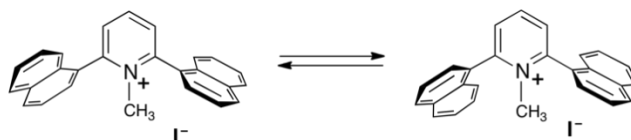
Figure 7. Two examples of non-binaphthyl or nitrogen heterocycle based asymmetric catalyst.

The current work focuses on the pyridine system with emphasis on atropisomerism on the 2,6-position. Previous work from our laboratory focused on the 2,6-diarylpyridine ^1H DNMR studies, which show that the barrier to rotation was significantly below room temperature (Figure 8)¹⁰. Additionally, the deciphering of ^1H DNMR of the 2,6-dinaphthylpyridine molecule were found to be too complicated and the line broadening issues added to further the complexity. In order to increase the barrier to rotation of the neutral form, 3,5-dimethyl-2,6-diarylpyridine system was investigated (Figure 9).



9, Barrier to rotation $\Delta G^* = 39.3$ kJ/mole

10, $\Delta G^* = >92.0$ kJ/mole



11, $\Delta G^* = >92.0$ kJ/mole

Figure 8: Barrier to rotation for 2,6-diarylpyridine

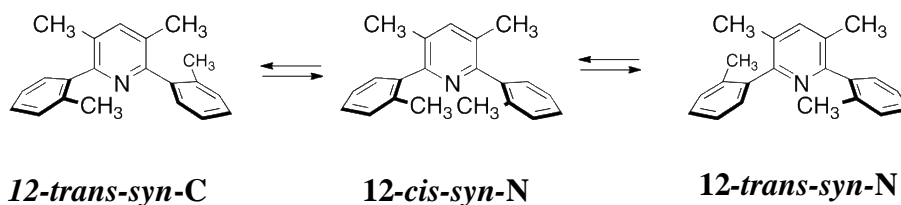


Figure 9: Atropisomer conformations of 3,5-Dimethyl-2,6-di(2-methylphenyl)pyridine

The pyridine moiety is a common group present in many pharmaceutical products and biologically active compounds. In recent years, the phenomenon of atropisomerism has proven to be a major factor in helping to focus biological activity. Furthermore, the pyridine functional group has also proven to be a useful component in designing asymmetric catalysts owing to the presence of the nitrogen lone pair electrons. Taking these factors into account, it is our belief that atropisomerism has the potential to be very useful in focusing biological activity and also in designing practical asymmetric catalysts.

RESULTS

In this section, the results of our investigations are presented. The results involve the work in synthesizing the relevant compounds. For each, we carried out computational work, crystal structure data, and dynamic NMR. These works combined result in the calculations and experimental information on the dihedral angles, relative stability of the isomers, and the barrier to rotation of the atropoisomers.

Synthesis

Dibromo Lutidine Starting Material Synthesis

The successful synthesis of the titled compounds 3,5-dimethyl-2,6-di(2-methyl)pyridine (**12**), 3,5-dimethyl-2,6-di(3-methyl)pyridine (**13**), 3,5-dimethyl-2,6-di(naphth-1-yl)pyridine (**14**), and 3,5-dimethyl-2,6-di(2-isopropyl)pyridine (**15**) was achieved using the Suzuki-Miyaura cross coupling reaction of the 2,6-dibromo-3,5-dimethylpyridine (**21**) moiety and the corresponding arylboronic acid substrates. Additionally, through the use of careful method development, the synthesis of the monoarylated versions of each of these compounds was accomplished (*vide supra*). But prior to performing these syntheses, it was necessary to first synthesize the 2,6-dibromo-3,5-dimethylpyridine (**21**) starting material. The synthesis of **21** involved very harsh conditions. Commercially available lutidine (**20**) was treated with oleum and Br₂ under reflux conditions.¹¹ Once the reaction was finished, the product was recrystallized using hot EtOH. One of the key realizations obtained from this reaction is the importance of the speed of the dropwise addition of the Br₂. When the Br₂ was added in a quick dropwise manner, the reaction temperature dropped quickly so that the target reaction did not have the required activation energy to form product. This only resulted in a continuous reflux of excess Br₂. When the Br₂ was added quickly, even after continuous reaction for 72 hours, no sign of Br₂ consumption was

observed (the excess Br₂ in the flask would reflux back into the dripper). When the Br₂ was added in a much slower dropwise manner instead, the reaction temperature was not affected drastically, and the target reaction was achieved leading to a 36% yield of the desired product after the reaction was refluxed for 48 hours. It is also important to note that this reaction was performed using 20-30% oleum. It may be possible to perform this reaction with 10% oleum, however it is presumed that the reaction time would need to be increased significantly.

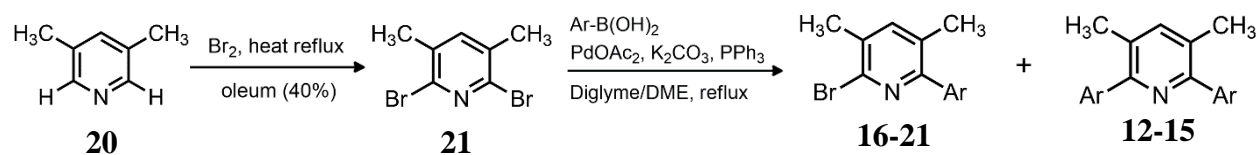
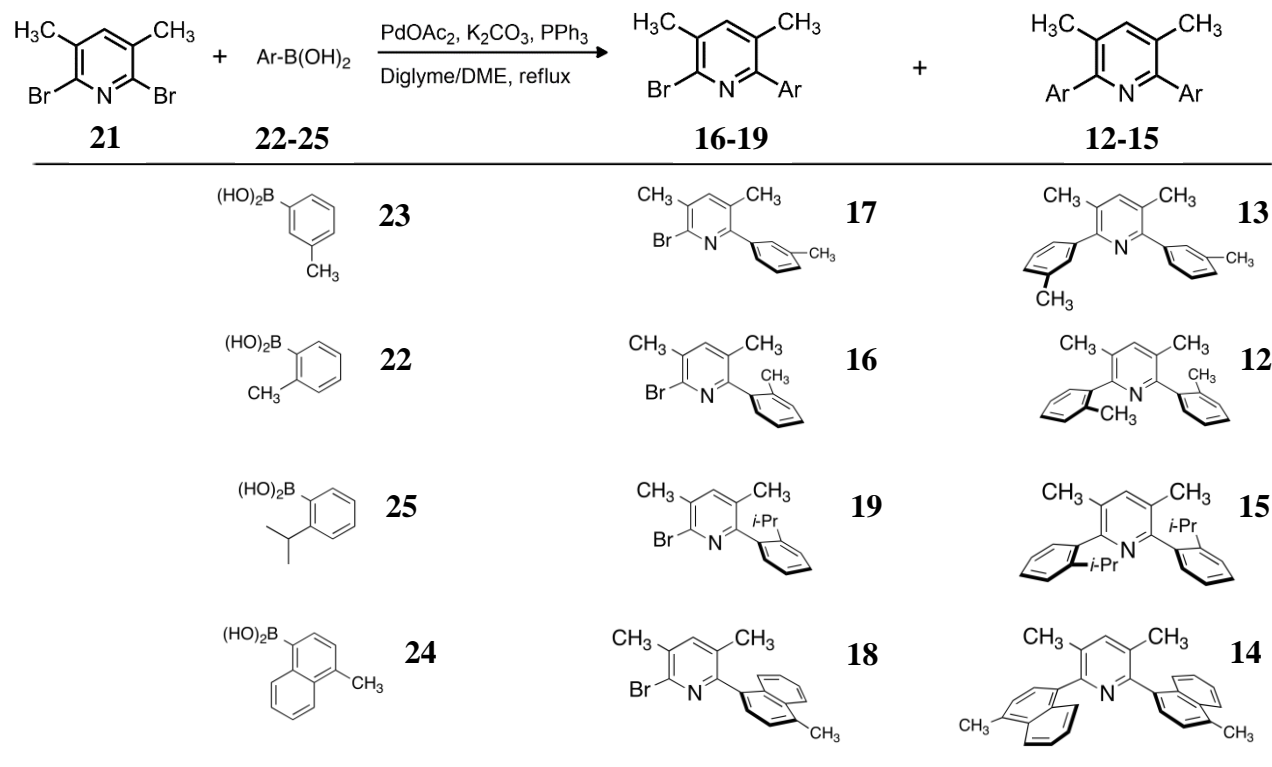


Figure 10: Synthesis approach of 3,5-dimethyl-2,6-diarylpyridine

The four substrates required were 2-methylphenylboronic acid (**22**), 3-methylphenylboronic acid (**23**), 4-methyl-1-naphthaleneboronic acid (**24**), and (2-isopropylphenyl)boronic acid (**25**). For the Suzuki-Miyaura cross coupling, Pd(OAc)₂ was used as the source of palladium in DME or diglyme solvent.¹² However, to achieve the monoarylated version of these compounds, the first modification to the procedure was to the equivalents of the boronic acid substrate. For example, on the first attempt at synthesizing 2-bromo-3,5-dimethyl-6-(2-methylphenyl)pyridine (**16**), only one equivalent of **21** was added for two equivalents of **22**. This reaction was run for four hours and it resulted in the desired product **16** with a yield of 24.9%. This reaction also afforded a secondary product (~ 12%) which, after further analysis, revealed itself to be the dimer of the boronic acid: 2,2'-dimethyl-1,1'-biphenyl (**30**). In the following experiment, all conditions were unaltered, except the equivalent of **22** was decreased to 1.25 for every 1 equivalent of **21**. This resulted in the formation of **12** with a net yield of

52.4% and no target compound **16** was observed to have formed. The formation of some **16** was expected since the boronic acid concentration was decreased by 0.63 times. The high yield of **12** was attributed to the long reaction time. In the following experiment, with the aid of periodic TLC monitoring, the reaction time was reduced to only two hours and this resulted in the formation of target compound **16** with a net yield of 17.9% and the formation of side product **12** with a yield of 52.1%. The next modification made was the replacement of the dimethoxyethane solvent with 2-methoxyethyl ether (diglyme) solvent. This would help to determine the impact of differences in-solvent properties. It was determined that due to the slightly higher reflux temperature attribute of diglyme, the diarylated version of the pyridine would form in much higher yield. As a result, a switch to ethylene glycol dimethoxy ethyl ether (DME) was made in addition to using only one equivalent of the boronic acid substrate instead of the 1.25 in an attempt to achieve high yield synthesis of the monoarylated products (**16-19**). This modification was experimented with using the **22** substrate and it was determined that the target compound **16** yield increased by ~3% (final yield: 22.7%) and the side product **12** yield decreased by ~30% (final yield: 22.2%). The highest yield of 37.5% for the monoarylated pyridine product was achieved with substrate **24** for target compound **18**, where the equivalent ratio of starting material to substrate was 1:1, and the reaction time period was 45 minutes. Interestingly, when the equivalent ratio of starting material to substrate was changed from 1:1 to 1:1.25 and the other conditions were unchanged, the monoarylated pyridine product yield remained consistent (~35%) while the diarylated pyridine yield increased from ~18% to ~60%. This result is especially surprising, since common intuition would suggest that increasing the substrate equivalent would lead to higher yields for both the monoarylated and diarylated pyridines.

Table 1: Syntheses of 3,5-dimethyl-2,6-diarylpyridine

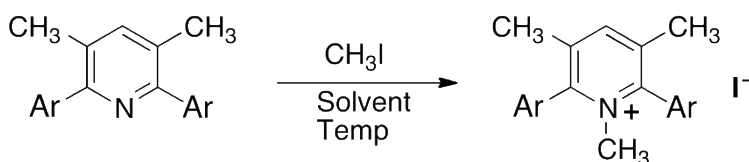


Boronic Acid	Equivalent(s) of Boronic Acid	Reaction Time (minutes)	Reaction Solvent	% Yield	
				Mono-Arylated	Di-Arylated
	1	45	DME	22.7%	22.2%
	1.6	45	Diglyme	12.9%	66.7%
	1.6	45	DME	24.0%	74.3%
	2	45	Diglyme	Not isolated	86.0%
	1	45	DME	37.5%	18.4%
	1.6	45	Diglyme	21.7%	57.6%
	1	45	DME	35.1%	27.7%
	2.5	45	Diglyme	Not isolated	102.8%

The synthesis of the diarylated pyridine product was straightforward. The highest yield was obtained in experiments where the substrate to starting material ratio was 2:1. Although, when experiments with higher substrate concentrations were attempted, it was determined that a

large amount of the dimerized substrate formed, in addition to the formation of the target compound. The removal of this side product was easily achieved using column chromatography. Furthermore, in the initial experiments the reaction time of 18 hours was used for convenience, however, after performing periodic TLC testing of the reaction mixture, it was determined that the majority of the reaction is complete within 45 minutes.

The selective diarylated products were N-methylated to provide the N-methylpyridinium diaryl compounds for investigations as well. The two atropisomers of the methylated pyridinium compounds were readily separated and there was no indication of isomerization on separation to date.



- 26**, Ar = 2-methylphenyl, 97.2 %
27, Ar = 3-methylphenyl, 99.1 %
28, Ar = 4-methylnaphth-1-yl, 98.7%

Figure 11. N-methylation of selected diarylated compounds.

***Ab-initio* modeling**

As has already been discussed, the aryl substrates for the diarylated pyridine molecules are bonded to the pyridine ring by a single covalent bond. As a result, the substrates have the ability to freely rotate around that bond axis. It is the presence of steric effects that prevent free rotation around the single bond from taking place, forcing the aryl groups into a particular conformation, which then results in atropisomer formations. In addition to this, conjugative effects, places additional restrictions on the free rotation of the pyridine-phenyl substrates by adding stability when π -orbital overlap is exhibited. Both the steric effects and the conjugative

effects work to position the aryl moiety with an opposite agenda. The steric effects prevent the r-phenyl group from being coplanar and instead force an orthogonal dihedral angle with the pyridine ring, primarily due to steric repulsion from the 3,5-methyl groups. The conjugative effect on the other hand, forces the r-phenyl substrate in the coplanar position, since it allows for maximum π orbital overlap. In both cases, the molecule will attempt to achieve the lowest energy state possible. As a result of these opposite forces, the phenyl substrates will orient themselves with a dihedral angle between 0° to 90° and 0° to 180° . Due to the symmetry of the molecules synthesized in this project, it is important to designate the different possibilities of atropisomer configurations. The 2-bromo-3,5-dimethyl-6-(2-methylphenyl)pyridine is used as an example in figure 12. The differences in barriers to rotation between *cis-syn-N*, *cis-anti*, and *cis-syn-C* are very small and are negligible for this work. It is the differences between the *cis*- and *trans*-diarylpyridine that will be the focus of our investigation.

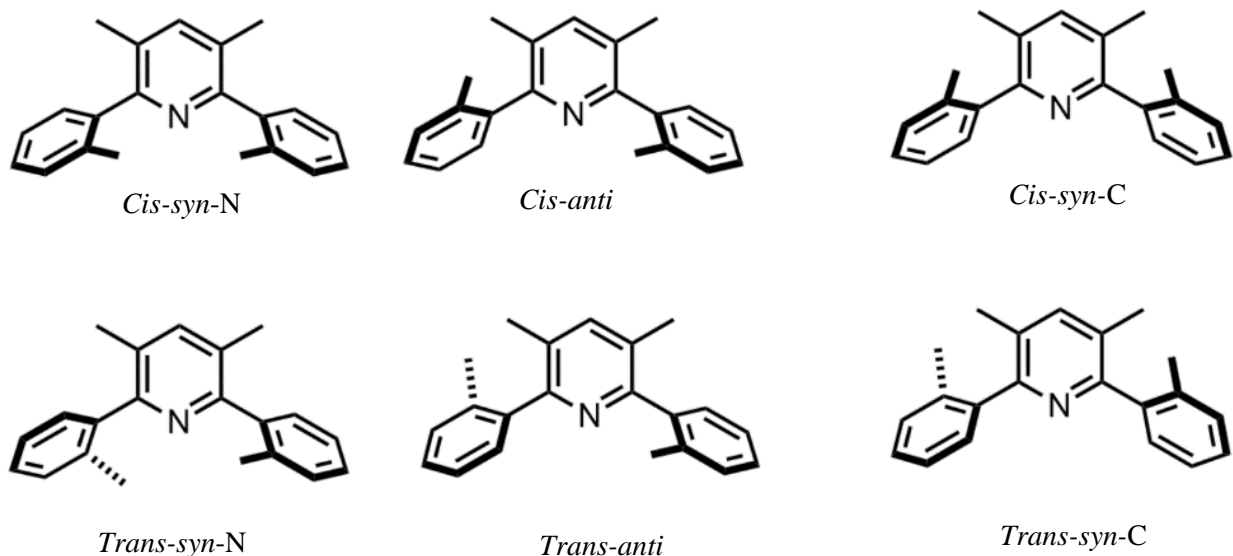


Figure 12: Minimized possible conformations of 3,5-dimethyl-2,6-di(2-methylphenyl)pyridine (**12**).

Prior to obtaining experimental data regarding the structures of the compounds synthesized in this project, a number of *ab-initio* calculations were performed as a way to predict the most stable form of each molecule. The software, Spartan platform was used with the application of the Density Functional approach, at the level of B3LYP, 6-311+G** equilibrium geometry in vacuum.¹³ One of the first molecules examined was the 3,5-dimethyl-2,6-di-*p*-tolylpyridine (**29**). Despite this molecule not having cis- or trans-isomers, modeling the molecule gives configurational information without the presence of any substituents on the aryl groups which could cause significant steric hinderances. Modeling shows that when the 4-methylphenyl substrates are in the *syn*-position and anti-position, the relative energies are 2.12 kJ/mol and 0.00 kJ/mole (Figure 13). This increase in energy can be explained by the small amount of steric effects between the methyl on the pyridine moiety and the ortho-hydrogen on the 4-methylphenylboronic acid group. In the *syn*-conformation, the dihedral angles between the pyridyl and the phenyl groups were calculated to be 44.74° and 45.06°.

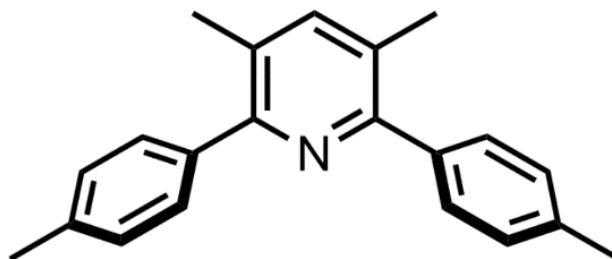
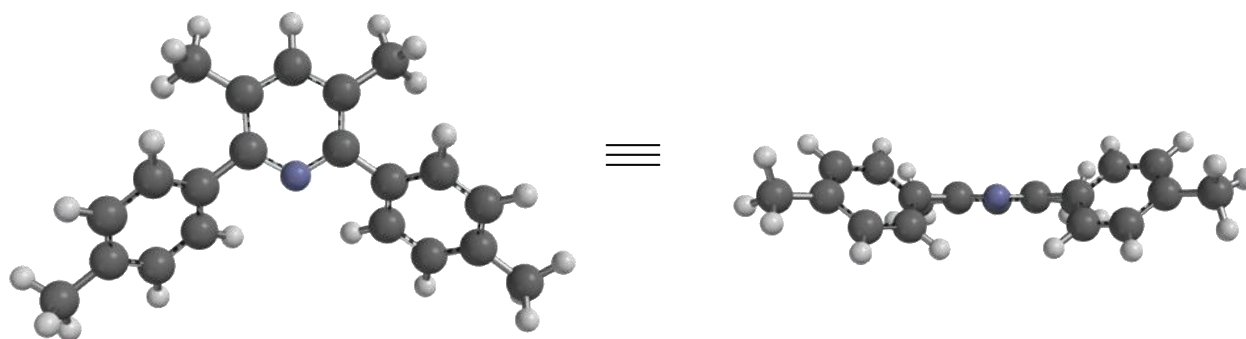


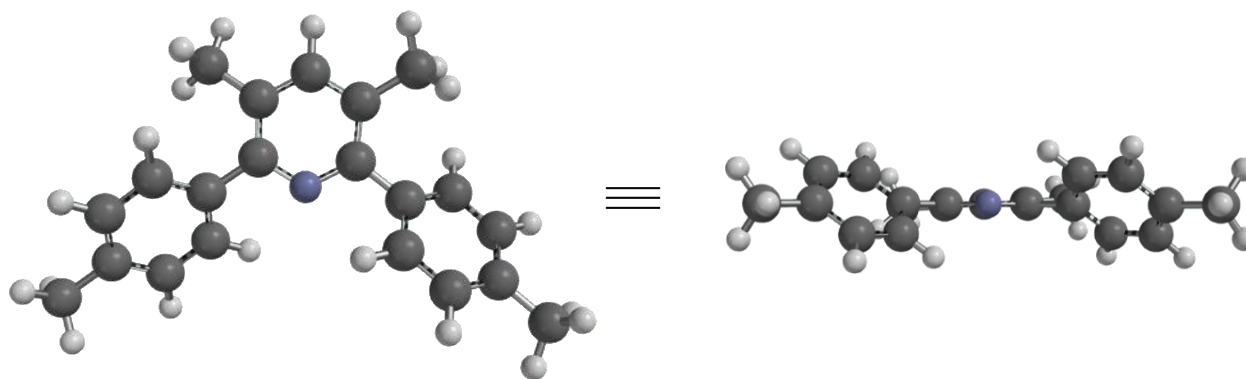
Figure 13: Configuration of di(4-methylphenyl)-3,5-dimethylpyridine (**29**).

In the following scenario, one of the phenyl substrates was rotated further so that the dihedral angle between the substrate and the pyridine ring was 90°. In this constraint, the conjugative effect had been completely removed (at least from the substrate that was rotated) which would lead to the conclusion that the energy of the system should be lower when comparing the energy of the system during the *trans* condition. However, since the substrate is

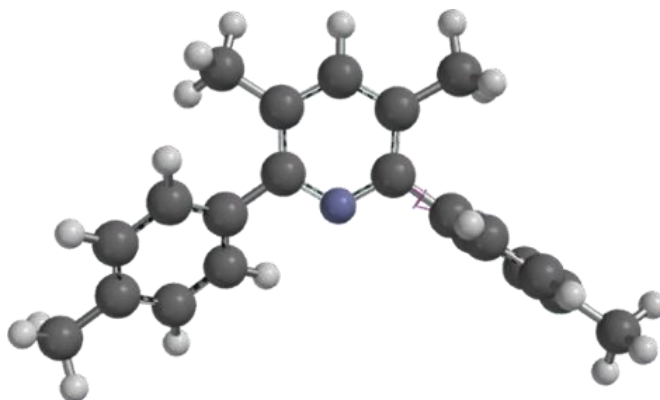
rotated so that the dihedral angle is a complete 90° , this condition will allow for minimum steric effects due to the proton-1 of the phenyl substrate being furthest away from the methyl of the pyridine system. This reduction in energy is enough, as a result of the optimum steric conformation, to compensate for the reduced conjugative effects, which then results in an overall system energy of 4.48 kJ/mol. In the final scenario, the phenyl substrate is constrained so that the dihedral angle between it and the phenyl ring is 0° . This results in one of the most destabilized conformations of the system possible with an overall system energy of 48.60 kJ/mol. The steric repulsive effects between proton 1 and the pyridine methyl are strong enough to increase the energy by a magnitude of 10, when comparing the system's energy to the 90° constraint scenario.



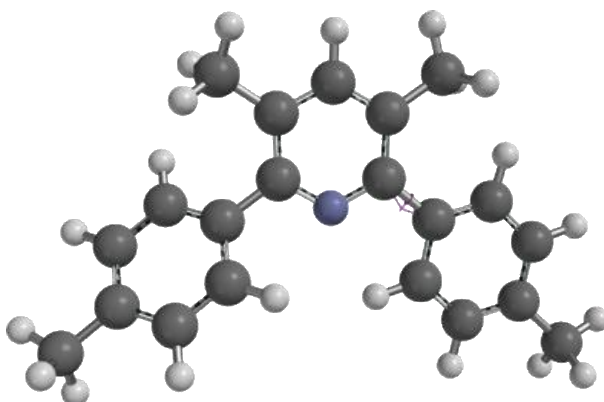
29-syn-isomer, 2.12 kJ/mol, dihedral angles, 47.11° , 46.84°



29-anti-isomer, 0.00 kJ/mole, dihedral angles, -44.93° , -45.10°



6.60 kJ/mole, dihedral angle constrained at 90° , -45.21°

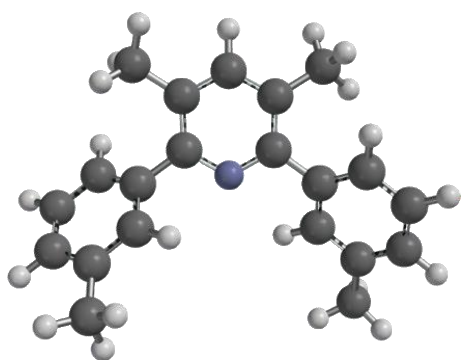


486.0 kJ/mole, dihedral angle constrained at 0° , -45.21°

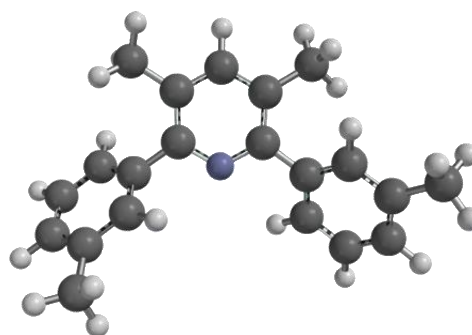
Figure 14: Modeling of 3,5-dimethyl-2,6-di(4-methylphenyl)pyridine (**29**). The given dihedral angles were from the modeling experiment. When one of the aryl dihedral angles were constrained, the other was allowed to rotate in the calculations.

With these modeling predictions in hand, the modeling was advanced to species that were successfully synthesized in this project. Starting with 3,5-dimethyl-2,6-di(3-methylphenyl)pyridine (**13**), the results were expectedly similar to the methyl in the *meta*-position. More specifically, **13** does not have significant steric effects when compared to the system where the methyl is in the 4-position (**29**). As shown in the Figure 15, the *cis*-isomer overall system energy was calculated to be 1.13 kJ/mole higher than the *trans*-isomer. The

energies were also calculated with the dihedral angles fixed at 90° and planar 180° for only one of the aryl groups. The energies calculated out to 5.4 and 39.6 kJ/mole respectively. When fixing the dihedral angle of 180° , the methyl group is oriented towards the nitrogen. This is considered to be the lower energy position as opposed to the methyl group or the aryl ring being oriented towards the methyl group of the pyridine ring. It is important to note that in all modeling experiments, the dihedral angles presented, were measured from the C2- or C2'-pyridine and the tolyl ring carbon distal from the methyl group on the phenyl system.

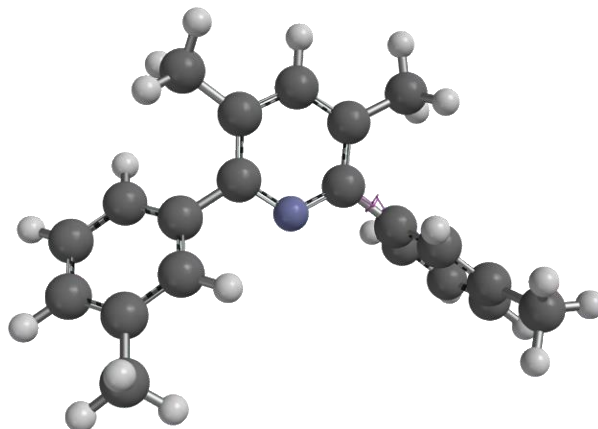


13-cis-anti-isomer, 1.13 kJ/mole

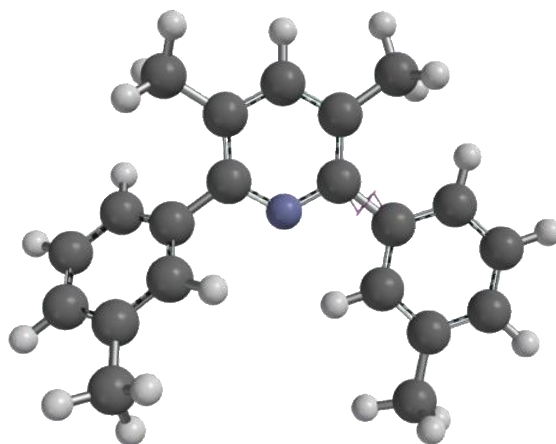


13-trans-anti-isomer, 0.00 kJ/mole

dihedral angles, 67.28° , 48.37°



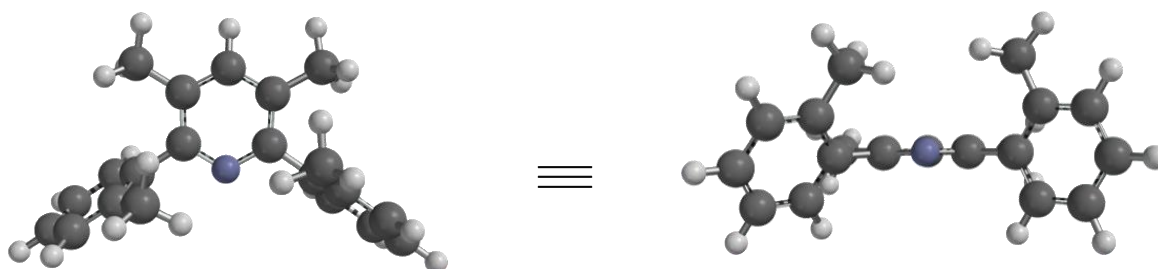
5.4 kJ/mole, dihedral angle constrained 90° , -137.63°



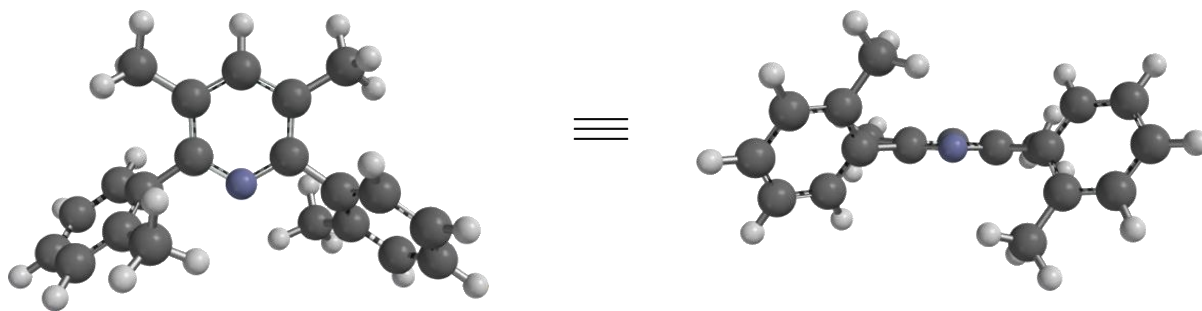
39.6 kJ/mole , dihedral angle constrained 180° , -101.49°

Figure 15: Modeling of 3,5-dimethyl-2,6-di(3-methylphenyl)pyridine (**13**). The given dihedral angles were from the modeling. When one of the aryl dihedral angles were constrained, the other aryl group was allowed to rotate in the calculations.

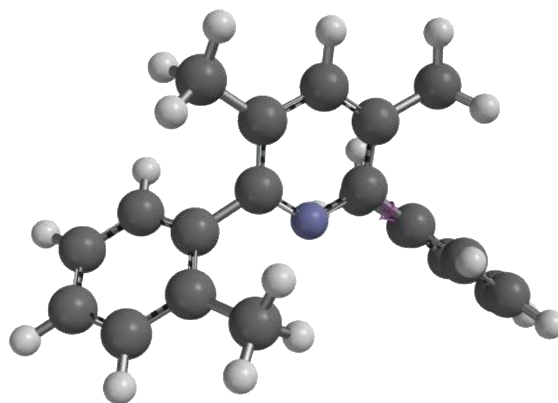
The ortho-substituted methyl groups on the other hand can have a larger impact on the energies since the substrate methyl groups are now in much closer proximity to the pyridine methyl groups (Figure 16). The relative overall system energy for the *cis-syn*-isomer calculated to 2.76 kJ/mole higher than the *trans*-isomer. When the dihedral angles are fixed at 90° and 180° for one of the aryl groups, the energies calculated out to 1.01 kJ/mole and 39.6 kJ/mole. Once again, when the 180° position is fixed, the methyl group is oriented toward the nitrogen of the pyridine. The dihedral angles turn out to be non-symmetrical between the pyridyl system and the 3-methylphenyl groups.



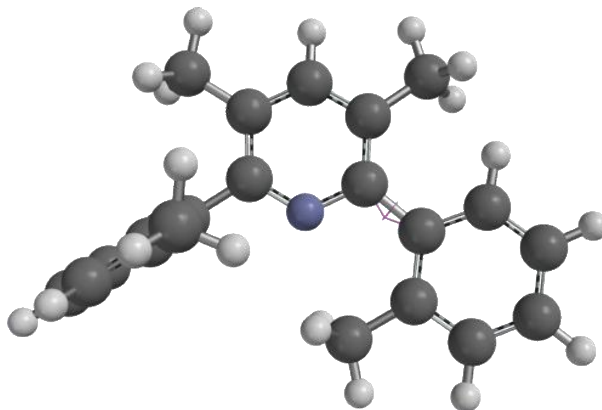
12-cis-syn-isomer, 2.76 kJ/mole, dihedral angles, -89.54° , 66.48°



12-trans-anti-isomer, 0.00 kJ/mole, dihedral angles, 64.87°, 64.94°



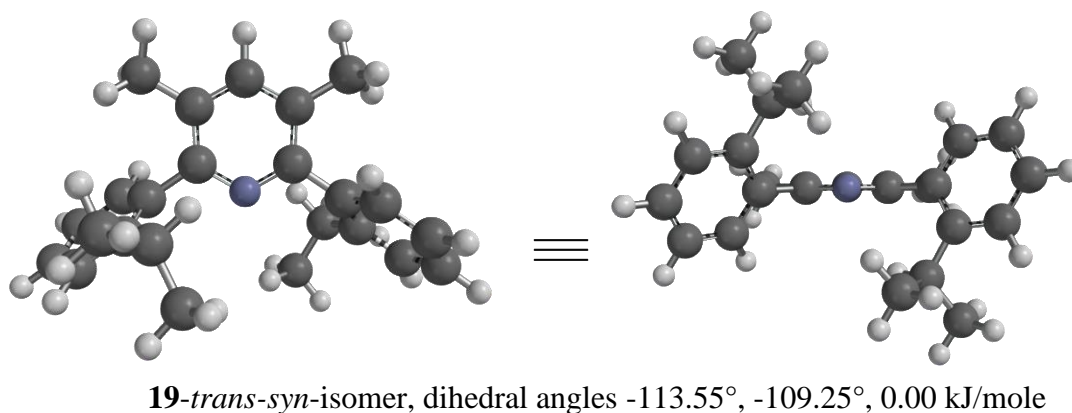
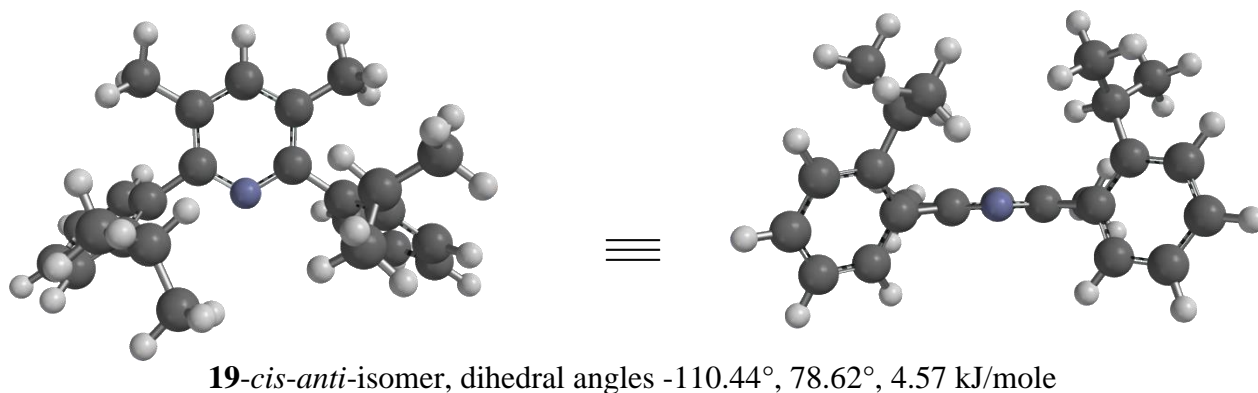
1.01 kJ/mole, dihedral angle constrained 90°, -115.08°

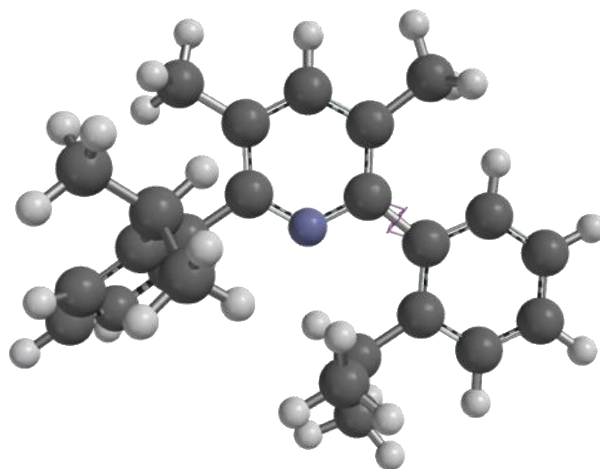


39.6 kJ/mole, dihedral angle constrained at 180°, -101.49°

Figure 16: Modeling of 3,5-dimethyl-2,6- di(2-methylphenyl)pyridine (**12**). The given dihedral angles were from the modeling. When one of the aryl dihedral angles were constrained, the other aryl group was allowed to rotate in the calculations.

The 2-isopropylphenyl group is expected to play a much larger role due to the relatively electron rich C-C bonds in such close proximity with respect to each other. The *cis*-isomer calculated to 4.57 kJ/mole higher than the trans-isomer. Consequently, the trans-isomer calculated to be the most stable conformation. With the dihedral angle constrained at 90° for one of the aryl groups and with the iso-propyl group oriented toward the nitrogen, the minimization provided an overall system energy of 52.92 kJ/mole. In **19**, there seems to be some interaction between the two isopropyl groups in the *cis*-isomer of this molecule. This same interaction, however, is not present in the trans-isomer (Figure 17).

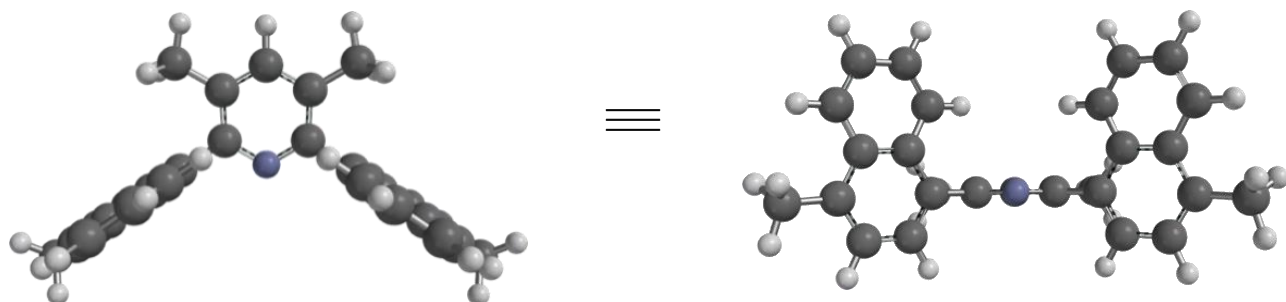




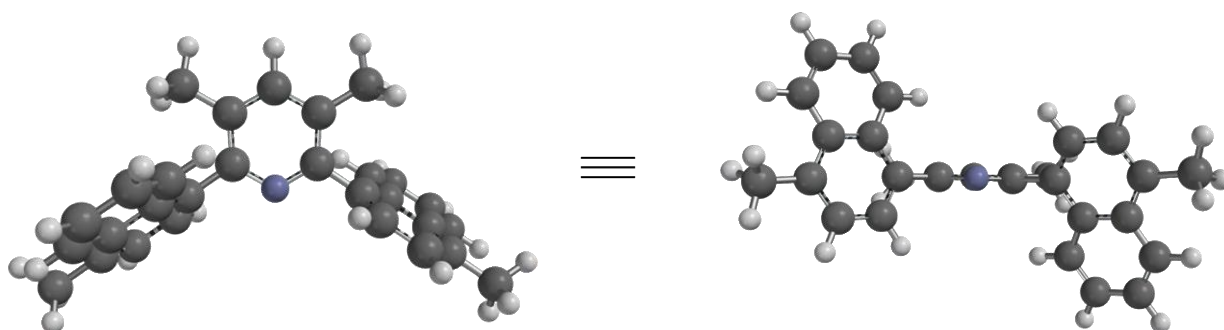
dihedral constrained 180° , -76.10° , 54.92 kJ/mol

Figure 17: Modeling of 3,5-dimethyl-2,6-di(2-isopropylphenyl)pyridine (**15**). The given dihedral angles were from the modeling. When one of the aryl dihedral angles were constrained, the other aryl group was allowed to rotate in the calculations.

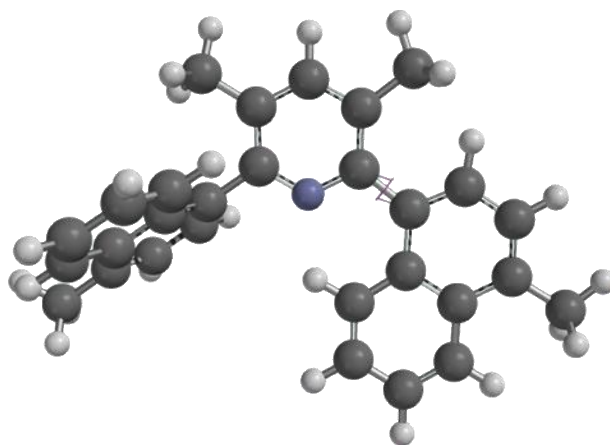
The binaphthyl case should also have relatively larger system energies due to the existence of two adjacent aromatic rings occupying space of the pyridine methyl (Figure 18). The calculations gave similar energies as in the isopropyl case. In the case of the *cis*-isomer, the relative overall energy of the system was calculated at 0.34 kJ/mol. On the other hand, the *trans*-isomer calculated to be the most stable conformation with an overall system energy of 0.00 kJ/mol. When one of the naphthyl groups is constrained at dihedral angles of 90° and 180° with respect to the pyridine ring, the system energies calculated out to 0.34 kJ/mol and 45.26 kJ/mol respectively. Once again, the naphthyl group was oriented toward the nitrogen in the dihedral angle 180° constraint. The high energy of the system can be explained by the large amount of steric interactions between the pyridine ring methyl and the naphthyl portion of **14**.



14-cis-isomer, dihedral angle -91.07° , 91.00° , 0.34 kJ/mole



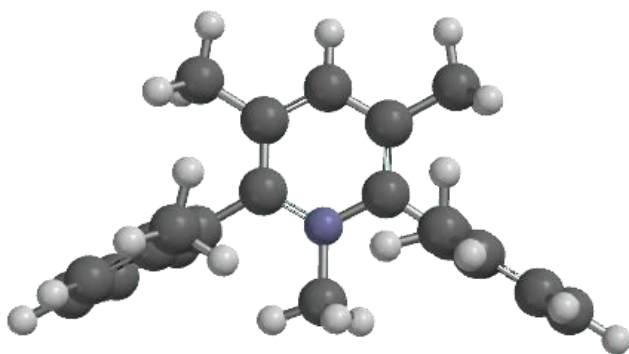
14-trans-isomer, dihedral angle -78.42° , -73.55° , 0.00 kJ/mole



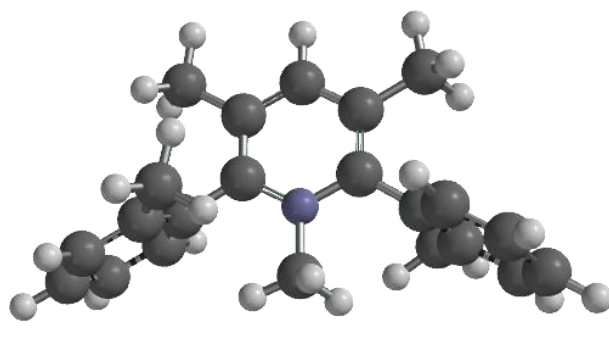
dihedral angle constrained 180° , -76.46° , 45.3 kJ/mole

Figure 18: Modeling of 3,5-dimethyl-2,6-di(4-methylnaphthyl-1-yl)pyridine (**14**). The given dihedral angles were from the modeling. When one of the aryl dihedral angles were constrained, the other aryl group was allowed to rotate in the calculations.

Computational modeling was also carried out with *cis*- and *trans*-isomer of 1,3,5-trimethyl-2,6-di(2-methylphenyl)pyridinium (**26**) as well as *cis*- and *trans*-isomers of 1,3,5-trimethyl-2,6-di(2-methylphenyl)pyridinium iodide. For the pyridinium compounds, the calculation shows that the *cis*-pyridinium compound *trans*-conformation is 0.4 kJ/mole higher than the *cis*-conformation (Figure 19). Consistently, the when iodide anion is inserted into the calculation, the *trans*-isomer is still higher by 56.1 kJ/mol. Closer inspection of the molecule shows that in the *cis*-conformation, the iodide anion is closer to the nitrogen cation ion site. This seems to be the likely cause for the large difference in the calculated energies. The initial position of the iodide anion was chosen by position of the iodide in the crystal structure. When performing calculations of the *cis*- or *trans*-1,3,5-trimethyl-2,6-di(2-methylphenyl)pyridinium the 1-methyl carbon is placed the same plane with the pyridine ring. However, once the iodide has been added, the N-methyl is no longer in the same plane as the pyridine ring system. Interestingly, the crystal structure of the *trans*-1,3,5-trimethyl-2,6-di(2-methylphenyl)pyridinium iodide show that N-methyl is in the same plane as the pyridine ring (*vide supra*). In some attempted calculations where the iodide was not able to move, the computation did not converge.



26-cis-isomer dihedral angle, -129.44° , 125.46° , 0.59 kJ/mole



26-trans-isomer 0.00 kJ/mole

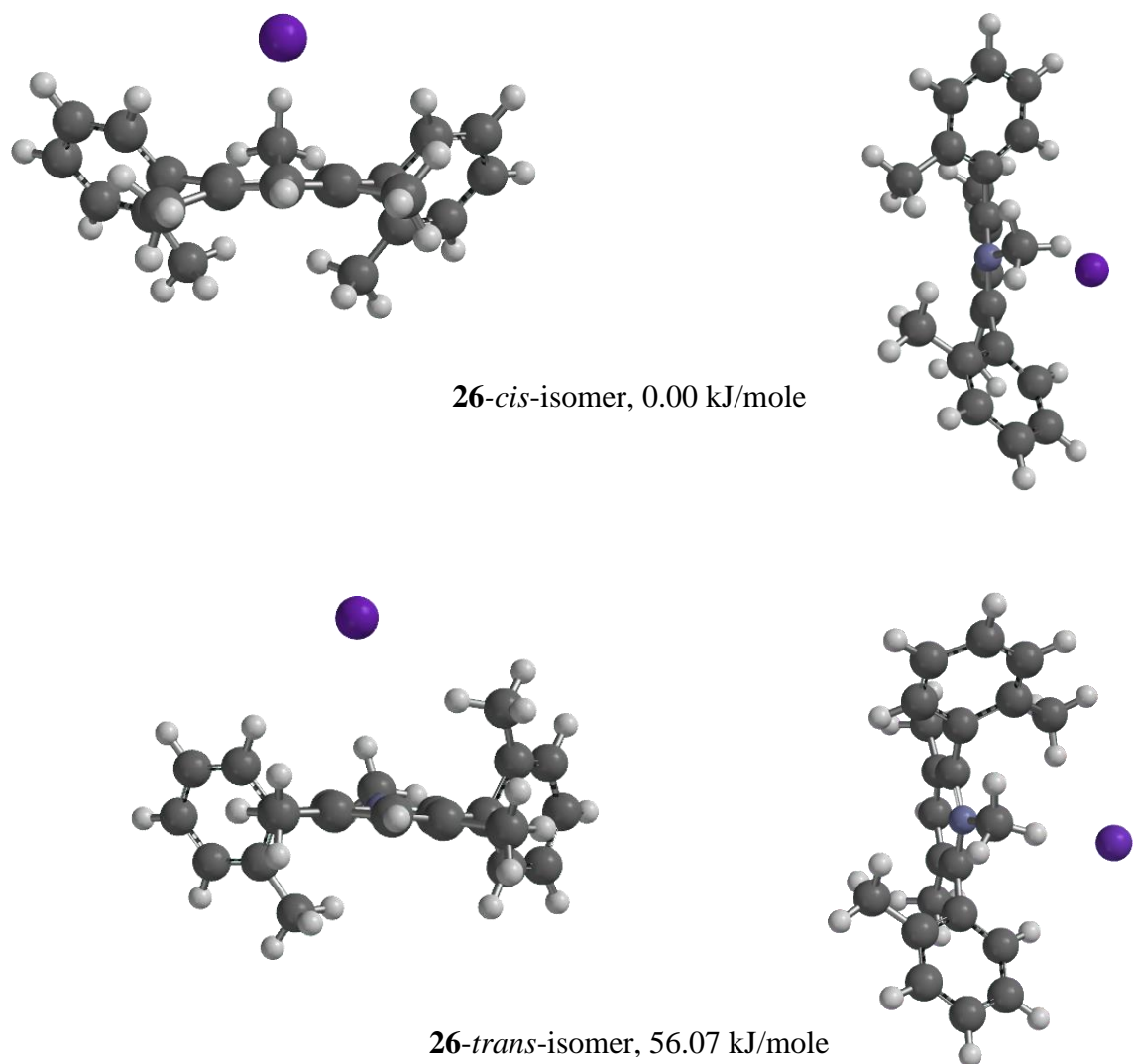
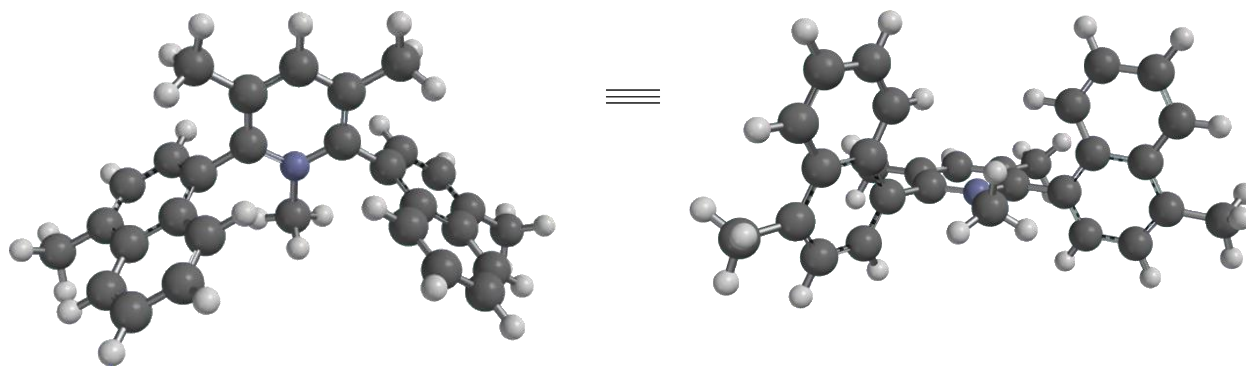
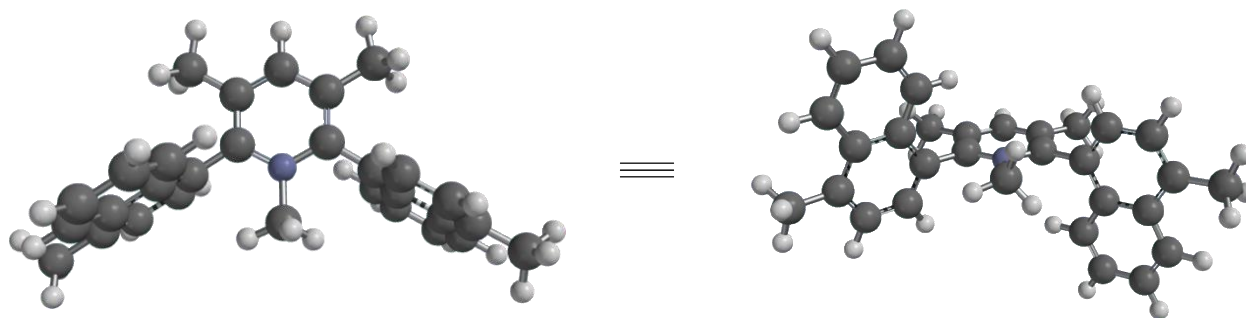


Figure 19: Modeling of *cis*- and *trans*-isomer of 1,3,5-trimethyl-2,6-di(2-methylphenyl)pyridinium and *cis*- and *trans*-isomer of 1,3,5-trimethyl-2,6-di(2-methylphenyl)pyridinium iodide (**26**).

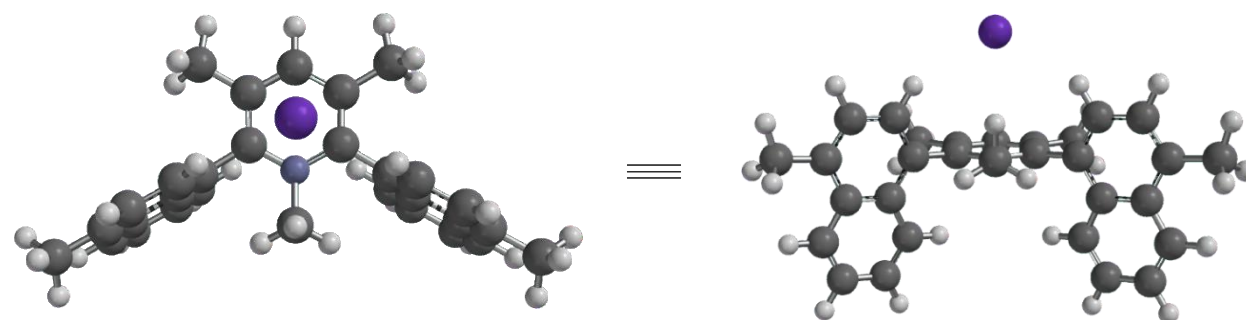
Analogue calculations were carried out for *cis*- and *trans*-1,3,5-trimethyl-2,6-di(4-methylnaphthyl-1-yl)pyridinium and *cis*- and *trans*-isomer of 1,3,5-trimethyl-2,6-di(4-methylnaphthyl-1-yl)pyridinium iodide (**28**). When iodide was involved, it was placed in the position that is indicated by the crystal structures, followed by minimization.



28-cis-isomer 0.00 kJ/mole, dihedral angles, 96.08°, -96.08°



28-trans-isomer 1.4 kJ/mole, dihedral angles, -88.50°, -92.64°



28-cis-isomer, 0.00 kJ/mole, dihedral angle 85.57° and 92.46°

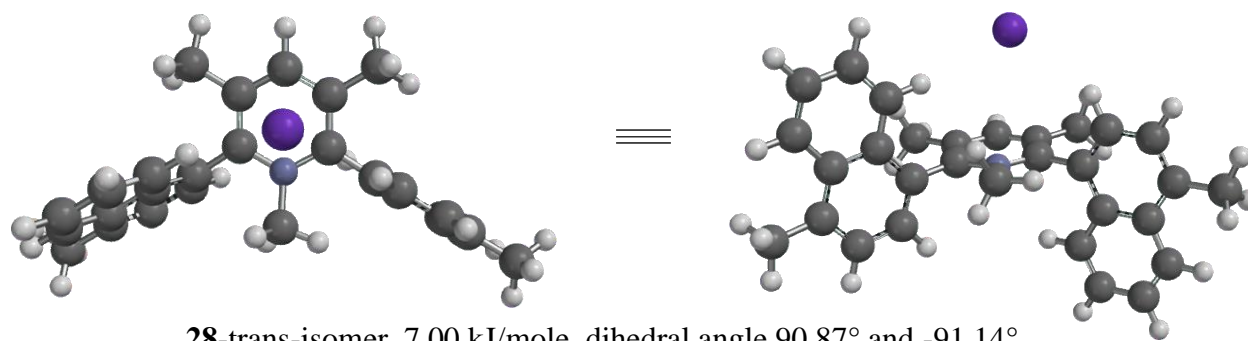


Figure 20: Modeling of *cis*- and *trans*-isomer of 1,3,5-trimethyl-2,6-di(4-methylnaphthyl-1-yl)pyridinium and *cis*- and *trans*-isomer of 1,3,5-trimethyl-2,6-di(4-methylnaphthyl-1-yl)pyridinium iodide.

N-methyl 3,5-dimethyl-2,6-di(3-methylphenyl)pyridinium compound gave uncertain results (*vide supra*) and further calculations were carried out to resolve the issue. Table 2 shows the results of these calculations. Starting with the minimized *cis*-conformation of the pyridinium compound, one of the 3-methylphenyl group was rotated and the energy calculated without minimization (Table 2, entries 1-12). In addition, the highest energy with dihedral angles at -180.0° and 0.0° were constrained while the rest of the structure was minimized (entries 13 and 14). This simple approach shows that the barrier to rotation is quite high as a result of the methyl groups on the carbon and nitrogen of the pyridinium ring. When the methyl on the phenyl is oriented towards the N-methyl of the pyridinium, the structure is more stable compared to when it is oriented towards the C-methyl group (entries 6 and 12). This is also true when the structure is minimized with the dihedral angles constrained (entries 13 and 14).

Table 2 summarizes the results of the calculations of the *cis*- and *trans*-isomers. The calculations show that *trans*-isomers are slightly lower in energy, however, when iodide is included in the calculations, the *cis*-isomer was lower in energy. This may be a result of the iodide and the methyl on the 2-position of the aromatic substrate being close together in the

trans- isomer. In the *cis*-isomer both substituents are further from the iodide. The results of these *Ab-initio* calculations gave us a prelude to the energies in the DNMR studies of the systems.

Table 2: Summary of the calculated energies (kJ/mol)

Compound/Substrate	<i>Cis</i>-isomer	<i>Trans</i>-isomer
2,6- di(4-methylphenyl)	2.12	0.00
2,6- di(3-methylphenyl)	1.13	0.00
2,6- di(2-methylphenyl)	2.76	0.00
2,6-di(2-isopropylphenyl)	4.57	0.00
2,6- di(4-methylnaphth-1-yl)	0.34	0.00
2,6- di(2-methylphenyl)pyridinium ion	0.59	0.00
2,6- di(2-methylphenyl)pyridinium iodide	0.00	56.1
2,6- di(4-methylnaphth-1-yl)pyridinium ion	0.59	0.00
2,6- di(4-methylnaphth-1-yl)pyridinium iodide	0.00	7.00

Single crystal X-ray structures

Some of the products were amenable to growing a single crystal and this allowed us to confirm the structure of the corresponding products. This gave us an opportunity to obtain the actual dihedral angles between the aryl substrates and the pyridine rings in a crystal lattice. The crystals were grown using the evaporation method, where the solvent was allowed to evaporate to dryness. This method provided sufficient crystals for X-ray analysis purposes; however, these crystals were not necessarily the crystals of the most stable isomer. In some cases, the crystal retrieved was formed from a mix of *cis*- and *trans*-isomers while in other cases only one isomer was present. One exception was the 1,3,5-trimethyl-2,6-di(2-methylphenyl)pyridinium iodide (**26**), which crystalized well. The solution was not allowed to completely evaporate, but when a small crystal appeared it was removed from the mother liquor to give the *trans*-isomer.

The crystal retrieved for the 3,5-dimethyl-2,6-di(3-methylphenyl)pyridine (**13**) gave the *cis-anti*-isomer with symmetrical dihedral angles of 138.21° between the pyridine system and the 3-methylphenylboronic acid substrate (Figure 21). The dihedral angles for this crystal were symmetrical between the two 3-methylphenylboronic acid groups, however, the other crystals show non-symmetrical dihedral angles (*vide-supra*).

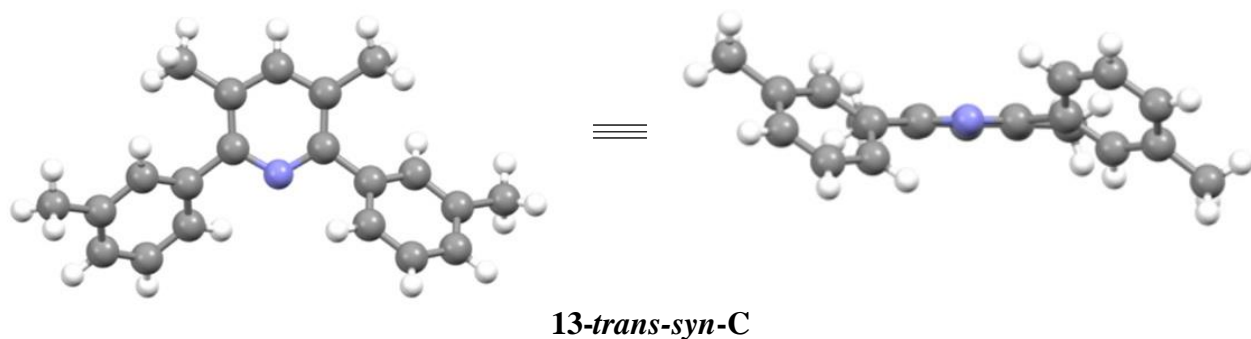


Figure 21: *Trans-syn*-crystal structure of 3,5-dimethyl-2,6-di(3-methylphenyl)pyridine (**13**) dihedral angle between 3-methylphenyl group from the substituted side and pyridine from the methyl substituted carbon -46.32° and -46.32° .

The crystal structure from the 3,5-dimethyl-2,6-di(2-methylphenyl)pyridine (**12**) contained both the *cis*- and *trans*- isomers in the unit cell (Figure 22). This crystal could only be refined to get two structures. The unrefined crystal structure of *trans-anti*-isomer gave dihedral angles of -117.37° (or 62.63°) and -96.64° (or 83.36°). The *cis-syn*-isomer gave dihedral angles of -92.34° and 97.81° . Improved crystals gave structure of only *trans-anti*-isomer (Figure 23). The dihedral angles were -104.18° and -72.88° .

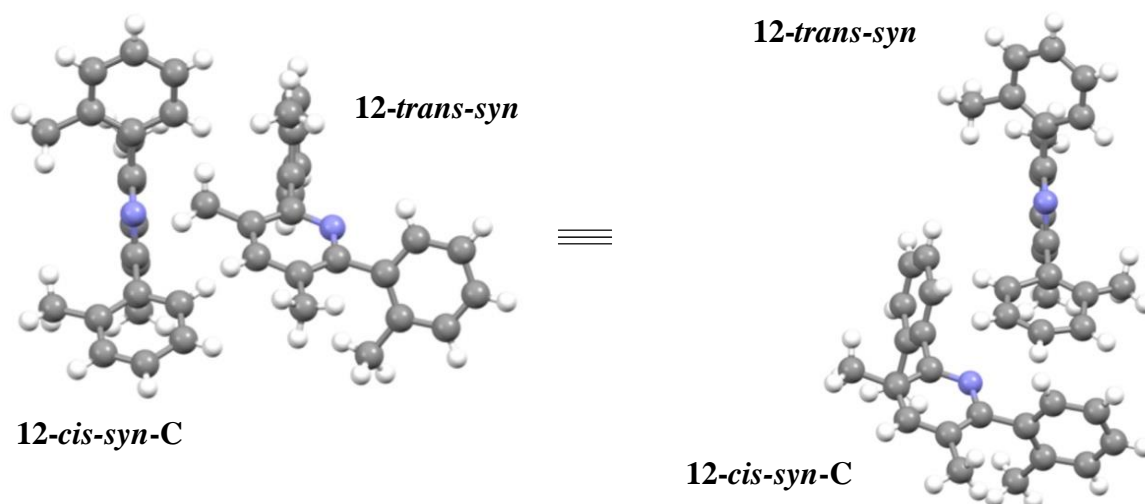


Figure 22: Crystal structure of *cis*- and *trans*-3,5-dimethyl-2,6-di(2-methylphenyl)pyridine (**12**) dihedral angle between 2-methylphenylboronic acid group and pyridine in *trans-syn*-isomer, 84.55°, -64.60°. For *cis-syn*-isomer 91.25°, -84.20°.

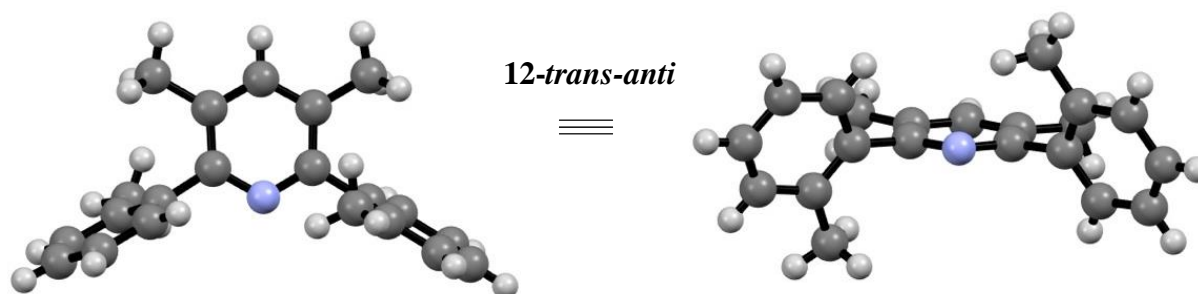


Figure 23: Crystal structure of 3,5-dimethyl-2,6-di(2-methylphenyl)pyridine show *trans-syn* isomer with dihedral angle 73.81°, 106.74°.

The crystal structure of 3,5-dimethyl-2,6-di(2-isopropylphenyl)pyridine (**15**) show *cis-syn*-isomer (Figure 24). The dihedral angles of the aryl group and pyridine were 108.82° and 98.87°. As the crystals were grown by the evaporation method, it is not clear whether the *cis-syn*-isomer is the more stable in the crystal structure or that by chance, the crystal chosen for analysis happens to be this isomer. Molecular modeling indicates the *trans*-isomer as the more stable isomer than the *cis*-isomer by 4.57 kJ/mole.

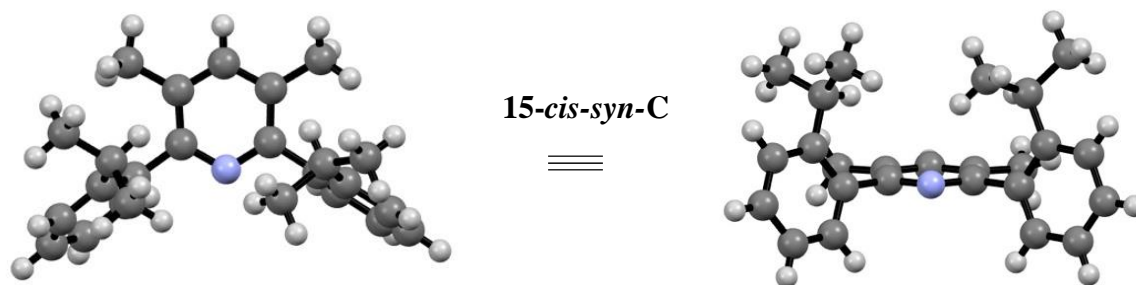


Figure 24: *Cis-syn-C* crystal structure of 3,5-dimethyl-2,6-di(2-isopropyl)pyridine (**15**), dihedral angles of -75.33° , -81.78° .

Crystal structure of 3,5-dimethyl-2,6-di(4-methylnaphthyl-1-yl)pyridine (**14**) show *trans-anti* conformation (Figure 25). The dihedral measurements gave 70.36° and 70.35° . In another sample, the crystal unit cell consisted of two *trans*-isomer structures, see Appendix B.

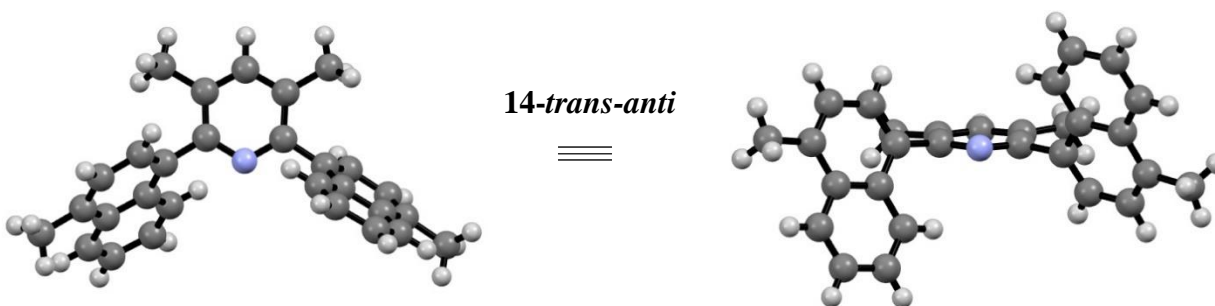


Figure 25: Crystal structure of 3,5-dimethyl-2,6-di(4-methylnaphthyl-1-yl)pyridine showing *trans-anti* conformation with dihedral angles of 111.35° and 111.35° (**14**).

2-Bromo-6-(4-methylnaphthyl-1-yl)pyridine (**18**) was obtained and a single crystal of X-ray quality was grown (Figure 26). The crystal structure dihedral angle measured at -109.08° .

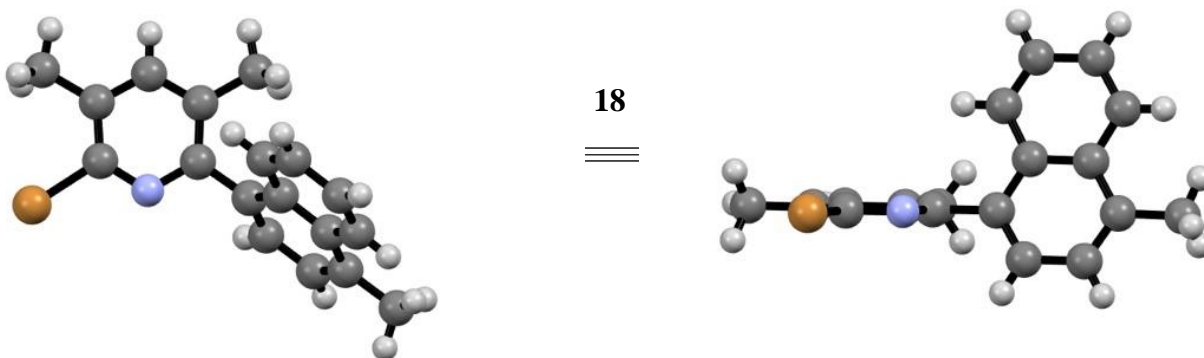


Figure 26: Crystal structure of 2-bromo-3,5-dimethyl-6-(4-methylnaphthyl-1-yl)pyridine with dihedral angle of 73.88° (**18**).

Crystal structure of *cis-syn*-isomer of N-methyl 3,5-dimethyl-2,6-di(2-methylphenyl)pyridinium iodide (**23**) was also obtained (Figure 27). The iodide anion closest to the nitrogen is located on the face of the pyridinium on the side of aryl groups distal to the 2-methyl group. The measurement of the dihedral angles gave 92.85° and -89.29° , very close to the orthogonal position between the aryl and the pyridyl groups.

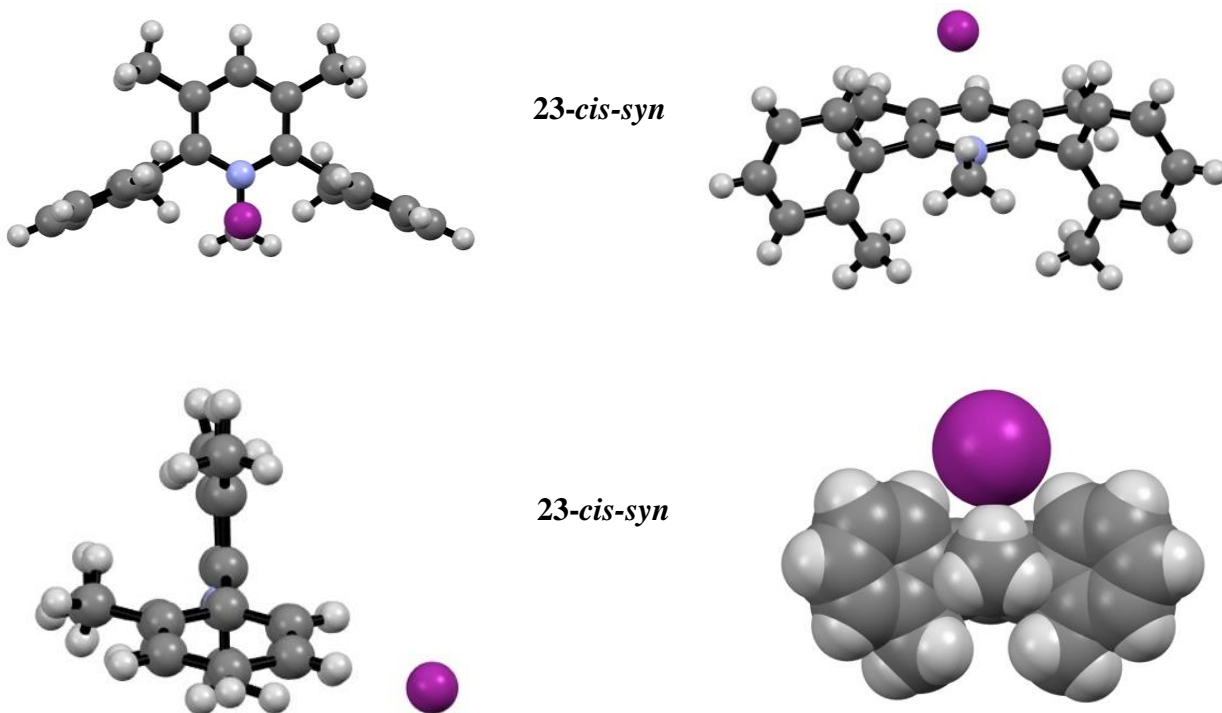
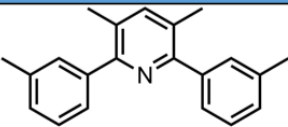
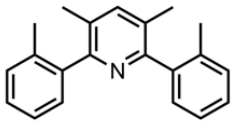
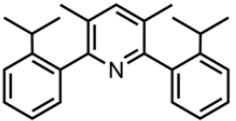
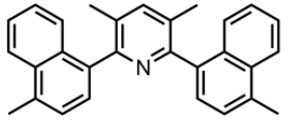
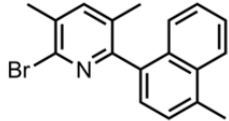
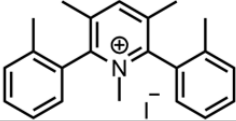


Figure 27: Four views of crystal structure of 1,3,5-trimethyl-cis-2,6-di(2-methylphenyl)pyridinium iodide showing *cis-syn*-isomer with dihedral angles of 83.85° and -82.16°.

Summary of the compounds and information obtained from the single crystal structures are presented in Table 3.

Table 3: Summary of the conformation and dihedral angles from the crystal structures

Compound	Calculated Dihedral Angles	Conformation found in X-Ray Crystal Structures	X-Ray Crystal Structure Dihedral Angles
	67.28°, 48.37°	<i>Trans</i> -	46.32°, -46.32°
	-89.54°, 66.48°	<i>Trans- and Cis</i> -	95.47°, -118.74° (<i>Trans</i>) 97.83, 90.15 (<i>cis</i>)
	-110.44°, 78.62°	<i>Cis</i> -	108.82°, 98.87°
	-78.42°, -73.55°	<i>Trans</i> -	70.36°, -70.35°
	73.91	-	73.88°
 *	-129.44, 125.46	<i>Cis</i> -	98.70°, 94.01°

* The computer modeling of this compound was initiated with the iodide in position as in the crystal structure but did not converge unless the iodide shifted quite a bit from the position located in the crystal structure (*vide infra*).

Variable Temperature ^1H NMRs

Variable temperatures were taken to elucidate the barriers to rotation using the dynamic NMR (DNMR) method.¹⁴ The 3,5-dimethyl-2,6-di(3-methylphenyl)pyridine (**13**) barrier of rotation was not obtained as it is a symmetrical compound and the cis-trans isomerization is meaningless. Also, a comparable analog was not used since the barrier to rotation of this compound would be very low and the limitations of the temperature capability of the available NMR spectrometer would not allow us to gather reasonable data. Prior to the discussion of the DNMR data, it should be noted that there is drift in the absorption with temperature in some peaks. Additionally, the analysis needs to take into account coincidental absorptions versus coalescence absorptions.

There are three major issues on the error of the DNMR line analysis. First, is the calibration of the temperature probe. Second, the multiple spectra taken at temperatures around the coalescence temperature to predict an accurate coalescence temperature. Third, when the spectra were obtained, it resulted in differences in the frequency of the absorbances of the two isomers. One of the approaches in the calculation uses an activation energy variable, which requires this information.

DNMR of 3,5-dimethyl-2,6-di(2-isopropylphenyl)pyridine

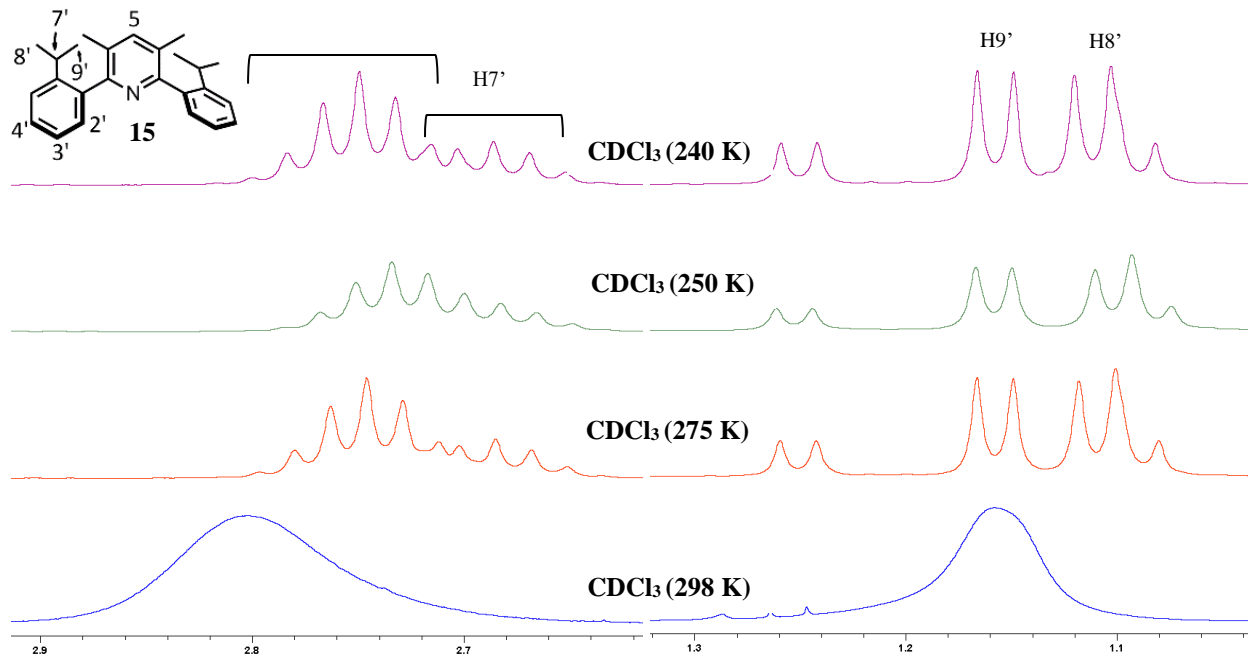


Figure 28: Low temperature variable temperature ^1H NMR of molecule **15** in CDCl_3 . Of the 1.1–1.2 and 2.6–2.9 ppm region.

Initial ^1H NMR indicates there are two sets of conformational isomerizations that are relatively slow by the NMR time scale (Figure 28). The *cis-trans* atropisomers and the rotations around the phenyl-isopropyl groups. This results in a broad absorbance for the protons of the isopropyl methyl groups, as can be seen by the broad peak in the 2.7 – 2.9 ppm range for the methine and 1.1–1.2 ppm for the methyl groups. As the temperature is lowered, the rotations decrease enough to allow for the NMR to distinguish the single peak to be 2 sets of septet, one from each atropisomer for the methine. The methyl peaks from the isopropyl group show doublet from the *cis-trans* isomers and so do the slowed rotations from isopropyl groups. The broad peak in the 1.1 to 1.3 ppm region separates into four sets of doublets.

The 7.45–7.55 ppm range of the NMR spectra, there are two observable singlets (Figure 29). These signals have been assigned as the hydrogen atom on C-5 of the pyridine moiety. The

integration of the corresponding singlets indicates a ratio of 2.5:1 for the more stable atropisomer. This is corroborated by the methyl peaks in 1.3-1.0 ppm range, since they also gave the same ratio. The methine peaks, distinguishable in the 2.85-2.60 ppm range confirms this ratio as well. Although the peaks are not completely separated, an approximate integration analysis reveals that the peak of the H7' proton from one atropisomer integrates 2.8x higher than the peak of the H7' proton from the other atropisomer.

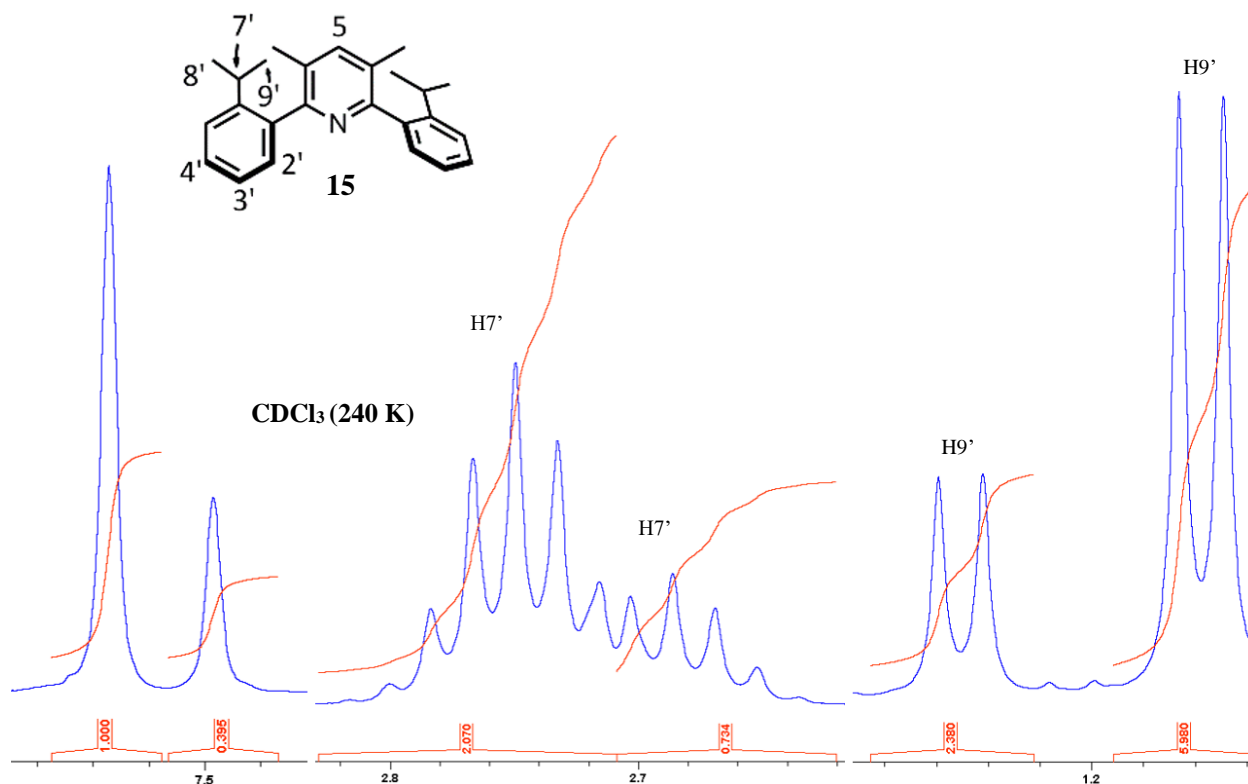


Figure 29: Low temperature spectra of the methyl and C-5 hydrogen atom region for **15**.

Molecular modeling indicates that the *trans*-isomer is stable by 4.57 kJ/mole at room temperature. For this reason, the *trans*-isomer has been assigned to be the more stable isomer. Hand held model indicates there is some steric interaction of the the two isopropyl groups in the *cis*-isomer. Using the integration, at 240 K, the enthalpy of *trans*-isomer is stable by 1.9 kJ/mole.

The di(2-isopropylphenyl) arylated pyridine **15** was also subjected to higher temperature D-NMR experiments in DMSO-d₆ (Figure 30). Above room temperature the cis-trans isomerization as well as the rotation of the isopropyl groups are at such a high rate that only a single sets appears.

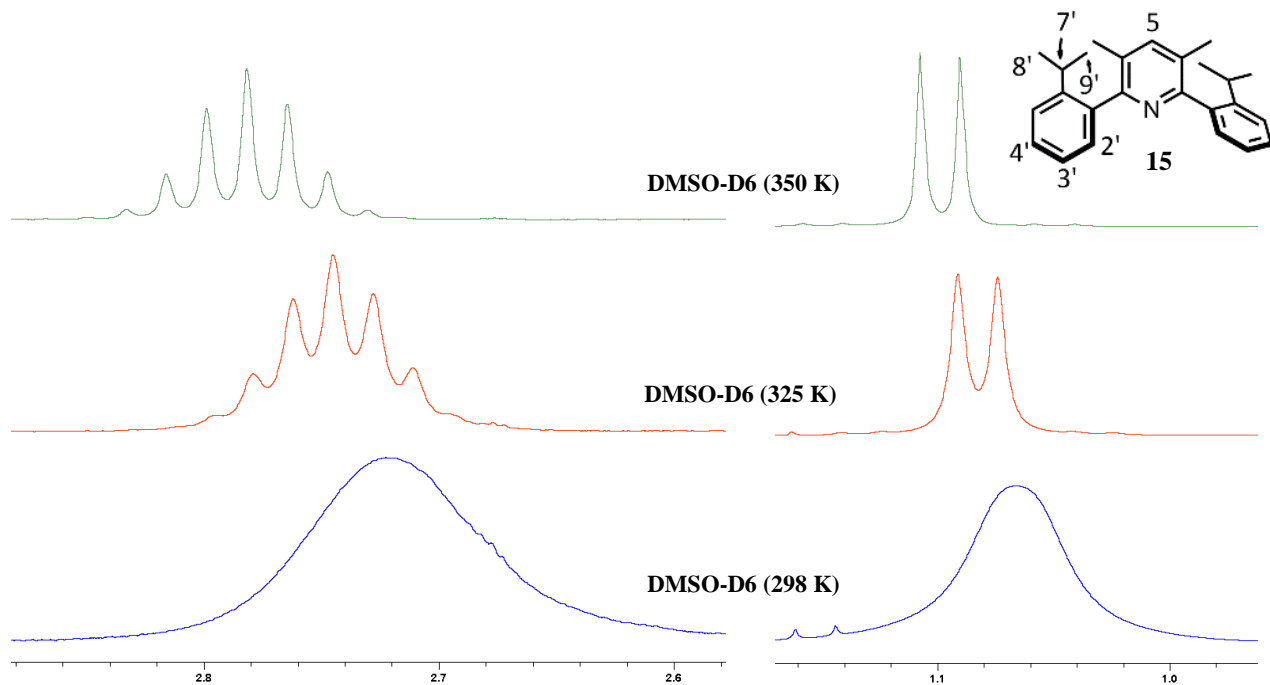


Figure 30: High temperature spectra of the isopropyl region in DMSO-d₆.

The relevant areas were simulated, Figures 30 and 31. The correlation between the experimental and simulated spectra fit well.

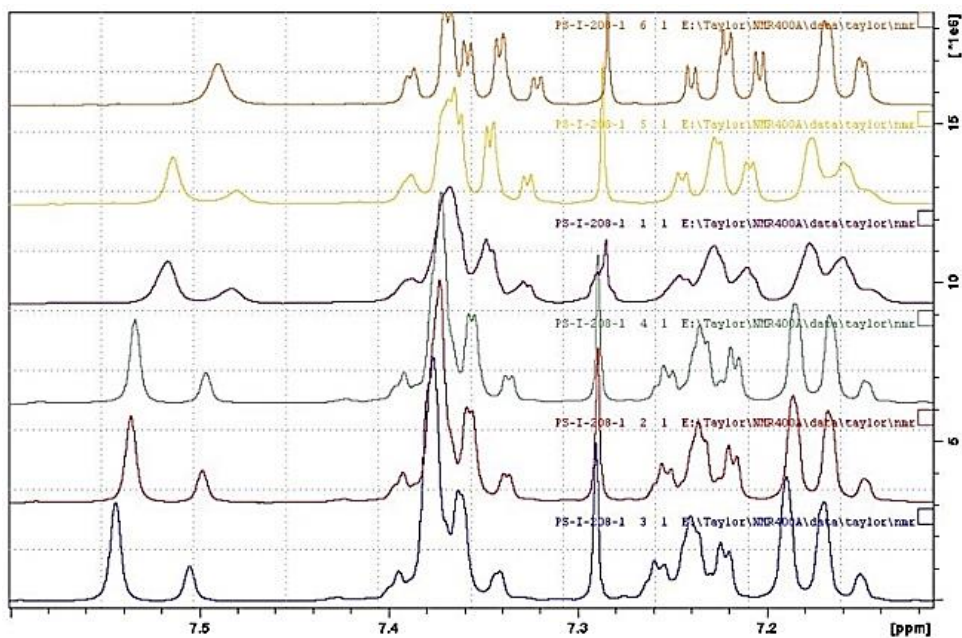


Figure 31: ^1H DNMR simulations of 3,5-dimethyl-2,6-di(2-isopropyl)pyridine (**15**), 7.1-7.6 ppm. The temperatures from top to bottom are 298K, 275K, 275K, 250K, 250K, 240K.

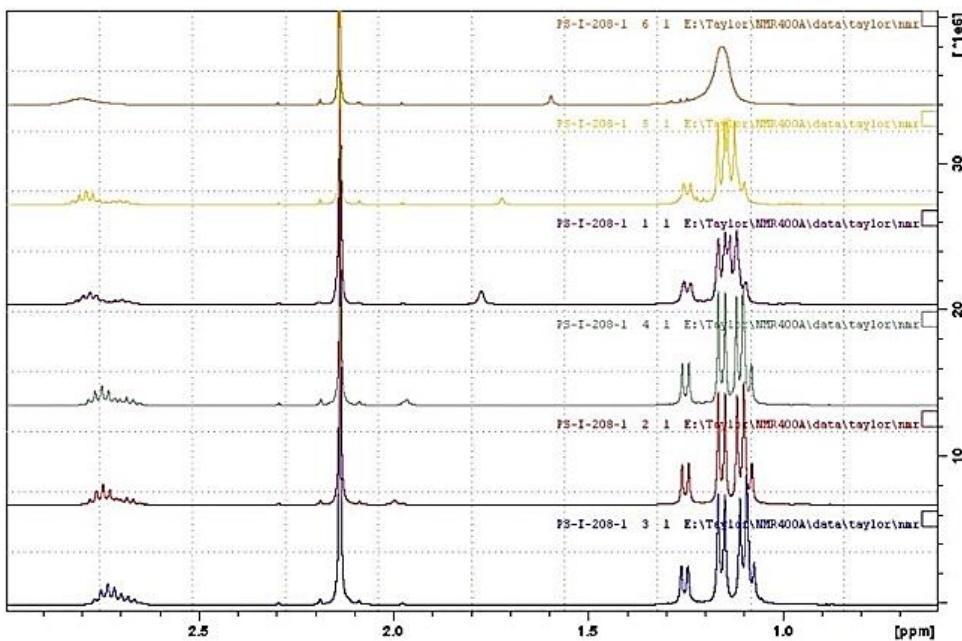


Figure 32: ^1H DNMR simulations of 3,5-dimethyl-2,6-di(2-isopropyl)pyridine (**15**), 0-3.0 ppm. The temperatures from top to bottom are 298K, 275K, 275K, 250K, 250K, 240K.

3,5-Dimethyl-2,6-di(2-methylphenyl)pyridine

As expected, the barrier to rotation for this molecule was low and the coalescence temperature was 275K. The rotational barrier is an estimate. Due to the instrument having a temperature limitation of 240K, it was not confirmed whether the separation of the absorption of the two atropisomers have reached their maximum point (Figure 33). Within these limits, the complete line analysis gave a barrier to rotation of 56.3 kJ/mol.

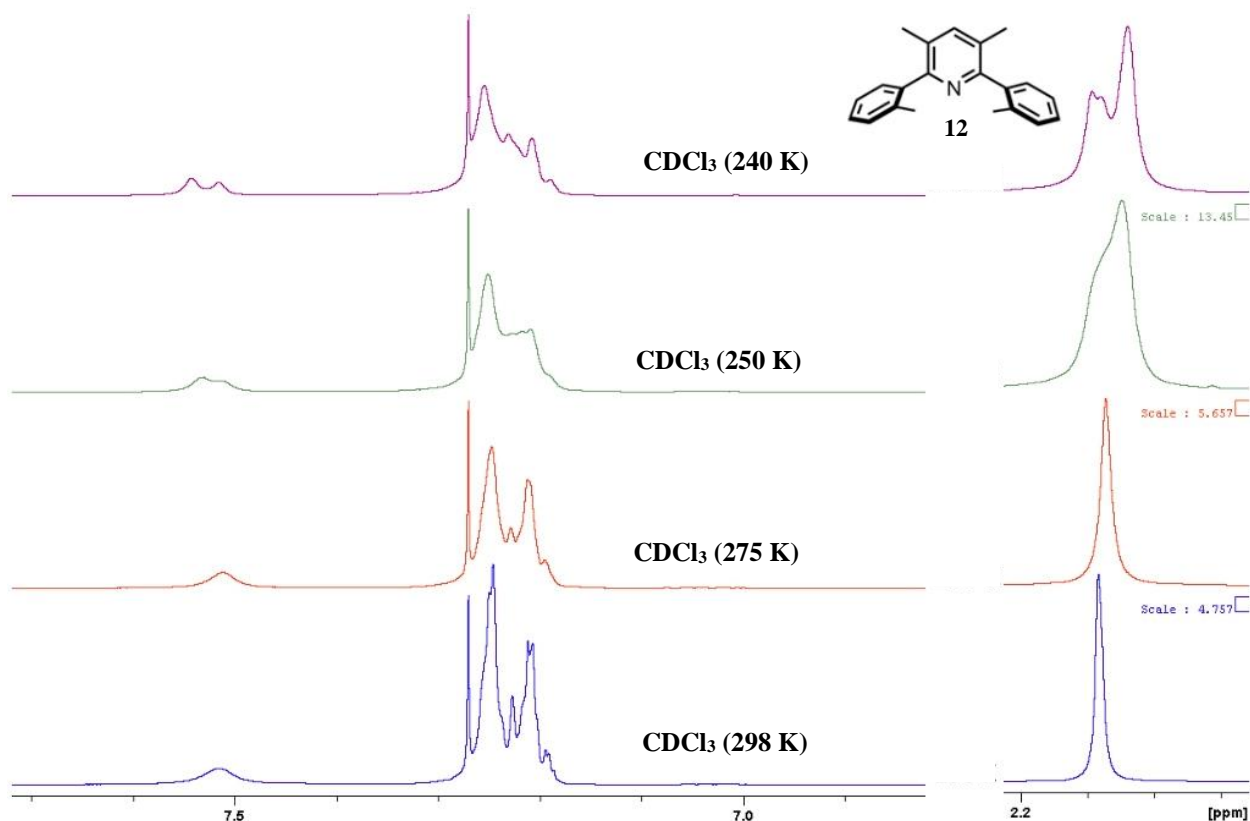


Figure 33: Variable temperature of **12** in CDCl₃.

3,5-Dimethyl-2,6-di(3-methylphenyl)pyridine

The 3-methylphenyl disubstituted compound did not have any separation of the *cis*- and *trans*-isomer even at low temperatures (See Appendix D).

3,5-Dimethyl-2,6-Di(4-methylnaphthyl-1-yl)pyridine

Figures 34 and 35 show the variable temperature of the relevant areas of the ^1H NMR. The peaks at 8.04 and 7.63 ppm show that the coalescence temperature is 2°C as indicated by the slight shouldering of the peaks. At lower temperatures there are distinct doublet of doublets present from each isomer. This is confirmed by the naphthylmethyl resonances between 2.15 and 2.20 ppm (Figure 35).

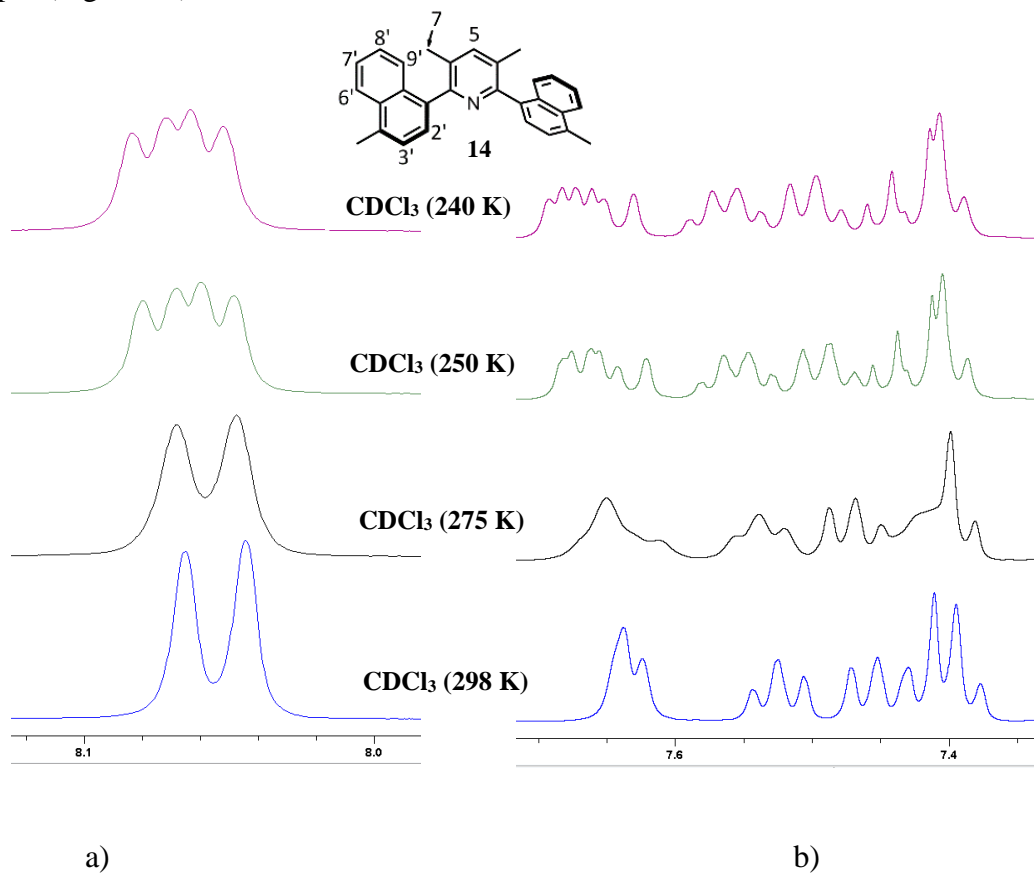


Figure 34. Variable temperature ^1H NMR spectra of the aromatic region of **14**.

The NMR indicates that the ratios of the cis- to trans-atropisomers was close to 1:1. The methyl peak region gave the cleanest separation. As a result, it was used to calculate the barrier to rotation. This allows the use of the coalescence temperature rate constant, given by equations 2 and 3 (Appendix C), which lead to a calculated rotational barrier energy of 60.9 kJ/mol (see

Appendix C). Complete line analysis gave barrier to rotation of 60.5 kJ/mol. This is a lower limit of the estimate. Due to the constraints of the NMR, the instrument could not go lower in temperature to confirm that the methyl peaks on pyridine, used for the calculations, had reached the maximum separation. Complete line analysis approach gave 60.5 kJ/mole and the two approaches are consistent.

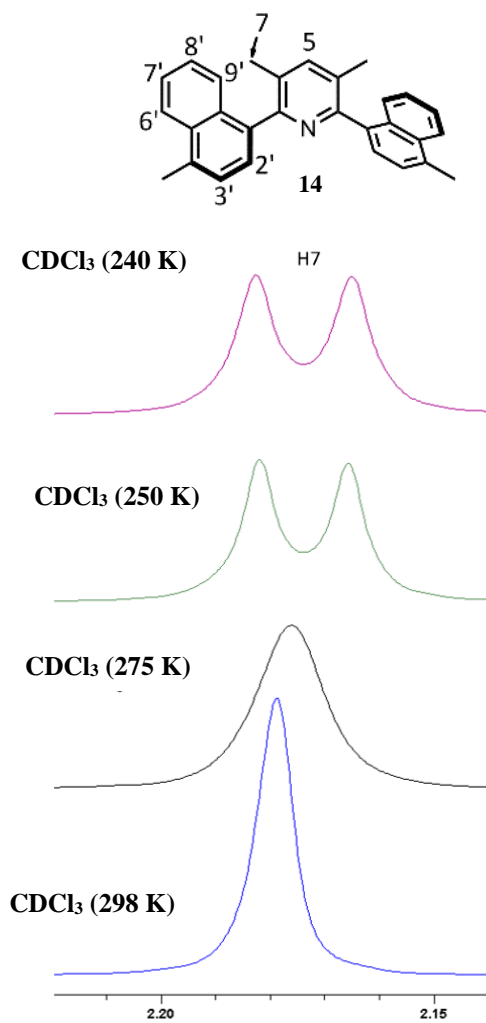


Figure 35. Variable temperature ¹H NMR simulation of the naphthylmethyl region for **14**. The spectra indicate a coalescence temperature of 275K.



Figure 36: ^1H NMR simulation of the aromatic region for **14**. The temperatures from top to bottom are 298K, 275K, 250K, 240K.

The relevant areas were simulated, Figure 36 and 37. The correlation between the experimental and simulated spectra fit well.

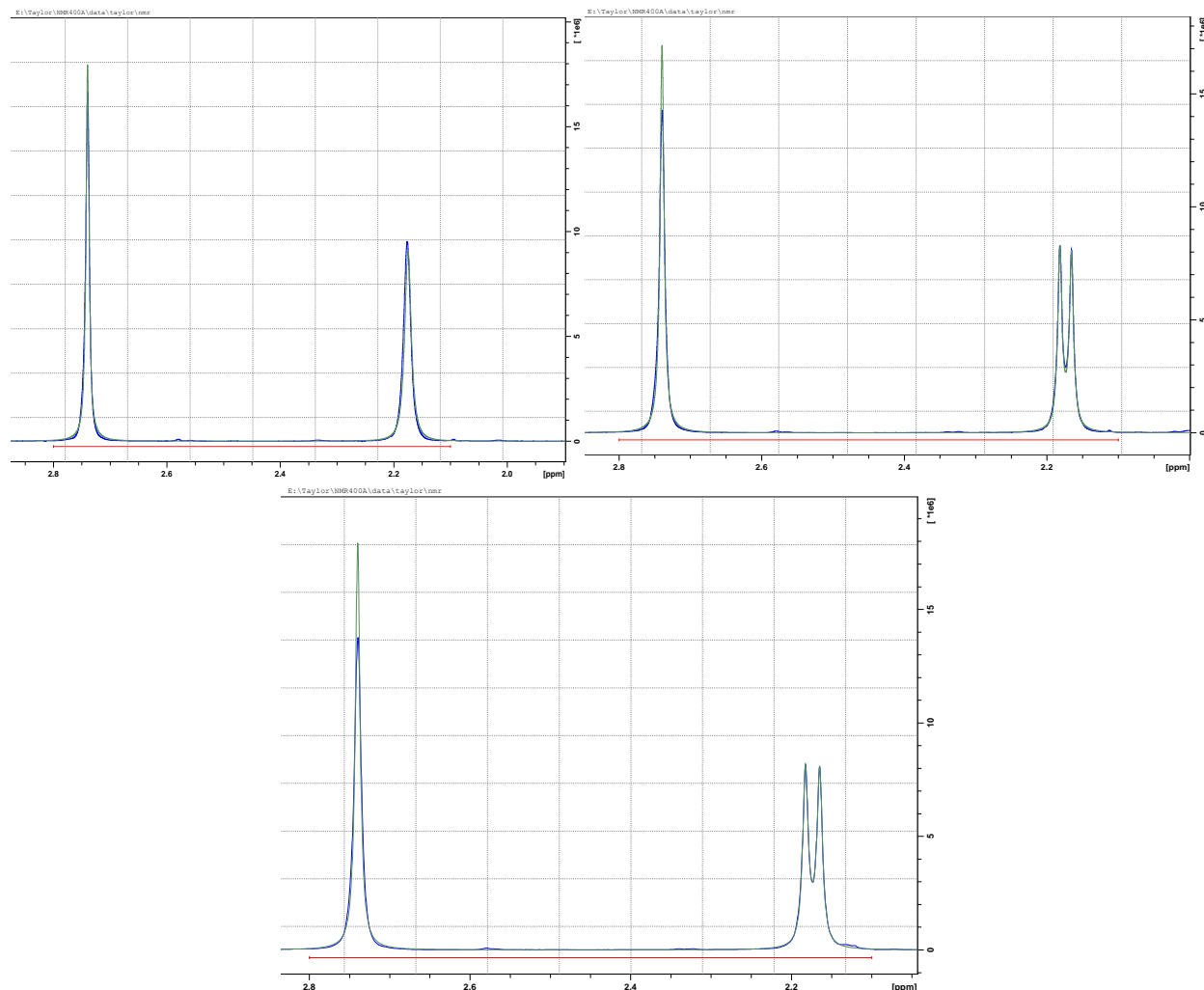


Figure 37: ^1H NMR simulation of the methyl region for **14**. The temperatures are 275K and 250K respectively (Top), and 240K (Bottom).

1,3,5-trimethyl-2,6-di-(2-methylphenyl)pyridinium Iodide

For this molecule, low temperature as well as higher temperature ^1H NMR (up to 350 K) show only one of the atropisomers. ^1H NMR was retaken as the sample temperature was dropped from 350 K down to 298 K and there was no indication of absorbance from the other atropisomer, which indicates that there is no isomerization even at 350 K (Figure 38). The most distinct areas for this analysis are the phenyl-methyl and pyridine-methyl absorption area of the variable temperature ^1H NMR in DMSO-d_6 . There are three distinct peaks in each area. By integration analysis, either the pyridine-methyl absorptions or phenyl-methyl absorptions from

the two isomers make up six protons and the third peak make up for the other six protons. As the temperature is increased, there is drift, but the two peaks do not coalesce. Within the limits of the NMR spectrometer, it is estimated that the barrier to rotation is >92 kJ/mole. This is in line with published work on related compound **31** (Figure 39).¹⁵ The authors were able to separate and detect the *cis*- and *trans*-isomers of compound **31** by GCMS with elution time and temperature of ~25 minutes and at 280-290°C. The authors were also able to separate the *cis-trans*-isomers by column chromatography. However, they do not provide the barrier to rotation information.

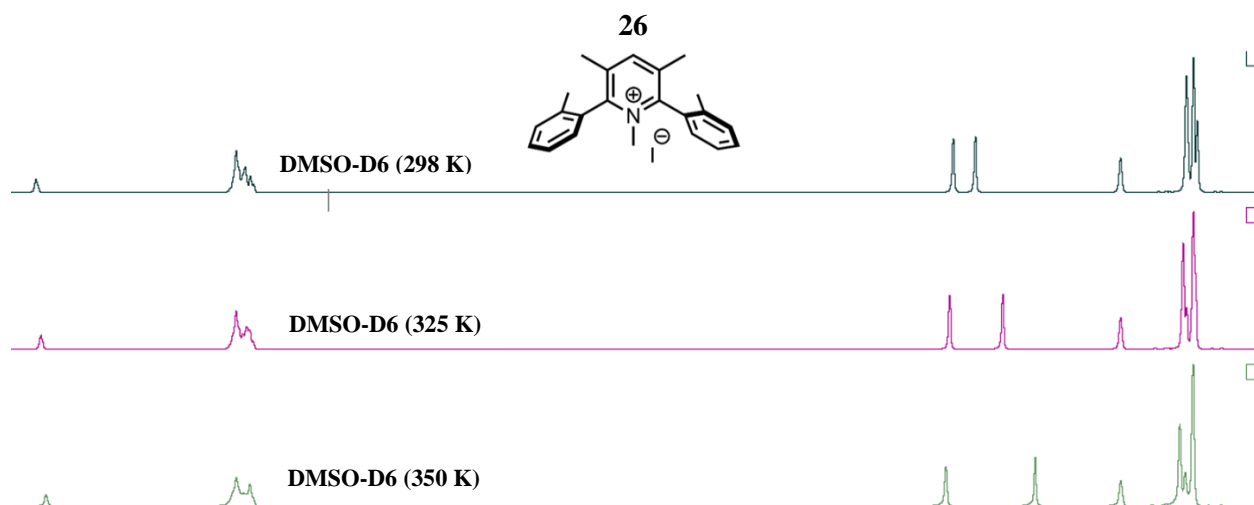


Figure 38: Variable temperature NMR in DMSO- d_6 of 1,3,5-trimethyl-2,6-di-(2-methylphenyl)pyridinium iodide, **26**.

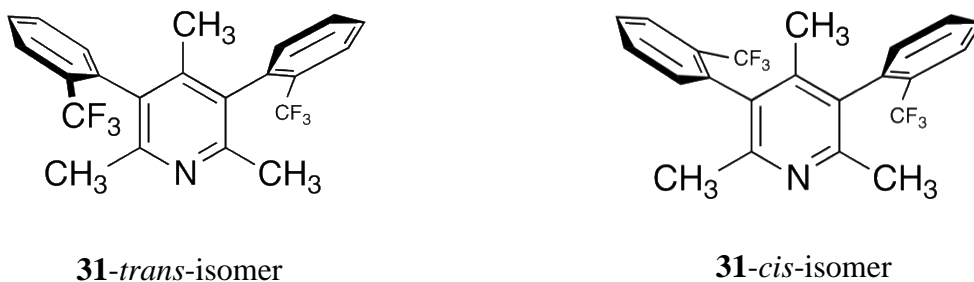


Figure 39: Cis- and trans-isomer of **31**.

1,3,5-Dimethyl-2,6-Di(4-methylnaphthyl-1-yl)pyridinium Iodide

The N-methylated 4-methylnaphthyl (**28**) disubstituted compound show the same properties. The N-methyl group and the methyl groups on the naphthyl moiety do not coalesce at the 350 K mark indicating that the barrier to rotation is >92 kJ/mole Figure 40.

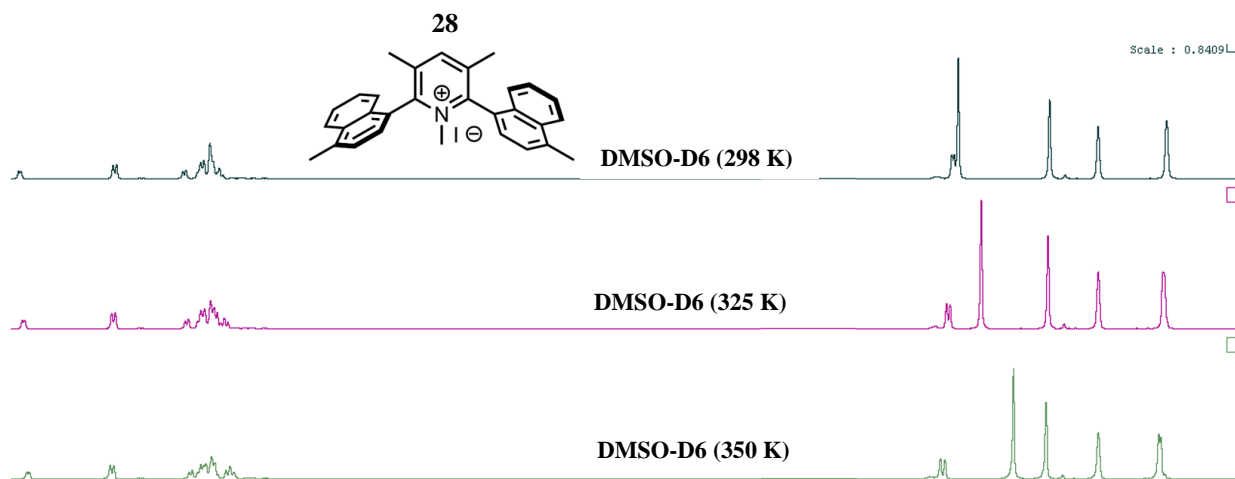


Figure 40: Variable temperature of **28** in DMSO-d₆

1,3,5-trimethyl-2,6-di-(3-methylphenyl)pyridinium Iodide

The variable temperature of this compound did not provide an obvious conclusion for the DNMR analysis. The compound may be undergoing rotation even at 240K. On the other hand, it is also possible that the absorptions of the two isomers are coincidental. Molecular modeling suggests that the barrier to rotation is high and previous work with compound **27** analog shows experimentally that the barrier to rotation is >50 kJ/mol.¹⁰

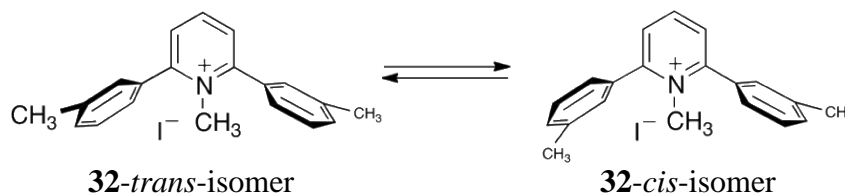


Figure 41: Cis-trans isomerization of **27** analog, **32**.

DISCUSSION

The barrier to rotation for the substrates is summarized in Table 4. The rotation of the 2,6-diaryl compounds are unique. Due to the symmetry, there are two potential routes for the

Table 4. Summary of the barrier to rotation.

Aryl group	Barrier to rotation	
	Experimental	Calculated
3-methylphenylboronic acid (23)	not determined	not determined
2-methylphenylboronic acid (22)	56.3 kJ/mol	not determined
2-isopropylphenylboronic acid (24)	4.57 kJ/mol	1.9 kJ/mol
(4-methylnaphthalen-1-yl) boronic acid (25)	60.5 kJ/mol	60.9 kJ/mol
3-methylphenylboronic acid (23) N-methylated	not determined	not determined
2-methylphenylboronic acid (22) N-methylated	>92 kJ/mol	not determined
(4-methylnaphthalen-1-yl) boronic acid (25) N-methylated	>92 kJ/mol	not determined

cis-trans isomerization. First, rotation of the 2-aryl or the 5-aryl groups lead to the same isomers. Second, the neutral nitrogen with nonbonding lone pairs in the plane of the ring does not provide steric hinderance and provides a path for the ease of rotation. Therefore, the sterically hindered side (R^L) will rotate through the nitrogen side of pyridine. What prevents the rotation is the less hindered side (R^S), which will rotate past the pyridine-methyl groups (Figure 42). For the 2,6-diisopropylphenyl group, there is some interaction between the two isopropyl groups in the cis-position, which affects the cis-trans isomer ratios as well as the barrier to rotation (*vide infra*). Methyl pyridinium compounds (**12-15** and **26-28**), on the other hand, do provide hinderance via the methyl groups.

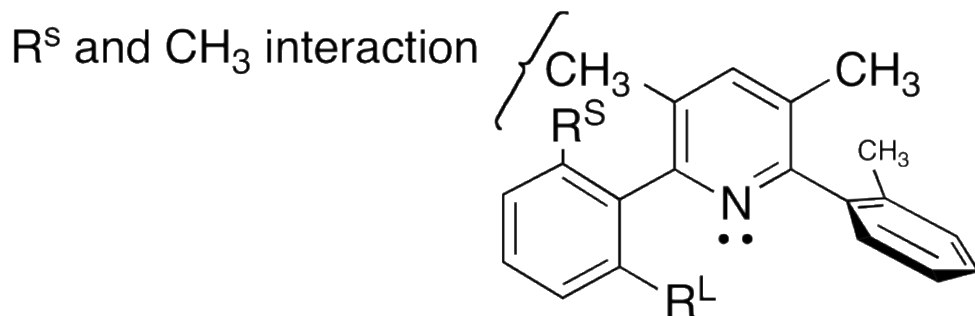


Figure 42: The more sterically hindered group rotates toward the pyridine nitrogen side.

In applying the Eyring equation, the transmission coefficient is usually taken as one, as shown in Pathway I (Figure 43). In some cases, when there is more than one path, Pathway II can partially be used. In the cases of this thesis, there are not two pathways, but instead two sites that lead to the same result (Pathway III). The rotation of each site behaves essentially independently, which causes the equilibrium rate to be doubled. Therefore, to get the barrier to rotation of each site, the rate must be halved.

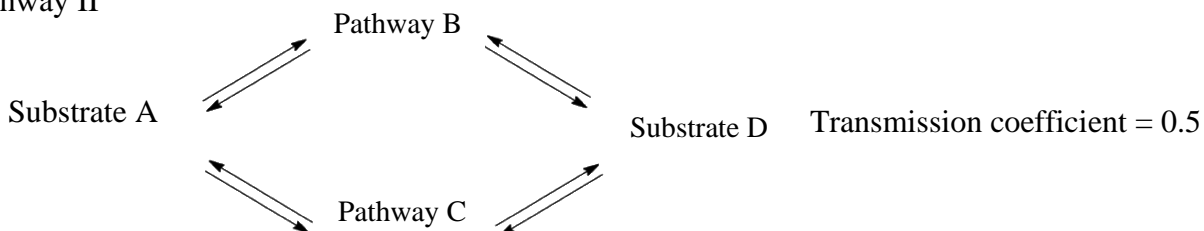
Eyring Equation

$$k_c = \kappa \frac{k_B T_c}{h} e^{-\Delta G^\ddagger / RT_c} \quad \kappa = \text{transmission coefficient}$$

Pathway I



Pathway II



Pathway III

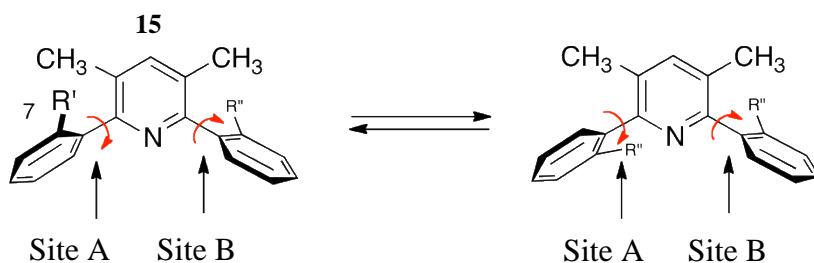


Figure 43: Eyring equation and three pathways.

3,5-Dimethyl-2,6-di(2-isopropyl)pyridine (15) has two potential type of rotational barriers. One is the rotations leading to the *cis-trans* isomer of the phenyl group and the pyridine. The second is the rotations of the isopropyl and the phenyl moiety (Figure 44). ^1H NMR at 240 K show *cis-trans* ratio of 1:2.76 or $\Delta G_0 = 2.03$ kJ/mole using the absorbance for *cis*- and *trans*-isomer for protons on C-4, C-7 and C-9 (Figure 28). Computations show that the *trans*-isomer is 4.57 kJ/mol more stable than the *cis*-isomer. In the *cis*-conformation, the two isopropyl group seem to have interaction to a small extent and is probably the cause of the lower stability. There are two sets of isopropyl methyl absorbances. One set shows the *cis-trans*-isomer ratios, while the other set shows the isopropyl methyl peaks with a 1:1 ratio. This indicates that there are the two methyl groups causing the low rotation rate of the isopropyl-phenyl bond. The two have similar coalescence temperatures at 298K. The dihedral angles between the two phenyl and pyridyl groups from the crystal structures were 108.82° and 98.87° . This is relatively close to 90° .

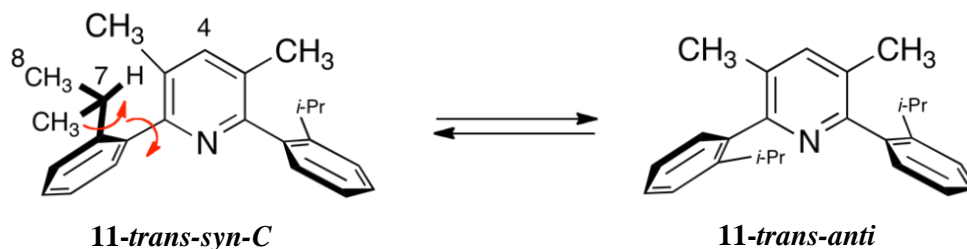


Figure 44: Two locations where atropisomerism occurs.

The barrier to rotation of the two rotations can be found by the DNMR results. The calculations from the DNMR gives the barrier to rotation of the *cis-trans* isomerization to be at least 64.2 kJ/mole. The rotations of the isopropyl group for the *trans*-isomer came out to be 93.0 kJ/mole whereas the *cis*-isomer came out to be 60.5 kJ/mole. These are considered to be minimum due to the limitation of the NMR instrument in that the lower temperature could not be reached and access to the instrument was highly limited.

For the 3,5-dimethyl-2,6-di(4-methylnaphthyl-1-yl)pyridine (**28**) two approaches were used. Since the methyl groups on the naphthyl groups were singlets, equations 2 and 3 (Appendix C) can be used and the values were confirmed by complete line analysis.

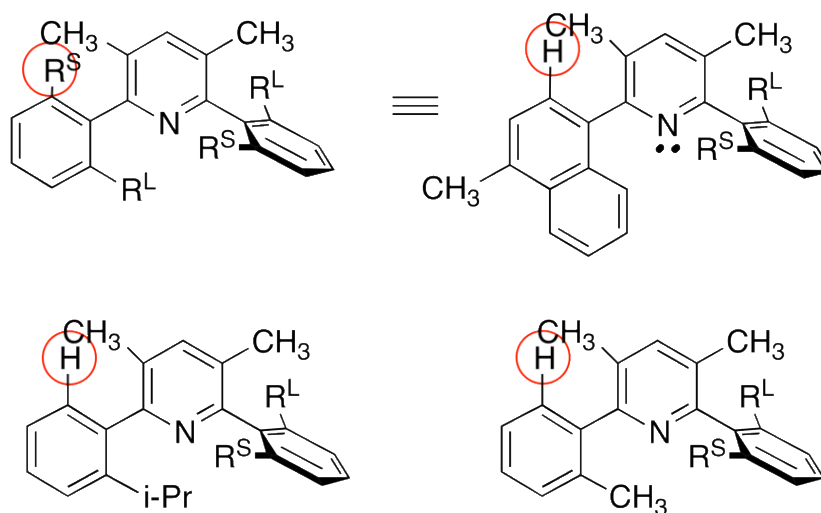
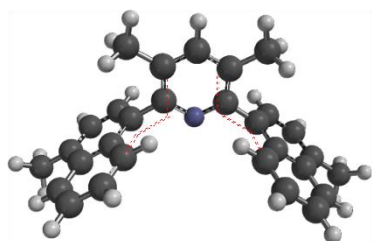


Figure 45: R^S - causing the hinderance to rotation

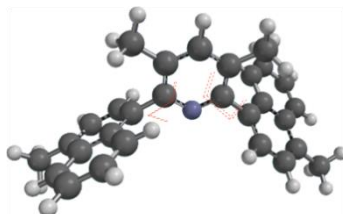
The 2-methylphenyl (**12**), 2-isopropylphenyl (**15**), and the 4-methylnaphthyl (**14**) substituted substrates all gave similar barrier to rotation. This is a result of the *R*s- substituents all being similar, resulting in similar barriers to rotations (Figure 45).

The NMR of 1,3,5-Dimethyl-2,6-di(3-methylphenyl)pyridinium (**27**) iodide show either only one isomer or both *cis*- and *trans*-isomer. The ¹HNMR were too similar to distinguish between them. The 3-methyl position is further from the axes of rotation of our interest. ¹HNMR spectra in DMSO-d₆ and chloroform-d at room temperature gave somewhat different absorptions. In going up or down in temperature, there was a drift in alkyl and aromatic regions, but nothing worthy of note. As indicated in the modeling of this compound, the barrier to rotation was significant. The proximity of the N-methyl adds significant steric hinderance.

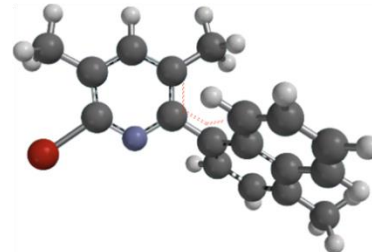
Comparing the energies and bond angles of the *cis*-, *trans*-3,5-dimethyl-2,6-di(4-methylnaphthyl-1-yl)pyridine (**14**) and the 2-bromo-3,5-dimethyl-6-(4-methylnaphthyl-1-yl)pyridine (**18**) compounds, it is possible to see the level of interaction between the two aryl groups. Modeling show that energies between the *cis*- and *trans*-isomers are very close, 0.34 kJ/mol (Figure 46). However, the dihedral angles do differ by 13.28° and 15.45°. The dihedral angels of the *trans*-isomer from



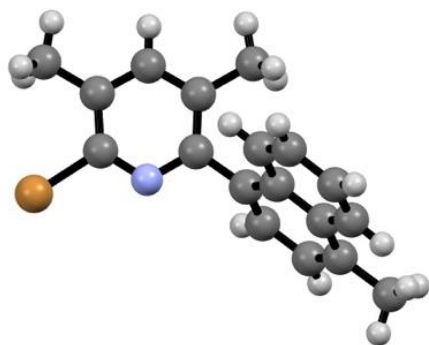
14-cis-, -91.7°, 91.00°
calculated



14-trans-, -78.42°, -73.55°
calculated

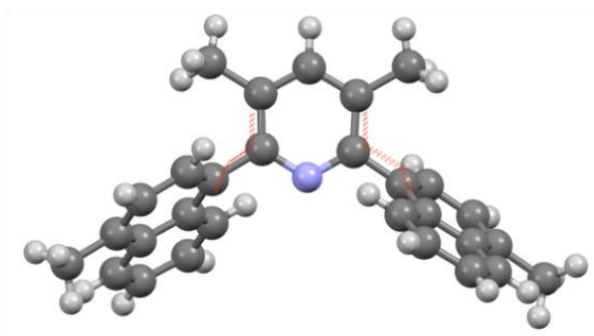


18, 73.9°
calculated



18, 70.2°

crystal structures



14-trans-, -68.55°, -68.55°

crystal structures

Figure 46: Modeled / Experimental Dihedral angle comparisons between molecules **14** and **18**.

modeling and crystal structures are within 10° and 5°. These dihedral angles are within 8° and 2° from the mononaphthylated pyridine (**18**). Comparing the *cis*- and *trans*-3,5-dimethyl-2,6-di(2-isopropyl)pyridine (**15**), the calculated energy differences were only 4.57 kJ/mol in favor of the *trans*-isomer. The *cis*-isomer dihedral angles from modeling are -110.44°, 78.62° and for the *trans*-isomer, the dihedral angles are -113.55°, 70.75°. The *cis*-crystal structure gives dihedral angles -104.67° and 81.78°. The dihedral angles determined using calculations and crystal structures are compared with the understanding that the calculations were carried out in vacuum. Additionally, it is important to take into account that the X-ray structures are of crystals where the packing pattern can have an effect on the conformation as well.

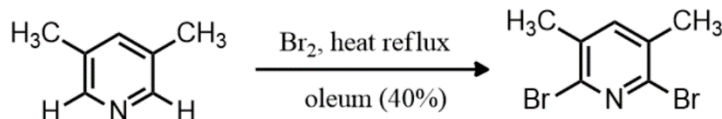
In conclusion, the 2,6-diaryllutidine was successfully synthesized by the palladium catalyzed cross coupling reaction. The computational investigations correlated well with the crystal structures with the exception of the 2,6-di(2-methylphenyl)pyridinium iodide. In this case, the computation only converged when the iodide made a significant shift in the position of the iodide relative to the compound. When the iodide could not move due to being in an energy well, the computation could not converge and it produced an error. Compounds with a

substitution in the 2-position of the aromatic group gave dihedral angles closer to 90° as indicated by the computation and the X-ray structures. As expected, the barrier to rotations for the 2-substituted phenyl were similar and this is due to the fact the bulky substituent in the 2-position can rotate to the less hindered side of the nitrogen position in the lutidine system. The rotational barrier is between the methyl of the lutidine and the hydrogen in the 2-position of the phenyl and the naphthyl group.

EXPERIMENTAL

All reactions were performed in either flame-dried or oven-dried apparatus, under an inert atmosphere of N₂ through the use of a dual vacuum/nitrogen manifold. All reagents were used as obtained from Aldrich Chemical Co., unless noted otherwise. Flash column chromatography was performed using SiO₂ (32-63 μm) and solvent mixtures as specified in the text. ¹H and ¹³C NMR spectra were recorded on Bruker Advance III 400 spectrometer using CDCl₃ (δ_{ref} = 7.27), DMSO-*d*₆ (δ_{ref} = 2.50), or as noted in the text. The ¹H and ¹³C assignments were based on samples taken at room temperature. Coupling constants (*J*) are reported in Hertz. FT-IR spectra were recorded on a Perkin Elmer Spectrum 100 FT-IR spectrometer equipped with an ATR unit. Melting points were taken on a Mel-Temp apparatus.

2,6-Dibromo-3,5-dimethylpyridine



To a stirred oleum solution (300 mL) of 3,5-dimethylpyridine (30.36 g, 283 mmol) at 277 K was added Br₂ (15.9 mL, 308 mmol) dropwise. The solution was stirred for 30 min at this temperature. It was warmed to 442 K and refluxed for 48 h. The solution was cooled to room temperature, poured into water slowly, neutralized by aqueous NaOH. The crude product was isolated by recrystallization using hot EtOH (26.68 g, 36%) as a white solid,

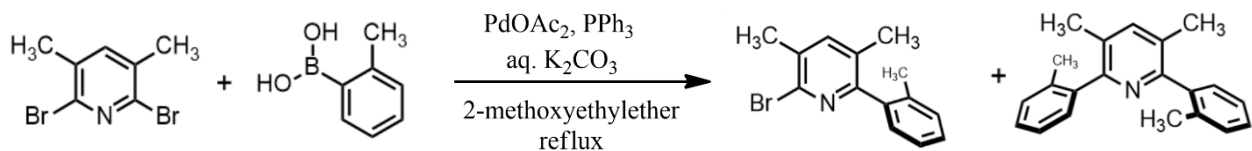
2,6-Dibromo-3,5-dimethylpyridine

TLC: R_f = 0.30 (SiO₂; DCM)

MP: 102-103 °C

¹H NMR (400 MHz, CDCl₃): δ 7.35 (s, 1H), 2.30 (s, 6H)

2-Bromo-3,5-dimethyl-6-(2-methylphenyl)pyridine 3,5-Dimethyl-2,6-di(2-methylphenyl)pyridine



To a 10 mL round bottom flask, 2,6-dibromo-3,5-lutidine (106 mg, 0.400 mmol), 2-methylphenylboronic acid (88.7 mg, 0.652 mmol), and triphenylphosphine (11.6, 0.044) were added in addition to a stir bar. To this, 2-methoxy-ethyl ether (2 mL) and 2M aqueous potassium carbonate (0.7 mL) solution were added using a syringe. The reaction was stirred until all solids appeared to have dissolved and the solution was then purged using nitrogen. This was followed by palladium acetate (8.5 mg, 0.038 mmol) was added and upon further stirring, the reaction solution turned into an orange color and then a dark green color. The solution was then refluxed at 174 °C for 45 minutes. The solution was then allowed to cool to room temperature and then extracted twice using ethyl acetate. The extracted organic layers were combined, washed with brine, dried over magnesium sulfate, filtered, and concentrated to yield a yellow crude oil. This crude was dissolved in CH₂Cl₂ and adsorbed onto silica gel and subject to flash column chromatography (SiO₂, hexanes:ethyl acetate 64:1 to 32:1 to 16:1 to 1:1 to ethyl acetate gradient). The collected fractions yielded the two products, mono-arylated compound as an oil (19.7 mg, 17.9%) and diarylated compound as a white solid (59.7 mg, 52.1%) assumed to be mixtures of cis- trans-isomers.

2-bromo-3,5-dimethyl-6-(2-methylphenyl)pyridine

TLC: R_f = 0.37 (SiO₂; hexanes:ethyl acetate 16:1)

MP: oil

IR (cm⁻¹): 3058, 3022, 2953.5, 2921.7, 2854.7

¹HNMR (400 MHz, CDCl₃): δ 7.42 (s, 1H), 7.31-7.21 (m, 3H), 7.15 (d, J= 7.42 Hz, 1H), 2.416 (s, 3H), 2.11 (s, 3H), 2.05 (s, 3H)

¹³CNMR (100 MHz, CDCl₃): δ 157.6, 140.7, 140.6, 138.7, 135.7, 133.2, 130.9, 130.2, 128.7, 128.2, 125.7, 21.5, 19.4, 18.1

MS (EI 70eV): calculated for C₁₄H₁₄BrN, 275.0, 277.0; found 274.5, 276.6

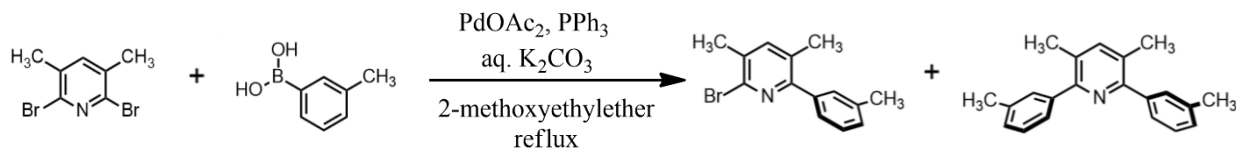
3,5-Dimethyl-2,6-di(2-methylphenyl)pyridine
TLC: R_f = 0.262 (SiO₂; hexanes:ethyl acetate 16:1)
MP: 67-75 °C
IR (cm⁻¹): 3066, 3021.0, 2968.6, 2960.9, 2925.5, 2866.2

¹HNMR (400 MHz, CDCl₃): δ 7.49 (s, 1H), 7.26-7.19 (m, 8H), 2.14 (s, 6H), 2.13 (s, 6H)

¹³CNMR (100 MHz, CDCl₃): δ 156.5, 140.3, 139.5, 135.7, 130.0, 129.7, 128.8, 127.6, 125.5, 19.5, 18.6

MS (EI 70eV): calculated for C₂₁H₂₁N, 287.2; found 286.6

2-Bromo-3,5-dimethyl-6-(3-methylphenyl)pyridine 3,5-Dimethyl-2,6-di(3-methylphenyl)pyridine



To a 10 mL round bottom flask, 2,6-dibromo-3,5-lutidine (107.7 mg, 0.406 mmol), 3-methylphenylboronic acid (90.4 mg, 0.665 mmol), and triphenylphosphine (9.8 mg, 0.037) were added in addition to a stir bar. To this, 2-methoxy-ethyl ether (2 mL) and 2M aqueous potassium carbonate (0.7 mL) solution were added using a syringe. The reaction was stirred until all solids appeared to have dissolved and the solution was then purged using nitrogen. This was followed by palladium acetate (8.0 mg, 0.036 mmol) and upon further stirring, the reaction solution turned into an orange color, followed by a dark green color. The solution was then refluxed with 174 °C oil bath for 45 minutes. The solution was then allowed to cool to room temperature and then extracted twice using ethyl acetate. The organic layers were then combined and washed with brine, dried over magnesium sulfate, filtered, and concentrated to yield a dark orange crude oil. This crude was then dissolved in CH₂Cl₂ and adsorbed onto silica gel and subject to flash column chromatography (SiO₂, hexanes:ethyl acetate 64:1 to 32:1 to 16:1 to 1:1 to EtOAc gradient). The collected fractions yielded the two products, mono-arylated compound as an oil (7.1 mg, 6.3%) and di-arylated compound as a white solid (98.4 mg, 84.3%) assumed to be mixtures of cis-trans-isomers.

2-bromo-3,5-dimethyl-6-(3-methylphenyl)pyridine
TLC: R_f = 0.44 (SiO₂; hexanes:ethyl acetate 16:1)

IR (cm⁻¹): 3039.4, 3022.3, 2954.7, 2921.8, 2854.2

¹HNMR (400 MHz, CDCl₃): δ 7.42 (s, 1H), 7.34 (s, 1H), 7.32 (d, 1H), 7.30 (s, 1H), 7.212 (dm, J = 6.4 Hz, 1H), 2.42, (s, 3H), 2.41 (s, 3H), 2.30 (s, 3H)

¹³CNMR (100 MHz, CDCl₃): δ 141.35, 130.08, 129.76, 128.91, 127.94, 126.04, 21.47, 21.41, 19.18

MS (EI 70eV): calculated C₁₄H₁₄BrN, 275.0, 277.0; found 274.5, 276.5

3,5-Dimethyl-2,6-di(3-methylphenyl)pyridine

TLC: R_f = 0.64 (SiO₂; hexanes:ethyl acetate 16:1)

MP: 52-62°C

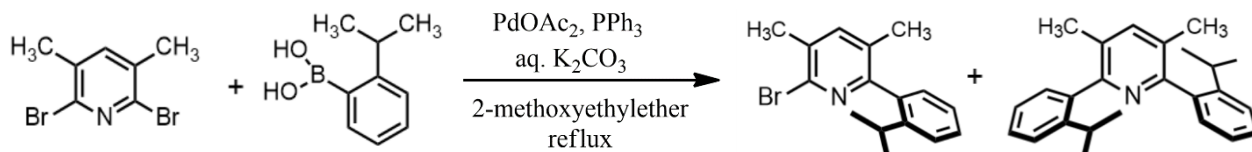
IR (cm⁻¹): 3036.2, 3021.6, 2979.6, 2954.2, 2916, 2855, 2730.6

¹HNMR (400 MHz, CDCl₃): δ 7.48 (s, 1H), 7.42 (s, 2H), 7.37 (d, J = 7.6 Hz, 2H), 7.33 (t, J = 7.48 Hz, 2H), 7.19 (d, J = 7.28 Hz, 2H), 2.43 (s, 6H), 2.38 (s, 6H)

¹³CNMR (100 MHz, CDCl₃): δ 155.96, 141.03, 140.63, 137.72, 129.98, 129.07, 128.4, 127.86, 126.28, 21.55, 19.63

MS(EI 70eV): calculated C₂₁H₂₁N 287.2; found 286.6

2-Bromo-6-(2-isopropylphenyl)-3,5-dimethyl pyridine
2,6-Bis(2-isopropylphenyl)-3,5-dimethyl pyridine



To a 10 mL round bottom flask, 2,6-dibromo-3,5-lutidine (109.4 mg, 0.413 mmol), (2-isopropylphenyl)boronic acid (114.4 mg, 0.698 mmol), and triphenylphosphine (7.3 mg, 0.028) were added in addition to a stir bar. To this, 2-methoxy-ethyl ether (2 mL) and 2M aqueous potassium carbonate (0.7 mL) solution were added using a syringe. The reaction was stirred until all solids appeared to have dissolved and the solution was then purged using nitrogen. This was followed by palladium acetate (8.8 mg, 0.039 mmol) was added and upon further stirring, the reaction solution turned into an orange color, then a dark green color. The solution was then refluxed at 174 °C for 45 minutes. The solution was then allowed to cool to room temperature and then extracted twice using ethyl acetate. The extracted organic layers were combined and washed with brine dried over magnesium sulfate, filtered, and concentrated to yield a bright yellow crude oil. The crude was then adsorbed onto silica gel and subject to flash column chromatography (SiO₂, hexanes:ethyl acetate 64:1 to 32:1 to 16:1 to 1:1 to ethyl acetate gradient). The collected fractions yielded two products, mono-arylated compound as an oil (43.8

mg, 34.5%) and diarylated compound as an oil (82.9 mg, 58.4%) assumed to be mixtures of cis-trans- isomers.

2-bromo-6-(2-isopropylphenyl)-3,5-dimethyl pyridine

TLC: $R_f = 0.42$ (SiO₂; hexanes:ethyl acetate 16:1)

IR (cm⁻¹): 3067.8, 3036.0, 3007.1, 2960.13, 2925.2, 2867.3

¹HNMR (400 MHz, CDCl₃): δ 7.43 (s, 1H), 7.42 - 7.35 (m, 2H), 7.23 (dt, $J = 1.96, 7.16$ Hz, 1H), 7.11 (dd, $J = 0.92, 7.40$ Hz, 1H), 2.67 (septet, $J =$, 1H), 2.43 (s, 3H), 2.05 (s, 3H), 1.16 (d, $J = 6.84$ Hz, 6H)

¹³CNMR (100 MHz, CDCl₃): δ 157.80, 146.48, 141.13, 140.59, 140.53, 139.54, 137.78, 134.23, 133.16, 131.07, 128.82, 128.58, 125.58, 125.53, 29.99, 13.94, 21.55, 20.99, 18.47

MS (EI 70 eV): calculated for C₁₆H₁₈BrN, 303.1, 305.1; found 303.1

2,6-bis(2-isopropylphenyl)-3,5-dimethyl pyridine

TLC: $R_f = 0.31$ (SiO₂; hexanes:ethyl acetate 16:1)

MP: 48-60 °C

IR (cm⁻¹): 3067.0, 2959.9, 2925.8, 2867.2

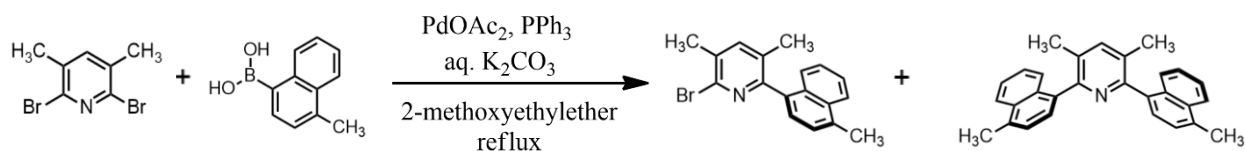
¹HNMR (400 MHz, CDCl₃): δ 7.49 (s, 1H), 7.37 (dd, $J = 1.32, 7.76$ Hz, 2H), 7.36 (dt, $J = 1.44, 7.92$ Hz, 2H), 7.22 (dt, $J = 1.68, 7.56$ Hz, 2H), 7.16 (dd, $J = 1.16, 7.40$ Hz, 2H), 2.80 (brs, 2H), 2.14 (s, 6H), 1.15 (brs, 12 H)

¹³CNMR (100 MHz, CDCl₃): δ 156.59, 146.29, 139.32, 129.97, 128.95, 128.06, 125.58, 125.22, 29.92, 24.04, 18.98

MS (EI 70 eV): calculated for C₂₅H₂₉N, 343.2; found 343.9

2-Bromo-3,5-dimethyl-6-(4-methylnaphthyl-1-yl)pyridine

3,5-Dimethyl-2,6-Di(4-methylnaphthyl-1-yl)pyridine



To a 10 mL round bottom flask, 2,6-dibromo-3,5-lutidine (105.8 mg, 0.399 mmol), 4-methyl-1-naphthalene boronic acid (123.1 mg, 0.662 mmol), and triphenylphosphine (10.1, 0.044 mmol) were added in addition to a stir bar. To this, 2-methoxy-ethyl ether (2 mL) and 2M aqueous potassium carbonate (0.7 mL) solution were added using a syringe. The reaction was stirred until all solids appeared to have dissolved and the solution was then purged using nitrogen. This was

followed by the addition of palladium acetate (10.1 mg, 0.045 mmol) and upon further stirring, the reaction solution turned into an orange color then dark green color. The solution was then refluxed with 174 °C oil bath for 45 minutes. The solution was then allowed to cool to room temperature and then extracted twice using ethyl acetate. The extracted organic layers were combined, washed with brine, dried over magnesium sulfate, filtered, and concentrated to yield an amber oil. This crude was dissolved in CH₂Cl₂ then adsorbed onto silica and subject to flash column chromatography (SiO₂, hexanes:ethyl acetate 64:1 to 32:1 to 16:1 to 1:1 to ethyl acetate gradient). The collected fractions yielded the two products, mono-arylated compound as a yellow solid (28.2 mg, 21.7%) and di-arylated compound as an oil (89.1 mg, 57.6%) assumed to be mixtures of cis- trans-isomers.

2-bromo-3,5-dimethyl-6-(4-methylnaphthyl-1-yl)pyridine

TLC: R_f = 0.32 (SiO₂; hexanes:ethyl acetate 16:1)

MP: 75-80 °C

IR (cm⁻¹): 3065.8, 3037.5, 2984.1, 2952.5, 2921.5, 2854.3

¹HNMR (400 MHz, CDCl₃): δ 8.08 (d, J= 8.4 Hz, 1H), 7.54 (ddd, J=2.3, 5.8, 8.2 Hz, 1H), 7.50 (s, 1H), 7.46-7.42 (m, 2H), 7.40 (d, J= 7.4 Hz, 1H), 7.32 (d, J= 7.1 Hz, 1H), 2.77 (s, 3H), 2.48 (s, 3H), 2.02 (s, 3H).

¹³CNMR (100 MHz, CDCl₃): δ 156.84, 140.97, 140.67, 135.14, 134.95, 133.51, 132.75, 132.07, 131.39, 126.49, 126.06, 125.97, 125.92, 125.68, 124.47, 21.61, 19.58, 18.43.

MS (EI, 70 eV): calculated for C₁₈H₁₆BrN, 325.1, 327.0; found, 324.0, 326.1

3,5-dimethyl-2,6-Di(4-methylnaphthyl-1-yl)pyridine

TLC: R_f = 0.31 (SiO₂; hexanes:ethyl acetate 16:1)

MP: 41-70 °C

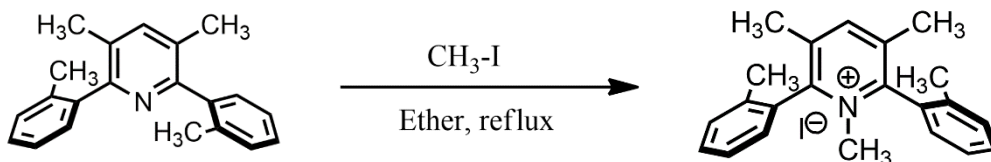
IR= 3098.8, 3062.0, 3020.7, 2968.4, 2949.0, 2921.4, 2852.6, 2734.8 (cm⁻¹): 2920.7

¹HNMR (400 MHz, CDCl₃): δ 8.06 (d, J= 8.2 Hz, 2H), 7.65 (s, 1H), 7.64 (d, J= 7.1 Hz, 2H), 7.53 (dt, J= 1.32, 7.56 Hz, 2H), 7.47 (dd, J= 1.28, 7.0 Hz, 2H), 7.47-7.38 (m, 4H), 2.74 (s, 6H), 2.18 (s, 6H).

¹³CNMR (100 MHz, CDCl₃): δ 155.76, 139.84, 136.52, 134.37, 132.85, 131.84, 131.33, 126.59, 126.29, 126.17, 125.72, 125.49, 124.41, 19.58, 19.03.

MS (EI, 70 eV): calculated for C₂₉H₂₅N, 387.2; found 387.0

1,3,5-trimethyl-2,6-di-(2-methylphenyl)pyridinium iodide



To a 50 mL pressure vessel with 3,5-dimethyl-2,6-di(2-methylphenyl)pyridine (84.0 mg, 0.292 mmol) ether (0.8 mL) and stir bar was added. The reaction was stirred until all solids appeared to have dissolved. To this, methyl-iodide (0.3 mL) was added using a syringe. The solution was then purged using nitrogen. The solution was then refluxed with 120°C oil bath for 15 minutes. The solution was then allowed to cool to room temperature. A solid layer and a liquid layer were observed to have formed. Both layers were dissolved in DCM and the solvent was then removed under pressure and the solid product formed (124.4 mg, 99.3%).

1,3,5-trimethyl-2,6-di(2-methylphenyl)pyridinium iodide

MP: 215-225 °C

IR (cm⁻¹): 3706.3, 3681.6, 3666.0, 3657.0, 3645.8, 2974.4, 2938.4, 2922.1, 2864.2, 2844.8, 2831.6

¹HNMR major atropisomer (400 MHz, CDCl₃): δ 8.25 (s, 1H), 7.67 (d, *j* = 1.44 Hz, 1H), 7.65 (d, *j* = 1.68 Hz), 7.56-7.45 (m, 8H), 3.63 (s, 1H), 2.231 (s, 3H), 2.05 (s, 3H)

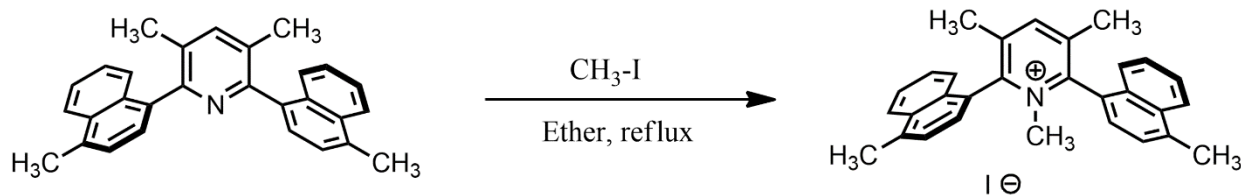
¹HNMR minor atropisomer (400 MHz, CDCl₃): δ 8.510 (s, 1H), 8.38-8.34 (m, 4H), 7.42-7.39 (m, 4H), 2.29 (s, 3H), 2.27 (s, 3H)

¹³CNMR (100 MHz, CDCl₃): δ 147.45, 137.71, 135.59, 133.57, 131.58, 131.35, 131.30, 131.01, 130.92, 130.74, 130.42, 129.60, 128.59, 128.49, 128.26, 127.79, 44.61, 20.36, 19.79, 19.74, 19.63, 18.98.

MS (EI, 70 ev) major atropisomer: calculated for C₂₂H₂₄N⁺ 302.2; found 302.1

MS (EI, 70 ev) minor atropisomer: calculated for C₂₂H₂₄N⁺ 302.2; found 302.1 and 302.8.

1,3,5-trimethyl-2,6-bis(4-methylnaphthalen-1-yl)pyridinium iodide



To a 50 mL pressure vessel, 3,5-dimethyl-2,6-bis(4-methylnaphthalen-1-yl)pyridine (87.7 mg, 0.305 mmol), followed by the addition of ether (0.8 mL) in addition to a stir bar. The reaction was stirred until all solids appeared to have dissolved. To this, methyl-iodide (0.3 mL) was added

using a syringe. The solution was then purged using nitrogen. The solution was then refluxed with 120°C oil bath for 15 minutes. The solution was then allowed to cool to room temperature. A solid layer and a liquid layer were observed to have formed. Both layers were dissolved in DCM and the solvent was then removed under pressure and the solid product formed (129.1 mg, 98.7% yield).

1,3,5-trimethyl-2,6-bis(4-methylnaphthalen-1-yl)pyridin-1-ium iodide

MP: 151-190 °C

IR (cm⁻¹): 3565.3, 3515.3, 3452.5, 3445.4, 3067.5, 3030.9, 2977.4, 2945.7, 2923.2, 2899.9, 2859.4

¹HNMR Major Atropisomer (400 MHz, CDCl₃): δ 8.63 (d, *j* = 7.24 Hz, 2H), 8.330 (s, 1H), 8.20-8.15 (m, 4H), 7.73-7.55 (m, 11H), 7.21 (d, *j* = 7.80 Hz, 2H), 3.56 (s, 3H), 2.82 (s, 3H), 2.23 (s, 3H)

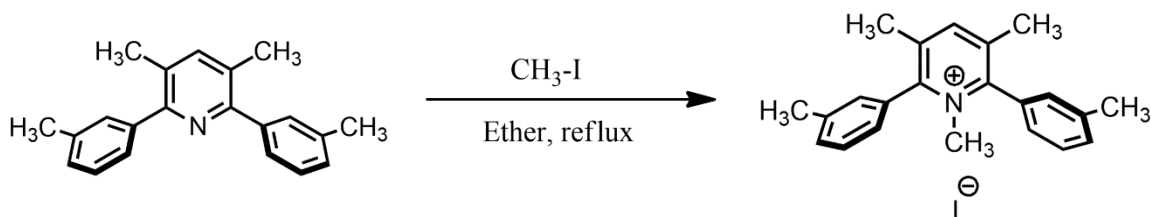
¹HNMR Minor Atropisomer (400 MHz, CDCl₃): δ 8.52 (s, 1H), 8.01 (d, *j* = 7.24 Hz, 2H), 7.79-7.77 (m, 4H), 7.73-7.55 (m, 11H), 3.53 (s, 3H), 2.82 (s, 3H), 2.29 (s, 3H)

¹³CNMR (100 MHz, CDCl₃): δ 206.97, 152.86, 152.63, 149.19, 147.97, 138.51, 138.39, 132.82, 129.83, 129.76, 129.36, 128.67, 128.47, 128.11, 127.90, 127.73, 127.68, 127.51, 127.46, 127.13, 125.88, 125.80, 124.81, 124.68, 45.49, 44.94, 31.15, 19.68, 19.43, 19.32

MS (EI, 70 ev) for major atropisomer: calculated for C₃₀H₂₈N⁺, 402.2; found 402.1 and 403.1

MS (EI, 70 ev) for minor atropisomer: calculated for C₃₀H₂₈N⁺, 402.2; found 401.9 and 403.1

3,5-Dimethyl-2,6-di(3-methylphenyl)pyridine



To a 10 mL round bottom flask, 3,5-Dimethyl-2,6-di(3-methylphenyl)pyridine (84.0 mg, 0.292 mmol), followed by the addition of ether (0.8 mL) in addition to a stir bar. The reaction was stirred until all solids appeared to have dissolved. To this, methyl-iodide (0.3 mL) was added using a syringe. The solution was then purged using nitrogen. The solution was then refluxed with 120 °C oil bath for 15 minutes. The solution was then allowed to cool to room temperature. A solid layer and a liquid layer were observed to have formed. Both layers were dissolved in DCM and the solvent was then removed under pressure and the solid product formed (124.4 mg, 99.3%).

1,3,5-trimethyl-2,6-di-m-tolylpyridin-1-ium iodide

TLC: N/A

MP: 208-218 °C

IR (cm⁻¹): 3051.6, 3031.8, 3005.9, 2974.2, 2955.0, 2920.2, 2857.2

¹HNMR (400 MHz, CDCl₃): δ 8.18 (s, 1H), 7.61 (d, J = 26.5 Hz, 2H), 7.60 (d, J = 11.6 Hz, 2H), 7.50 (t, j = 7.60 Hz, 2H), 7.38 (d, j = 7.20 Hz, 2H), 3.72 (s, 3H), 2.48 (s, 6H), 2.27 (s, 6H)

¹³CNMR (100 MHz, CDCl₃): δ 147.23, 147.20, 140.04, 140.01, 137.47, 131.80, 131.50, 129.77, 129.04, 128.98, 125.81, 125.76, 121.18, 72.08, 60.82, 46.32, 45.40, 41.06, 29.69, 21.45, 20.36, 18.57

MS (EI, 70 ev): calculated for C₂₂H₂₄N⁺ 302.2; found 302.1 and 303.3.

REFERENCES

1. Laplante, Steven R, D Fader, Lee, Fandrlick, Keith R, Fandrlick, Daniel R, Hucke, Oliver, Kemper, Ray, Miller, Stephen P F, and Edwards, Paul J. "Assessing Atropisomer Axial Chirality in Drug Discovery and Development." *Journal of Medicinal Chemistry* 54.20 (2011): 7005-7022. Web.
2. Bringmann, Gerhard, Gulder, Tanja, Gulder, Tobias A M, and Breuning, Matthias. "Atroposelective Total Synthesis of Axially Chiral Biaryl Natural Products." *Chemical Reviews* 111.2 (2011): 563-639. Web.
3. Ming Ge, H.; Yun Zhang, W.; Ding, G.; Saparpakorn, P.; Chun Song, Y.; Hannongbua, S.; Xiang Tan, R. Chaetoglobins A and B, Two Unusual Alkaloids from Endophytic *Chaetomium Globosum* Culture. *Chem. Commun.* **2008**, 5978– 5980, DOI: 10.1039/b812144c. b) Bringmann, G.; Gulder, T.; Gulder, T. A. M.; Breuning, M. Atroposelective Total Synthesis of Axially Chiral Biaryl Natural Products. *Chem. Rev.* 2011, *111*, 563-639.
4. Hubbard, B. K.; Walsh, C. T. Vancomycin Assembly: Nature's Way. *Angew. Chem. Int. Ed.* 2003, *42*, 730-765.
5. Lanman, Brian A, et al. "Discovery of a Covalent Inhibitor of KRASG12C (AMG 510) for the Treatment of Solid Tumors." *Journal of Medicinal Chemistry*, vol. 63, no. 1, 2020, pp. 52–65.
6. McCarthy, Mary, and Patrick J Guiry. "Axially Chiral Bidentate Ligands in Asymmetric Catalysis." *Tetrahedron* 57.18 (2001): 3809-844. Web.
7. Oh, T.; Lopez, P.; Reilly, M. Simultaneous coordination of dimethyl crotonthioamide by 1,8-naphthalenediylbis(mercuritri-fluoroacetate). Synthesis of optically pure 2,2'-bisboryl-,

- bismERIC-, bisSilyl- bisstannyl-substituted 1,1'-binaphthyl compounds. Catalysis of Diels-Alder reactions of O-ethyl crotonthioate by 2,2'-bismERIC-1,1'-binaphthalene. *Eur. J. Org. Chem.* **2000**, 2901-2903.
8. Lin Pu. 1,1'-binaphthyl Dimers, Oligomers, and Polymers: Molecular Recognition, Asymmetric Catalysis, and New Materials. *Chemical Reviews* 98.7 (1998): 2405-2494. Web.
 9. Gottarelli, Giovanni, et al. Induction of the Cholesteric Mesophase in Nematic Liquid Crystals: Mechanism and Application to the Determination of Bridged Biaryl Configurations. *Journal of the American Chemical Society*, Vol. 105, no. 25, 1983, pp. 7318–7321.
 10. Yulek, C. Atropisomerism in Pyridyl Systems. M.S. Thesis, California State University, Northridge, CA, 2006.
 11. Dunn, A. D.; Guillermic, S. The Bromination of Lutidines. *Zeitschrift fur chemie*, 1988, 28(2) 59-60. b) Pugh, D. 2,6-Dibromo-3,5-dimethylpyridine and 2,6-diiodo-3,5-dimethylpyridine. *Acta Cryst.* **2006**, C62, o590-o592.
 12. Huang, W., Hu, M., Wan, X. *et al.* Facilitating the transmetalation step with aryl-zincates in nickel-catalyzed enantioselective arylation of secondary benzylic halides. *Nat Commun* **10**, 2963 (2019). <https://doi.org/10.1038/s41467-019-10851-4> Spartan 14 by Wavefunction Inc. 18401 Von Karman Ave., Suite 370, Irvine, CA 92612, 2014.
 13. Gunther, H. The Influence of Dynamic Effects on ¹H Nuclear Magnetic Resonance Spectra. In *NMR Spectroscopy*, 2nd ed.; Wiley, 1995, pp 335-390.
 14. Friebolin, H. Dynamic NMR Spectroscopy (DNMR) In Basic One- and Two-Dimensional NMR Spetroscopy, 3rd ed.; Wiley-VCH, 1998, pp301-330.

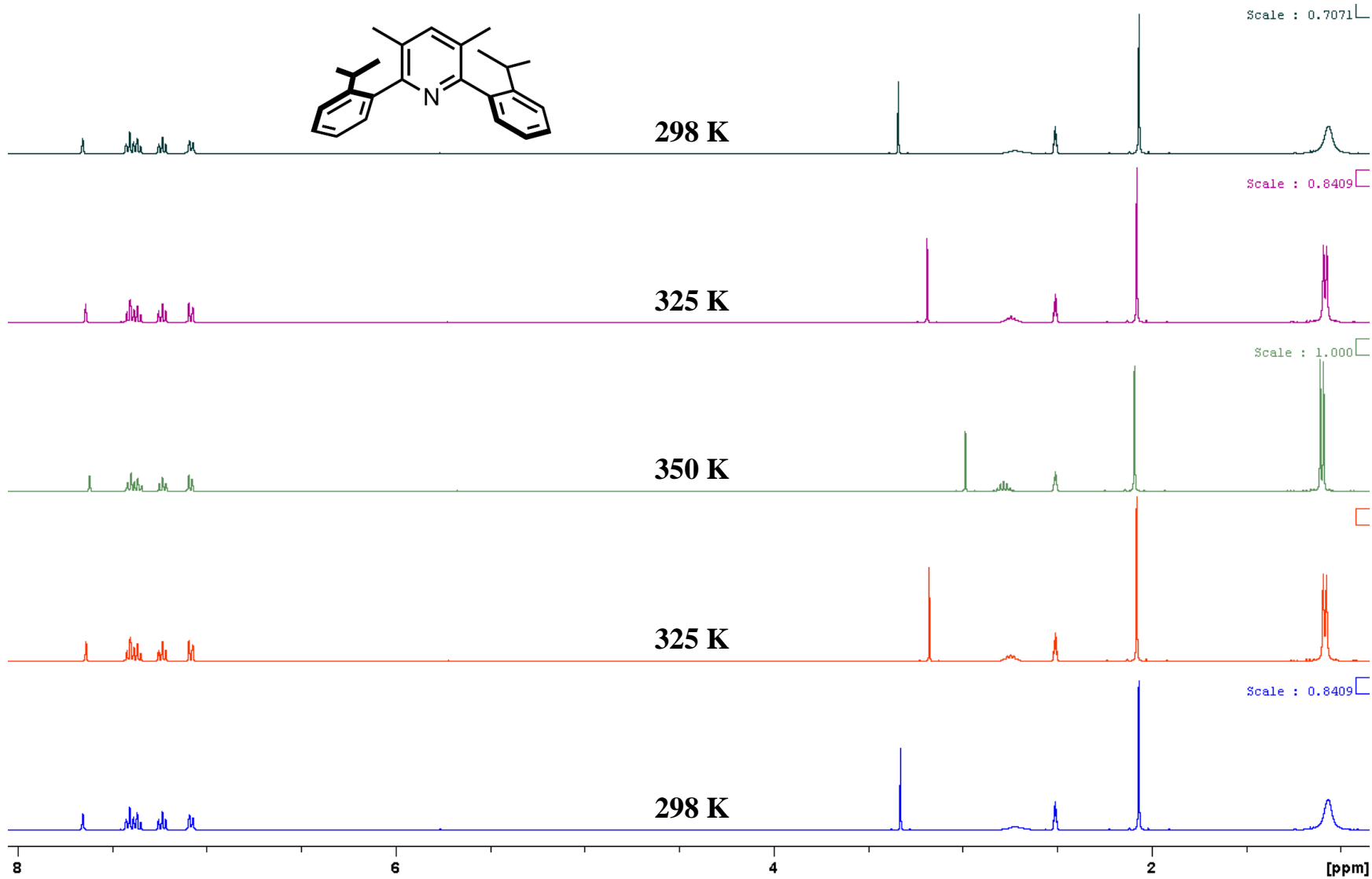
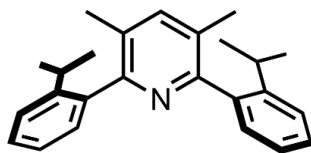
15. Szawkalo, J.; Blachut, D.; Roszkowski, P.; Pomaranski, P.; Maurin, J. K.; Budzianowski, A.; Czarnocki, Z. New stable atropisomers derived from 2,4,6-collidine and related compounds. *Tetrahedron*, **2016**, 72, 6779-6787.

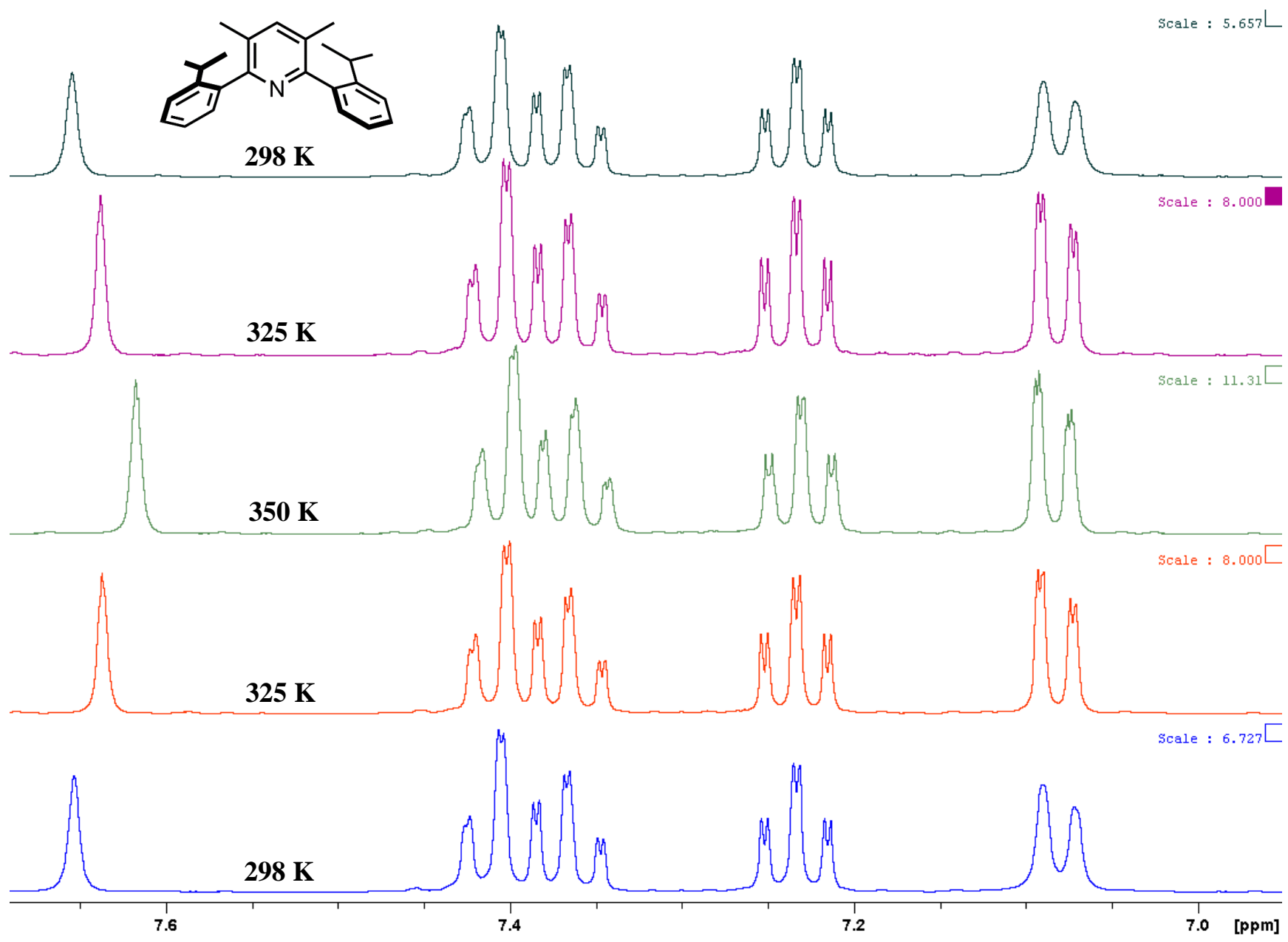
APPENDIX A: DYNAMIC ¹H NMR

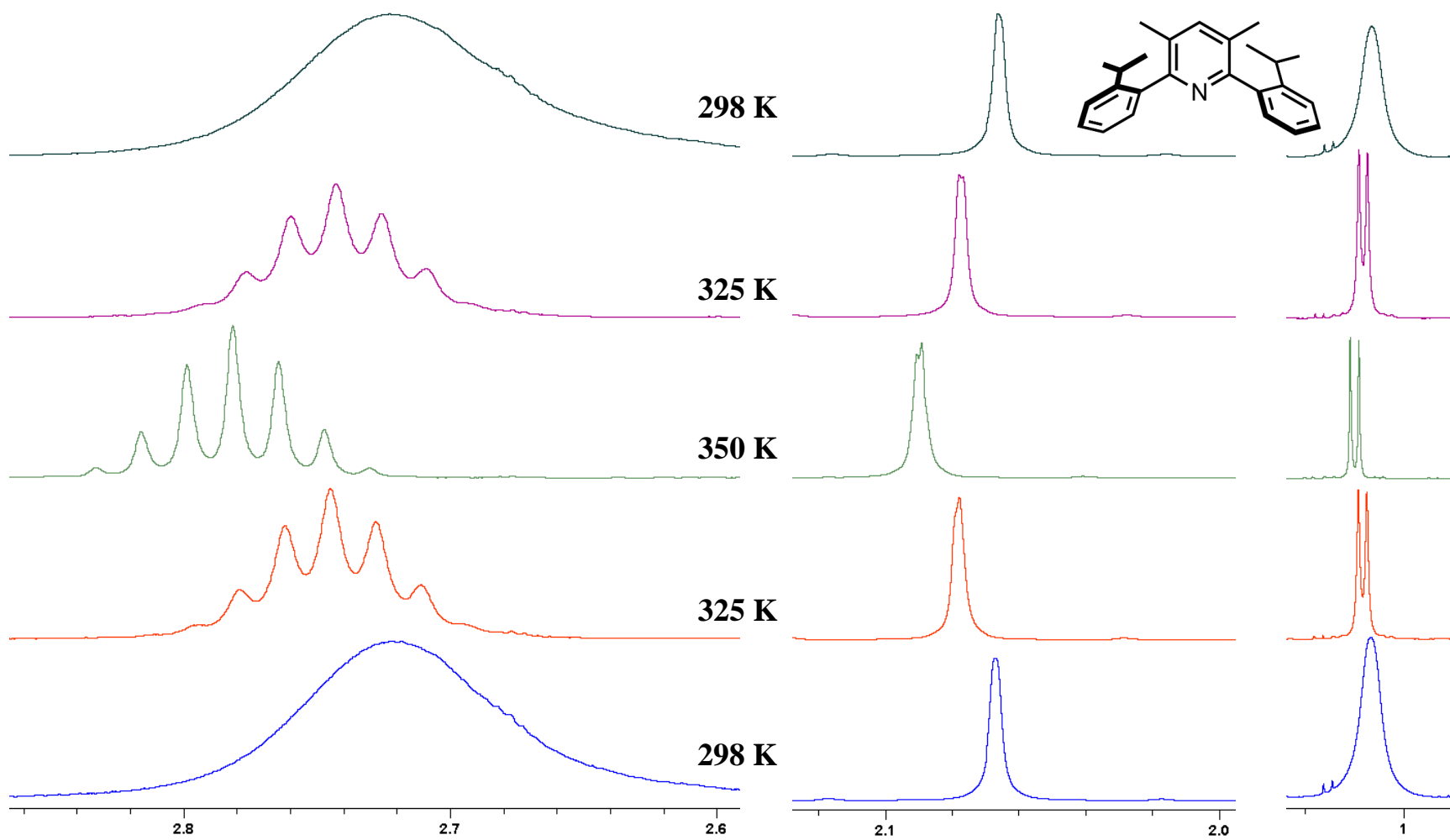
Compound	Page
3,5-Dimethyl-2,6-di(2-isopropylphenyl)pyridine.....	65
3,5-Dimethyl-2,6-di(2-methylphenyl)pyridine.....	71
3,5-Dimethyl-2,6-Di(4-methylnaphthyl-1-yl)pyridine.....	77
1,3,5-Trimethyl-2,6-di-(2-methylphenyl)pyridinium iodide.....	83
1,3,5-Dimethyl-2,6-Di(4-methylnaphthyl-1-yl)pyridinium iodide.....	89
1,3,5-trimethyl-2,6-di-(3-methylphenyl)pyridinium iodide.....	97

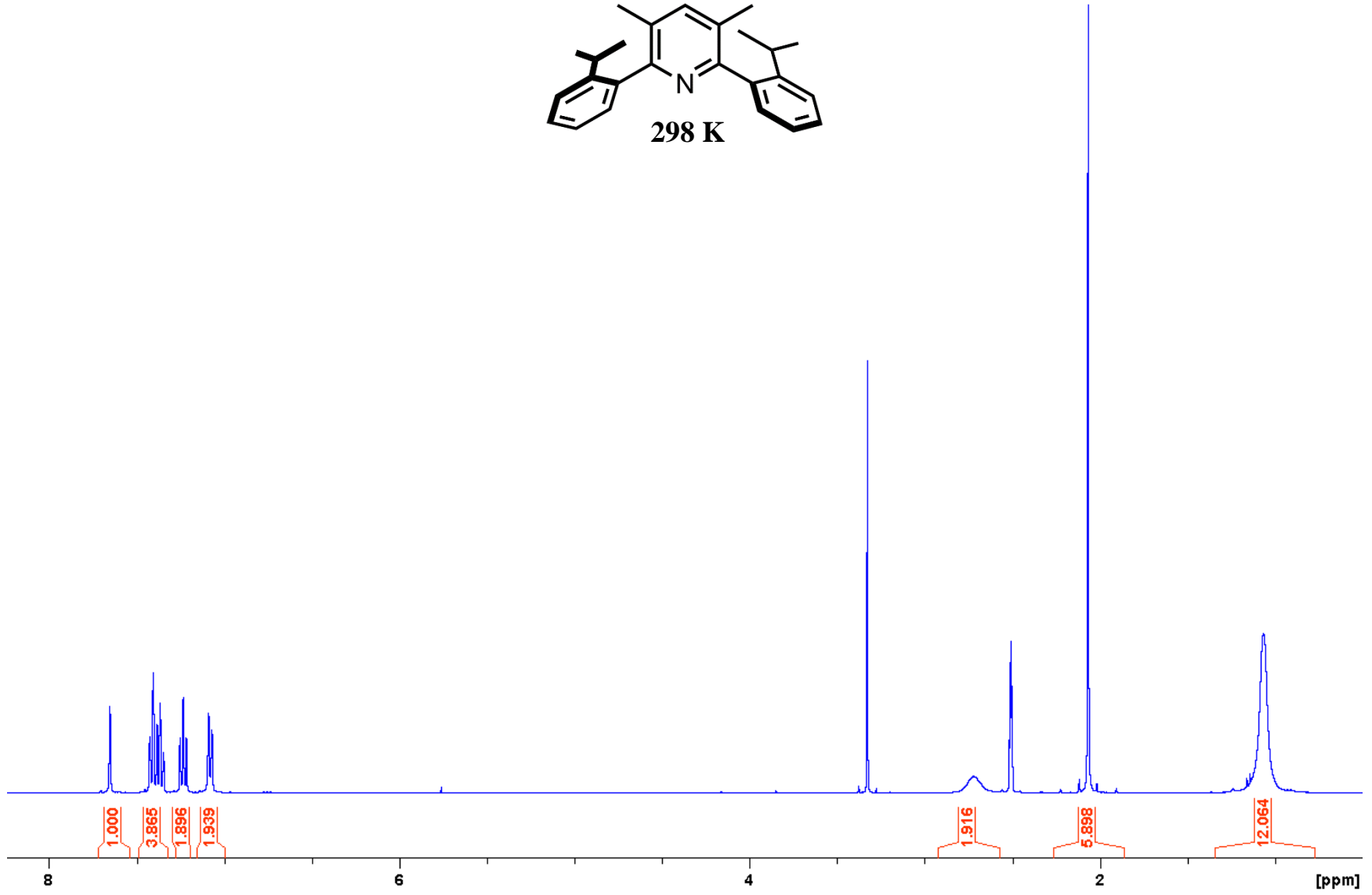
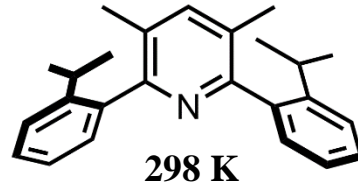
The dynamic ¹H NMR were taken starting at room temperature. The ¹H NMR were taken in increments of temperature as indicated. While decreasing the temperature, if temperature stabilized was observed, the spectrum was obtained. The NMR was also taken at the same temperature while increasing temperature back to room temperature. This same procedure was followed for NMRs obtained when temperature was increased above room temperature. As a result, some DNMR data have two spectra at the same temperature.

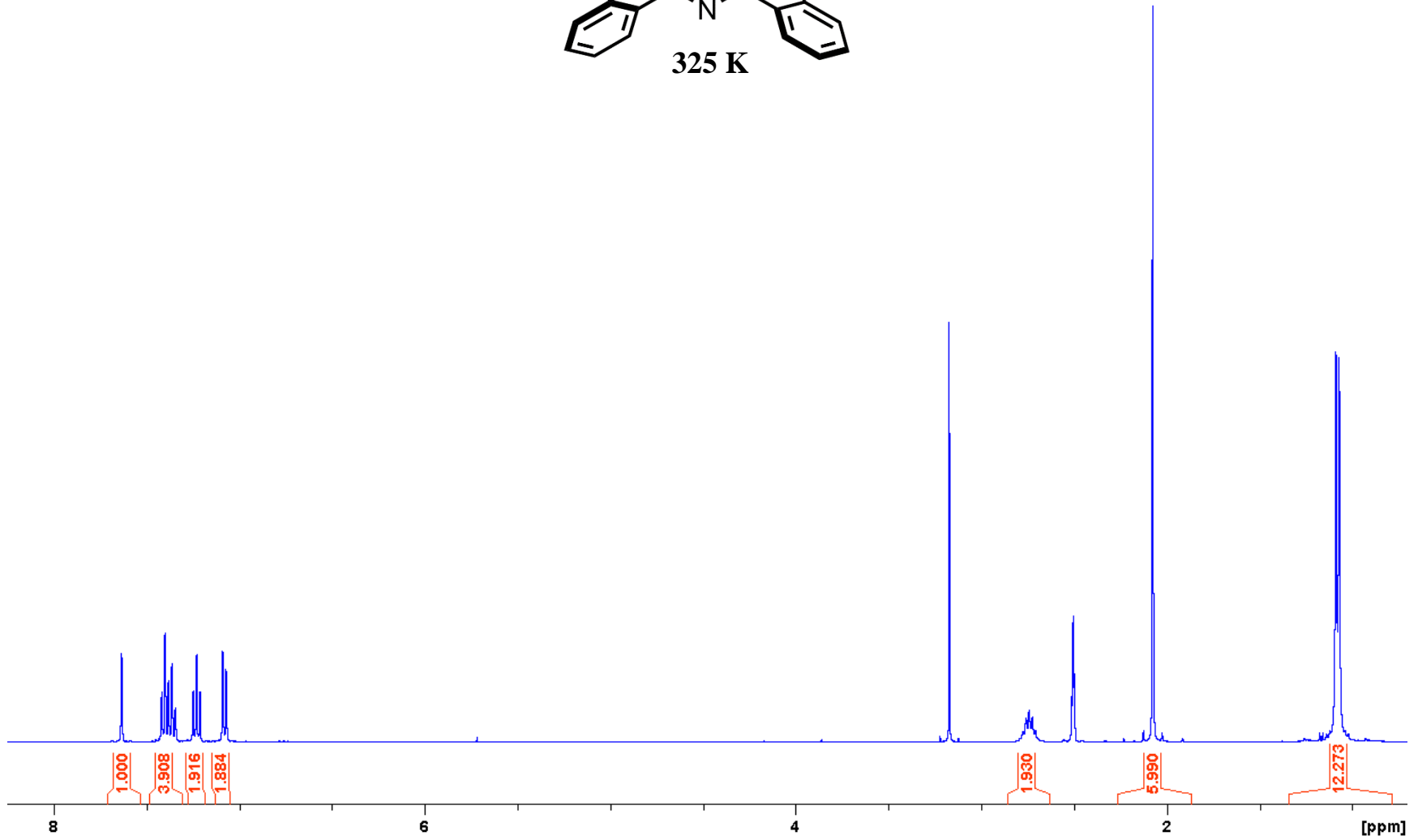
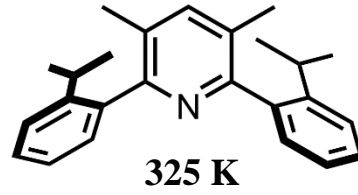
3,5-Dimethyl-2,6-di(2-isopropylphenyl)pyridine

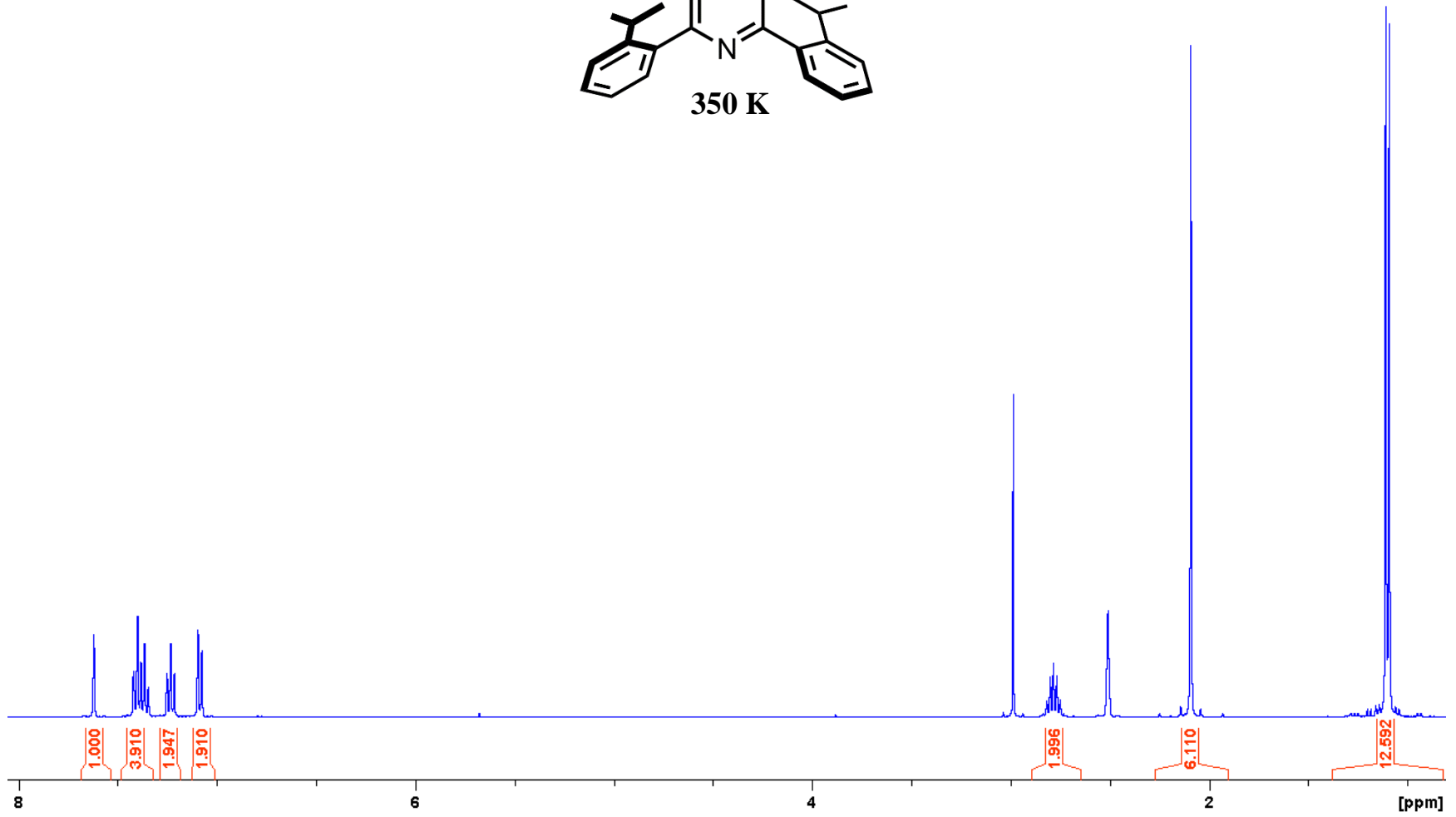
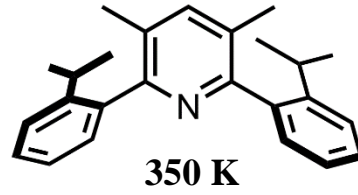




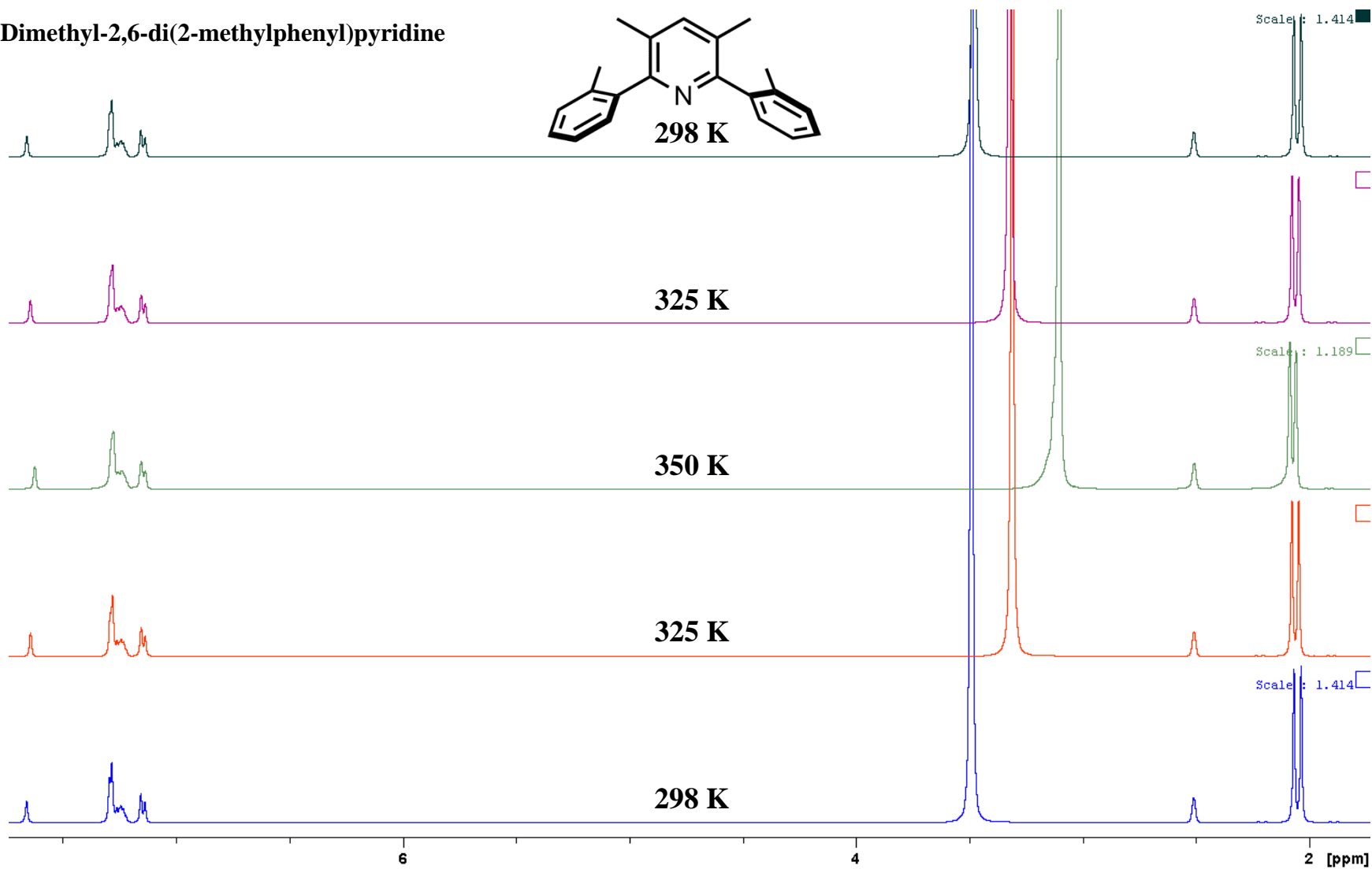
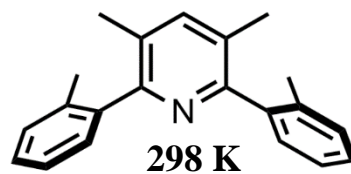


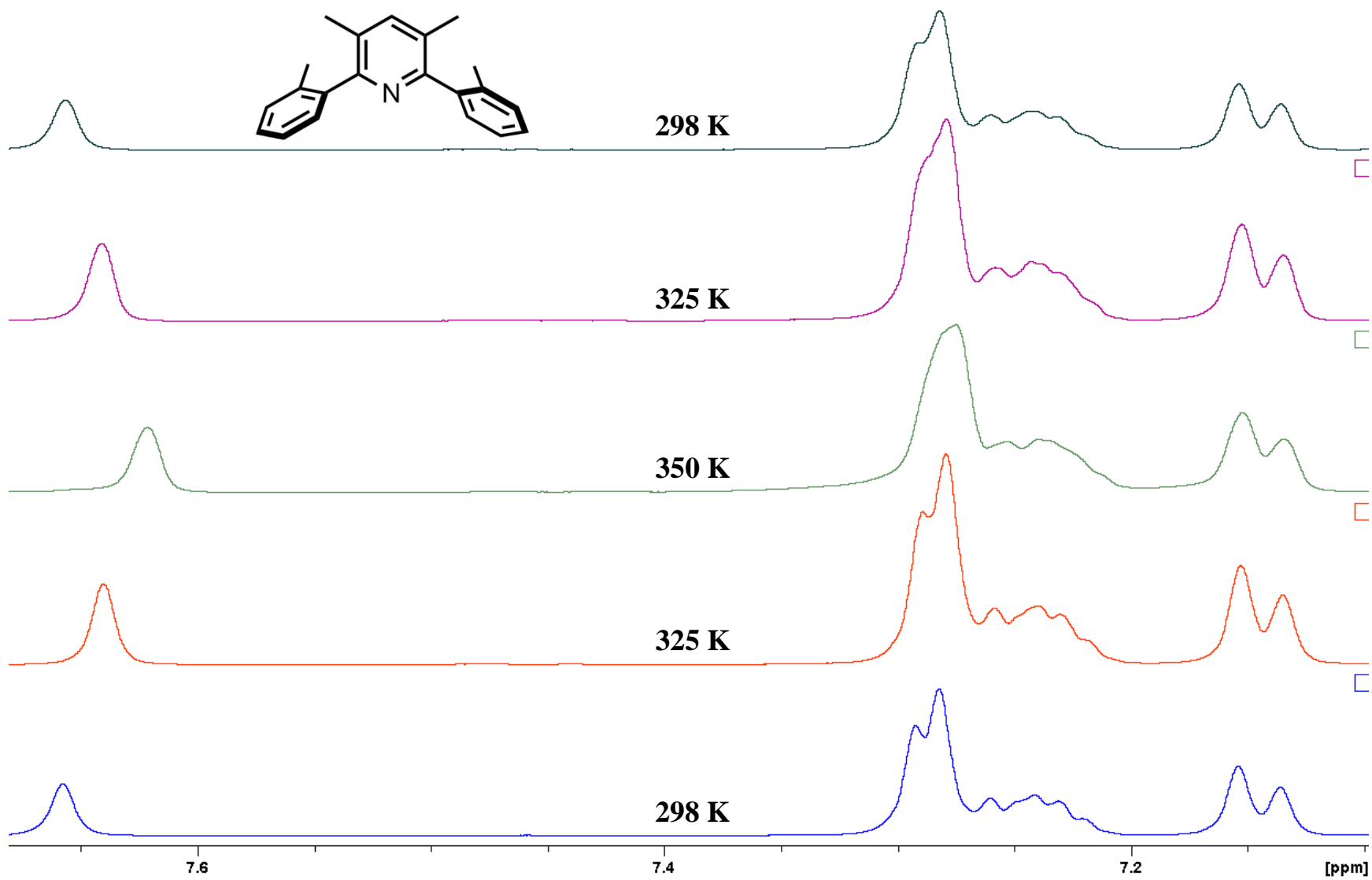


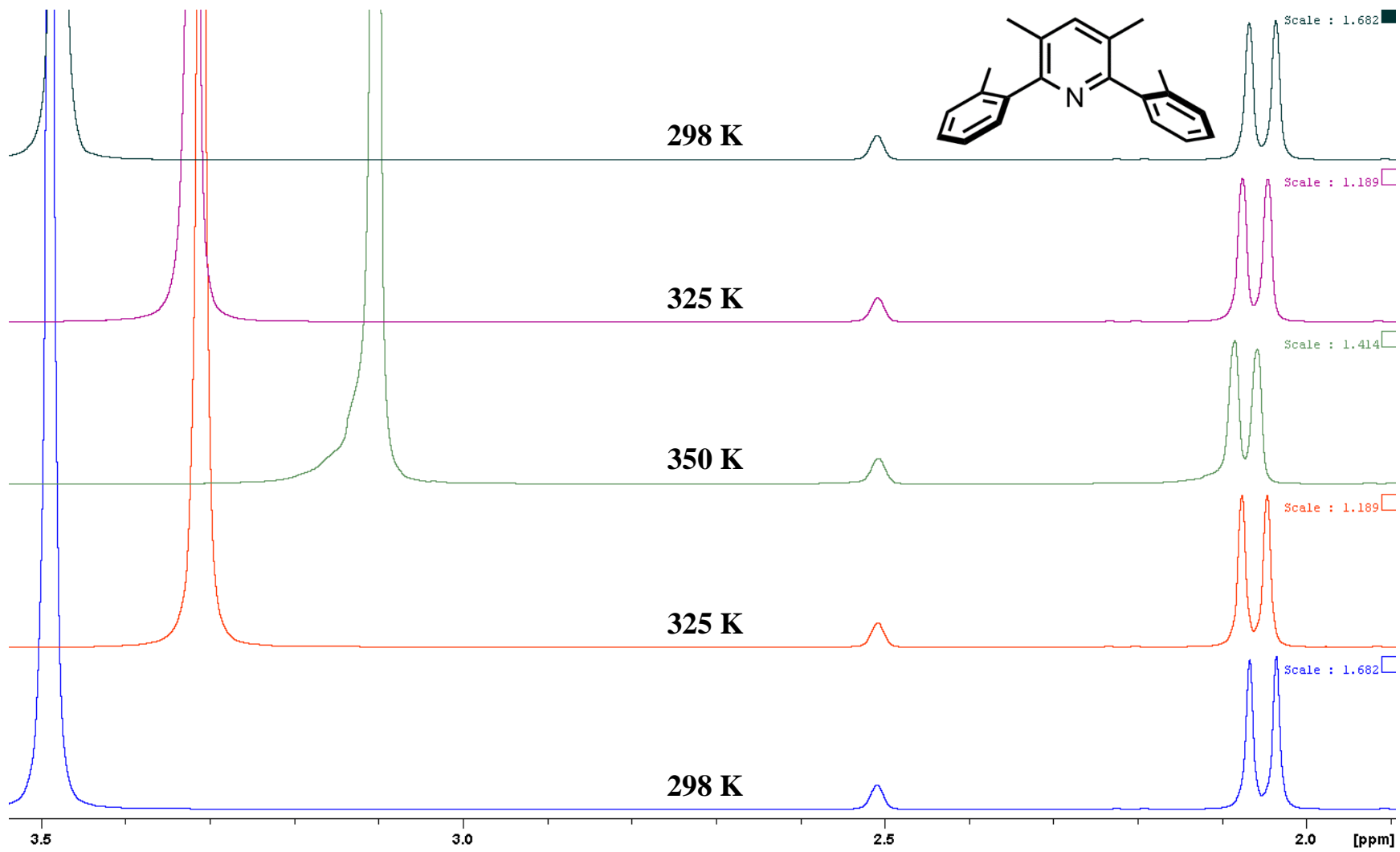


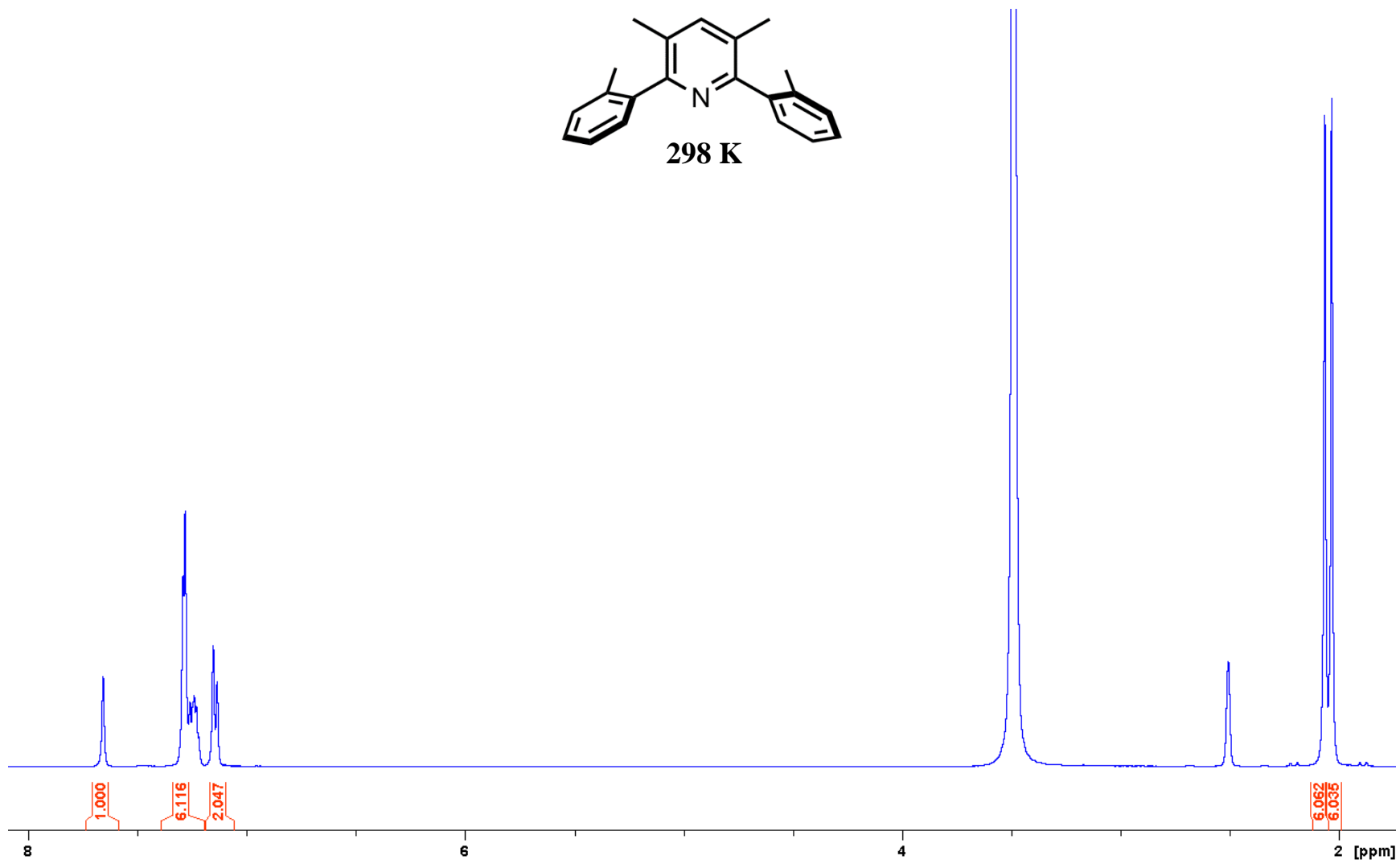
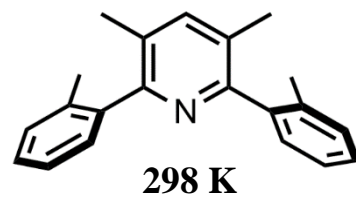


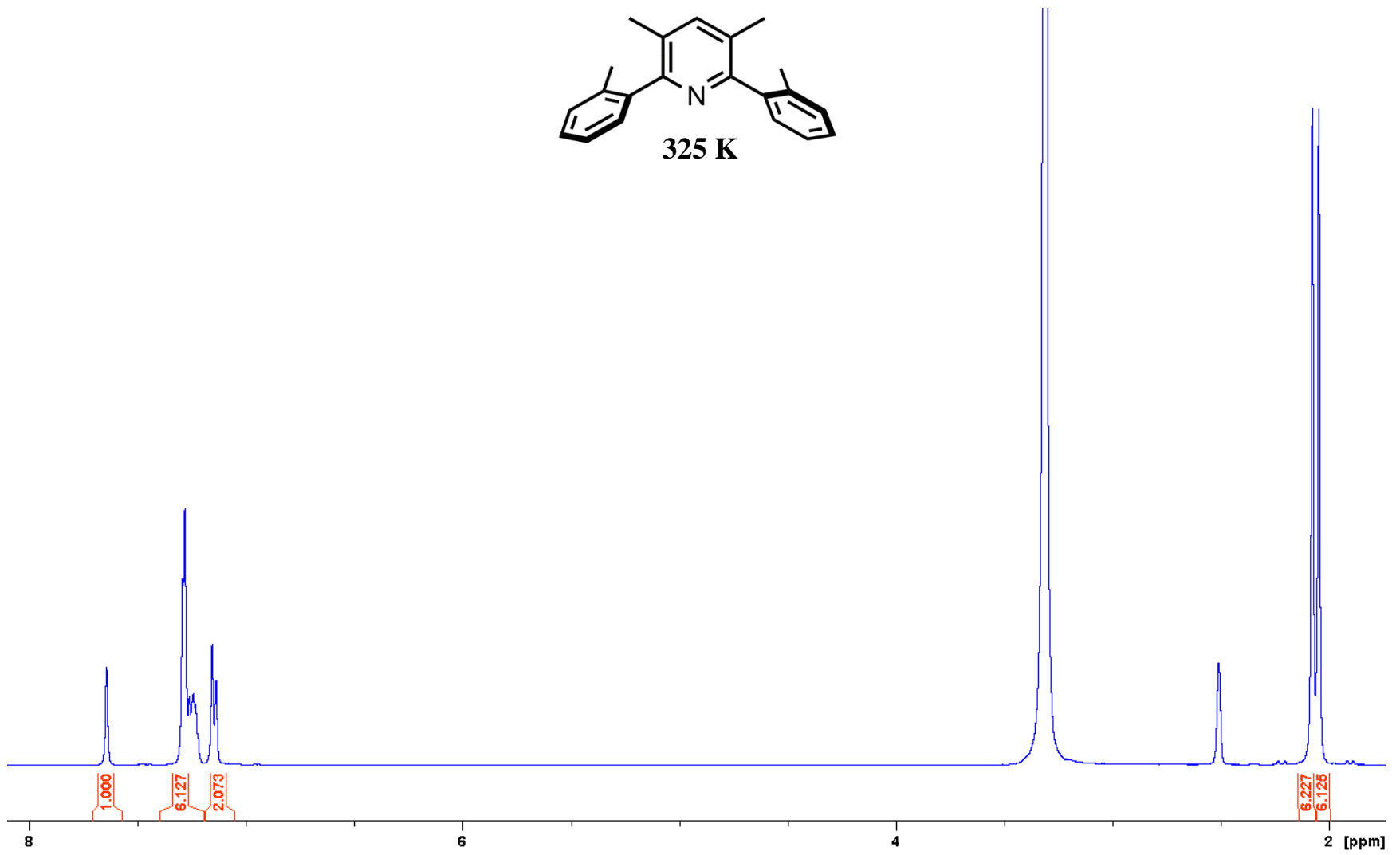
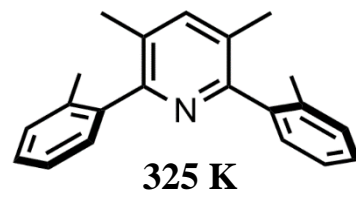
3,5-Dimethyl-2,6-di(2-methylphenyl)pyridine

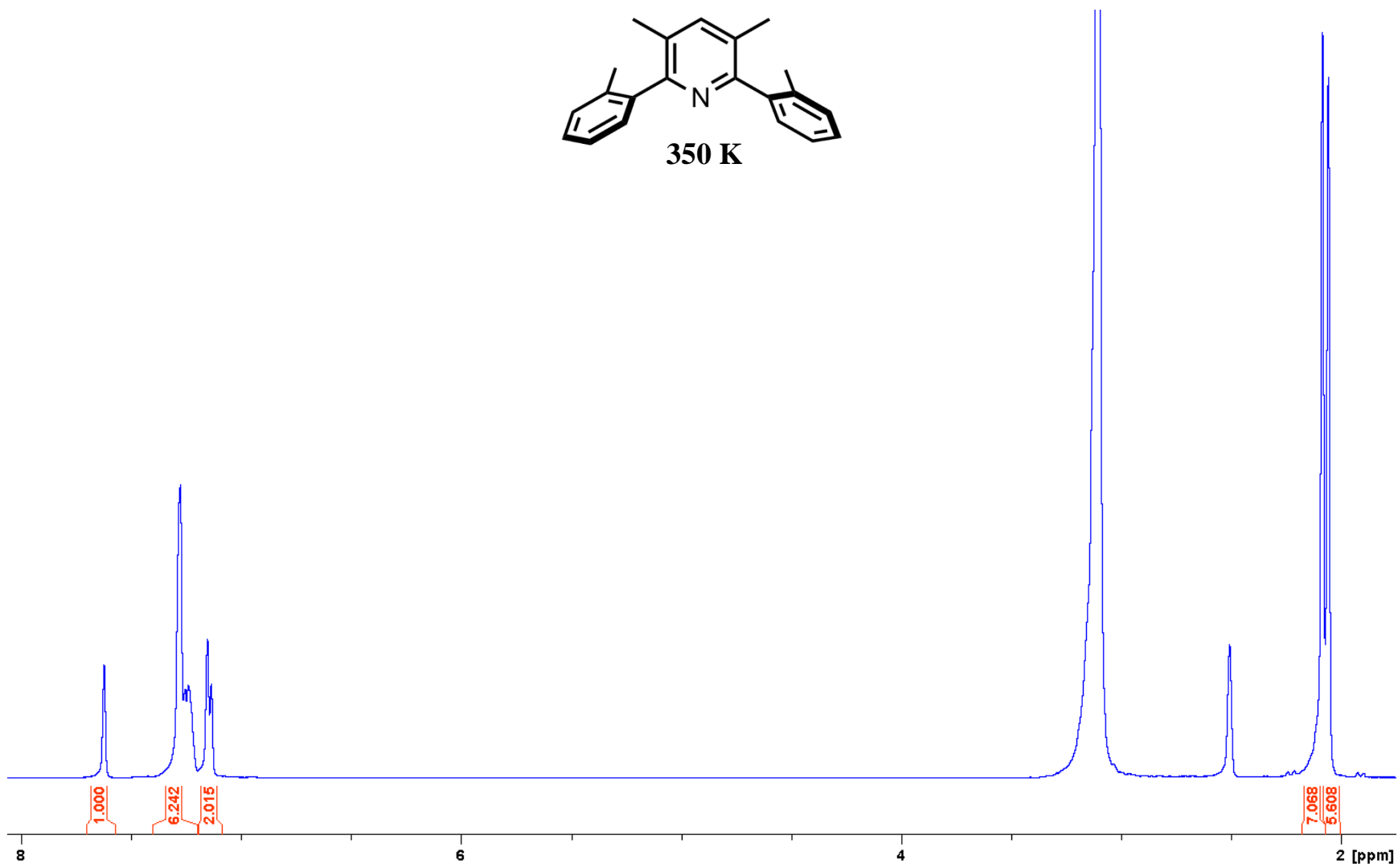
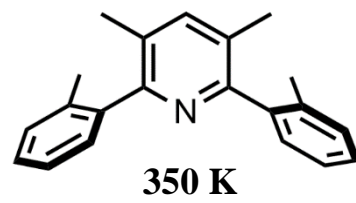




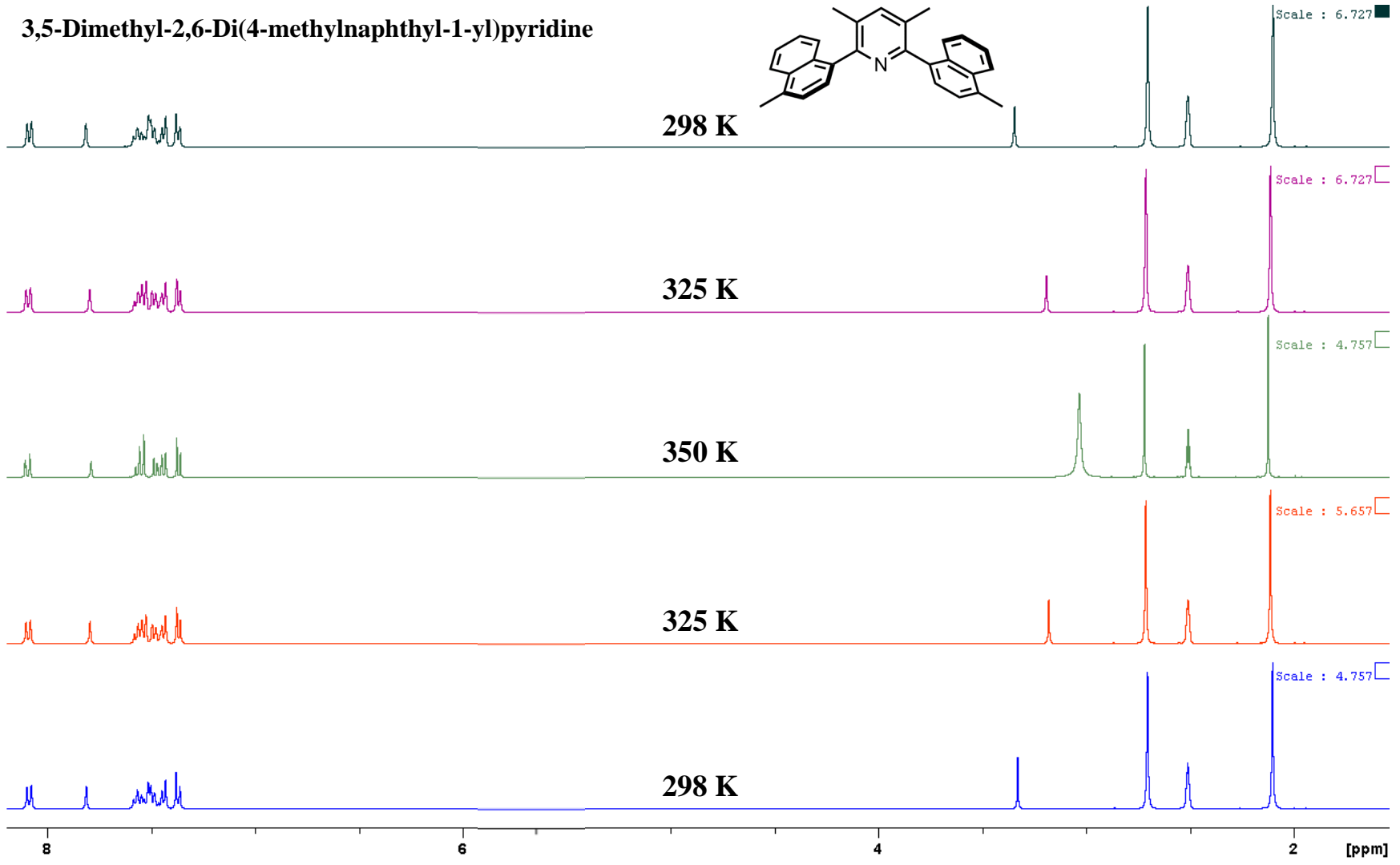
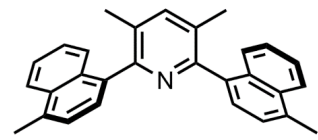


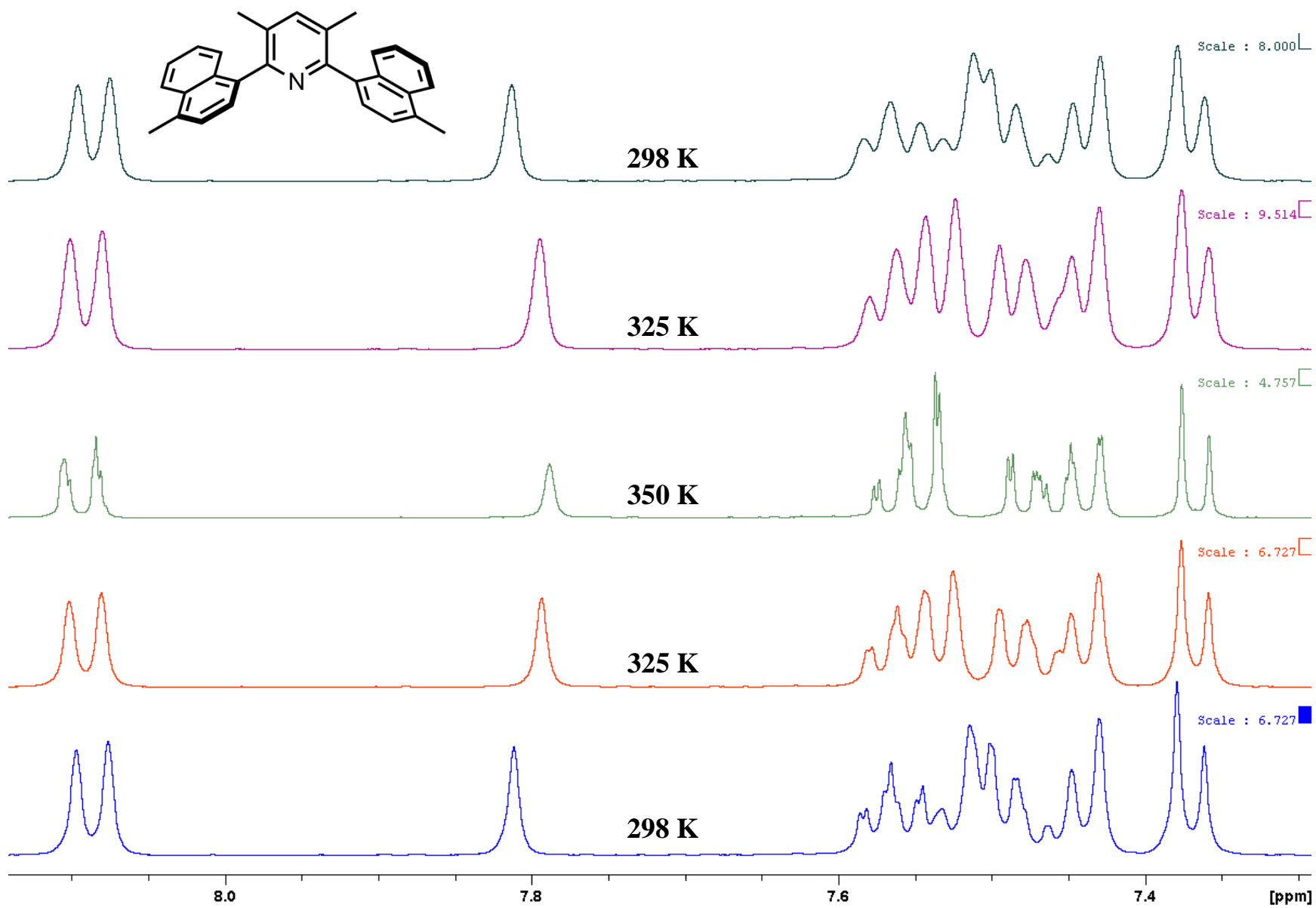


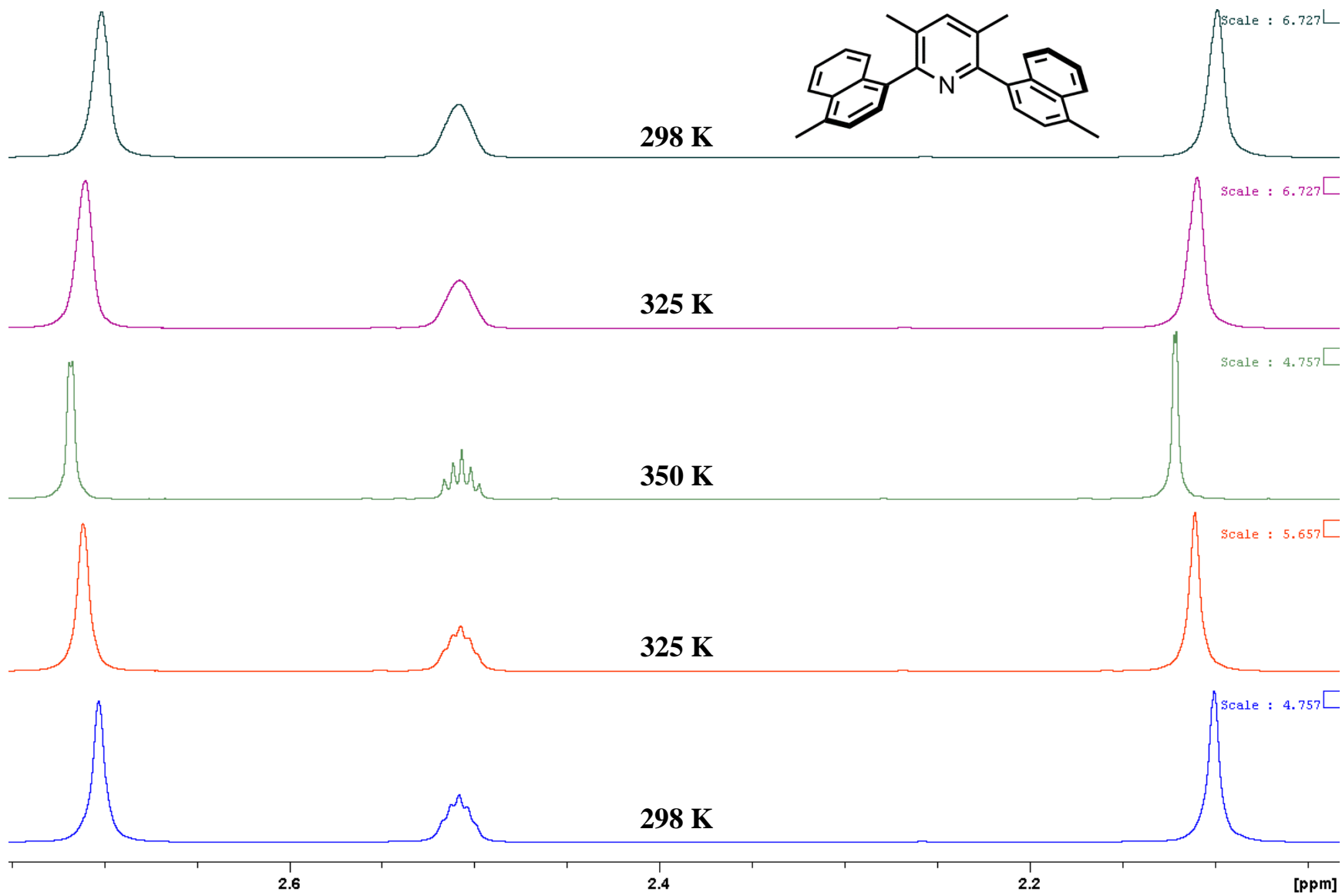


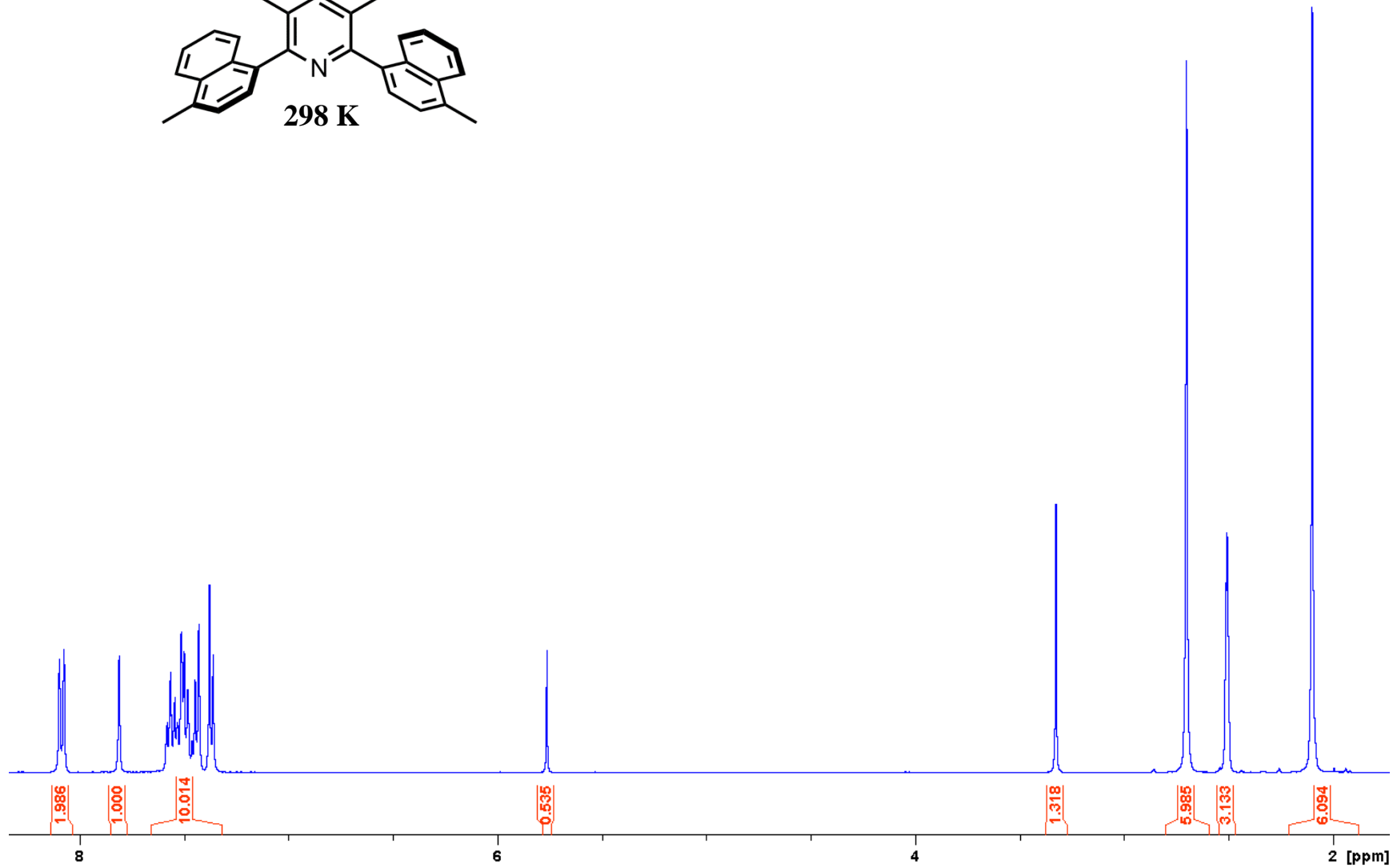
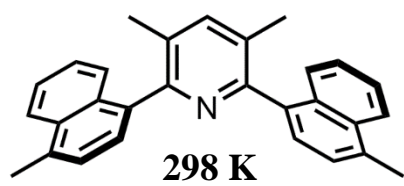


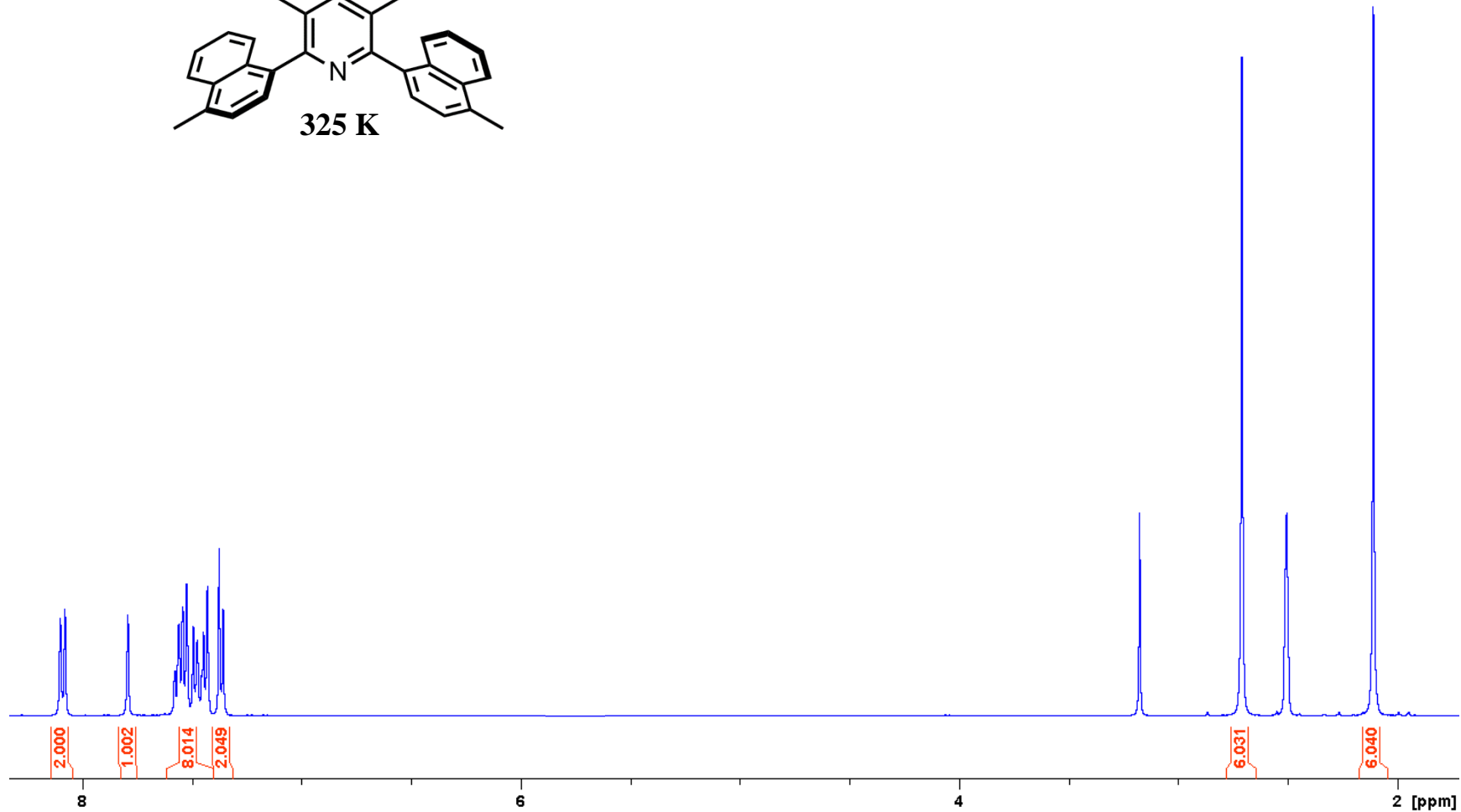
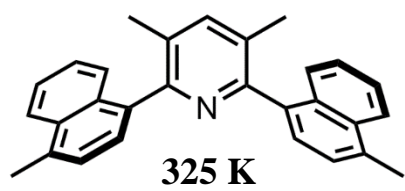
3,5-Dimethyl-2,6-Di(4-methylnaphthyl-1-yl)pyridine

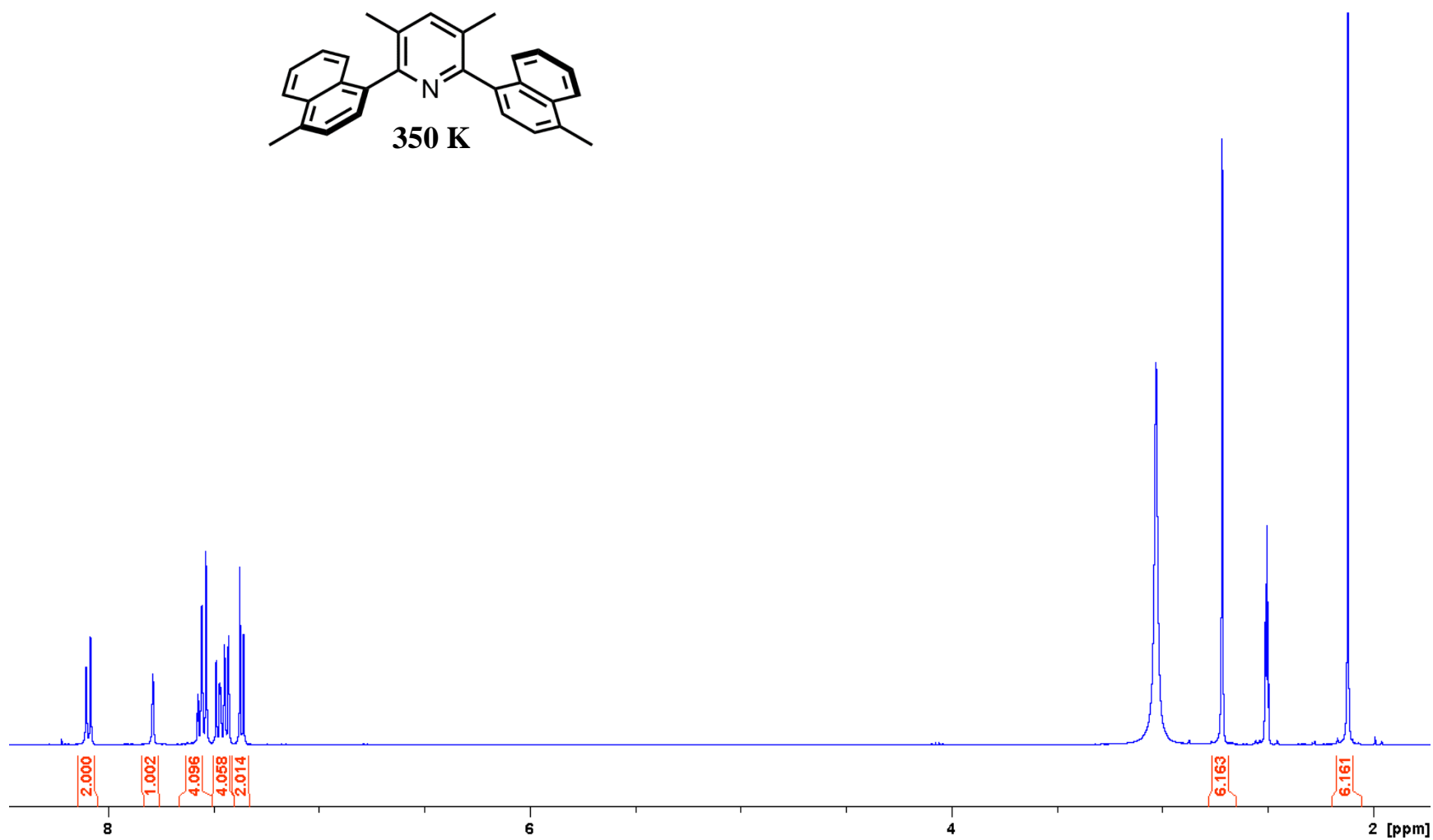
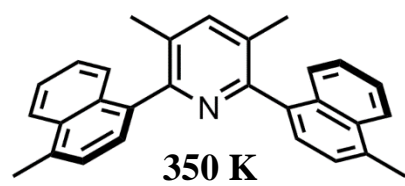




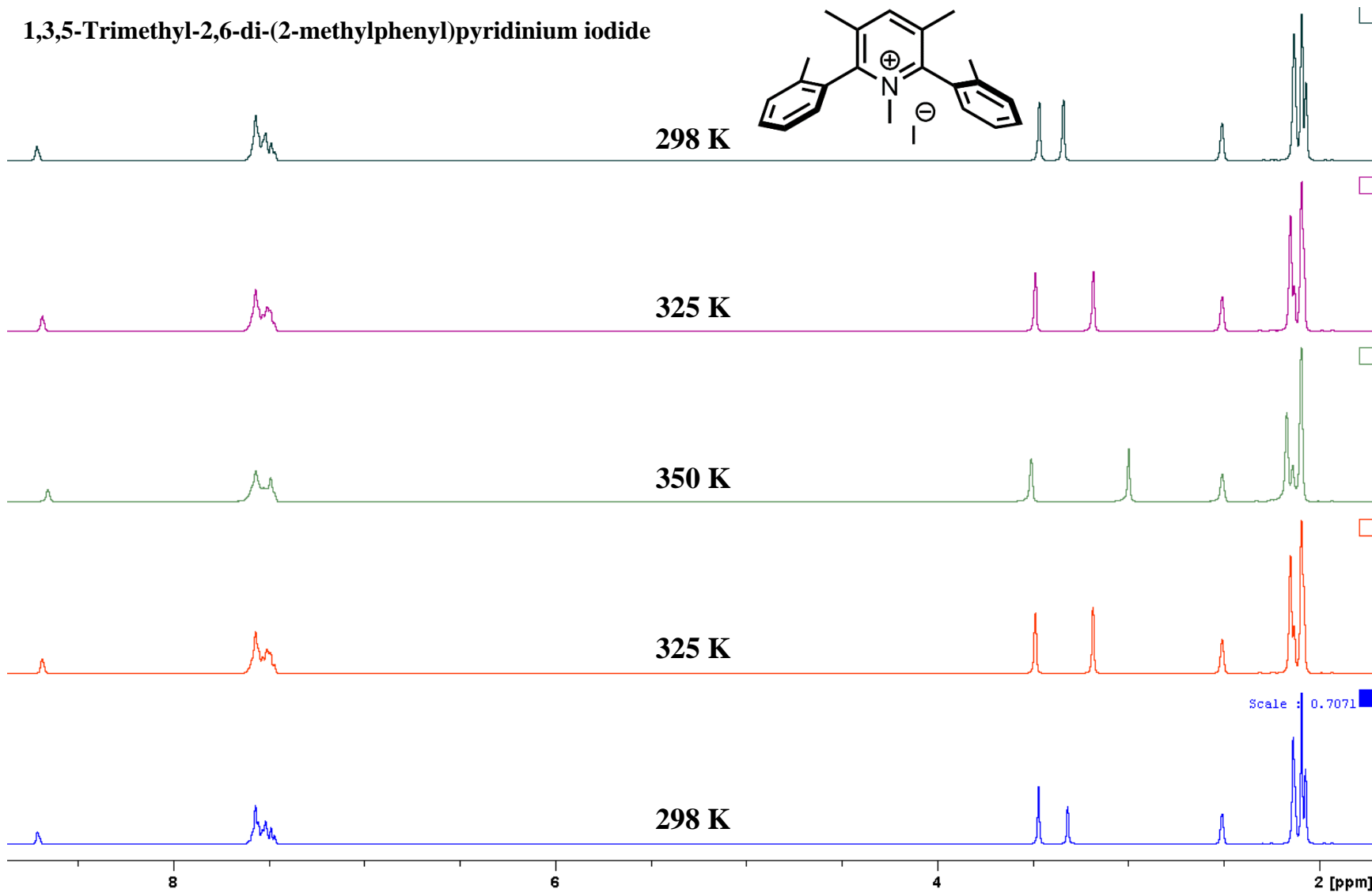
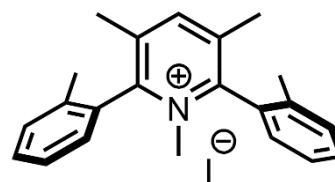


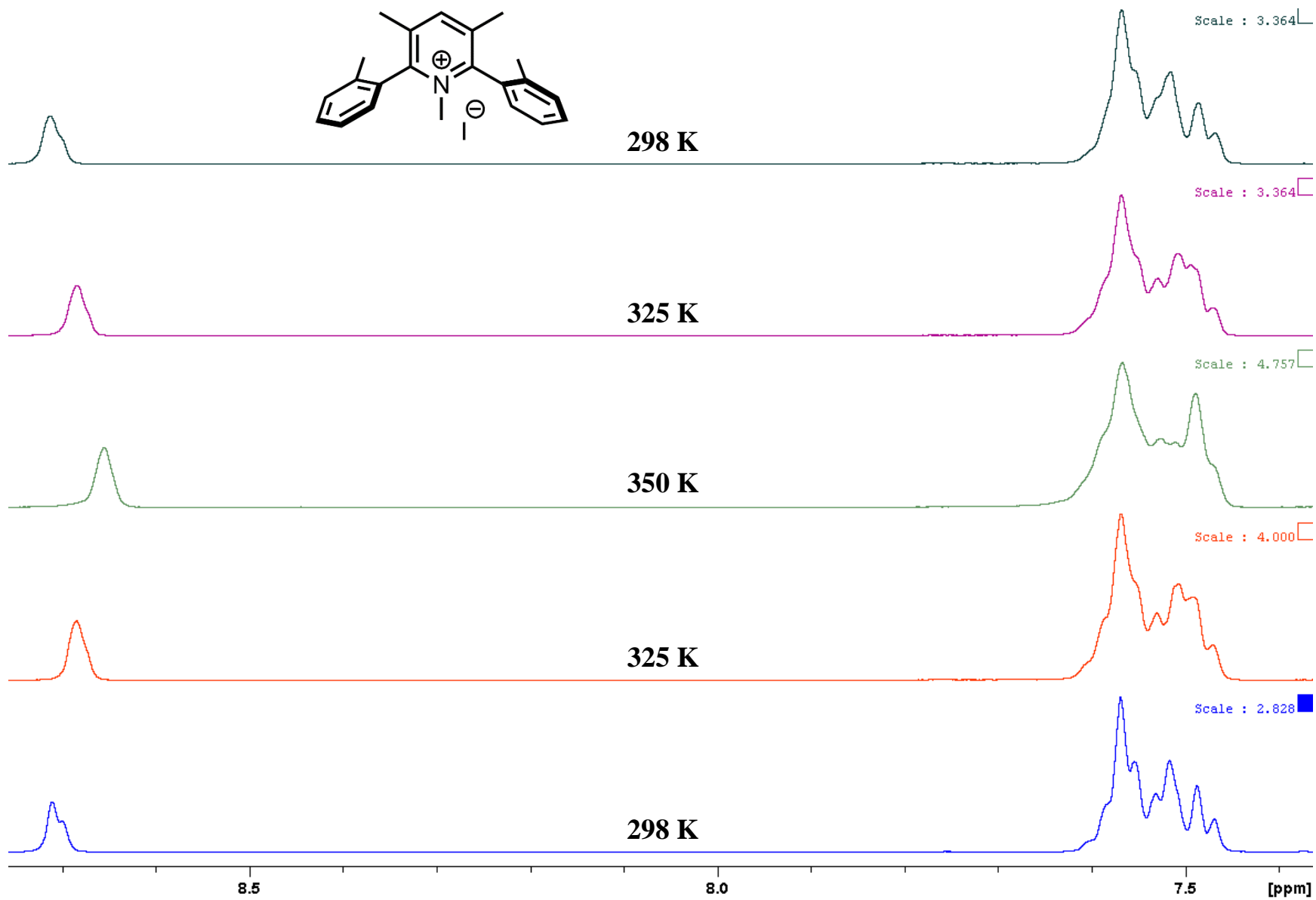


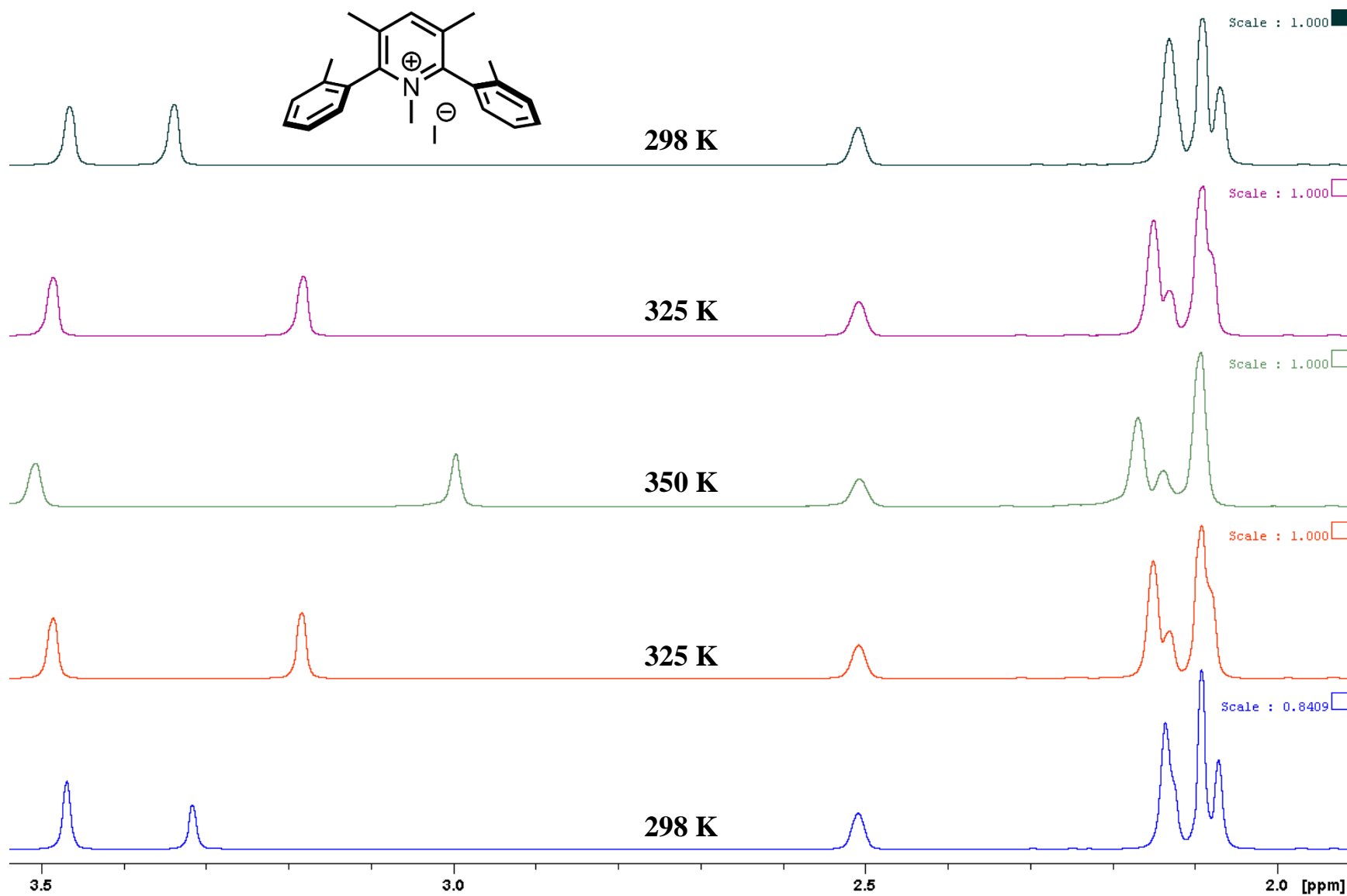


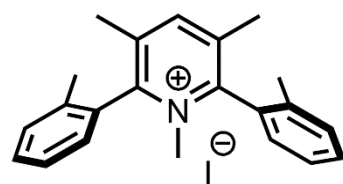


1,3,5-Trimethyl-2,6-di-(2-methylphenyl)pyridinium iodide

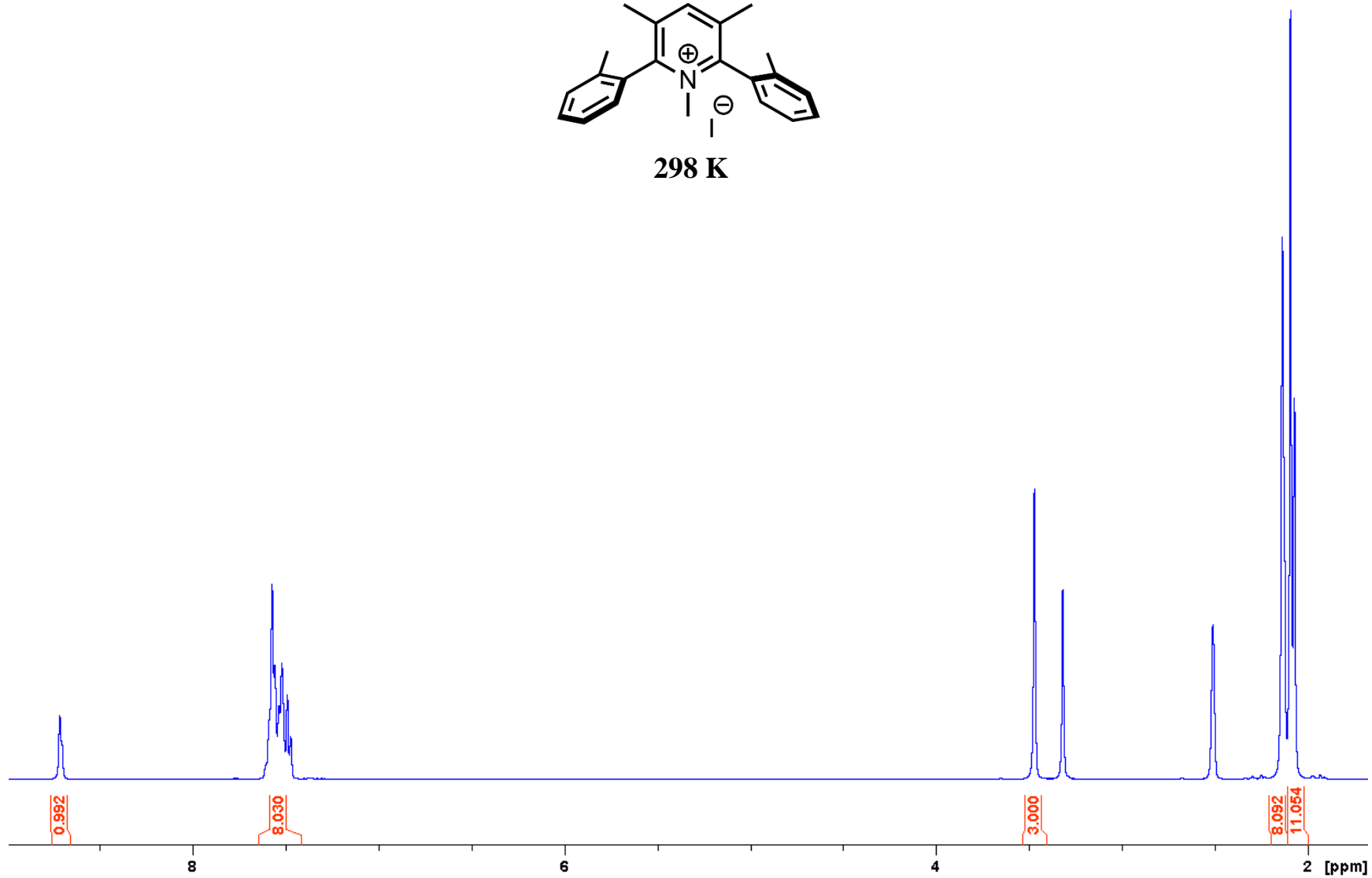


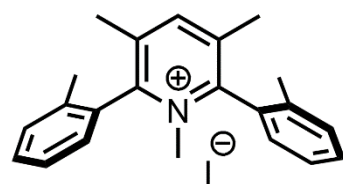




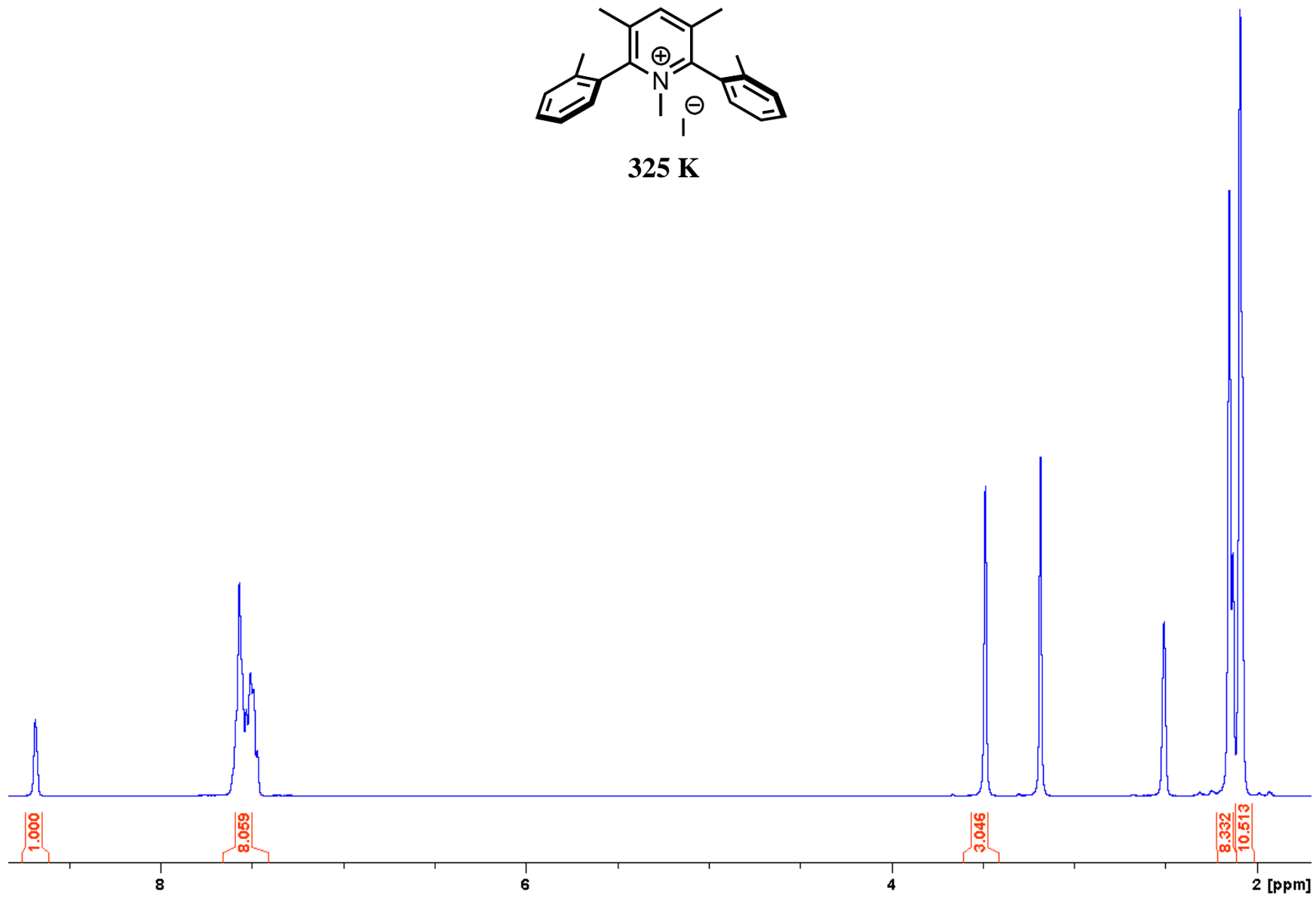


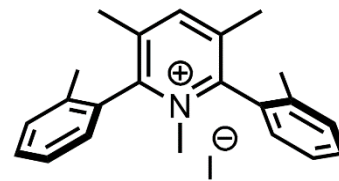
298 K



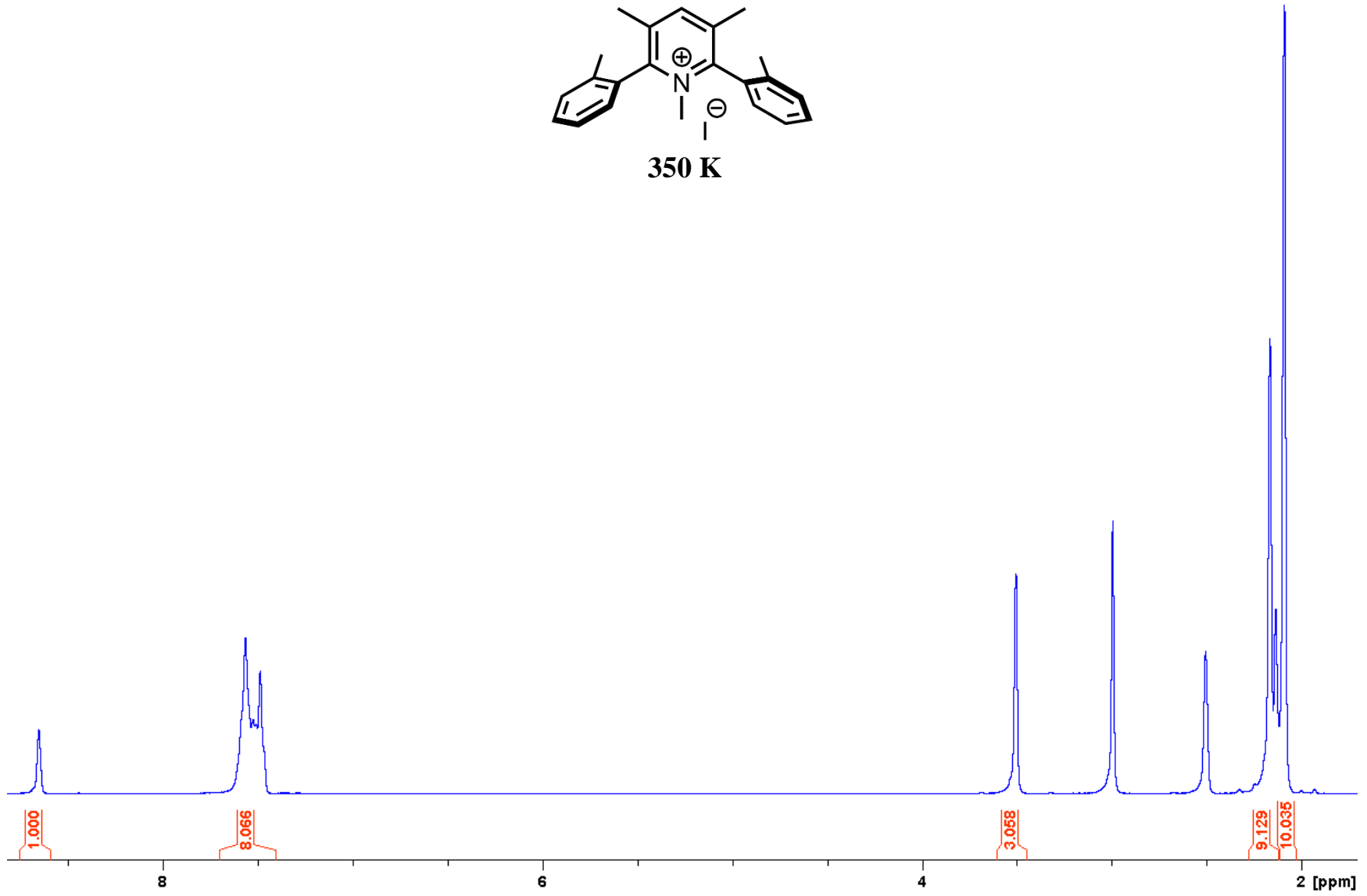


325 K

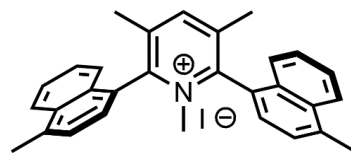




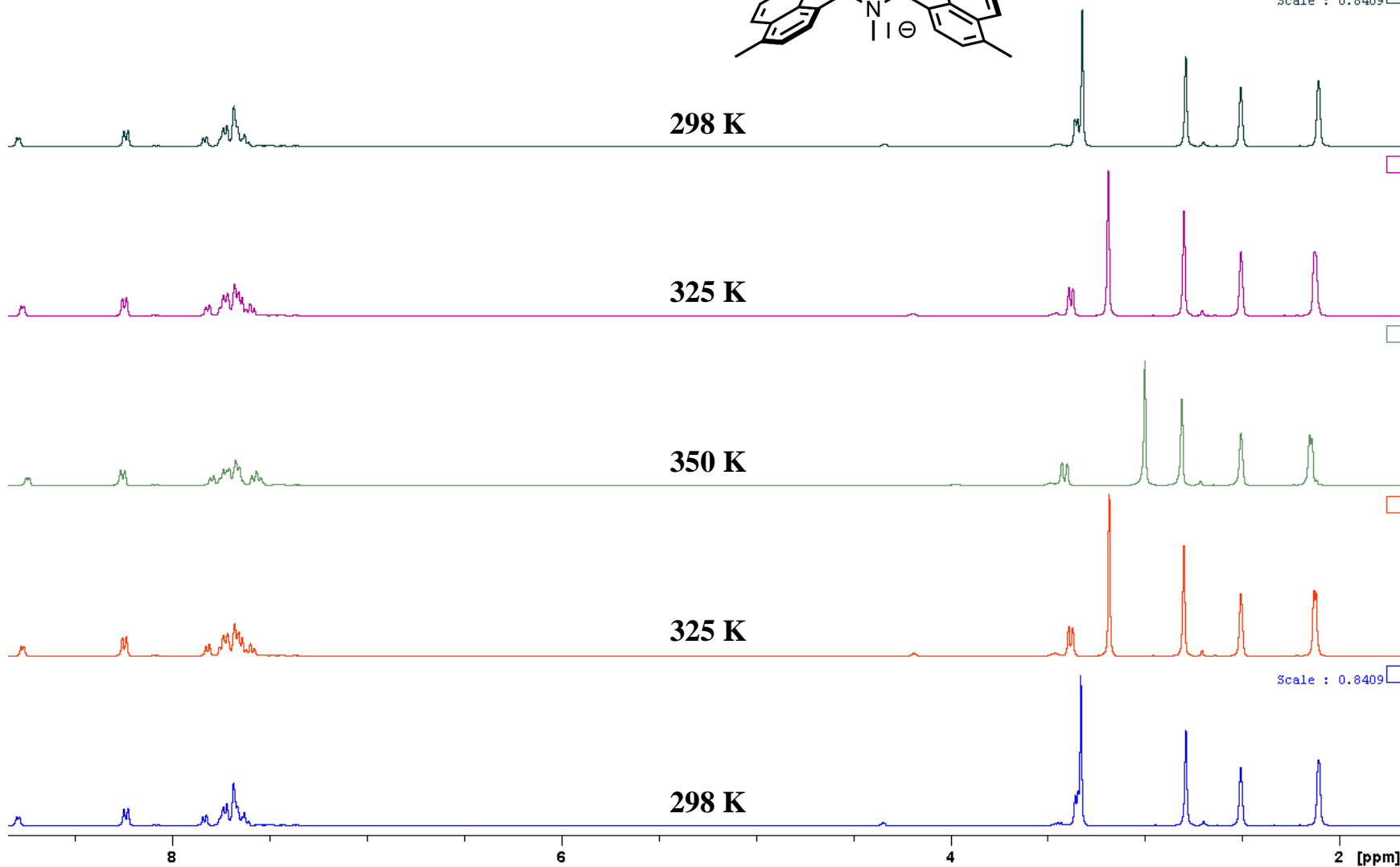
350 K

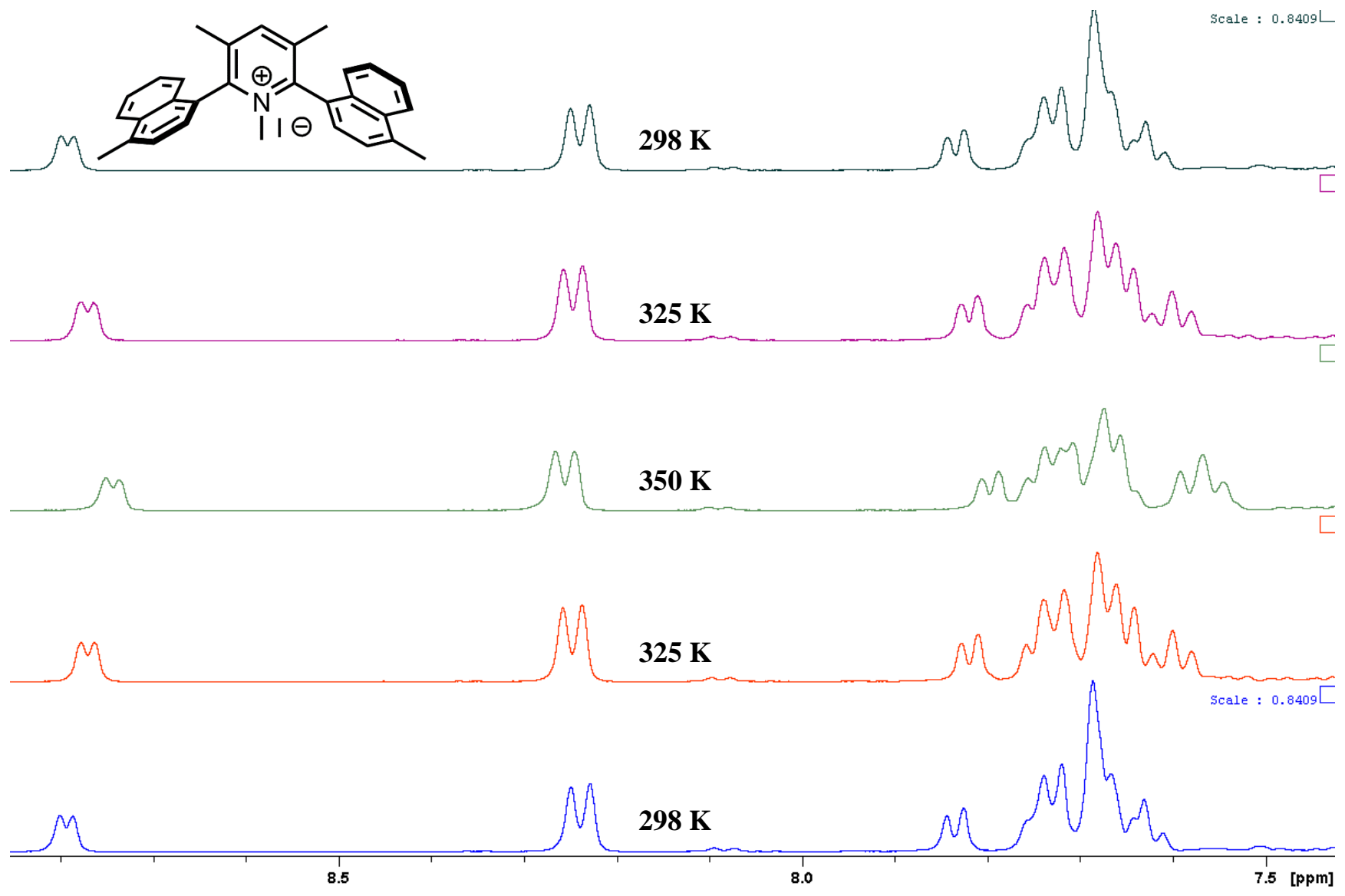


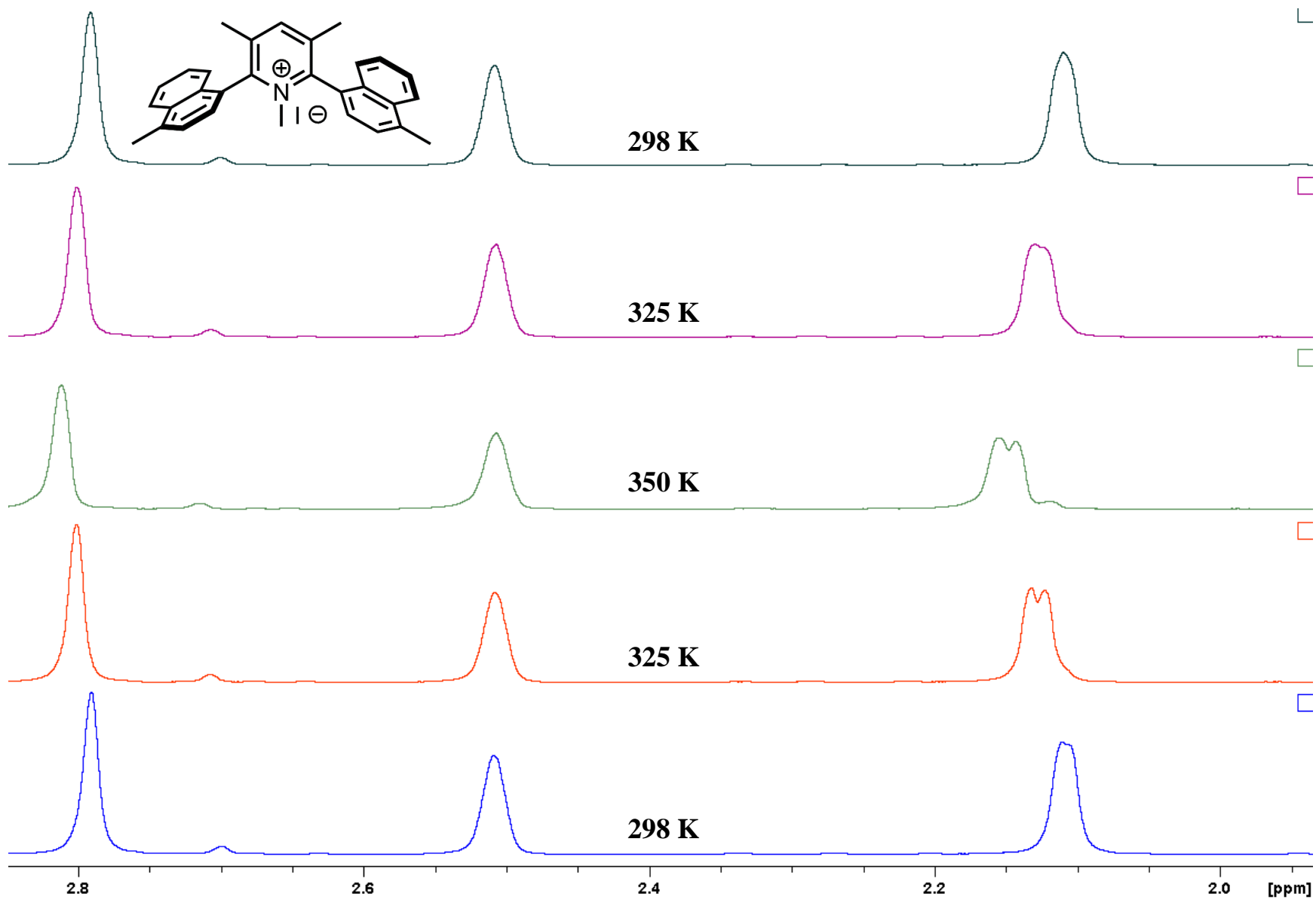
1,3,5-Dimethyl-2,6-Di(4-methylnaphthyl-1-yl)pyridinium iodide

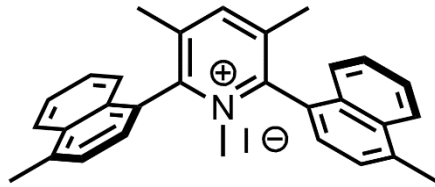


Scale : 0.8409

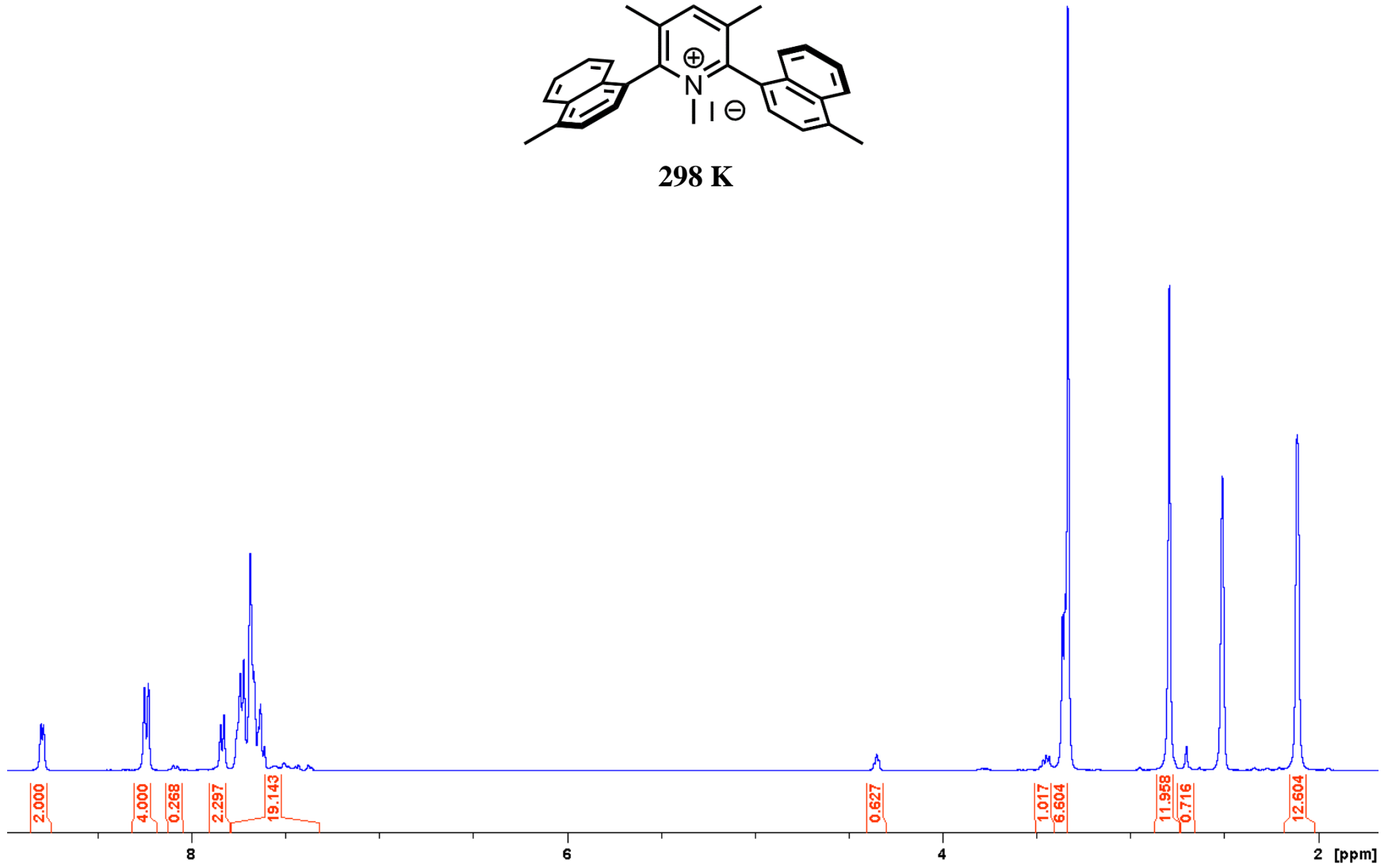


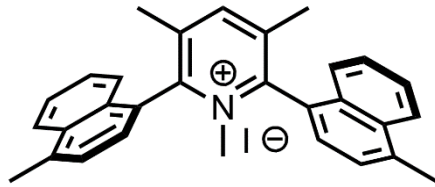




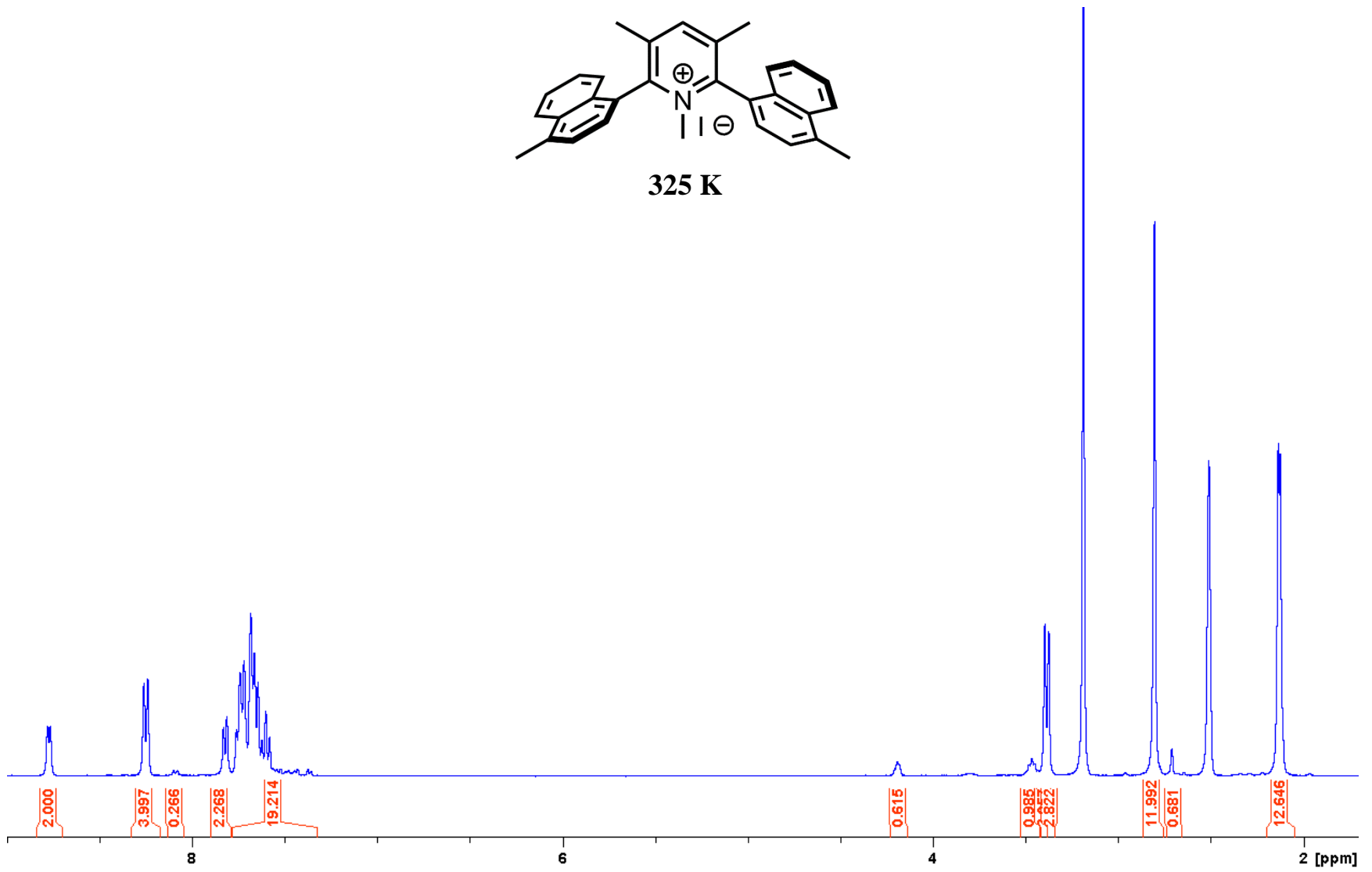


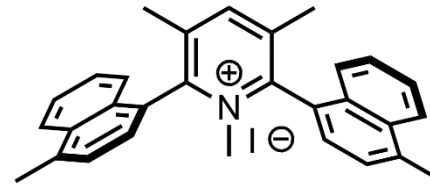
298 K



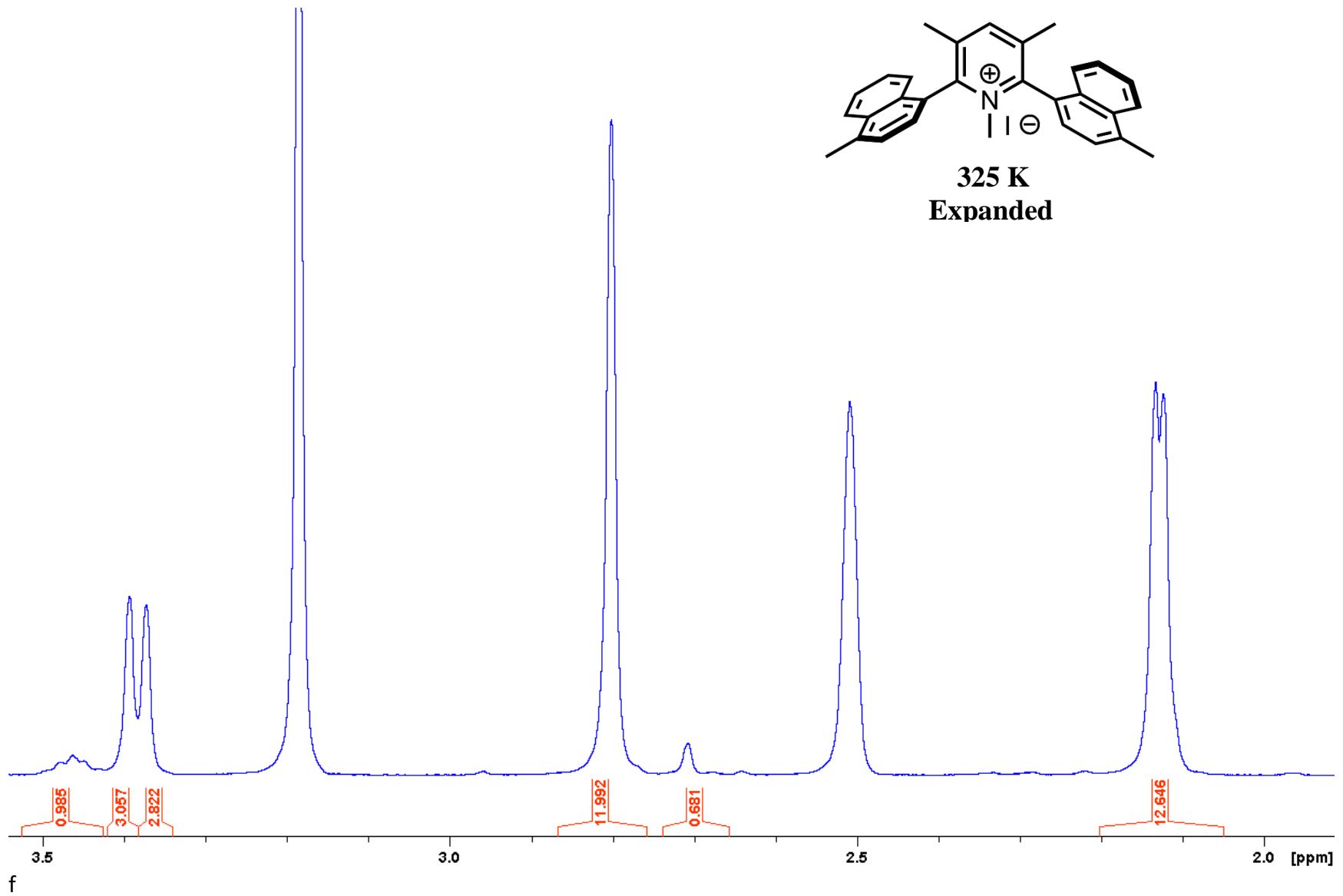


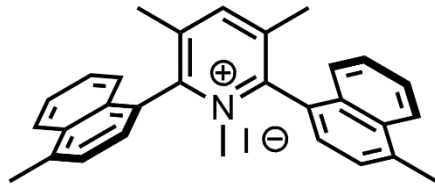
325 K



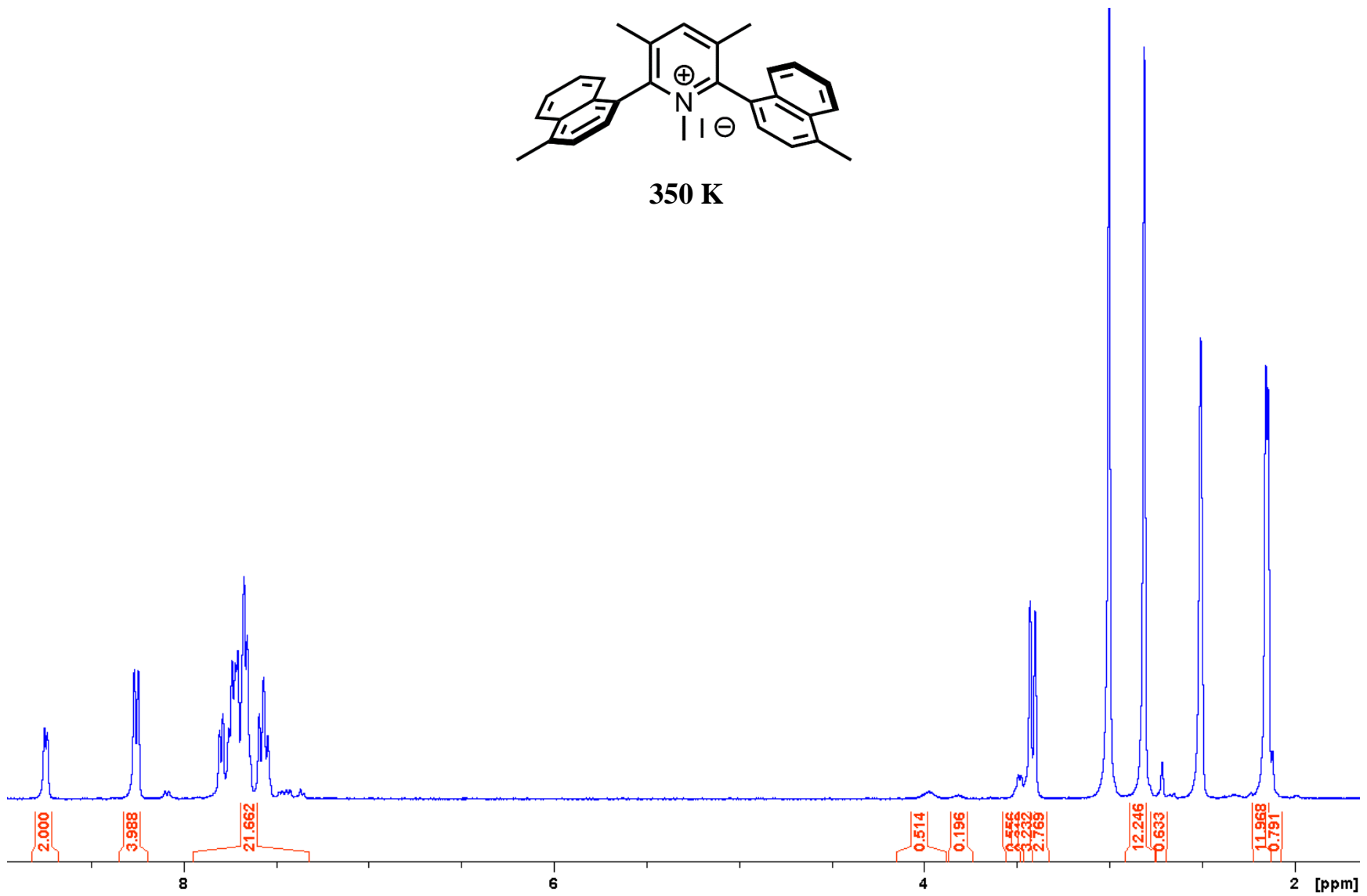


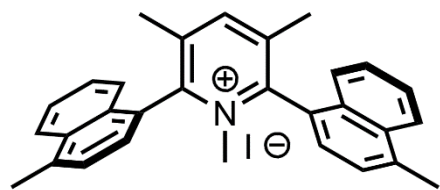
325 K
Expanded



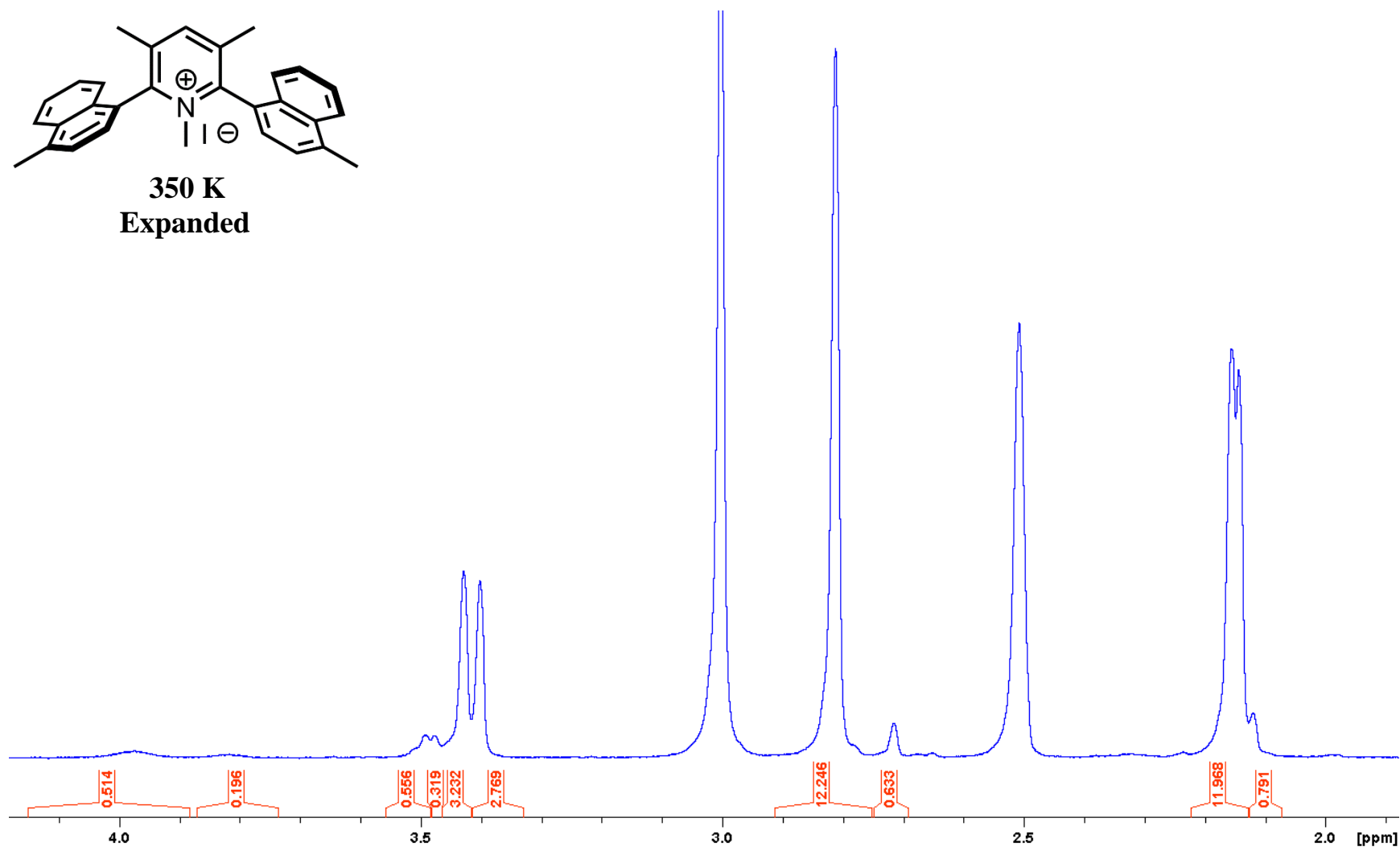


350 K

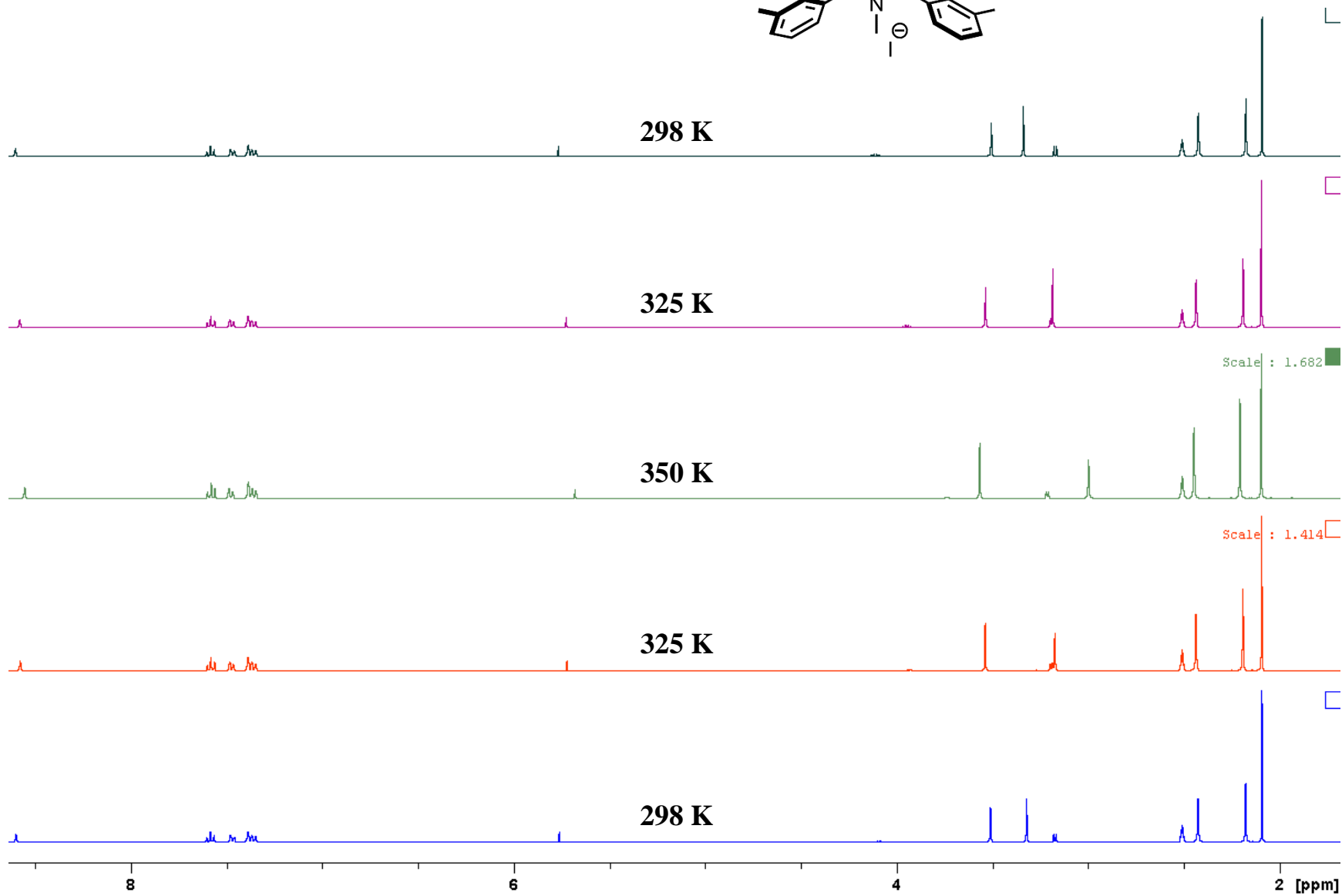
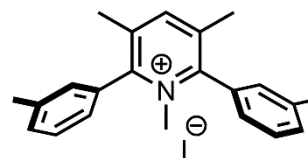


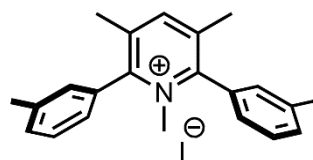


350 K
Expanded

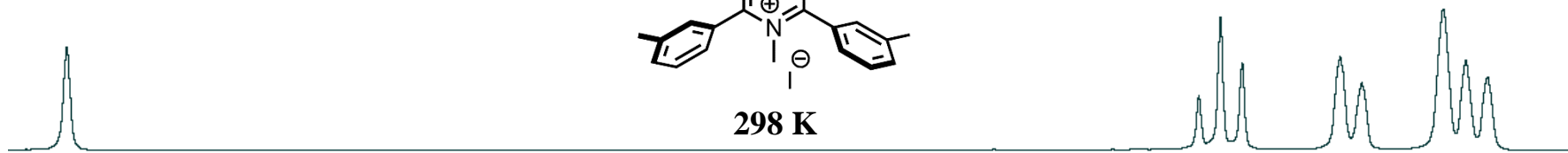


1,3,5-trimethyl-2,6-di-(3-methylphenyl)pyridinium iodide





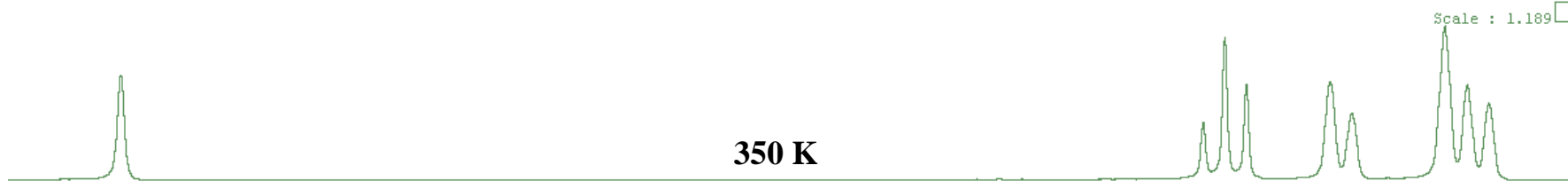
298 K



325 K



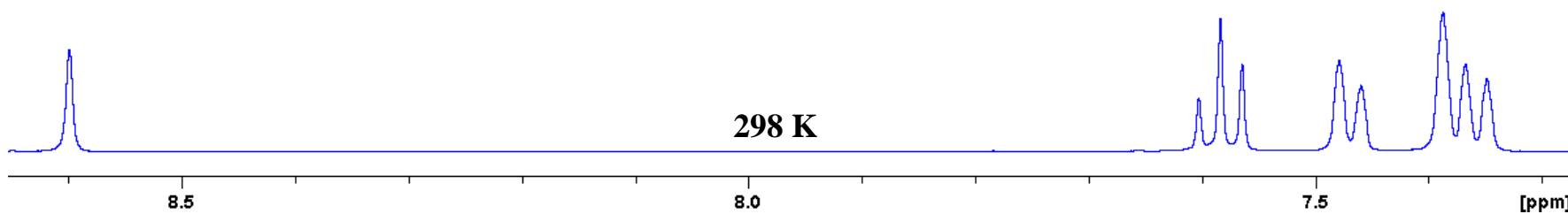
350 K

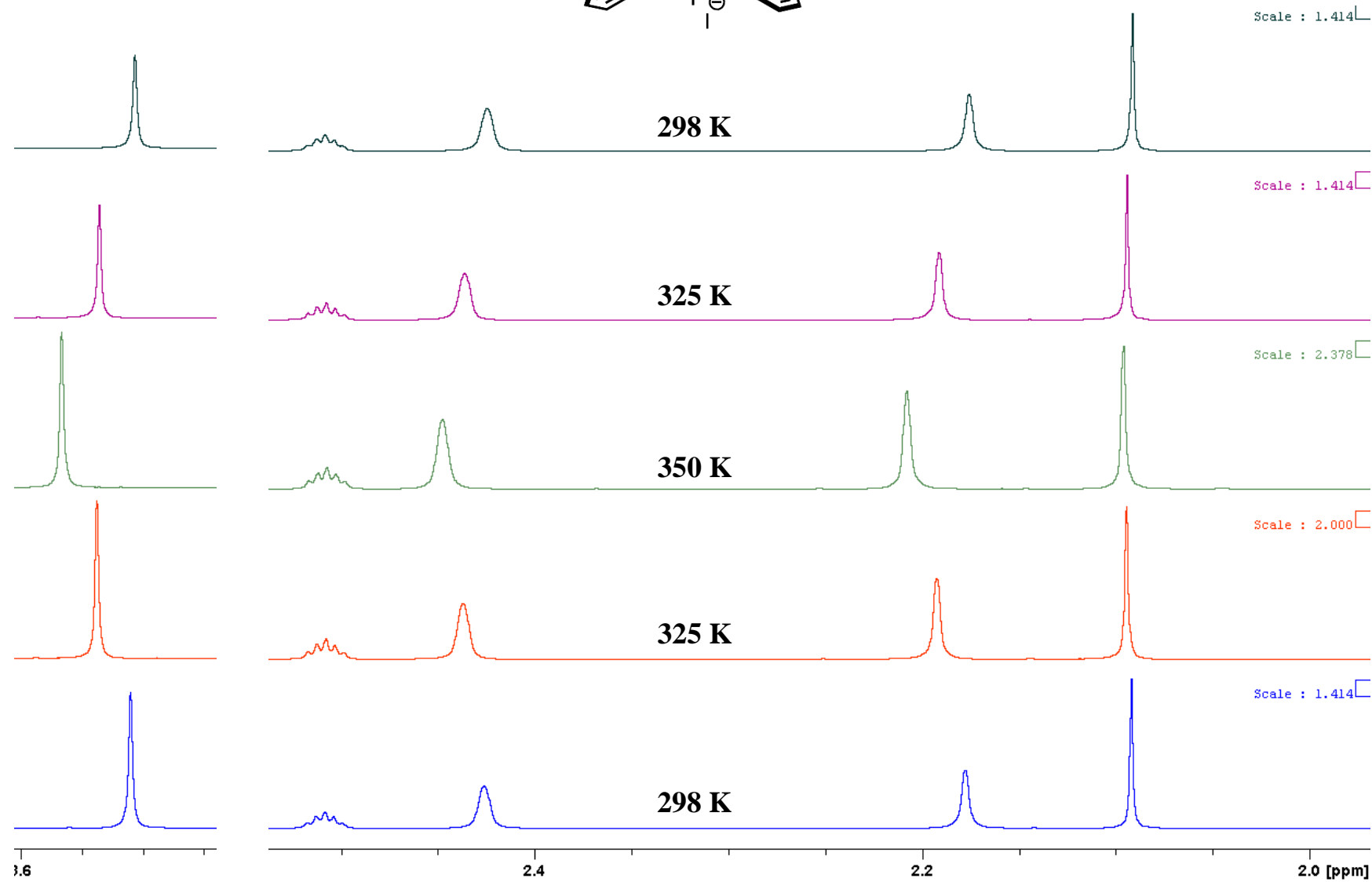
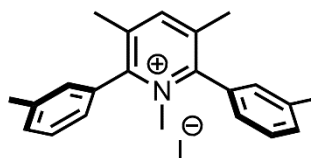


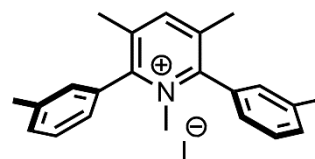
325 K



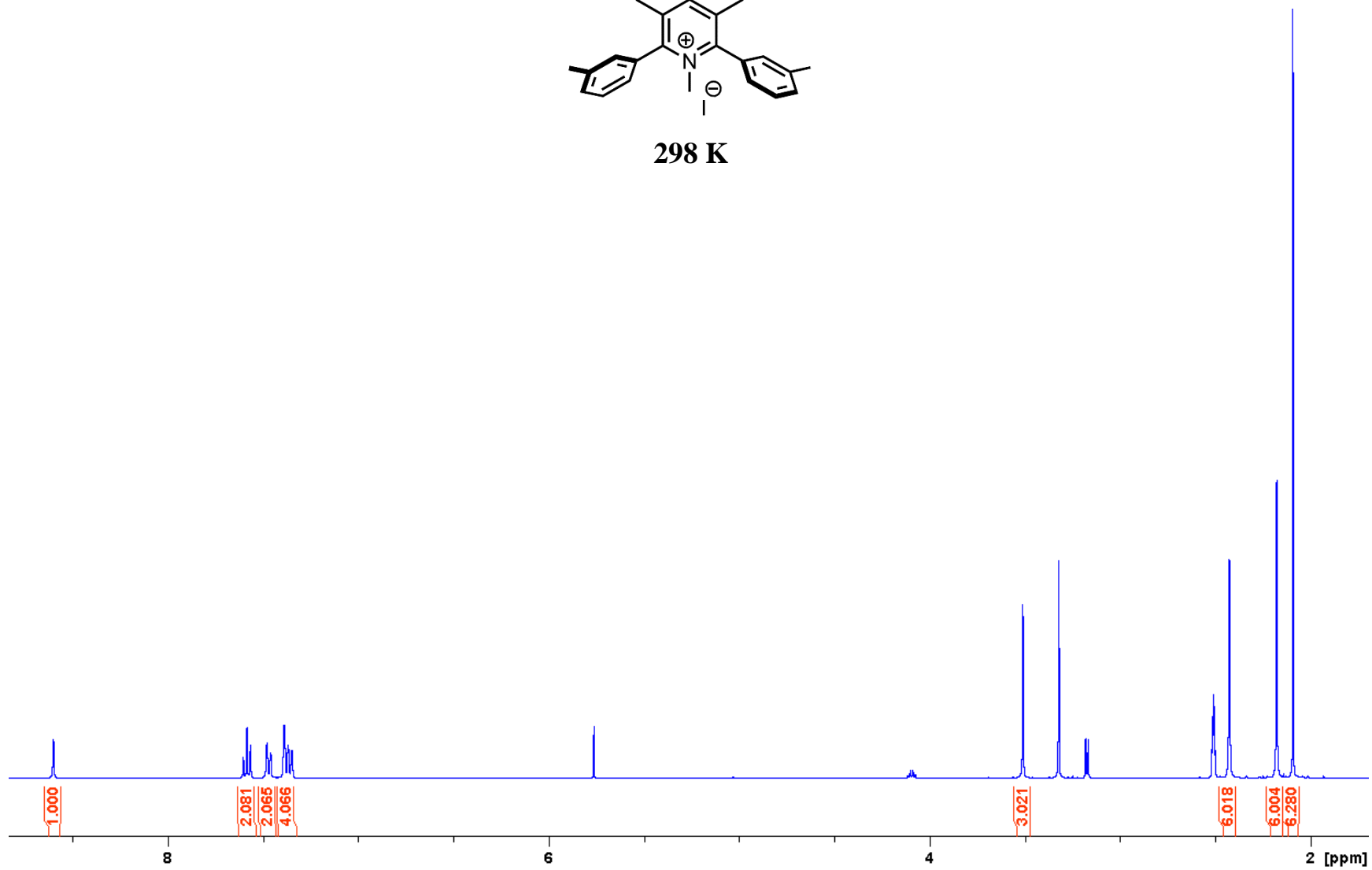
298 K

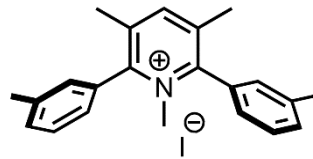




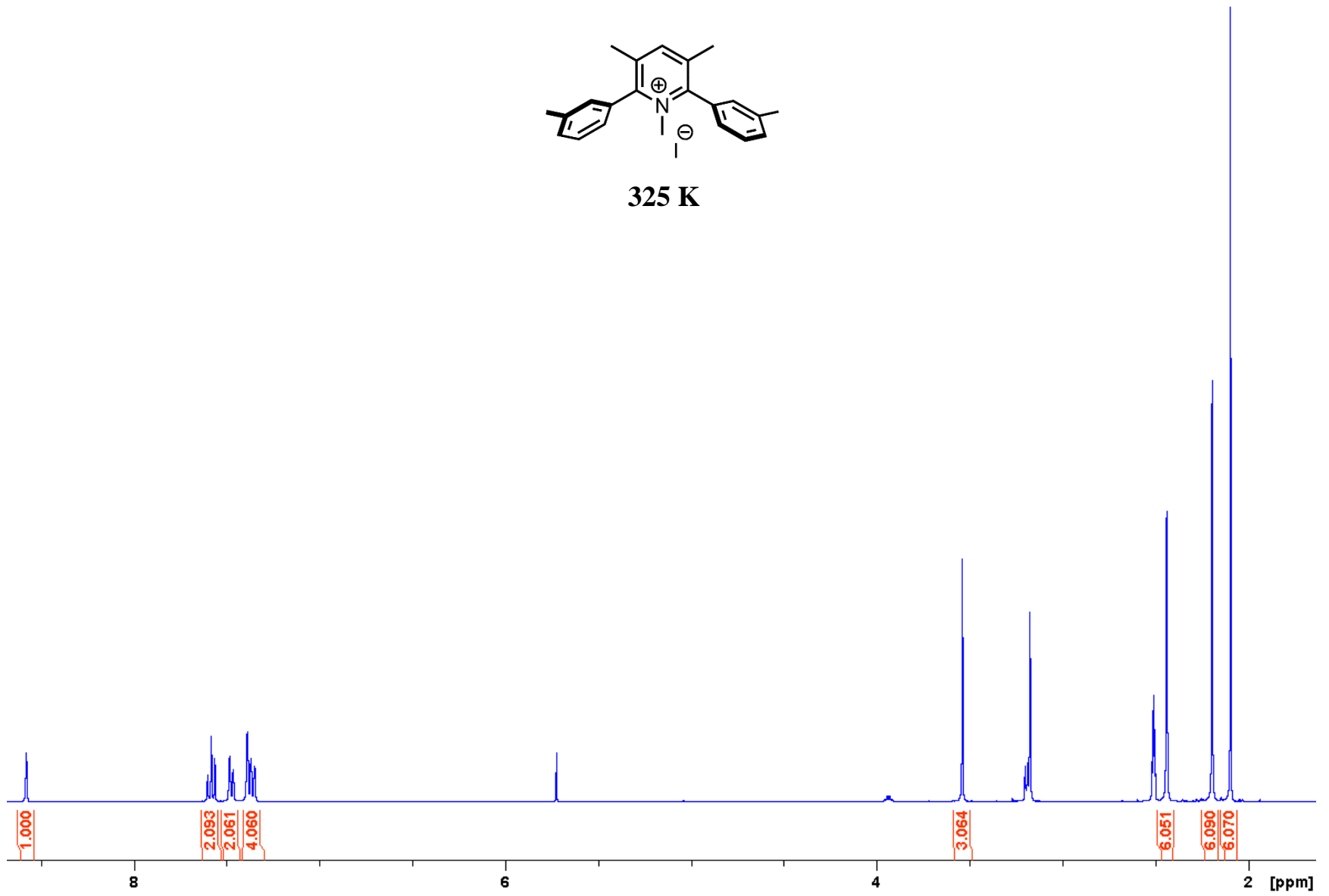


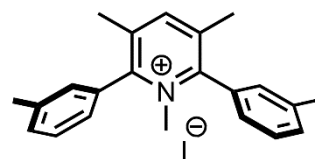
298 K



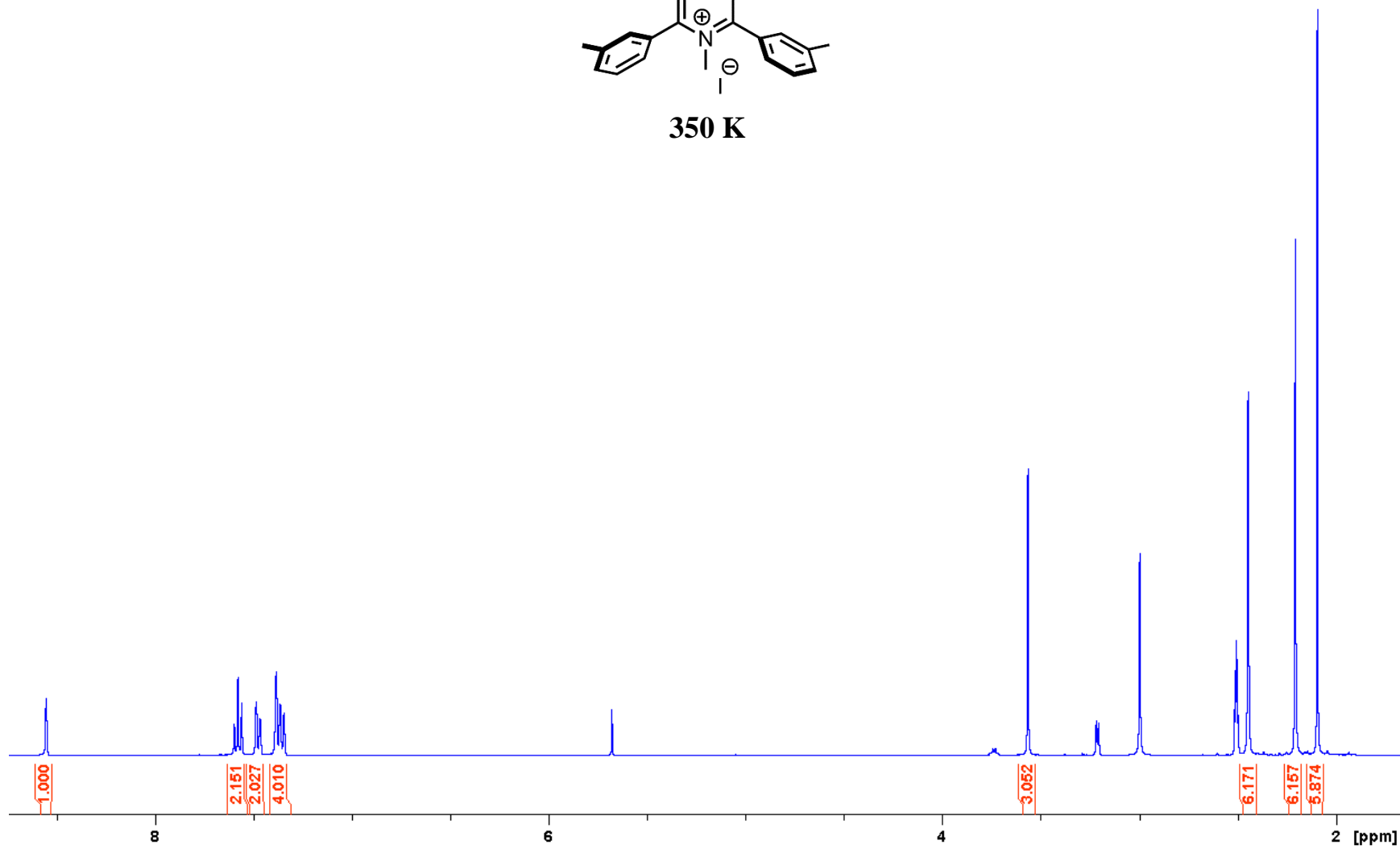


325 K





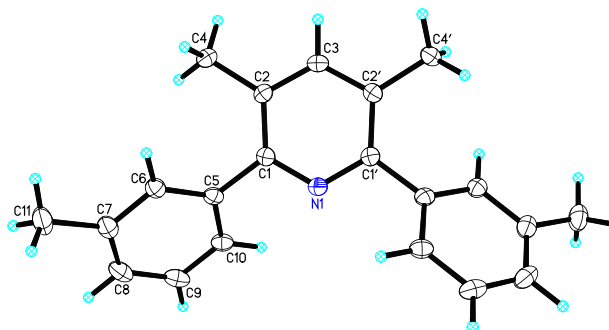
350 K



APPENDIX B: X-RAY DIFFRACTION DATA

Compound	Page
3,5-Dimethyl-2,6-di(3-methylphenyl)pyridine.....	104
<i>cis</i> - and <i>trans</i> 3,5-Dimethyl-2,6-di(2-methylphenyl)pyridine	111
<i>cis</i> -2,6-Di(2-isopropylphenyl)-3,5-dimethyl pyridine.....	127
<i>trans</i> -3,5-Dimethyl-2,6-di(4-methylnaphthyl-1-yl)pyridine unit cell A.....	137
<i>trans</i> -3,5-Dimethyl-2,6-di(4-methylnaphthyl-1-yl)pyridine unit cell B	147
<i>cis</i> -1,3,5-Trimethyl-2,6-di- <i>o</i> -tolylpyridinium iodide.....	166

3,5-Dimethyl-2,6-di(3-methylphenyl)pyridine



X-ray Data Collection, Structure Solution and Refinement.

A colorless crystal of approximate dimensions 0.322 x 0.380 x 0.548 mm was mounted on a glass fiber and transferred to a Bruker SMART APEX II diffractometer. The APEX2¹ program package was used to determine the unit-cell parameters and for data collection (10 sec/frame scan time for a sphere of diffraction data). The raw frame data was processed using SAINT² and SADABS³ to yield the reflection data file. Subsequent calculations were carried out using the SHELXTL⁴ program. The diffraction symmetry was *mmm* and the systematic absences were consistent with the orthorhombic space group *Pbcn* that was later determined to be correct.

The structure was solved by dual space methods and refined on F^2 by full-matrix least-squares techniques. The analytical scattering factors⁵ for neutral atoms were used throughout the analysis. Hydrogen atoms were located from a difference-Fourier map and refined (x, y, z and U_{iso}). The molecule was located on a two-fold rotation axis.

Least-squares analysis yielded $wR2 = 0.1132$ and $Goof = 1.039$ for 143 variables refined against 1987 data (0.74 Å), $R1 = 0.0413$ for those 1694 data with $I > 2.0\sigma(I)$.

References.

1. APEX2 Version 2014.11-0, Bruker AXS, Inc.; Madison, WI 2014.
2. SAINT Version 8.34a, Bruker AXS, Inc.; Madison, WI 2013.
3. Sheldrick, G. M. SADABS, Version 2014/5, Bruker AXS, Inc.; Madison, WI 2014.
4. Sheldrick, G. M. SHELXTL, Version 2014/7, Bruker AXS, Inc.; Madison, WI 2014.
5. International Tables for Crystallography 1992, Vol. C., Dordrecht: Kluwer Academic Publishers.

Definitions:

$$wR2 = [\sum[w(F_o^2 - F_c^2)^2] / \sum[w(F_o^2)^2]]^{1/2}$$

$$R1 = \sum||F_o| - |F_c|| / \sum|F_o|$$

$Goof = S = [\sum[w(F_o^2 - F_c^2)^2] / (n-p)]^{1/2}$ where n is the number of reflections and p is the total number of parameters refined. The thermal ellipsoid plot is shown at the 50% probability level.

Table 1. Crystal data and structure refinement.

Identification code	toh8 (Tae Oh)	
Empirical formula	C ₂₁ H ₂₁ N	
Formula weight	287.39	
Temperature	133(2) K	
Wavelength	0.71073 Å	
Crystal system	Orthorhombic	
Space group	<i>Pbcn</i>	
Unit cell dimensions	a = 23.404(2) Å	∠ = 90°.
	b = 8.7793(8) Å	∠ = 90°.
	c = 7.7596(7) Å	∠ = 90°.
Volume	1594.4(2) Å ³	
Z	4	
Density (calculated)	1.197 Mg/m ³	
Absorption coefficient	0.069 mm ⁻¹	
F(000)	616	
Crystal color	colorless	
Crystal size	0.548 x 0.380 x 0.322 mm ³	
Theta range for data collection	1.740 to 28.746°	
Index ranges	-30 ≤ h ≤ 31, -11 ≤ k ≤ 11, -10 ≤ l ≤ 10	
Reflections collected	13138	
Independent reflections	1987 [R(int) = 0.0312]	
Completeness to theta = 25.500°	100.0 %	
Absorption correction	Semi-empirical from equivalents	
Max. and min. transmission	0.8621 and 0.7777	
Refinement method	Full-matrix least-squares on F ²	
Data / restraints / parameters	1987 / 0 / 143	
Goodness-of-fit on F ²	1.039	
Final R indices [I > 2σ(I) = 1694 data]	R1 = 0.0413, wR2 = 0.1073	
R indices (all data, 0.74 Å)	R1 = 0.0496, wR2 = 0.1132	
Largest diff. peak and hole	0.345 and -0.216 e.Å ⁻³	

Table 2. Atomic coordinates ($\times 10^4$) and equivalent isotropic displacement parameters ($\text{\AA}^2 \times 10^3$). $U(\text{eq})$ is defined as one third of the trace of the orthogonalized U^{ij} tensor.

	x	y	z	$U(\text{eq})$
N(1)	5000	2124(1)	2500	18(1)
C(1)	5445(1)	1363(1)	1831(1)	17(1)
C(2)	5470(1)	-237(1)	1823(1)	17(1)
C(3)	5000	-993(2)	2500	18(1)
C(4)	5961(1)	-1150(1)	1111(2)	22(1)
C(5)	5888(1)	2371(1)	1047(1)	18(1)
C(6)	6474(1)	2156(1)	1303(1)	20(1)
C(7)	6877(1)	3145(1)	578(1)	24(1)
C(8)	6682(1)	4337(1)	-448(2)	27(1)
C(9)	6102(1)	4573(1)	-706(2)	26(1)
C(10)	5707(1)	3610(1)	56(1)	21(1)
C(11)	7504(1)	2949(2)	938(2)	32(1)

Table 3. Bond lengths [\AA] and angles [$^\circ$].

N(1)-C(1)	1.3426(12)
N(1)-C(1)#1	1.3427(12)
C(1)-C(2)	1.4059(15)
C(1)-C(5)	1.4925(14)
C(2)-C(3)	1.3882(12)
C(2)-C(4)	1.5056(14)
C(3)-C(2)#1	1.3882(12)
C(5)-C(6)	1.3974(15)
C(5)-C(10)	1.3979(15)
C(6)-C(7)	1.3995(15)
C(7)-C(8)	1.3920(17)
C(7)-C(11)	1.5047(17)
C(8)-C(9)	1.3866(17)
C(9)-C(10)	1.3859(16)
C(1)-N(1)-C(1)#1	120.30(13)
N(1)-C(1)-C(2)	122.07(10)
N(1)-C(1)-C(5)	113.70(9)
C(2)-C(1)-C(5)	124.18(9)
C(3)-C(2)-C(1)	116.34(10)
C(3)-C(2)-C(4)	119.26(10)
C(1)-C(2)-C(4)	124.39(9)
C(2)#1-C(3)-C(2)	122.84(14)
C(6)-C(5)-C(10)	118.72(10)
C(6)-C(5)-C(1)	122.92(9)
C(10)-C(5)-C(1)	118.34(9)
C(5)-C(6)-C(7)	121.34(10)
C(8)-C(7)-C(6)	118.39(11)
C(8)-C(7)-C(11)	120.77(11)
C(6)-C(7)-C(11)	120.81(11)
C(9)-C(8)-C(7)	121.02(11)
C(10)-C(9)-C(8)	120.01(11)
C(9)-C(10)-C(5)	120.47(10)

Symmetry transformations used to generate equivalent atoms:

#1 $-x+1, y, -z+1/2$

Table 4. Anisotropic displacement parameters ($\text{\AA}^2 \times 10^3$) for toh8. The anisotropic displacement factor exponent takes the form: $-2\pi^2 [h^2 a^{*2}U^{11} + \dots + 2 h k a^* b^* U^{12}]$

	U ¹¹	U ²²	U ³³	U ²³	U ¹³	U ¹²
N(1)	18(1)	16(1)	18(1)	0	-2(1)	0
C(1)	17(1)	18(1)	16(1)	0(1)	-3(1)	-1(1)
C(2)	17(1)	19(1)	16(1)	-1(1)	-4(1)	2(1)
C(3)	22(1)	15(1)	17(1)	0	-5(1)	0
C(4)	22(1)	19(1)	26(1)	-2(1)	1(1)	3(1)
C(5)	22(1)	16(1)	16(1)	-4(1)	-1(1)	-2(1)
C(6)	21(1)	20(1)	19(1)	-2(1)	0(1)	-2(1)
C(7)	24(1)	26(1)	21(1)	-6(1)	3(1)	-5(1)
C(8)	35(1)	24(1)	23(1)	-1(1)	5(1)	-11(1)
C(9)	38(1)	18(1)	21(1)	2(1)	-2(1)	-4(1)
C(10)	27(1)	17(1)	20(1)	-2(1)	-3(1)	-1(1)
C(11)	22(1)	40(1)	35(1)	-6(1)	5(1)	-7(1)

Table 5. Hydrogen coordinates ($\times 10^4$) and isotropic displacement parameters ($\text{\AA}^2 \times 10^3$).

	x	y	z	U(eq)
H(3)	5000	-2100(20)	2500	25(5)
H(4A)	5816(6)	-2153(17)	719(19)	30(4)
H(4B)	6154(6)	-634(16)	130(20)	30(4)
H(4C)	6252(6)	-1343(17)	2010(20)	36(4)
H(6)	6615(5)	1290(14)	2033(16)	14(3)
H(8)	6963(6)	5029(18)	-1010(20)	33(4)
H(9)	5978(6)	5392(16)	-1440(20)	32(4)
H(10)	5290(5)	3767(15)	-101(17)	25(3)
H(11A)	7729(8)	3100(20)	-50(30)	64(6)
H(11B)	7595(8)	1910(20)	1410(30)	67(6)
H(11C)	7648(8)	3640(20)	1840(30)	71(6)

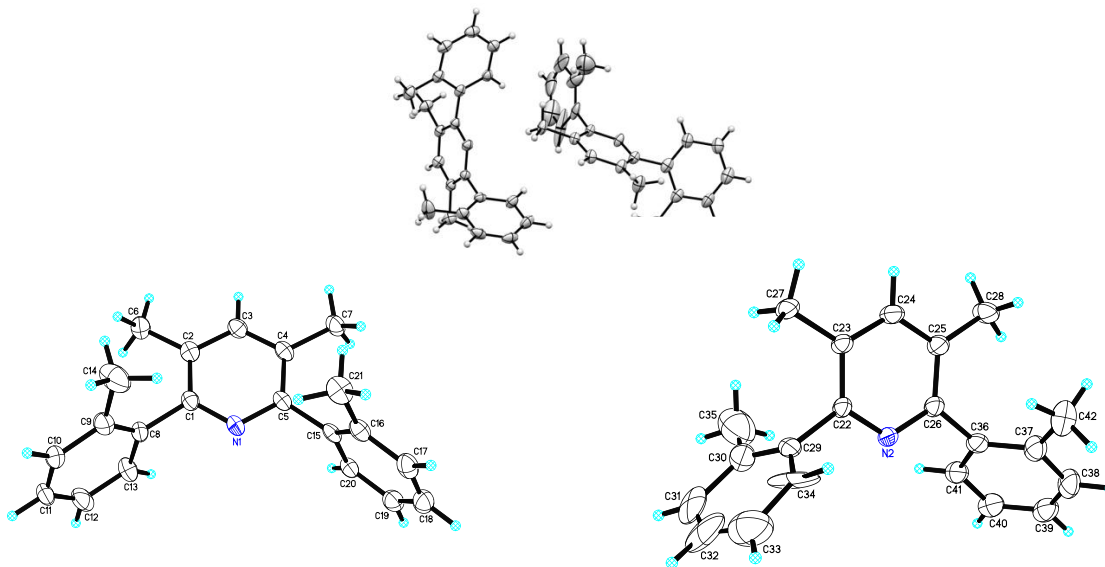
Table 6. Torsion angles [°].

C(1)#1-N(1)-C(1)-C(2)	-0.98(7)
C(1)#1-N(1)-C(1)-C(5)	176.55(9)
N(1)-C(1)-C(2)-C(3)	1.86(13)
C(5)-C(1)-C(2)-C(3)	-175.40(8)
N(1)-C(1)-C(2)-C(4)	-179.22(9)
C(5)-C(1)-C(2)-C(4)	3.52(16)
C(1)-C(2)-C(3)-C(2)#1	-0.88(6)
C(4)-C(2)-C(3)-C(2)#1	-179.86(10)
N(1)-C(1)-C(5)-C(6)	136.20(10)
C(2)-C(1)-C(5)-C(6)	-46.33(15)
N(1)-C(1)-C(5)-C(10)	-41.80(12)
C(2)-C(1)-C(5)-C(10)	135.67(11)
C(10)-C(5)-C(6)-C(7)	-0.57(16)
C(1)-C(5)-C(6)-C(7)	-178.56(10)
C(5)-C(6)-C(7)-C(8)	-1.50(16)
C(5)-C(6)-C(7)-C(11)	176.86(11)
C(6)-C(7)-C(8)-C(9)	1.92(17)
C(11)-C(7)-C(8)-C(9)	-176.44(11)
C(7)-C(8)-C(9)-C(10)	-0.24(18)
C(8)-C(9)-C(10)-C(5)	-1.90(17)
C(6)-C(5)-C(10)-C(9)	2.29(16)
C(1)-C(5)-C(10)-C(9)	-179.63(10)

Symmetry transformations used to generate equivalent atoms:

#1 -x+1,y,-z+1/2

cis- and *trans* 3,5-Dimethyl-2,6-di(2-methylphenyl)pyridine



X-ray Data Collection, Structure Solution and Refinement.

A colorless crystal of approximate dimensions 0.349 x 0.398 x 0.412 mm was mounted on a glass fiber and transferred to a Bruker SMART APEX II diffractometer. The APEX2¹ program package was used to determine the unit-cell parameters and for data collection (10 sec/frame scan time for a sphere of diffraction data). The raw frame data was processed using SAINT² and SADABS³ to yield the reflection data file. Subsequent calculations were carried out using the SHELXTL⁴ program. The diffraction symmetry was $2/m$ and the systematic absences were consistent with the monoclinic space group $P2_1/c$ that was later determined to be correct.

The structure was solved by dual space methods and refined on F^2 by full-matrix least-squares techniques. The analytical scattering factors⁵ for neutral atoms were used throughout the analysis. Hydrogen atoms were included using a riding model. There were two molecules of the formula-unit present ($Z = 8$).

Least-squares analysis yielded $wR2 = 0.2455$ and $Goof = 1.032$ for 405 variables refined against 6026 data (0.83 \AA), $R1 = 0.0880$ for those 5006 data with $I > 2.0\sigma(I)$.

The molecule defined by atoms N(2)-C(42) was not well resolved. It is probable that some of the atoms (C(29)-C(35)) are disordered, however, a good disordered model could not be refined.

References.

1. APEX2 Version 2014.11-0, Bruker AXS, Inc.; Madison, WI 2014.
2. SAINT Version 8.34a, Bruker AXS, Inc.; Madison, WI 2013.

3. Sheldrick, G. M. SADABS, Version 2014/5, Bruker AXS, Inc.; Madison, WI 2014.
 4. Sheldrick, G. M. SHELXTL, Version 2014/7, Bruker AXS, Inc.; Madison, WI 2014
 5. International Tables for Crystallography 1992, Vol. C., Dordrecht: Kluwer Academic Publishers.
-

Definitions:

$$wR2 = [\Sigma[w(F_o^2 - F_c^2)^2] / \Sigma[w(F_o^2)^2]]^{1/2}$$

$$R1 = \Sigma||F_o| - |F_c|| / \Sigma|F_o|$$

Goof = S = $[\Sigma[w(F_o^2 - F_c^2)^2] / (n-p)]^{1/2}$ where n is the number of reflections and p is the total number of parameters refined.

The thermal ellipsoid plot is shown at the 50% probability level.

Table 1. Crystal data and structure refinement.

Identification code	toh9 (Tae Oh)	
Empirical formula	C ₂₁ H ₂₁ N	
Formula weight	287.39	
Temperature	88(2) K	
Wavelength	0.71073 Å	
Crystal system	Monoclinic	
Space group	P2 ₁ /c	
Unit cell dimensions	a = 10.3366(4) Å	β = 90°.
	b = 13.3041(5) Å	γ = 91.2328(7)°.
	c = 23.8255(9) Å	α = 90°.
Volume	3275.7(2) Å ³	
Z	8	
Density (calculated)	1.165 Mg/m ³	
Absorption coefficient	0.067 mm ⁻¹	
F(000)	1232	
Crystal color	colorless	
Crystal size	0.412 x 0.398 x 0.349 mm ³	
Theta range for data collection	1.710 to 25.398°	
Index ranges	-12 ≤ h ≤ 12, -16 ≤ k ≤ 15, -28 ≤ l ≤ 28	
Reflections collected	35004	
Independent reflections	6026 [R(int) = 0.0310]	
Completeness to theta = 25.398°	99.7 %	
Absorption correction	Semi-empirical from equivalents	
Max. and min. transmission	0.8620 and 0.8404	
Refinement method	Full-matrix least-squares on F ²	
Data / restraints / parameters	6026 / 0 / 405	
Goodness-of-fit on F ²	1.032	
Final R indices [I > 2σ(I) = 5006 data]	R1 = 0.0880, wR2 = 0.2318	
R indices (all data, 0.83 Å)	R1 = 0.1017, wR2 = 0.2455	
Largest diff. peak and hole	1.748 and -0.627 e.Å ⁻³	

Table 2. Atomic coordinates ($\times 10^4$) and equivalent isotropic displacement parameters ($\text{\AA}^2 \times 10^3$). $U(\text{eq})$ is defined as one third of the trace of the orthogonalized U^{ij} tensor.

	x	y	z	$U(\text{eq})$
N(1)	751(2)	8599(2)	1346(1)	25(1)
C(1)	1798(3)	8522(2)	1024(1)	24(1)
C(2)	2143(3)	9255(2)	633(1)	25(1)
C(3)	1326(3)	10085(2)	581(1)	26(1)
C(4)	233(3)	10179(2)	903(1)	24(1)
C(5)	-15(3)	9413(2)	1290(1)	23(1)
C(6)	3343(3)	9153(2)	290(1)	32(1)
C(7)	-647(3)	11082(2)	847(1)	31(1)
C(8)	2605(3)	7604(2)	1126(1)	26(1)
C(9)	2478(3)	6751(2)	787(1)	34(1)
C(10)	3241(4)	5913(3)	916(1)	37(1)
C(11)	4113(3)	5921(3)	1360(2)	37(1)
C(12)	4233(3)	6766(3)	1697(2)	40(1)
C(13)	3469(3)	7600(3)	1582(1)	33(1)
C(14)	1561(5)	6734(3)	289(2)	53(1)
C(15)	-1129(3)	9439(2)	1684(1)	24(1)
C(16)	-2320(3)	9015(2)	1530(1)	27(1)
C(17)	-3298(3)	9010(2)	1927(2)	33(1)
C(18)	-3102(3)	9406(2)	2459(2)	35(1)
C(19)	-1917(3)	9828(2)	2606(1)	33(1)
C(20)	-929(3)	9847(2)	2220(1)	26(1)
C(21)	-2540(3)	8550(3)	966(1)	36(1)
N(2)	4010(2)	8814(2)	3728(1)	26(1)
C(22)	2976(3)	8732(2)	3380(1)	22(1)
C(23)	2563(3)	7807(2)	3157(1)	23(1)
C(24)	3269(3)	6962(2)	3316(1)	28(1)
C(25)	4336(3)	7028(2)	3682(1)	28(1)
C(26)	4681(3)	7988(2)	3876(1)	25(1)
C(27)	1388(3)	7727(2)	2774(1)	30(1)
C(28)	5024(4)	6089(2)	3875(2)	39(1)
C(29)	2304(3)	9706(2)	3252(2)	39(1)

C(30)	1271(4)	10043(4)	3526(2)	62(1)
C(31)	757(5)	11113(4)	3369(3)	83(2)
C(32)	1479(5)	11536(5)	2955(2)	74(2)
C(33)	2461(7)	11280(4)	2695(3)	86(2)
C(34)	2868(7)	10319(3)	2796(3)	112(3)
C(35)	672(6)	9467(5)	3896(3)	85(2)
C(36)	5784(3)	8180(2)	4292(1)	30(1)
C(37)	7063(3)	7981(3)	4170(2)	35(1)
C(38)	8016(3)	8212(3)	4581(2)	42(1)
C(39)	7693(3)	8620(3)	5084(2)	41(1)
C(40)	6428(3)	8832(3)	5206(2)	38(1)
C(41)	5465(3)	8603(2)	4810(1)	33(1)
C(42)	7468(4)	7580(3)	3615(2)	47(1)

Table 3. Bond lengths [\AA] and angles [$^\circ$].

N(1)-C(1)	1.344(4)
N(1)-C(5)	1.346(4)
C(1)-C(2)	1.401(4)
C(1)-C(8)	1.496(4)
C(2)-C(3)	1.393(4)
C(2)-C(6)	1.506(4)
C(3)-C(4)	1.384(4)
C(4)-C(5)	1.401(4)
C(4)-C(7)	1.511(4)
C(5)-C(15)	1.502(4)
C(8)-C(13)	1.390(4)
C(8)-C(9)	1.398(4)
C(9)-C(10)	1.398(4)
C(9)-C(14)	1.501(5)
C(10)-C(11)	1.374(5)
C(11)-C(12)	1.386(5)
C(12)-C(13)	1.386(4)
C(15)-C(16)	1.397(4)
C(15)-C(20)	1.399(4)
C(16)-C(17)	1.398(4)
C(16)-C(21)	1.492(4)
C(17)-C(18)	1.386(5)
C(18)-C(19)	1.385(5)
C(19)-C(20)	1.390(5)
N(2)-C(26)	1.342(4)
N(2)-C(22)	1.342(4)
C(22)-C(23)	1.402(4)
C(22)-C(29)	1.498(4)
C(23)-C(24)	1.388(4)
C(23)-C(27)	1.508(4)
C(24)-C(25)	1.393(4)
C(25)-C(26)	1.402(4)
C(25)-C(28)	1.505(4)
C(26)-C(36)	1.516(4)

C(29)-C(30)	1.340(6)
C(29)-C(34)	1.487(8)
C(30)-C(35)	1.331(8)
C(30)-C(31)	1.563(8)
C(31)-C(32)	1.371(8)
C(32)-C(33)	1.247(9)
C(33)-C(34)	1.366(7)
C(36)-C(37)	1.386(5)
C(36)-C(41)	1.403(5)
C(37)-C(38)	1.409(5)
C(37)-C(42)	1.494(5)
C(38)-C(39)	1.364(5)
C(39)-C(40)	1.376(5)
C(40)-C(41)	1.390(5)

C(1)-N(1)-C(5)	118.9(2)
N(1)-C(1)-C(2)	123.1(3)
N(1)-C(1)-C(8)	115.0(2)
C(2)-C(1)-C(8)	121.9(3)
C(3)-C(2)-C(1)	116.6(3)
C(3)-C(2)-C(6)	121.9(3)
C(1)-C(2)-C(6)	121.5(3)
C(4)-C(3)-C(2)	121.6(3)
C(3)-C(4)-C(5)	117.4(3)
C(3)-C(4)-C(7)	121.3(3)
C(5)-C(4)-C(7)	121.2(3)
N(1)-C(5)-C(4)	122.4(3)
N(1)-C(5)-C(15)	114.4(2)
C(4)-C(5)-C(15)	123.2(2)
C(13)-C(8)-C(9)	120.0(3)
C(13)-C(8)-C(1)	118.5(3)
C(9)-C(8)-C(1)	121.5(3)
C(10)-C(9)-C(8)	118.3(3)
C(10)-C(9)-C(14)	120.4(3)
C(8)-C(9)-C(14)	121.3(3)
C(11)-C(10)-C(9)	121.4(3)

C(10)-C(11)-C(12)	120.2(3)
C(11)-C(12)-C(13)	119.3(3)
C(12)-C(13)-C(8)	120.8(3)
C(16)-C(15)-C(20)	120.5(3)
C(16)-C(15)-C(5)	120.7(3)
C(20)-C(15)-C(5)	118.7(3)
C(15)-C(16)-C(17)	118.1(3)
C(15)-C(16)-C(21)	121.3(3)
C(17)-C(16)-C(21)	120.5(3)
C(18)-C(17)-C(16)	121.6(3)
C(19)-C(18)-C(17)	119.8(3)
C(18)-C(19)-C(20)	119.9(3)
C(19)-C(20)-C(15)	120.1(3)
C(26)-N(2)-C(22)	119.7(2)
N(2)-C(22)-C(23)	122.5(3)
N(2)-C(22)-C(29)	114.5(2)
C(23)-C(22)-C(29)	123.0(2)
C(24)-C(23)-C(22)	116.9(3)
C(24)-C(23)-C(27)	121.3(3)
C(22)-C(23)-C(27)	121.8(3)
C(23)-C(24)-C(25)	121.6(3)
C(24)-C(25)-C(26)	117.1(3)
C(24)-C(25)-C(28)	120.1(3)
C(26)-C(25)-C(28)	122.7(3)
N(2)-C(26)-C(25)	122.2(3)
N(2)-C(26)-C(36)	114.3(3)
C(25)-C(26)-C(36)	123.4(3)
C(30)-C(29)-C(34)	120.0(4)
C(30)-C(29)-C(22)	124.1(4)
C(34)-C(29)-C(22)	115.9(4)
C(35)-C(30)-C(29)	121.1(5)
C(35)-C(30)-C(31)	121.5(5)
C(29)-C(30)-C(31)	117.3(5)
C(32)-C(31)-C(30)	111.0(5)
C(33)-C(32)-C(31)	134.9(6)
C(32)-C(33)-C(34)	114.8(7)

C(33)-C(34)-C(29)	121.2(7)
C(37)-C(36)-C(41)	120.3(3)
C(37)-C(36)-C(26)	122.6(3)
C(41)-C(36)-C(26)	117.1(3)
C(36)-C(37)-C(38)	117.9(3)
C(36)-C(37)-C(42)	122.7(3)
C(38)-C(37)-C(42)	119.3(3)
C(39)-C(38)-C(37)	121.2(3)
C(38)-C(39)-C(40)	121.3(3)
C(39)-C(40)-C(41)	118.8(3)
C(40)-C(41)-C(36)	120.5(3)

Table 4. Anisotropic displacement parameters ($\text{\AA}^2 \times 10^3$). The anisotropic displacement factor exponent takes the form: $-2\pi^2 [h^2 a^{*2}U^{11} + \dots + 2 h k a^* b^* U^{12}]$

	U ¹¹	U ²²	U ³³	U ²³	U ¹³	U ¹²
N(1)	24(1)	20(1)	29(1)	1(1)	-2(1)	5(1)
C(1)	24(1)	22(1)	25(1)	-3(1)	-3(1)	3(1)
C(2)	24(1)	23(2)	28(2)	-3(1)	-3(1)	-1(1)
C(3)	27(2)	20(1)	31(2)	2(1)	-2(1)	-1(1)
C(4)	24(1)	19(1)	30(2)	0(1)	-5(1)	1(1)
C(5)	23(1)	19(1)	26(1)	-1(1)	-5(1)	2(1)
C(6)	29(2)	30(2)	39(2)	-1(1)	3(1)	2(1)
C(7)	30(2)	23(2)	39(2)	7(1)	2(1)	6(1)
C(8)	24(1)	24(2)	29(2)	2(1)	4(1)	6(1)
C(9)	42(2)	28(2)	31(2)	-1(1)	1(1)	9(1)
C(10)	52(2)	27(2)	34(2)	2(1)	12(2)	14(2)
C(11)	36(2)	31(2)	46(2)	13(2)	13(2)	16(1)
C(12)	29(2)	42(2)	47(2)	11(2)	-5(2)	10(2)
C(13)	26(2)	30(2)	42(2)	-1(1)	-5(1)	6(1)
C(14)	83(3)	31(2)	45(2)	-9(2)	-21(2)	12(2)
C(15)	26(2)	14(1)	31(2)	4(1)	-4(1)	4(1)
C(16)	27(2)	19(1)	35(2)	2(1)	-4(1)	2(1)
C(17)	27(2)	23(2)	48(2)	6(1)	2(1)	1(1)
C(18)	33(2)	28(2)	44(2)	5(1)	7(1)	4(1)
C(19)	37(2)	30(2)	32(2)	1(1)	-1(1)	7(1)
C(20)	26(2)	24(2)	28(2)	0(1)	-5(1)	6(1)
C(21)	33(2)	32(2)	42(2)	-5(1)	-8(1)	-4(1)
N(2)	23(1)	19(1)	34(1)	3(1)	-8(1)	-1(1)
C(22)	19(1)	22(1)	26(1)	3(1)	-6(1)	-1(1)
C(23)	23(1)	20(1)	26(1)	3(1)	-3(1)	-4(1)
C(24)	32(2)	20(1)	31(2)	0(1)	-6(1)	-5(1)
C(25)	28(2)	20(1)	35(2)	5(1)	-7(1)	-2(1)
C(26)	22(1)	23(1)	31(2)	4(1)	-4(1)	-2(1)
C(27)	31(2)	24(2)	34(2)	-1(1)	-14(1)	-3(1)
C(28)	45(2)	20(2)	51(2)	3(1)	-18(2)	2(1)
C(29)	39(2)	24(2)	52(2)	-12(2)	-32(2)	5(1)

C(30)	38(2)	52(3)	94(4)	-33(3)	-15(2)	9(2)
C(31)	46(2)	98(4)	102(4)	-71(4)	-46(3)	17(3)
C(32)	56(3)	102(4)	62(3)	16(3)	-37(3)	-36(3)
C(33)	98(5)	61(3)	96(4)	21(3)	-33(4)	-20(3)
C(34)	162(6)	16(2)	154(5)	41(3)	-137(5)	-36(3)
C(35)	102(4)	72(4)	80(4)	-15(3)	-13(3)	21(3)
C(36)	30(2)	18(1)	43(2)	7(1)	-7(1)	-2(1)
C(37)	30(2)	34(2)	42(2)	7(1)	-5(1)	2(1)
C(38)	31(2)	47(2)	47(2)	8(2)	-11(2)	7(2)
C(39)	38(2)	37(2)	48(2)	8(2)	-12(2)	-5(2)
C(40)	42(2)	36(2)	34(2)	4(1)	-6(2)	-4(2)
C(41)	35(2)	28(2)	34(2)	1(1)	-9(1)	0(1)
C(42)	33(2)	66(3)	43(2)	5(2)	0(2)	5(2)

Table 5. Hydrogen coordinates ($\times 10^4$) and isotropic displacement parameters ($\text{\AA}^2 \times 10^3$).

	x	y	z	U(eq)
H(3A)	1523	10597	319	31
H(6A)	4091	9027	540	48
H(6B)	3482	9775	79	48
H(6C)	3237	8591	27	48
H(7A)	-448	11449	503	46
H(7B)	-514	11525	1172	46
H(7C)	-1550	10858	829	46
H(10A)	3155	5324	693	45
H(11A)	4634	5347	1435	45
H(12A)	4834	6773	2005	47
H(13A)	3537	8175	1817	40
H(14A)	747	7060	388	80
H(14B)	1389	6036	180	80
H(14C)	1947	7093	-24	80
H(17A)	-4116	8727	1828	39
H(18A)	-3778	9390	2723	42
H(19A)	-1780	10103	2971	40
H(20A)	-116	10138	2320	31
H(21A)	-2459	9065	675	54
H(21B)	-3409	8257	945	54
H(21C)	-1895	8022	908	54
H(24A)	3018	6324	3172	33
H(27A)	1341	7049	2614	45
H(27B)	1451	8220	2471	45
H(27C)	607	7858	2988	45
H(28A)	5448	6212	4240	59
H(28B)	5675	5903	3601	59
H(28C)	4396	5542	3910	59
H(31A)	40	11430	3539	99
H(32A)	1155	12172	2838	89
H(33A)	2892	11719	2446	103

H(34A)	3523	10037	2571	135
H(35A)	385	8844	3714	127
H(35B)	-79	9827	4040	127
H(35C)	1270	9307	4208	127
H(38A)	8900	8082	4507	50
H(39A)	8355	8760	5356	49
H(40A)	6215	9130	5555	45
H(41A)	4585	8734	4891	39
H(42A)	6756	7657	3340	71
H(42B)	7688	6866	3653	71
H(42C)	8225	7953	3488	71

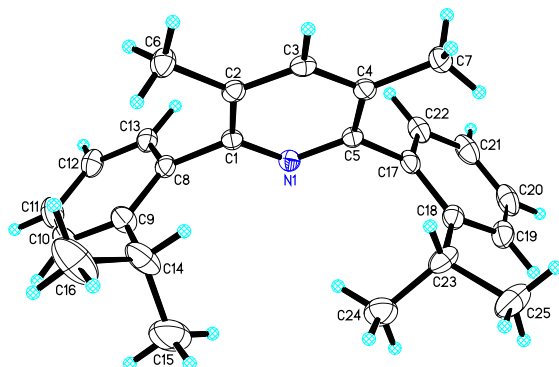
Table 6. Torsion angles [°].

C(5)-N(1)-C(1)-C(2)	0.7(4)
C(5)-N(1)-C(1)-C(8)	178.6(2)
N(1)-C(1)-C(2)-C(3)	-1.1(4)
C(8)-C(1)-C(2)-C(3)	-178.9(3)
N(1)-C(1)-C(2)-C(6)	178.4(3)
C(8)-C(1)-C(2)-C(6)	0.6(4)
C(1)-C(2)-C(3)-C(4)	0.3(4)
C(6)-C(2)-C(3)-C(4)	-179.2(3)
C(2)-C(3)-C(4)-C(5)	0.8(4)
C(2)-C(3)-C(4)-C(7)	179.8(3)
C(1)-N(1)-C(5)-C(4)	0.6(4)
C(1)-N(1)-C(5)-C(15)	-178.0(2)
C(3)-C(4)-C(5)-N(1)	-1.3(4)
C(7)-C(4)-C(5)-N(1)	179.7(3)
C(3)-C(4)-C(5)-C(15)	177.1(3)
C(7)-C(4)-C(5)-C(15)	-1.9(4)
N(1)-C(1)-C(8)-C(13)	-80.2(3)
C(2)-C(1)-C(8)-C(13)	97.8(4)
N(1)-C(1)-C(8)-C(9)	97.8(3)
C(2)-C(1)-C(8)-C(9)	-84.2(4)
C(13)-C(8)-C(9)-C(10)	-0.4(5)
C(1)-C(8)-C(9)-C(10)	-178.4(3)
C(13)-C(8)-C(9)-C(14)	-179.6(3)
C(1)-C(8)-C(9)-C(14)	2.5(5)
C(8)-C(9)-C(10)-C(11)	-1.0(5)
C(14)-C(9)-C(10)-C(11)	178.2(4)
C(9)-C(10)-C(11)-C(12)	1.3(5)
C(10)-C(11)-C(12)-C(13)	-0.1(5)
C(11)-C(12)-C(13)-C(8)	-1.3(5)
C(9)-C(8)-C(13)-C(12)	1.6(5)
C(1)-C(8)-C(13)-C(12)	179.6(3)
N(1)-C(5)-C(15)-C(16)	-90.2(3)
C(4)-C(5)-C(15)-C(16)	91.2(3)
N(1)-C(5)-C(15)-C(20)	86.2(3)

C(4)-C(5)-C(15)-C(20)	-92.3(3)
C(20)-C(15)-C(16)-C(17)	0.0(4)
C(5)-C(15)-C(16)-C(17)	176.3(3)
C(20)-C(15)-C(16)-C(21)	-178.2(3)
C(5)-C(15)-C(16)-C(21)	-1.9(4)
C(15)-C(16)-C(17)-C(18)	-0.4(4)
C(21)-C(16)-C(17)-C(18)	177.8(3)
C(16)-C(17)-C(18)-C(19)	0.5(5)
C(17)-C(18)-C(19)-C(20)	-0.2(5)
C(18)-C(19)-C(20)-C(15)	-0.2(4)
C(16)-C(15)-C(20)-C(19)	0.3(4)
C(5)-C(15)-C(20)-C(19)	-176.1(3)
C(26)-N(2)-C(22)-C(23)	-0.5(4)
C(26)-N(2)-C(22)-C(29)	179.5(3)
N(2)-C(22)-C(23)-C(24)	0.6(4)
C(29)-C(22)-C(23)-C(24)	-179.4(3)
N(2)-C(22)-C(23)-C(27)	179.1(3)
C(29)-C(22)-C(23)-C(27)	-0.9(5)
C(22)-C(23)-C(24)-C(25)	0.2(4)
C(27)-C(23)-C(24)-C(25)	-178.3(3)
C(23)-C(24)-C(25)-C(26)	-1.1(5)
C(23)-C(24)-C(25)-C(28)	175.9(3)
C(22)-N(2)-C(26)-C(25)	-0.5(4)
C(22)-N(2)-C(26)-C(36)	-177.1(3)
C(24)-C(25)-C(26)-N(2)	1.2(5)
C(28)-C(25)-C(26)-N(2)	-175.7(3)
C(24)-C(25)-C(26)-C(36)	177.6(3)
C(28)-C(25)-C(26)-C(36)	0.6(5)
N(2)-C(22)-C(29)-C(30)	-95.5(4)
C(23)-C(22)-C(29)-C(30)	84.5(4)
N(2)-C(22)-C(29)-C(34)	83.3(4)
C(23)-C(22)-C(29)-C(34)	-96.6(4)
C(34)-C(29)-C(30)-C(35)	173.4(4)
C(22)-C(29)-C(30)-C(35)	-7.9(6)
C(34)-C(29)-C(30)-C(31)	-3.5(5)
C(22)-C(29)-C(30)-C(31)	175.3(3)

C(35)-C(30)-C(31)-C(32)	-176.1(5)
C(29)-C(30)-C(31)-C(32)	0.7(5)
C(30)-C(31)-C(32)-C(33)	-3.2(8)
C(31)-C(32)-C(33)-C(34)	7.9(9)
C(32)-C(33)-C(34)-C(29)	-9.7(7)
C(30)-C(29)-C(34)-C(33)	8.4(6)
C(22)-C(29)-C(34)-C(33)	-170.5(4)
N(2)-C(26)-C(36)-C(37)	-118.8(3)
C(25)-C(26)-C(36)-C(37)	64.6(4)
N(2)-C(26)-C(36)-C(41)	59.2(4)
C(25)-C(26)-C(36)-C(41)	-117.4(3)
C(41)-C(36)-C(37)-C(38)	0.4(5)
C(26)-C(36)-C(37)-C(38)	178.3(3)
C(41)-C(36)-C(37)-C(42)	-176.8(3)
C(26)-C(36)-C(37)-C(42)	1.1(5)
C(36)-C(37)-C(38)-C(39)	-0.1(5)
C(42)-C(37)-C(38)-C(39)	177.2(3)
C(37)-C(38)-C(39)-C(40)	-0.8(6)
C(38)-C(39)-C(40)-C(41)	1.4(5)
C(39)-C(40)-C(41)-C(36)	-1.1(5)
C(37)-C(36)-C(41)-C(40)	0.3(5)
C(26)-C(36)-C(41)-C(40)	-177.8(3)

cis-2,6-di(2-isopropylphenyl)-3,5-dimethyl pyridine



X-ray Data Collection, Structure Solution and Refinement.

A colorless crystal of approximate dimensions 0.182 x 0.263 x 0.300 mm was mounted on a glass fiber and transferred to a Bruker SMART APEX II diffractometer. The APEX2¹ program package was used to determine the unit-cell parameters and for data collection (90 sec/frame scan time for a sphere of diffraction data). The raw frame data was processed using SAINT² and SADABS³ to yield the reflection data file. Subsequent calculations were carried out using the SHELXTL⁴ program. The diffraction symmetry was $2/m$ and the systematic absences were consistent with the monoclinic space group $P2_1/c$ that was later determined to be correct.

The structure was solved by dual space methods and refined on F^2 by full-matrix least-squares techniques. The analytical scattering factors⁵ for neutral atoms were used throughout the analysis. Hydrogen atoms were located from a difference-Fourier map and refined (x, y, z and U_{iso}).

Least-squares analysis yielded $wR2 = 0.1020$ and $Goof = 1.033$ for 351 variables refined against 4180 data (80 Å), $R1 = 0.0396$ for those 3505 data with $I > 2.0\sigma(I)$.

References.

6. APEX2 Version 2014.11-0, Bruker AXS, Inc.; Madison, WI 2014.
 7. SAINT Version 8.34a, Bruker AXS, Inc.; Madison, WI 2013.
 8. Sheldrick, G. M. SADABS, Version 2014/5, Bruker AXS, Inc.; Madison, WI 2014.
 9. Sheldrick, G. M. SHELXTL, Version 2014/7, Bruker AXS, Inc.; Madison, WI 2014
 10. International Tables for Crystallography 1992, Vol. C., Dordrecht: Kluwer Academic Publishers.
-

Definitions:

$$wR2 = [\Sigma[w(F_o^2 - F_c^2)^2] / \Sigma[w(F_o^2)^2]]^{1/2}$$

$$R1 = \Sigma||F_o| - |F_c|| / \Sigma|F_o|$$

Goof = S = $[\Sigma[w(F_o^2 - F_c^2)^2] / (n-p)]^{1/2}$ where n is the number of reflections and p is the total number of parameters refined.

The thermal ellipsoid plot is shown at the 50% probability level.

Table 1. Crystal data and structure refinement.

Identification code	toh7 (Tae Oh)	
Empirical formula	C ₂₅ H ₂₉ N	
Formula weight	343.49	
Temperature	133(2) K	
Wavelength	0.71073 Å	
Crystal system	Monoclinic	
Space group	<i>P</i> 2 ₁ / <i>c</i>	
Unit cell dimensions	a = 11.0625(5) Å	∠ = 90°.
	b = 14.9273(7) Å	∠ = 110.1561(7)°.
	c = 13.1903(6) Å	∠ = 90°.
Volume	2044.76(16) Å ³	
Z	4	
Density (calculated)	1.116 Mg/m ³	
Absorption coefficient	0.064 mm ⁻¹	
F(000)	744	
Crystal color	colorless	
Crystal size	0.300 x 0.263 x 0.182 mm ³	
Theta range for data collection	1.961 to 26.372°	
Index ranges	-13 ≤ <i>h</i> ≤ 13, -18 ≤ <i>k</i> ≤ 18, -16 ≤ <i>l</i> ≤ 16	
Reflections collected	24672	
Independent reflections	4180 [R(int) = 0.0279]	
Completeness to theta = 25.500°	100.0 %	
Absorption correction	Semi-empirical from equivalents	
Max. and min. transmission	0.8622 and 0.8050	
Refinement method	Full-matrix least-squares on F ²	
Data / restraints / parameters	4180 / 0 / 351	
Goodness-of-fit on F ²	1.033	
Final R indices [I > 2σ(I) = 3505 data]	R1 = 0.0396, wR2 = 0.0963	
R indices (all data, 0.80 Å)	R1 = 0.0490, wR2 = 0.1020	
Largest diff. peak and hole	0.237 and -0.190 e.Å ⁻³	

Table 2. Atomic coordinates ($\times 10^4$) and equivalent isotropic displacement parameters ($\text{\AA}^2 \times 10^3$) for toh7. $U(\text{eq})$ is defined as one third of the trace of the orthogonalized U^{ij} tensor.

	x	y	z	$U(\text{eq})$
N(1)	3144(1)	7355(1)	3146(1)	18(1)
C(1)	3931(1)	7135(1)	2607(1)	17(1)
C(2)	3723(1)	7416(1)	1547(1)	18(1)
C(3)	2642(1)	7939(1)	1054(1)	18(1)
C(4)	1816(1)	8183(1)	1596(1)	18(1)
C(5)	2110(1)	7867(1)	2650(1)	18(1)
C(6)	4638(1)	7191(1)	967(1)	26(1)
C(7)	678(1)	8784(1)	1077(1)	24(1)
C(8)	5081(1)	6588(1)	3237(1)	19(1)
C(9)	5188(1)	5675(1)	3044(1)	26(1)
C(10)	6278(1)	5219(1)	3704(1)	34(1)
C(11)	7227(1)	5641(1)	4530(1)	32(1)
C(12)	7121(1)	6542(1)	4713(1)	27(1)
C(13)	6053(1)	7010(1)	4068(1)	22(1)
C(14)	4139(2)	5164(1)	2190(1)	39(1)
C(15)	3440(2)	4545(1)	2725(2)	58(1)
C(16)	4666(2)	4644(1)	1430(2)	59(1)
C(17)	1287(1)	8095(1)	3309(1)	21(1)
C(18)	149(1)	7621(1)	3191(1)	24(1)
C(19)	-568(1)	7882(1)	3828(1)	31(1)
C(20)	-177(1)	8579(1)	4561(1)	34(1)
C(21)	944(1)	9039(1)	4677(1)	32(1)
C(22)	1670(1)	8797(1)	4046(1)	26(1)
C(23)	-254(1)	6837(1)	2411(1)	28(1)
C(24)	510(2)	5994(1)	2904(1)	36(1)
C(25)	-1697(2)	6636(1)	2023(1)	44(1)

Table 3. Bond lengths [\AA] and angles [$^\circ$].

N(1)-C(1)	1.3408(14)
N(1)-C(5)	1.3439(14)
C(1)-C(2)	1.4009(16)
C(1)-C(8)	1.4988(15)
C(2)-C(3)	1.3878(16)
C(2)-C(6)	1.5028(16)
C(3)-C(4)	1.3902(16)
C(4)-C(5)	1.3958(16)
C(4)-C(7)	1.5035(16)
C(5)-C(17)	1.4986(16)
C(8)-C(13)	1.3936(16)
C(8)-C(9)	1.3988(17)
C(9)-C(10)	1.3975(18)
C(9)-C(14)	1.5155(18)
C(10)-C(11)	1.378(2)
C(11)-C(12)	1.379(2)
C(12)-C(13)	1.3838(17)
C(14)-C(15)	1.526(3)
C(14)-C(16)	1.534(2)
C(17)-C(22)	1.3928(17)
C(17)-C(18)	1.4047(17)
C(18)-C(19)	1.3954(18)
C(18)-C(23)	1.5205(19)
C(19)-C(20)	1.384(2)
C(20)-C(21)	1.378(2)
C(21)-C(22)	1.3883(18)
C(23)-C(25)	1.5279(19)
C(23)-C(24)	1.529(2)
C(1)-N(1)-C(5)	118.73(9)
N(1)-C(1)-C(2)	122.81(10)
N(1)-C(1)-C(8)	114.97(9)
C(2)-C(1)-C(8)	122.19(10)
C(3)-C(2)-C(1)	117.14(10)

C(3)-C(2)-C(6)	120.65(10)
C(1)-C(2)-C(6)	122.19(10)
C(2)-C(3)-C(4)	121.24(10)
C(3)-C(4)-C(5)	117.08(10)
C(3)-C(4)-C(7)	121.12(10)
C(5)-C(4)-C(7)	121.78(10)
N(1)-C(5)-C(4)	122.99(10)
N(1)-C(5)-C(17)	115.62(10)
C(4)-C(5)-C(17)	121.39(10)
C(13)-C(8)-C(9)	119.54(11)
C(13)-C(8)-C(1)	117.84(10)
C(9)-C(8)-C(1)	122.59(10)
C(10)-C(9)-C(8)	118.06(12)
C(10)-C(9)-C(14)	119.58(12)
C(8)-C(9)-C(14)	122.30(11)
C(11)-C(10)-C(9)	121.90(12)
C(10)-C(11)-C(12)	119.82(12)
C(11)-C(12)-C(13)	119.40(12)
C(12)-C(13)-C(8)	121.28(11)
C(9)-C(14)-C(15)	109.92(14)
C(9)-C(14)-C(16)	112.02(14)
C(15)-C(14)-C(16)	111.27(15)
C(22)-C(17)-C(18)	120.11(11)
C(22)-C(17)-C(5)	118.45(11)
C(18)-C(17)-C(5)	121.44(11)
C(19)-C(18)-C(17)	117.80(12)
C(19)-C(18)-C(23)	121.82(12)
C(17)-C(18)-C(23)	120.37(11)
C(20)-C(19)-C(18)	121.63(13)
C(21)-C(20)-C(19)	120.32(12)
C(20)-C(21)-C(22)	119.21(13)
C(21)-C(22)-C(17)	120.94(13)
C(18)-C(23)-C(25)	113.97(12)
C(18)-C(23)-C(24)	110.81(11)
C(25)-C(23)-C(24)	110.02(12)

Table 4. Anisotropic displacement parameters ($\text{\AA}^2 \times 10^3$) for toh7. The anisotropic displacement factor exponent takes the form: $-2\pi^2 [h^2 a^{*2}U^{11} + \dots + 2 h k a^* b^* U^{12}]$

	U ¹¹	U ²²	U ³³	U ²³	U ¹³	U ¹²
N(1)	18(1)	17(1)	19(1)	0(1)	6(1)	0(1)
C(1)	16(1)	15(1)	20(1)	-1(1)	6(1)	-2(1)
C(2)	18(1)	18(1)	20(1)	-2(1)	7(1)	-3(1)
C(3)	20(1)	18(1)	16(1)	1(1)	5(1)	-4(1)
C(4)	16(1)	16(1)	21(1)	-1(1)	4(1)	-2(1)
C(5)	16(1)	16(1)	21(1)	-1(1)	6(1)	-1(1)
C(6)	24(1)	33(1)	23(1)	2(1)	12(1)	4(1)
C(7)	21(1)	26(1)	24(1)	6(1)	7(1)	4(1)
C(8)	18(1)	22(1)	19(1)	2(1)	9(1)	2(1)
C(9)	27(1)	22(1)	28(1)	1(1)	7(1)	3(1)
C(10)	35(1)	24(1)	39(1)	2(1)	9(1)	11(1)
C(11)	25(1)	37(1)	31(1)	6(1)	6(1)	12(1)
C(12)	20(1)	36(1)	24(1)	0(1)	6(1)	3(1)
C(13)	20(1)	25(1)	22(1)	0(1)	9(1)	2(1)
C(14)	40(1)	20(1)	43(1)	-4(1)	-3(1)	3(1)
C(15)	43(1)	34(1)	79(1)	4(1)	0(1)	-10(1)
C(16)	77(1)	34(1)	49(1)	-17(1)	-1(1)	10(1)
C(17)	21(1)	23(1)	19(1)	6(1)	7(1)	7(1)
C(18)	21(1)	29(1)	21(1)	9(1)	8(1)	5(1)
C(19)	26(1)	40(1)	31(1)	15(1)	16(1)	10(1)
C(20)	40(1)	41(1)	30(1)	12(1)	21(1)	22(1)
C(21)	42(1)	30(1)	27(1)	2(1)	14(1)	15(1)
C(22)	28(1)	25(1)	25(1)	2(1)	9(1)	8(1)
C(23)	24(1)	39(1)	23(1)	3(1)	10(1)	-8(1)
C(24)	38(1)	30(1)	41(1)	-6(1)	14(1)	-8(1)
C(25)	29(1)	63(1)	37(1)	7(1)	9(1)	-15(1)

Table 5. Hydrogen coordinates ($\times 10^4$) and isotropic displacement parameters ($\text{\AA}^2 \times 10^3$).

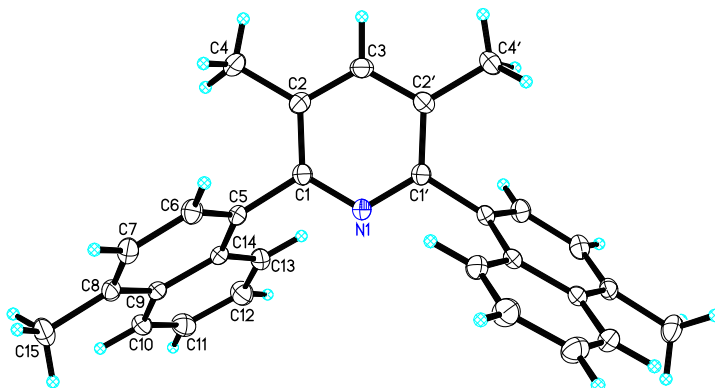
	x	y	z	U(eq)
H(3A)	2468(12)	8141(8)	316(11)	20(3)
H(6A)	5510(20)	7321(14)	1401(17)	74(6)
H(6B)	4399(17)	7489(13)	280(16)	56(5)
H(6C)	4620(20)	6567(16)	811(17)	79(7)
H(7A)	-3(18)	8723(12)	1397(15)	53(5)
H(7B)	310(20)	8694(13)	332(18)	69(6)
H(7C)	935(19)	9397(15)	1174(17)	73(6)
H(10A)	6332(15)	4579(11)	3594(13)	43(4)
H(11A)	7972(15)	5292(10)	4990(13)	38(4)
H(12A)	7779(14)	6855(10)	5289(12)	33(4)
H(13A)	5957(13)	7654(10)	4192(11)	26(3)
H(14A)	3514(15)	5600(10)	1752(12)	36(4)
H(15A)	2700(20)	4261(14)	2198(17)	73(6)
H(15B)	3060(20)	4874(14)	3218(17)	66(6)
H(15C)	4040(19)	4075(14)	3152(17)	65(6)
H(16A)	3920(20)	4380(15)	867(18)	77(6)
H(16B)	5251(19)	4157(14)	1821(16)	61(5)
H(16C)	5170(20)	5072(17)	1092(19)	89(8)
H(19A)	-1355(15)	7565(10)	3760(12)	33(4)
H(20A)	-694(16)	8735(11)	5005(13)	43(4)
H(21A)	1228(15)	9523(11)	5205(13)	39(4)
H(22A)	2481(15)	9124(10)	4120(12)	34(4)
H(23A)	-43(13)	6988(9)	1793(12)	24(3)
H(24A)	314(16)	5509(11)	2377(14)	45(4)
H(24B)	260(16)	5781(11)	3537(14)	45(4)
H(24C)	1451(17)	6116(10)	3159(13)	42(4)
H(25A)	-1898(18)	6163(13)	1433(16)	60(5)
H(25B)	-2195(18)	7178(13)	1737(16)	59(5)
H(25C)	-1961(16)	6390(11)	2614(14)	45(4)

Table 6. Torsion angles [°].

C(5)-N(1)-C(1)-C(2)	0.03(16)
C(5)-N(1)-C(1)-C(8)	178.08(10)
N(1)-C(1)-C(2)-C(3)	-0.48(16)
C(8)-C(1)-C(2)-C(3)	-178.39(10)
N(1)-C(1)-C(2)-C(6)	177.85(11)
C(8)-C(1)-C(2)-C(6)	-0.06(17)
C(1)-C(2)-C(3)-C(4)	1.00(16)
C(6)-C(2)-C(3)-C(4)	-177.36(11)
C(2)-C(3)-C(4)-C(5)	-1.05(16)
C(2)-C(3)-C(4)-C(7)	177.24(11)
C(1)-N(1)-C(5)-C(4)	-0.09(16)
C(1)-N(1)-C(5)-C(17)	-179.18(10)
C(3)-C(4)-C(5)-N(1)	0.59(16)
C(7)-C(4)-C(5)-N(1)	-177.69(11)
C(3)-C(4)-C(5)-C(17)	179.62(10)
C(7)-C(4)-C(5)-C(17)	1.35(17)
N(1)-C(1)-C(8)-C(13)	-71.13(13)
C(2)-C(1)-C(8)-C(13)	106.93(13)
N(1)-C(1)-C(8)-C(9)	106.60(13)
C(2)-C(1)-C(8)-C(9)	-75.33(15)
C(13)-C(8)-C(9)-C(10)	0.08(18)
C(1)-C(8)-C(9)-C(10)	-177.61(11)
C(13)-C(8)-C(9)-C(14)	177.02(12)
C(1)-C(8)-C(9)-C(14)	-0.67(19)
C(8)-C(9)-C(10)-C(11)	0.5(2)
C(14)-C(9)-C(10)-C(11)	-176.53(14)
C(9)-C(10)-C(11)-C(12)	-0.8(2)
C(10)-C(11)-C(12)-C(13)	0.5(2)
C(11)-C(12)-C(13)-C(8)	0.06(18)
C(9)-C(8)-C(13)-C(12)	-0.36(17)
C(1)-C(8)-C(13)-C(12)	177.45(11)
C(10)-C(9)-C(14)-C(15)	69.57(18)
C(8)-C(9)-C(14)-C(15)	-107.33(15)
C(10)-C(9)-C(14)-C(16)	-54.67(19)

C(8)-C(9)-C(14)-C(16)	128.43(15)
N(1)-C(5)-C(17)-C(22)	81.21(13)
C(4)-C(5)-C(17)-C(22)	-97.89(13)
N(1)-C(5)-C(17)-C(18)	-99.12(13)
C(4)-C(5)-C(17)-C(18)	81.78(14)
C(22)-C(17)-C(18)-C(19)	0.28(17)
C(5)-C(17)-C(18)-C(19)	-179.39(10)
C(22)-C(17)-C(18)-C(23)	-178.21(11)
C(5)-C(17)-C(18)-C(23)	2.12(17)
C(17)-C(18)-C(19)-C(20)	-0.45(18)
C(23)-C(18)-C(19)-C(20)	178.02(12)
C(18)-C(19)-C(20)-C(21)	0.1(2)
C(19)-C(20)-C(21)-C(22)	0.41(19)
C(20)-C(21)-C(22)-C(17)	-0.58(19)
C(18)-C(17)-C(22)-C(21)	0.22(18)
C(5)-C(17)-C(22)-C(21)	179.91(11)
C(19)-C(18)-C(23)-C(25)	25.15(17)
C(17)-C(18)-C(23)-C(25)	-156.41(12)
C(19)-C(18)-C(23)-C(24)	-99.59(14)
C(17)-C(18)-C(23)-C(24)	78.85(14)

trans-3,5-Dimethyl-2,6-di(4-methylnaphthyl-1-yl)pyridine: Unit cell A



X-ray Data Collection, Structure Solution and Refinement.

A colorless crystal of approximate dimensions 0.270 x 0.283 x 0.396 mm was mounted on a glass fiber and transferred to a Bruker SMART APEX II diffractometer. The APEX2¹ program package was used to determine the unit-cell parameters and for data collection (15 sec/frame scan time for a sphere of diffraction data). The raw frame data was processed using SAINT² and SADABS³ to yield the reflection data file. Subsequent calculations were carried out using the SHELXTL⁴ program. The diffraction symmetry was *2/m* and the systematic absences were consistent with the monoclinic space groups *Cc* and *C2/c*. It was later determined that space group *C2/c* was correct.

The structure was solved by dual space methods and refined on F^2 by full-matrix least-squares techniques. The analytical scattering factors⁵ for neutral atoms were used throughout the analysis. Hydrogen atoms were located from a difference-Fourier map and refined (x, y, z and U_{iso}). The molecule was located on a two-fold rotation axis.

Least-squares analysis yielded $wR2 = 0.1187$ and $Goof = 1.080$ for 187 variables refined against 2590 data (0.74 Å), $R1 = 0.0411$ for those 2195 data with $I > 2.0\sigma(I)$.

References.

11. APEX2 Version 2014.11-0, Bruker AXS, Inc.; Madison, WI 2014.
12. SAINT Version 8.34a, Bruker AXS, Inc.; Madison, WI 2013.
13. Sheldrick, G. M. SADABS, Version 2014/5, Bruker AXS, Inc.; Madison, WI 2014.
14. Sheldrick, G. M. SHELXTL, Version 2014/7, Bruker AXS, Inc.; Madison, WI 2014.
15. International Tables for Crystallography 1992, Vol. C., Dordrecht: Kluwer Academic Publishers.

Definitions:

$$wR2 = [\Sigma[w(F_o^2 - F_c^2)^2] / \Sigma[w(F_o^2)^2]]^{1/2}$$

$$R1 = \Sigma||F_o| - |F_c|| / \Sigma|F_o|$$

Goof = $S = [\Sigma[w(F_o^2 - F_c^2)^2] / (n-p)]^{1/2}$ where n is the number of reflections and p is the total number of parameters refined.

The thermal ellipsoid plot is shown at the 50% probability level.

Table 1. Crystal data and structure refinement.

Identification code	toh6 (Tae Oh)	
Empirical formula	C ₂₉ H ₂₅ N	
Formula weight	387.50	
Temperature	133(2) K	
Wavelength	0.71073 Å	
Crystal system	Monoclinic	
Space group	C2/c	
Unit cell dimensions	a = 22.7935(15) Å	∠ = 90°.
	b = 7.4999(5) Å	∠ = 131.3330(6)°.
	c = 16.3915(11) Å	∠ = 90°.
Volume	2104.1(2) Å ³	
Z	4	
Density (calculated)	1.223 Mg/m ³	
Absorption coefficient	0.070 mm ⁻¹	
F(000)	824	
Crystal color	colorless	
Crystal size	0.396 x 0.283 x 0.270 mm ³	
Theta range for data collection	2.380 to 28.795°	
Index ranges	-30 ≤ h ≤ 30, -10 ≤ k ≤ 10, -22 ≤ l ≤ 21	
Reflections collected	12195	
Independent reflections	2590 [R(int) = 0.0214]	
Completeness to theta = 25.500°	100.0 %	
Absorption correction	Semi-empirical from equivalents	
Max. and min. transmission	0.8621 and 0.8183	
Refinement method	Full-matrix least-squares on F ²	
Data / restraints / parameters	2590 / 0 / 187	
Goodness-of-fit on F ²	1.080	
Final R indices [I > 2σ(I) = 2195 data]	R1 = 0.0411, wR2 = 0.1122	
R indices (all data, 0.74 Å)	R1 = 0.0488, wR2 = 0.1187	
Largest diff. peak and hole	0.342 and -0.261 e.Å ⁻³	

Table 2. Atomic coordinates ($\times 10^4$) and equivalent isotropic displacement parameters ($\text{\AA}^2 \times 10^3$). $U(\text{eq})$ is defined as one third of the trace of the orthogonalized U^{ij} tensor.

	x	y	z	$U(\text{eq})$
N(1)	10000	5066(2)	2500	18(1)
C(1)	9402(1)	4152(1)	2281(1)	17(1)
C(2)	9387(1)	2283(2)	2306(1)	18(1)
C(3)	10000	1375(2)	2500	20(1)
C(4)	8751(1)	1266(2)	2153(1)	25(1)
C(5)	8724(1)	5217(1)	1970(1)	17(1)
C(6)	8024(1)	5111(2)	923(1)	20(1)
C(7)	7367(1)	6094(2)	582(1)	21(1)
C(8)	7393(1)	7158(2)	1284(1)	19(1)
C(9)	8104(1)	7251(1)	2392(1)	17(1)
C(10)	8164(1)	8265(2)	3174(1)	21(1)
C(11)	8853(1)	8377(2)	4228(1)	26(1)
C(12)	9521(1)	7477(2)	4556(1)	26(1)
C(13)	9485(1)	6462(2)	3829(1)	21(1)
C(14)	8779(1)	6305(1)	2733(1)	16(1)
C(15)	6685(1)	8217(2)	884(1)	26(1)

Table 3. Bond lengths [\AA] and angles [$^\circ$].

N(1)-C(1)#1	1.3459(12)
N(1)-C(1)	1.3460(12)
C(1)-C(2)	1.4032(15)
C(1)-C(5)	1.4973(14)
C(2)-C(3)	1.3901(13)
C(2)-C(4)	1.5053(15)
C(3)-C(2)#1	1.3900(13)
C(5)-C(6)	1.3713(15)
C(5)-C(14)	1.4280(15)
C(6)-C(7)	1.4114(15)
C(7)-C(8)	1.3687(16)
C(8)-C(9)	1.4293(15)
C(8)-C(15)	1.5059(15)
C(9)-C(10)	1.4179(15)
C(9)-C(14)	1.4312(14)
C(10)-C(11)	1.3699(17)
C(11)-C(12)	1.4072(16)
C(12)-C(13)	1.3694(16)
C(13)-C(14)	1.4188(15)
C(1)#1-N(1)-C(1)	118.77(13)
N(1)-C(1)-C(2)	122.74(10)
N(1)-C(1)-C(5)	117.01(9)
C(2)-C(1)-C(5)	120.22(9)
C(3)-C(2)-C(1)	117.10(10)
C(3)-C(2)-C(4)	120.17(10)
C(1)-C(2)-C(4)	122.72(10)
C(2)#1-C(3)-C(2)	121.33(14)
C(6)-C(5)-C(14)	119.01(9)
C(6)-C(5)-C(1)	118.81(9)
C(14)-C(5)-C(1)	122.17(9)
C(5)-C(6)-C(7)	121.30(10)
C(8)-C(7)-C(6)	121.68(10)
C(7)-C(8)-C(9)	118.73(10)

C(7)-C(8)-C(15)	120.17(10)
C(9)-C(8)-C(15)	121.10(10)
C(10)-C(9)-C(8)	121.79(10)
C(10)-C(9)-C(14)	118.49(10)
C(8)-C(9)-C(14)	119.71(10)
C(11)-C(10)-C(9)	121.19(10)
C(10)-C(11)-C(12)	120.20(11)
C(13)-C(12)-C(11)	120.40(11)
C(12)-C(13)-C(14)	120.97(10)
C(13)-C(14)-C(5)	121.81(9)
C(13)-C(14)-C(9)	118.71(10)
C(5)-C(14)-C(9)	119.48(9)

Symmetry transformations used to generate equivalent atoms:

#1 $-x+2, y, -z+1/2$

Table 4. Anisotropic displacement parameters ($\text{\AA}^2 \times 10^3$) for toh6. The anisotropic displacement factor exponent takes the form: $-2\pi^2 [h^2 a^{*2}U^{11} + \dots + 2 h k a^* b^* U^{12}]$

	U ¹¹	U ²²	U ³³	U ²³	U ¹³	U ¹²
N(1)	17(1)	17(1)	23(1)	0	14(1)	0
C(1)	17(1)	18(1)	18(1)	0(1)	12(1)	0(1)
C(2)	19(1)	18(1)	19(1)	-2(1)	13(1)	-3(1)
C(3)	23(1)	16(1)	23(1)	0	16(1)	0
C(4)	25(1)	21(1)	35(1)	-3(1)	22(1)	-6(1)
C(5)	16(1)	16(1)	22(1)	2(1)	14(1)	-1(1)
C(6)	20(1)	23(1)	21(1)	0(1)	15(1)	-1(1)
C(7)	17(1)	26(1)	19(1)	3(1)	12(1)	0(1)
C(8)	17(1)	19(1)	24(1)	5(1)	14(1)	1(1)
C(9)	18(1)	14(1)	24(1)	2(1)	15(1)	0(1)
C(10)	22(1)	18(1)	28(1)	1(1)	18(1)	2(1)
C(11)	29(1)	24(1)	28(1)	-5(1)	20(1)	0(1)
C(12)	21(1)	27(1)	23(1)	-4(1)	11(1)	0(1)
C(13)	17(1)	20(1)	24(1)	-1(1)	12(1)	0(1)
C(14)	16(1)	15(1)	22(1)	1(1)	14(1)	-1(1)
C(15)	20(1)	31(1)	28(1)	6(1)	16(1)	7(1)

Table 5. Hydrogen coordinates ($\times 10^4$) and isotropic displacement parameters ($\text{\AA}^2 \times 10^3$).

	x	y	z	U(eq)
H(3)	10000	40(30)	2500	30(5)
H(4A)	8884(11)	40(30)	2336(16)	70(6)
H(4B)	8256(11)	1320(30)	1397(16)	60(6)
H(4C)	8594(11)	1810(20)	2540(15)	58(6)
H(6)	7983(7)	4397(19)	399(11)	24(3)
H(7)	6880(9)	6030(20)	-194(12)	32(4)
H(10)	7701(8)	8910(20)	2945(11)	26(3)
H(11)	8893(9)	9100(20)	4770(12)	36(4)
H(12)	10001(9)	7570(20)	5314(13)	32(4)
H(13)	9949(8)	5820(20)	4065(11)	25(3)
H(15A)	6269(9)	8070(20)	99(13)	34(4)
H(15B)	6800(8)	9520(20)	1036(12)	35(4)
H(15C)	6477(9)	7810(20)	1243(13)	41(4)

Table 6. Torsion angles [°].

C(1)#1-N(1)-C(1)-C(2)	2.18(7)
C(1)#1-N(1)-C(1)-C(5)	-176.06(10)
N(1)-C(1)-C(2)-C(3)	-4.21(14)
C(5)-C(1)-C(2)-C(3)	173.98(8)
N(1)-C(1)-C(2)-C(4)	174.77(9)
C(5)-C(1)-C(2)-C(4)	-7.03(16)
C(1)-C(2)-C(3)-C(2)#1	1.97(7)
C(4)-C(2)-C(3)-C(2)#1	-177.04(11)
N(1)-C(1)-C(5)-C(6)	111.17(10)
C(2)-C(1)-C(5)-C(6)	-67.13(13)
N(1)-C(1)-C(5)-C(14)	-70.35(12)
C(2)-C(1)-C(5)-C(14)	111.35(12)
C(14)-C(5)-C(6)-C(7)	1.92(16)
C(1)-C(5)-C(6)-C(7)	-179.55(9)
C(5)-C(6)-C(7)-C(8)	-1.75(17)
C(6)-C(7)-C(8)-C(9)	-0.71(16)
C(6)-C(7)-C(8)-C(15)	178.70(10)
C(7)-C(8)-C(9)-C(10)	-177.30(10)
C(15)-C(8)-C(9)-C(10)	3.30(16)
C(7)-C(8)-C(9)-C(14)	2.87(15)
C(15)-C(8)-C(9)-C(14)	-176.53(10)
C(8)-C(9)-C(10)-C(11)	-178.46(10)
C(14)-C(9)-C(10)-C(11)	1.37(16)
C(9)-C(10)-C(11)-C(12)	0.01(18)
C(10)-C(11)-C(12)-C(13)	-1.00(19)
C(11)-C(12)-C(13)-C(14)	0.54(19)
C(12)-C(13)-C(14)-C(5)	-178.40(11)
C(12)-C(13)-C(14)-C(9)	0.85(17)
C(6)-C(5)-C(14)-C(13)	179.53(10)
C(1)-C(5)-C(14)-C(13)	1.05(16)
C(6)-C(5)-C(14)-C(9)	0.28(15)
C(1)-C(5)-C(14)-C(9)	-178.19(9)
C(10)-C(9)-C(14)-C(13)	-1.78(15)
C(8)-C(9)-C(14)-C(13)	178.06(9)

C(10)-C(9)-C(14)-C(5)	177.49(9)
C(8)-C(9)-C(14)-C(5)	-2.68(15)

Symmetry transformations used to generate equivalent atoms:

#1 $-x+2, y, -z+1/2$

Empirical formula	C ₂₉ H ₂₅ N	
Formula weight	387.50	
Temperature	133(2) K	
Wavelength	0.71073 Å	
Crystal system	Monoclinic	
Space group	C2/c	
Unit cell dimensions	a = 22.4581(14) Å	β = 90°.
	b = 7.9134(5) Å	γ = 101.3638(10)°.
	c = 36.913(2) Å	α = 90°.
Volume	6431.7(7) Å ³	
Z	12	
Density (calculated)	1.201 Mg/m ³	
Absorption coefficient	0.069 mm ⁻¹	
F(000)	2472	
Crystal color	colorless	
Crystal size	0.289 x 0.234 x 0.211 mm ³	
Theta range for data collection	1.850 to 26.372°	
Index ranges	-28 ≤ h ≤ 28, -9 ≤ k ≤ 9, -46 ≤ l ≤ 46	
Reflections collected	37033	
Independent reflections	6568 [R(int) = 0.0577]	
Completeness to theta = 25.242°	100.0 %	
Absorption correction	Semi-empirical from equivalents	
Max. and min. transmission	0.8622 and 0.7662	
Refinement method	Full-matrix least-squares on F ²	
Data / restraints / parameters	6568 / 0 / 557	
Goodness-of-fit on F ²	1.057	
Final R indices [I > 2σ(I) = 5151 data]	R1 = 0.0507, wR2 = 0.1098	
R indices (all data, 0.80 Å)	R1 = 0.0684, wR2 = 0.1178	
Largest diff. peak and hole	0.345 and -0.192 e.Å ⁻³	

Table 2. Atomic coordinates ($\times 10^4$) and equivalent isotropic displacement parameters ($\text{\AA}^2 \times 10^3$) for toh13. $U(\text{eq})$ is defined as one third of the trace of the orthogonalized U^{ij} tensor.

	x	y	z	$U(\text{eq})$
N(1)	4426(1)	5048(2)	4172(1)	20(1)
C(1)	3922(1)	6012(2)	4107(1)	19(1)
C(2)	3923(1)	7718(2)	4208(1)	19(1)
C(3)	4476(1)	8421(2)	4372(1)	22(1)
C(4)	5007(1)	7470(2)	4435(1)	23(1)
C(5)	4955(1)	5765(2)	4335(1)	19(1)
C(6)	3351(1)	8760(2)	4149(1)	24(1)
C(7)	5606(1)	8265(3)	4607(1)	39(1)
C(8)	3346(1)	5198(2)	3909(1)	20(1)
C(9)	3108(1)	5644(2)	3551(1)	24(1)
C(10)	2541(1)	5035(3)	3365(1)	26(1)
C(11)	2205(1)	3938(2)	3534(1)	24(1)
C(12)	2451(1)	3380(2)	3900(1)	20(1)
C(13)	2140(1)	2189(2)	4087(1)	23(1)
C(14)	2366(1)	1708(2)	4441(1)	23(1)
C(15)	2923(1)	2377(2)	4632(1)	22(1)
C(16)	3244(1)	3493(2)	4461(1)	20(1)
C(17)	3024(1)	4016(2)	4091(1)	19(1)
C(18)	1579(1)	3405(3)	3342(1)	31(1)
C(19)	5495(1)	4618(2)	4404(1)	19(1)
C(20)	5717(1)	4021(2)	4753(1)	23(1)
C(21)	6223(1)	2926(2)	4824(1)	21(1)
C(22)	6513(1)	2417(2)	4550(1)	19(1)
C(23)	6296(1)	3024(2)	4182(1)	19(1)
C(24)	6574(1)	2558(2)	3883(1)	24(1)
C(25)	6362(1)	3143(3)	3534(1)	28(1)
C(26)	5861(1)	4249(3)	3462(1)	26(1)
C(27)	5580(1)	4731(2)	3742(1)	23(1)
C(28)	5784(1)	4133(2)	4109(1)	19(1)
C(29)	7043(1)	1227(3)	4634(1)	25(1)
N(2)	5000	7464(3)	2500	21(1)

C(30)	4587(1)	6598(2)	2645(1)	21(1)
C(31)	4574(1)	4828(2)	2657(1)	25(1)
C(32)	5000	3975(3)	2500	27(1)
C(33)	4136(1)	3841(3)	2838(1)	40(1)
C(34)	4116(1)	7620(2)	2782(1)	22(1)
C(35)	3518(1)	7398(3)	2612(1)	28(1)
C(36)	3047(1)	8309(3)	2722(1)	31(1)
C(37)	3159(1)	9450(3)	3004(1)	29(1)
C(38)	3776(1)	9735(2)	3188(1)	24(1)
C(39)	3924(1)	10908(2)	3480(1)	30(1)
C(40)	4508(1)	11170(3)	3656(1)	33(1)
C(41)	4981(1)	10246(3)	3550(1)	32(1)
C(42)	4861(1)	9101(3)	3268(1)	27(1)
C(43)	4258(1)	8810(2)	3077(1)	22(1)
C(44)	2642(1)	10371(3)	3118(1)	40(1)

Table 3. Bond lengths [\AA] and angles [$^\circ$] for toh13.

N(1)-C(5)	1.345(2)
N(1)-C(1)	1.348(2)
C(1)-C(2)	1.400(2)
C(1)-C(8)	1.499(2)
C(2)-C(3)	1.387(2)
C(2)-C(6)	1.505(2)
C(3)-C(4)	1.390(3)
C(3)-H(3A)	0.99(2)
C(4)-C(5)	1.398(3)
C(4)-C(7)	1.509(3)
C(5)-C(19)	1.496(2)
C(6)-H(6A)	0.99(2)
C(6)-H(6B)	0.99(3)
C(6)-H(6C)	0.98(2)
C(7)-H(7A)	0.94(3)
C(7)-H(7B)	1.02(3)
C(7)-H(7C)	0.97(3)
C(8)-C(9)	1.371(3)
C(8)-C(17)	1.428(2)
C(9)-C(10)	1.407(3)
C(9)-H(9A)	1.00(2)
C(10)-C(11)	1.376(3)
C(10)-H(10A)	0.967(18)
C(11)-C(12)	1.425(3)
C(11)-C(18)	1.506(3)
C(12)-C(13)	1.429(3)
C(12)-C(17)	1.432(2)
C(13)-C(14)	1.361(3)
C(13)-H(13A)	0.97(2)
C(14)-C(15)	1.413(3)
C(14)-H(14A)	1.00(2)
C(15)-C(16)	1.369(3)
C(15)-H(15A)	0.993(19)
C(16)-C(17)	1.419(2)

C(16)-H(16A)	0.939(18)
C(18)-H(18A)	1.03(2)
C(18)-H(18B)	1.00(2)
C(18)-H(18C)	1.03(2)
C(19)-C(20)	1.368(3)
C(19)-C(28)	1.429(2)
C(20)-C(21)	1.411(2)
C(20)-H(20A)	0.96(2)
C(21)-C(22)	1.368(2)
C(21)-H(21A)	0.984(18)
C(22)-C(23)	1.433(2)
C(22)-C(29)	1.501(2)
C(23)-C(24)	1.419(2)
C(23)-C(28)	1.428(2)
C(24)-C(25)	1.362(3)
C(24)-H(24A)	0.99(2)
C(25)-C(26)	1.409(3)
C(25)-H(25A)	0.98(2)
C(26)-C(27)	1.367(3)
C(26)-H(26A)	0.97(2)
C(27)-C(28)	1.421(2)
C(27)-H(27A)	0.944(19)
C(29)-H(29A)	0.99(2)
C(29)-H(29B)	0.99(2)
C(29)-H(29C)	1.01(2)
N(2)-C(30)	1.346(2)
N(2)-C(30)#1	1.346(2)
C(30)-C(31)	1.402(3)
C(30)-C(34)	1.497(2)
C(31)-C(32)	1.387(2)
C(31)-C(33)	1.511(3)
C(32)-C(31)#1	1.387(2)
C(32)-H(32A)	1.05(3)
C(33)-H(33A)	0.99(3)
C(33)-H(33B)	0.98(3)
C(33)-H(33C)	1.01(3)

C(34)-C(35)	1.375(3)
C(34)-C(43)	1.429(3)
C(35)-C(36)	1.404(3)
C(35)-H(35A)	1.00(2)
C(36)-C(37)	1.364(3)
C(36)-H(36A)	0.98(2)
C(37)-C(38)	1.435(3)
C(37)-C(44)	1.501(3)
C(38)-C(39)	1.411(3)
C(38)-C(43)	1.434(2)
C(39)-C(40)	1.362(3)
C(39)-H(39A)	1.01(2)
C(40)-C(41)	1.407(3)
C(40)-H(40A)	0.96(2)
C(41)-C(42)	1.367(3)
C(41)-H(41A)	0.94(2)
C(42)-C(43)	1.417(3)
C(42)-H(42A)	0.96(2)
C(44)-H(44A)	1.02(2)
C(44)-H(44B)	1.02(3)
C(44)-H(44C)	1.00(3)
C(5)-N(1)-C(1)	118.52(15)
N(1)-C(1)-C(2)	122.78(16)
N(1)-C(1)-C(8)	117.22(15)
C(2)-C(1)-C(8)	119.98(15)
C(3)-C(2)-C(1)	117.17(16)
C(3)-C(2)-C(6)	120.54(16)
C(1)-C(2)-C(6)	122.28(16)
C(2)-C(3)-C(4)	121.42(17)
C(2)-C(3)-H(3A)	118.9(13)
C(4)-C(3)-H(3A)	119.6(13)
C(3)-C(4)-C(5)	116.99(16)
C(3)-C(4)-C(7)	120.64(17)
C(5)-C(4)-C(7)	122.36(17)
N(1)-C(5)-C(4)	123.06(16)

N(1)-C(5)-C(19)	115.78(15)
C(4)-C(5)-C(19)	121.16(15)
C(2)-C(6)-H(6A)	110.8(13)
C(2)-C(6)-H(6B)	110.7(15)
H(6A)-C(6)-H(6B)	106(2)
C(2)-C(6)-H(6C)	111.4(14)
H(6A)-C(6)-H(6C)	107.0(19)
H(6B)-C(6)-H(6C)	111(2)
C(4)-C(7)-H(7A)	110.9(17)
C(4)-C(7)-H(7B)	112.4(18)
H(7A)-C(7)-H(7B)	107(2)
C(4)-C(7)-H(7C)	110.0(16)
H(7A)-C(7)-H(7C)	111(2)
H(7B)-C(7)-H(7C)	106(2)
C(9)-C(8)-C(17)	118.94(16)
C(9)-C(8)-C(1)	119.62(16)
C(17)-C(8)-C(1)	121.38(15)
C(8)-C(9)-C(10)	121.78(17)
C(8)-C(9)-H(9A)	118.0(11)
C(10)-C(9)-H(9A)	120.0(11)
C(11)-C(10)-C(9)	121.23(17)
C(11)-C(10)-H(10A)	120.4(10)
C(9)-C(10)-H(10A)	118.4(11)
C(10)-C(11)-C(12)	118.68(16)
C(10)-C(11)-C(18)	120.50(18)
C(12)-C(11)-C(18)	120.76(17)
C(11)-C(12)-C(13)	121.76(16)
C(11)-C(12)-C(17)	120.07(16)
C(13)-C(12)-C(17)	118.18(16)
C(14)-C(13)-C(12)	121.49(16)
C(14)-C(13)-H(13A)	119.6(12)
C(12)-C(13)-H(13A)	118.9(12)
C(13)-C(14)-C(15)	120.01(17)
C(13)-C(14)-H(14A)	120.1(12)
C(15)-C(14)-H(14A)	119.8(12)
C(16)-C(15)-C(14)	120.51(17)

C(16)-C(15)-H(15A)	119.0(11)
C(14)-C(15)-H(15A)	120.4(11)
C(15)-C(16)-C(17)	121.02(16)
C(15)-C(16)-H(16A)	121.4(11)
C(17)-C(16)-H(16A)	117.6(11)
C(16)-C(17)-C(8)	122.02(15)
C(16)-C(17)-C(12)	118.75(16)
C(8)-C(17)-C(12)	119.20(16)
C(11)-C(18)-H(18A)	110.4(12)
C(11)-C(18)-H(18B)	110.8(12)
H(18A)-C(18)-H(18B)	107.4(17)
C(11)-C(18)-H(18C)	109.7(13)
H(18A)-C(18)-H(18C)	108.2(18)
H(18B)-C(18)-H(18C)	110.3(18)
C(20)-C(19)-C(28)	119.21(16)
C(20)-C(19)-C(5)	120.31(15)
C(28)-C(19)-C(5)	120.48(15)
C(19)-C(20)-C(21)	121.23(16)
C(19)-C(20)-H(20A)	119.5(12)
C(21)-C(20)-H(20A)	119.2(12)
C(22)-C(21)-C(20)	121.75(17)
C(22)-C(21)-H(21A)	120.0(10)
C(20)-C(21)-H(21A)	118.3(10)
C(21)-C(22)-C(23)	118.69(16)
C(21)-C(22)-C(29)	120.30(16)
C(23)-C(22)-C(29)	121.00(16)
C(24)-C(23)-C(28)	118.30(16)
C(24)-C(23)-C(22)	122.02(16)
C(28)-C(23)-C(22)	119.68(15)
C(25)-C(24)-C(23)	121.31(17)
C(25)-C(24)-H(24A)	120.7(11)
C(23)-C(24)-H(24A)	118.0(11)
C(24)-C(25)-C(26)	120.57(17)
C(24)-C(25)-H(25A)	119.5(12)
C(26)-C(25)-H(25A)	119.9(12)
C(27)-C(26)-C(25)	119.95(18)

C(27)-C(26)-H(26A)	121.0(11)
C(25)-C(26)-H(26A)	119.0(11)
C(26)-C(27)-C(28)	121.14(17)
C(26)-C(27)-H(27A)	120.2(11)
C(28)-C(27)-H(27A)	118.6(11)
C(27)-C(28)-C(23)	118.72(15)
C(27)-C(28)-C(19)	121.84(16)
C(23)-C(28)-C(19)	119.43(15)
C(22)-C(29)-H(29A)	112.7(12)
C(22)-C(29)-H(29B)	110.6(13)
H(29A)-C(29)-H(29B)	107.3(17)
C(22)-C(29)-H(29C)	109.8(11)
H(29A)-C(29)-H(29C)	106.4(16)
H(29B)-C(29)-H(29C)	109.9(17)
C(30)-N(2)-C(30)#1	118.8(2)
N(2)-C(30)-C(31)	122.81(17)
N(2)-C(30)-C(34)	116.56(16)
C(31)-C(30)-C(34)	120.58(16)
C(32)-C(31)-C(30)	116.90(18)
C(32)-C(31)-C(33)	119.73(19)
C(30)-C(31)-C(33)	123.36(18)
C(31)#1-C(32)-C(31)	121.8(2)
C(31)#1-C(32)-H(32A)	119.11(12)
C(31)-C(32)-H(32A)	119.11(12)
C(31)-C(33)-H(33A)	112.7(16)
C(31)-C(33)-H(33B)	109.4(15)
H(33A)-C(33)-H(33B)	107(2)
C(31)-C(33)-H(33C)	111.4(18)
H(33A)-C(33)-H(33C)	109(2)
H(33B)-C(33)-H(33C)	107(2)
C(35)-C(34)-C(43)	118.91(17)
C(35)-C(34)-C(30)	118.00(17)
C(43)-C(34)-C(30)	123.09(15)
C(34)-C(35)-C(36)	121.79(19)
C(34)-C(35)-H(35A)	118.2(12)
C(36)-C(35)-H(35A)	120.0(12)

C(37)-C(36)-C(35)	121.52(18)
C(37)-C(36)-H(36A)	120.4(13)
C(35)-C(36)-H(36A)	118.1(13)
C(36)-C(37)-C(38)	118.86(17)
C(36)-C(37)-C(44)	119.91(19)
C(38)-C(37)-C(44)	121.2(2)
C(39)-C(38)-C(43)	118.49(17)
C(39)-C(38)-C(37)	121.72(17)
C(43)-C(38)-C(37)	119.79(17)
C(40)-C(39)-C(38)	121.63(19)
C(40)-C(39)-H(39A)	120.3(12)
C(38)-C(39)-H(39A)	118.1(12)
C(39)-C(40)-C(41)	119.82(19)
C(39)-C(40)-H(40A)	119.3(13)
C(41)-C(40)-H(40A)	120.8(13)
C(42)-C(41)-C(40)	120.76(19)
C(42)-C(41)-H(41A)	118.7(13)
C(40)-C(41)-H(41A)	120.4(13)
C(41)-C(42)-C(43)	120.77(18)
C(41)-C(42)-H(42A)	121.8(12)
C(43)-C(42)-H(42A)	117.5(12)
C(42)-C(43)-C(34)	122.35(16)
C(42)-C(43)-C(38)	118.52(17)
C(34)-C(43)-C(38)	119.12(16)
C(37)-C(44)-H(44A)	111.1(13)
C(37)-C(44)-H(44B)	109.3(14)
H(44A)-C(44)-H(44B)	108.7(19)
C(37)-C(44)-H(44C)	108.2(14)
H(44A)-C(44)-H(44C)	105.2(19)
H(44B)-C(44)-H(44C)	114(2)

Symmetry transformations used to generate equivalent atoms:

#1 $-x+1, y, -z+1/2$

Table 4. Anisotropic displacement parameters ($\text{\AA}^2 \times 10^3$) for toh13. The anisotropic displacement factor exponent takes the form: $-2\pi^2 [h^2 a^{*2}U^{11} + \dots + 2hka^*b^*U^{12}]$

	U ¹¹	U ²²	U ³³	U ²³	U ¹³	U ¹²
N(1)	16(1)	19(1)	26(1)	-1(1)	6(1)	1(1)
C(1)	16(1)	20(1)	21(1)	2(1)	6(1)	0(1)
C(2)	18(1)	19(1)	20(1)	3(1)	7(1)	2(1)
C(3)	23(1)	16(1)	28(1)	0(1)	7(1)	-1(1)
C(4)	18(1)	22(1)	28(1)	-1(1)	4(1)	-2(1)
C(5)	14(1)	22(1)	21(1)	1(1)	5(1)	0(1)
C(6)	20(1)	21(1)	33(1)	2(1)	6(1)	4(1)
C(7)	21(1)	26(1)	66(2)	-9(1)	-1(1)	-4(1)
C(8)	15(1)	18(1)	27(1)	-2(1)	6(1)	3(1)
C(9)	23(1)	24(1)	25(1)	1(1)	7(1)	1(1)
C(10)	24(1)	32(1)	21(1)	-2(1)	3(1)	5(1)
C(11)	20(1)	28(1)	26(1)	-8(1)	4(1)	2(1)
C(12)	14(1)	21(1)	25(1)	-6(1)	6(1)	1(1)
C(13)	16(1)	22(1)	31(1)	-8(1)	7(1)	-2(1)
C(14)	22(1)	16(1)	34(1)	-2(1)	11(1)	-1(1)
C(15)	20(1)	20(1)	26(1)	-2(1)	5(1)	3(1)
C(16)	15(1)	18(1)	25(1)	-3(1)	3(1)	1(1)
C(17)	14(1)	18(1)	27(1)	-4(1)	6(1)	3(1)
C(18)	22(1)	41(1)	29(1)	-7(1)	0(1)	-1(1)
C(19)	14(1)	20(1)	24(1)	-2(1)	4(1)	-2(1)
C(20)	20(1)	25(1)	25(1)	-2(1)	9(1)	1(1)
C(21)	19(1)	22(1)	23(1)	3(1)	3(1)	0(1)
C(22)	16(1)	15(1)	27(1)	-3(1)	4(1)	-3(1)
C(23)	15(1)	17(1)	26(1)	-4(1)	4(1)	-5(1)
C(24)	18(1)	24(1)	30(1)	-4(1)	6(1)	0(1)
C(25)	24(1)	35(1)	25(1)	-6(1)	9(1)	-4(1)
C(26)	24(1)	32(1)	22(1)	0(1)	3(1)	-5(1)
C(27)	16(1)	24(1)	27(1)	0(1)	2(1)	-2(1)
C(28)	14(1)	18(1)	24(1)	-3(1)	3(1)	-5(1)
C(29)	22(1)	23(1)	30(1)	0(1)	5(1)	4(1)
N(2)	18(1)	22(1)	22(1)	0	4(1)	0

C(30)	20(1)	25(1)	16(1)	1(1)	2(1)	0(1)
C(31)	27(1)	26(1)	21(1)	3(1)	3(1)	-4(1)
C(32)	36(2)	19(1)	23(1)	0	2(1)	0
C(33)	45(1)	32(1)	47(1)	10(1)	19(1)	-6(1)
C(34)	22(1)	26(1)	21(1)	4(1)	7(1)	-1(1)
C(35)	23(1)	38(1)	23(1)	2(1)	4(1)	-2(1)
C(36)	19(1)	48(1)	26(1)	11(1)	2(1)	4(1)
C(37)	24(1)	35(1)	29(1)	15(1)	10(1)	11(1)
C(38)	27(1)	20(1)	26(1)	9(1)	12(1)	3(1)
C(39)	39(1)	22(1)	32(1)	5(1)	18(1)	0(1)
C(40)	48(1)	24(1)	31(1)	-3(1)	18(1)	-8(1)
C(41)	29(1)	35(1)	33(1)	-5(1)	9(1)	-13(1)
C(42)	22(1)	30(1)	30(1)	-2(1)	10(1)	-3(1)
C(43)	22(1)	21(1)	24(1)	4(1)	8(1)	-2(1)
C(44)	32(1)	52(2)	38(1)	12(1)	11(1)	18(1)

Table 5. Hydrogen coordinates ($\times 10^4$) and isotropic displacement parameters ($\text{\AA}^2 \times 10^3$) for toh13.

	x	y	z	U(eq)
H(3A)	4492(10)	9630(30)	4440(6)	37(6)
H(6A)	3152(10)	8780(30)	3885(7)	44(6)
H(6B)	3445(11)	9950(40)	4220(7)	56(7)
H(6C)	3055(11)	8290(30)	4286(7)	48(7)
H(7A)	5923(13)	7830(40)	4500(7)	63(8)
H(7B)	5724(14)	8040(40)	4884(10)	92(11)
H(7C)	5579(12)	9480(40)	4583(7)	61(8)
H(9A)	3333(8)	6490(30)	3430(5)	24(5)
H(10A)	2388(8)	5420(20)	3115(5)	14(4)
H(13A)	1752(9)	1740(30)	3958(5)	25(5)
H(14A)	2145(10)	850(30)	4564(6)	38(6)
H(15A)	3078(8)	2090(20)	4895(5)	20(5)
H(16A)	3615(8)	3950(20)	4584(5)	15(4)
H(18A)	1561(9)	2110(30)	3305(6)	35(6)
H(18B)	1469(9)	3940(30)	3091(6)	32(6)
H(18C)	1268(10)	3730(30)	3500(6)	47(7)
H(20A)	5536(9)	4390(30)	4955(5)	26(5)
H(21A)	6369(8)	2540(20)	5079(5)	17(4)
H(24A)	6922(9)	1760(30)	3934(5)	25(5)
H(25A)	6564(9)	2810(30)	3334(6)	28(5)
H(26A)	5716(8)	4640(30)	3211(6)	24(5)
H(27A)	5250(8)	5490(20)	3696(5)	17(5)
H(29A)	7417(9)	1700(30)	4571(5)	30(5)
H(29B)	6952(10)	160(30)	4493(6)	39(6)
H(29C)	7141(8)	980(20)	4907(6)	23(5)
H(32A)	5000	2650(40)	2500	27(7)
H(33A)	4086(12)	4340(40)	3076(8)	66(8)
H(33B)	4289(12)	2680(40)	2889(7)	61(8)
H(33C)	3724(15)	3740(40)	2669(9)	89(11)
H(35A)	3425(9)	6580(30)	2400(6)	30(5)

H(36A)	2630(10)	8080(30)	2594(6)	34(6)
H(39A)	3581(10)	11580(30)	3553(6)	37(6)
H(40A)	4591(10)	11950(30)	3859(6)	39(6)
H(41A)	5388(10)	10440(30)	3665(6)	34(6)
H(42A)	5179(9)	8460(30)	3192(5)	26(5)
H(44A)	2650(10)	10220(30)	3393(7)	41(6)
H(44B)	2239(12)	9910(30)	2972(7)	55(7)
H(44C)	2701(10)	11610(30)	3084(6)	46(7)

Table 6. Torsion angles [°] for toh13.

C(5)-N(1)-C(1)-C(2)	-1.3(2)
C(5)-N(1)-C(1)-C(8)	177.11(15)
N(1)-C(1)-C(2)-C(3)	1.8(2)
C(8)-C(1)-C(2)-C(3)	-176.54(16)
N(1)-C(1)-C(2)-C(6)	-177.04(16)
C(8)-C(1)-C(2)-C(6)	4.6(2)
C(1)-C(2)-C(3)-C(4)	-0.3(3)
C(6)-C(2)-C(3)-C(4)	178.56(17)
C(2)-C(3)-C(4)-C(5)	-1.6(3)
C(2)-C(3)-C(4)-C(7)	178.85(19)
C(1)-N(1)-C(5)-C(4)	-0.8(3)
C(1)-N(1)-C(5)-C(19)	179.10(15)
C(3)-C(4)-C(5)-N(1)	2.2(3)
C(7)-C(4)-C(5)-N(1)	-178.25(19)
C(3)-C(4)-C(5)-C(19)	-177.71(16)
C(7)-C(4)-C(5)-C(19)	1.9(3)
N(1)-C(1)-C(8)-C(9)	-108.65(19)
C(2)-C(1)-C(8)-C(9)	69.8(2)
N(1)-C(1)-C(8)-C(17)	74.1(2)
C(2)-C(1)-C(8)-C(17)	-107.43(19)
C(17)-C(8)-C(9)-C(10)	3.2(3)
C(1)-C(8)-C(9)-C(10)	-174.04(16)
C(8)-C(9)-C(10)-C(11)	-1.1(3)
C(9)-C(10)-C(11)-C(12)	-2.0(3)
C(9)-C(10)-C(11)-C(18)	175.25(18)
C(10)-C(11)-C(12)-C(13)	-177.38(17)
C(18)-C(11)-C(12)-C(13)	5.4(3)
C(10)-C(11)-C(12)-C(17)	2.7(3)
C(18)-C(11)-C(12)-C(17)	-174.47(17)
C(11)-C(12)-C(13)-C(14)	-177.49(17)
C(17)-C(12)-C(13)-C(14)	2.4(3)
C(12)-C(13)-C(14)-C(15)	-0.6(3)
C(13)-C(14)-C(15)-C(16)	-0.9(3)
C(14)-C(15)-C(16)-C(17)	0.6(3)

C(15)-C(16)-C(17)-C(8)	178.99(16)
C(15)-C(16)-C(17)-C(12)	1.2(2)
C(9)-C(8)-C(17)-C(16)	179.84(16)
C(1)-C(8)-C(17)-C(16)	-2.9(2)
C(9)-C(8)-C(17)-C(12)	-2.4(2)
C(1)-C(8)-C(17)-C(12)	174.86(15)
C(11)-C(12)-C(17)-C(16)	177.26(16)
C(13)-C(12)-C(17)-C(16)	-2.6(2)
C(11)-C(12)-C(17)-C(8)	-0.6(2)
C(13)-C(12)-C(17)-C(8)	179.53(15)
N(1)-C(5)-C(19)-C(20)	-103.4(2)
C(4)-C(5)-C(19)-C(20)	76.5(2)
N(1)-C(5)-C(19)-C(28)	76.6(2)
C(4)-C(5)-C(19)-C(28)	-103.5(2)
C(28)-C(19)-C(20)-C(21)	-0.6(3)
C(5)-C(19)-C(20)-C(21)	179.42(16)
C(19)-C(20)-C(21)-C(22)	0.2(3)
C(20)-C(21)-C(22)-C(23)	0.3(3)
C(20)-C(21)-C(22)-C(29)	-178.95(17)
C(21)-C(22)-C(23)-C(24)	179.77(17)
C(29)-C(22)-C(23)-C(24)	-1.0(3)
C(21)-C(22)-C(23)-C(28)	-0.3(2)
C(29)-C(22)-C(23)-C(28)	178.97(16)
C(28)-C(23)-C(24)-C(25)	-0.1(3)
C(22)-C(23)-C(24)-C(25)	179.86(17)
C(23)-C(24)-C(25)-C(26)	0.7(3)
C(24)-C(25)-C(26)-C(27)	-0.6(3)
C(25)-C(26)-C(27)-C(28)	-0.1(3)
C(26)-C(27)-C(28)-C(23)	0.6(3)
C(26)-C(27)-C(28)-C(19)	-179.68(17)
C(24)-C(23)-C(28)-C(27)	-0.5(2)
C(22)-C(23)-C(28)-C(27)	179.50(15)
C(24)-C(23)-C(28)-C(19)	179.78(16)
C(22)-C(23)-C(28)-C(19)	-0.2(2)
C(20)-C(19)-C(28)-C(27)	-179.05(16)
C(5)-C(19)-C(28)-C(27)	0.9(2)

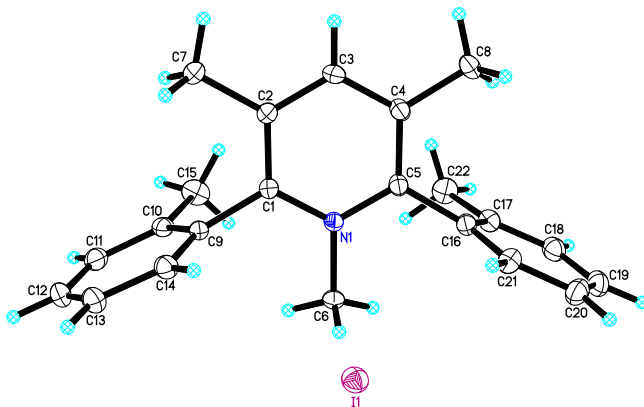
C(20)-C(19)-C(28)-C(23)	0.6(2)
C(5)-C(19)-C(28)-C(23)	-179.41(15)
C(30)#1-N(2)-C(30)-C(31)	1.10(13)
C(30)#1-N(2)-C(30)-C(34)	-176.39(17)
N(2)-C(30)-C(31)-C(32)	-2.1(2)
C(34)-C(30)-C(31)-C(32)	175.29(13)
N(2)-C(30)-C(31)-C(33)	176.50(17)
C(34)-C(30)-C(31)-C(33)	-6.1(3)
C(30)-C(31)-C(32)-C(31)#1	0.99(11)
C(33)-C(31)-C(32)-C(31)#1	-177.7(2)
N(2)-C(30)-C(34)-C(35)	117.23(18)
C(31)-C(30)-C(34)-C(35)	-60.3(2)
N(2)-C(30)-C(34)-C(43)	-62.6(2)
C(31)-C(30)-C(34)-C(43)	119.9(2)
C(43)-C(34)-C(35)-C(36)	0.1(3)
C(30)-C(34)-C(35)-C(36)	-179.72(17)
C(34)-C(35)-C(36)-C(37)	-0.6(3)
C(35)-C(36)-C(37)-C(38)	0.9(3)
C(35)-C(36)-C(37)-C(44)	-178.63(19)
C(36)-C(37)-C(38)-C(39)	179.49(18)
C(44)-C(37)-C(38)-C(39)	-1.0(3)
C(36)-C(37)-C(38)-C(43)	-0.7(3)
C(44)-C(37)-C(38)-C(43)	178.80(18)
C(43)-C(38)-C(39)-C(40)	-0.1(3)
C(37)-C(38)-C(39)-C(40)	179.68(18)
C(38)-C(39)-C(40)-C(41)	-0.7(3)
C(39)-C(40)-C(41)-C(42)	0.9(3)
C(40)-C(41)-C(42)-C(43)	-0.4(3)
C(41)-C(42)-C(43)-C(34)	-179.79(18)
C(41)-C(42)-C(43)-C(38)	-0.4(3)
C(35)-C(34)-C(43)-C(42)	179.42(18)
C(30)-C(34)-C(43)-C(42)	-0.8(3)
C(35)-C(34)-C(43)-C(38)	0.1(3)
C(30)-C(34)-C(43)-C(38)	179.87(16)
C(39)-C(38)-C(43)-C(42)	0.7(3)
C(37)-C(38)-C(43)-C(42)	-179.15(17)

C(39)-C(38)-C(43)-C(34)	-179.95(16)
C(37)-C(38)-C(43)-C(34)	0.2(2)

Symmetry transformations used to generate equivalent atoms:

#1 $-x+1, y, -z+1/2$

cis-1,3,5-Trimethyl-2,6-di-*o*-tolylpyridinium iodide



X-ray Data Collection, Structure Solution and Refinement.

A colorless crystal of approximate dimensions 0.197 x 0.204 x 0.401 mm was mounted on a glass fiber and transferred to a Bruker SMART APEX II diffractometer. The APEX2¹ program package was used to determine the unit-cell parameters and for data collection (15 sec/frame scan time for a sphere of diffraction data). The raw frame data was processed using SAINT² and SADABS³ to yield the reflection data file. Subsequent calculations were carried out using the SHELXTL⁴ program. The diffraction symmetry was $2/m$ and the systematic absences were consistent with the monoclinic space group $P2_1/n$ that was later determined to be correct.

The structure was solved by dual space methods and refined on F^2 by full-matrix least-squares techniques. The analytical scattering factors⁵ for neutral atoms were used throughout the analysis. Hydrogen atoms were included using a riding model.

Least-squares analysis yielded $wR2 = 0.0543$ and $Goof = 1.069$ for 222 variables refined against 5734 data (0.69 Å), $R1 = 0.0222$ for those 5304 data with $I > 2.0\sigma(I)$.

References.

16. APEX2 Version 2014.11-0, Bruker AXS, Inc.; Madison, WI 2014.
 17. SAINT Version 8.34a, Bruker AXS, Inc.; Madison, WI 2013.
 18. Sheldrick, G. M. SADABS, Version 2014/5, Bruker AXS, Inc.; Madison, WI 2014.
 19. Sheldrick, G. M. SHELXTL, Version 2014/7, Bruker AXS, Inc.; Madison, WI 2014
 20. International Tables for Crystallography 1992, Vol. C., Dordrecht: Kluwer Academic Publishers.
-

Definitions:

$$wR2 = [\Sigma[w(F_o^2 - F_c^2)^2] / \Sigma[w(F_o^2)^2]]^{1/2}$$

$$R1 = \Sigma||F_o| - |F_c|| / \Sigma|F_o|$$

Goof = S = $[\Sigma[w(F_o^2 - F_c^2)^2] / (n-p)]^{1/2}$ where n is the number of reflections and p is the total number of parameters refined.

The thermal ellipsoid plot is shown at the 50% probability level.

Table 1. Crystal data and structure refinement.

Identification code	toh10 (Tae Oh)	
Empirical formula	C ₂₂ H ₂₄ I N	
Formula weight	429.32	
Temperature	133(2) K	
Wavelength	0.71073 Å	
Crystal system	Monoclinic	
Space group	<i>P</i> 2 ₁ / <i>n</i>	
Unit cell dimensions	a = 10.6108(5) Å	∠ = 90°.
	b = 10.3795(5) Å	∠ = 94.9706(6)°.
	c = 17.2978(8) Å	∠ = 90°.
Volume	1897.93(16) Å ³	
Z	4	
Density (calculated)	1.502 Mg/m ³	
Absorption coefficient	1.690 mm ⁻¹	
F(000)	864	
Crystal color	colorless	
Crystal size	0.401 x 0.204 x 0.197 mm ³	
Theta range for data collection	2.171 to 31.130°	
Index ranges	-15 ≤ <i>h</i> ≤ 14, -14 ≤ <i>k</i> ≤ 14, -24 ≤ <i>l</i> ≤ 24	
Reflections collected	28662	
Independent reflections	5734 [R(int) = 0.0198]	
Completeness to theta = 25.500°	100.0 %	
Absorption correction	Semi-empirical from equivalents	
Max. and min. transmission	0.7462 and 0.6675	
Refinement method	Full-matrix least-squares on F ²	
Data / restraints / parameters	5734 / 0 / 222	
Goodness-of-fit on F ²	1.069	
Final R indices [I > 2σ(I) = 5304 data]	R1 = 0.0222, wR2 = 0.0532	
R indices (all data, 0.69 Å)	R1 = 0.0246, wR2 = 0.0543	
Largest diff. peak and hole	0.832 and -0.364 e.Å ⁻³	

Table 2. Atomic coordinates ($\times 10^4$) and equivalent isotropic displacement parameters ($\text{\AA}^2 \times 10^3$) for toh10. $U(\text{eq})$ is defined as one third of the trace of the orthogonalized U^{ij} tensor.

	x	y	z	$U(\text{eq})$
N(1)	9576(1)	4072(1)	6695(1)	14(1)
C(1)	9495(1)	3266(1)	6071(1)	14(1)
C(2)	10408(1)	3319(1)	5540(1)	16(1)
C(3)	11397(1)	4195(1)	5670(1)	17(1)
C(4)	11480(1)	5006(1)	6312(1)	17(1)
C(5)	10532(1)	4948(1)	6822(1)	15(1)
C(6)	8594(1)	3996(2)	7256(1)	18(1)
C(7)	10354(2)	2419(2)	4857(1)	22(1)
C(8)	12574(2)	5925(2)	6450(1)	23(1)
C(9)	8464(1)	2298(1)	5968(1)	15(1)
C(10)	8686(1)	1047(2)	6248(1)	18(1)
C(11)	7750(2)	120(2)	6073(1)	23(1)
C(12)	6643(2)	426(2)	5627(1)	26(1)
C(13)	6434(2)	1666(2)	5346(1)	24(1)
C(14)	7343(1)	2609(2)	5523(1)	19(1)
C(15)	9886(2)	713(2)	6730(1)	25(1)
C(16)	10546(1)	5848(1)	7498(1)	17(1)
C(17)	11303(1)	5564(2)	8180(1)	19(1)
C(18)	11416(2)	6500(2)	8765(1)	23(1)
C(19)	10770(2)	7658(2)	8683(1)	24(1)
C(20)	9987(2)	7914(2)	8017(1)	24(1)
C(21)	9877(2)	7017(2)	7416(1)	20(1)
C(22)	11933(2)	4281(2)	8288(1)	26(1)
I(1)	6364(1)	6423(1)	6055(1)	19(1)

Table 3. Bond lengths [\AA] and angles [$^\circ$].

N(1)-C(1)	1.3620(18)
N(1)-C(5)	1.3656(18)
N(1)-C(6)	1.4870(18)
C(1)-C(2)	1.3933(19)
C(1)-C(9)	1.4855(19)
C(2)-C(3)	1.392(2)
C(2)-C(7)	1.503(2)
C(3)-C(4)	1.391(2)
C(4)-C(5)	1.396(2)
C(4)-C(8)	1.505(2)
C(5)-C(16)	1.497(2)
C(9)-C(14)	1.398(2)
C(9)-C(10)	1.399(2)
C(10)-C(11)	1.397(2)
C(10)-C(15)	1.501(2)
C(11)-C(12)	1.385(2)
C(12)-C(13)	1.387(3)
C(13)-C(14)	1.389(2)
C(16)-C(17)	1.399(2)
C(16)-C(21)	1.407(2)
C(17)-C(18)	1.401(2)
C(17)-C(22)	1.494(2)
C(18)-C(19)	1.385(2)
C(19)-C(20)	1.386(2)
C(20)-C(21)	1.392(2)
C(1)-N(1)-C(5)	122.05(12)
C(1)-N(1)-C(6)	119.06(12)
C(5)-N(1)-C(6)	118.89(12)
N(1)-C(1)-C(2)	119.93(13)
N(1)-C(1)-C(9)	120.40(12)
C(2)-C(1)-C(9)	119.63(13)
C(3)-C(2)-C(1)	118.46(13)
C(3)-C(2)-C(7)	120.67(13)

C(1)-C(2)-C(7)	120.83(13)
C(4)-C(3)-C(2)	121.31(13)
C(3)-C(4)-C(5)	118.60(13)
C(3)-C(4)-C(8)	120.39(13)
C(5)-C(4)-C(8)	121.02(13)
N(1)-C(5)-C(4)	119.61(13)
N(1)-C(5)-C(16)	119.85(12)
C(4)-C(5)-C(16)	120.54(13)
C(14)-C(9)-C(10)	121.03(13)
C(14)-C(9)-C(1)	119.55(13)
C(10)-C(9)-C(1)	119.06(13)
C(11)-C(10)-C(9)	117.93(14)
C(11)-C(10)-C(15)	120.98(15)
C(9)-C(10)-C(15)	121.08(14)
C(12)-C(11)-C(10)	121.03(15)
C(11)-C(12)-C(13)	120.67(15)
C(12)-C(13)-C(14)	119.32(16)
C(13)-C(14)-C(9)	120.00(15)
C(17)-C(16)-C(21)	120.97(14)
C(17)-C(16)-C(5)	119.53(13)
C(21)-C(16)-C(5)	119.29(13)
C(16)-C(17)-C(18)	118.00(14)
C(16)-C(17)-C(22)	120.77(14)
C(18)-C(17)-C(22)	121.19(15)
C(19)-C(18)-C(17)	121.16(15)
C(18)-C(19)-C(20)	120.41(15)
C(19)-C(20)-C(21)	119.89(15)
C(20)-C(21)-C(16)	119.51(15)

Table 4. Anisotropic displacement parameters ($\text{\AA}^2 \times 10^3$). The anisotropic displacement factor exponent takes the form: $-2\pi^2 [h^2 a^{*2}U^{11} + \dots + 2 h k a^* b^* U^{12}]$

	U ¹¹	U ²²	U ³³	U ²³	U ¹³	U ¹²
N(1)	15(1)	14(1)	13(1)	0(1)	2(1)	-2(1)
C(1)	14(1)	13(1)	15(1)	-1(1)	2(1)	-1(1)
C(2)	17(1)	16(1)	15(1)	-2(1)	3(1)	-1(1)
C(3)	15(1)	18(1)	18(1)	0(1)	6(1)	-2(1)
C(4)	16(1)	16(1)	18(1)	0(1)	1(1)	-3(1)
C(5)	16(1)	14(1)	15(1)	-1(1)	1(1)	-2(1)
C(6)	18(1)	20(1)	16(1)	-2(1)	7(1)	-3(1)
C(7)	24(1)	24(1)	20(1)	-7(1)	7(1)	-5(1)
C(8)	20(1)	24(1)	26(1)	-3(1)	4(1)	-9(1)
C(9)	15(1)	17(1)	15(1)	-3(1)	4(1)	-3(1)
C(10)	18(1)	16(1)	19(1)	-1(1)	6(1)	-1(1)
C(11)	27(1)	16(1)	26(1)	-2(1)	11(1)	-4(1)
C(12)	22(1)	28(1)	28(1)	-9(1)	6(1)	-10(1)
C(13)	18(1)	32(1)	23(1)	-6(1)	1(1)	-4(1)
C(14)	18(1)	21(1)	18(1)	-1(1)	1(1)	-1(1)
C(15)	23(1)	24(1)	29(1)	8(1)	1(1)	3(1)
C(16)	18(1)	16(1)	16(1)	-1(1)	3(1)	-3(1)
C(17)	18(1)	19(1)	20(1)	1(1)	2(1)	-2(1)
C(18)	24(1)	27(1)	19(1)	-2(1)	2(1)	-6(1)
C(19)	29(1)	25(1)	20(1)	-5(1)	5(1)	-9(1)
C(20)	30(1)	17(1)	25(1)	-1(1)	7(1)	1(1)
C(21)	23(1)	18(1)	19(1)	-1(1)	2(1)	2(1)
C(22)	25(1)	26(1)	26(1)	2(1)	-1(1)	3(1)
I(1)	20(1)	21(1)	18(1)	1(1)	3(1)	-2(1)

Table 5. Hydrogen coordinates ($\times 10^4$) and isotropic displacement parameters ($\text{\AA}^2 \times 10^3$).

	x	y	z	U(eq)
H(3A)	12028	4239	5313	21
H(6A)	8959	4267	7771	27
H(6B)	8288	3108	7283	27
H(6C)	7887	4565	7086	27
H(7A)	9546	2531	4544	33
H(7B)	10427	1528	5042	33
H(7C)	11052	2613	4540	33
H(8A)	12920	5867	6993	34
H(8B)	12281	6806	6338	34
H(8C)	13232	5700	6110	34
H(11A)	7874	-733	6263	27
H(12A)	6021	-220	5512	31
H(13A)	5677	1869	5036	29
H(14A)	7202	3465	5341	23
H(15A)	10602	1146	6518	38
H(15B)	10016	-221	6722	38
H(15C)	9824	998	7266	38
H(18A)	11944	6337	9227	28
H(19A)	10863	8282	9086	29
H(20A)	9527	8699	7970	28
H(21A)	9354	7194	6955	24
H(22A)	12435	4108	7850	39
H(22D)	11288	3610	8314	39
H(22B)	12488	4284	8771	39

Table 6. Torsion angles [°].

C(5)-N(1)-C(1)-C(2)	0.2(2)
C(6)-N(1)-C(1)-C(2)	-179.82(13)
C(5)-N(1)-C(1)-C(9)	178.02(13)
C(6)-N(1)-C(1)-C(9)	-2.0(2)
N(1)-C(1)-C(2)-C(3)	0.8(2)
C(9)-C(1)-C(2)-C(3)	-177.07(14)
N(1)-C(1)-C(2)-C(7)	178.63(14)
C(9)-C(1)-C(2)-C(7)	0.8(2)
C(1)-C(2)-C(3)-C(4)	-0.2(2)
C(7)-C(2)-C(3)-C(4)	-178.04(15)
C(2)-C(3)-C(4)-C(5)	-1.3(2)
C(2)-C(3)-C(4)-C(8)	178.63(14)
C(1)-N(1)-C(5)-C(4)	-1.7(2)
C(6)-N(1)-C(5)-C(4)	178.26(13)
C(1)-N(1)-C(5)-C(16)	177.42(13)
C(6)-N(1)-C(5)-C(16)	-2.6(2)
C(3)-C(4)-C(5)-N(1)	2.3(2)
C(8)-C(4)-C(5)-N(1)	-177.68(14)
C(3)-C(4)-C(5)-C(16)	-176.89(14)
C(8)-C(4)-C(5)-C(16)	3.2(2)
N(1)-C(1)-C(9)-C(14)	92.85(17)
C(2)-C(1)-C(9)-C(14)	-89.29(18)
N(1)-C(1)-C(9)-C(10)	-94.01(17)
C(2)-C(1)-C(9)-C(10)	83.85(18)
C(14)-C(9)-C(10)-C(11)	-0.4(2)
C(1)-C(9)-C(10)-C(11)	-173.46(13)
C(14)-C(9)-C(10)-C(15)	-179.58(14)
C(1)-C(9)-C(10)-C(15)	7.4(2)
C(9)-C(10)-C(11)-C(12)	0.9(2)
C(15)-C(10)-C(11)-C(12)	-179.94(15)
C(10)-C(11)-C(12)-C(13)	-0.4(3)
C(11)-C(12)-C(13)-C(14)	-0.6(3)
C(12)-C(13)-C(14)-C(9)	1.1(2)
C(10)-C(9)-C(14)-C(13)	-0.6(2)

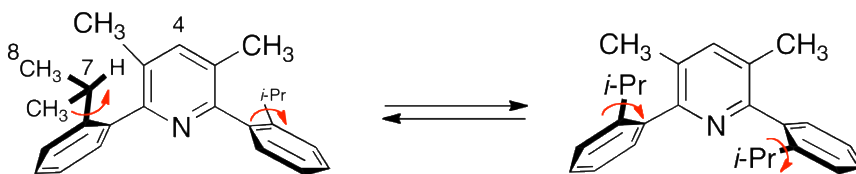
C(1)-C(9)-C(14)-C(13)	172.43(14)
N(1)-C(5)-C(16)-C(17)	98.70(17)
C(4)-C(5)-C(16)-C(17)	-82.16(18)
N(1)-C(5)-C(16)-C(21)	-86.50(18)
C(4)-C(5)-C(16)-C(21)	92.65(18)
C(21)-C(16)-C(17)-C(18)	-2.5(2)
C(5)-C(16)-C(17)-C(18)	172.26(14)
C(21)-C(16)-C(17)-C(22)	175.31(15)
C(5)-C(16)-C(17)-C(22)	-10.0(2)
C(16)-C(17)-C(18)-C(19)	1.8(2)
C(22)-C(17)-C(18)-C(19)	-176.01(15)
C(17)-C(18)-C(19)-C(20)	0.4(2)
C(18)-C(19)-C(20)-C(21)	-1.9(2)
C(19)-C(20)-C(21)-C(16)	1.2(2)
C(17)-C(16)-C(21)-C(20)	1.0(2)
C(5)-C(16)-C(21)-C(20)	-173.69(14)

APPENDIX C – ACTIVATION CALCULATIONS FROM ¹H DNMR DATA

When possible two methods were used. In the case where the cis-trans-isomer was not in equal amounts as indicated by the ¹H NMR, the complete line analysis is needed. In the case where the interested area has equal population, the simplified is probably more accurate. The major cause of the error in the calculation comes from the calibration of the temperature, which was not carried out. The second major issue is also related to temperature, the increments of the temperature should be closer around the coalescence temperature for better linear fit. The third issue is the lower temperature limits of the instrument, where equilibrium rates are slowed enough to obtain absorption peaks that are independent needed in the calculations and analysis. Access to the instrument was highly limited in this investigation.

3,5-Dimethyl-2,6-di(2-isopropyl)pyridine

Rotations of the isopropyl group



Method A

The two low energy points of rotations of the isopropyl group results in no change in the conformation. There is also rotational isomers for the trans- and *cis*-isomers.⁴⁴ Eyring equation is applied to find the ΔG^\ddagger (Equation 1). The coalescence rate constant, k_C , is given by equation 2, provided the two singlets have equal intensities and the two nuclei are not coupled.

$$k_C = \kappa \frac{k_B T_c}{h} e^{-\Delta G^\ddagger / RT_c} \quad (1)$$

k_C = rate constant at coalescence temperature

κ = transmission coefficient = the fraction of all reacting molecules reaching the transition state that proceed to deactivated product molecules.

k_B = Boltzmann's constant = 3.29986×10^{-24} cal K⁻¹ = 1.380662×10^{-23} J K⁻¹

h = Planck's constant = 1.58369×10^{-34} cal s = 6.626176×10^{-34} J s

R = gas constant = 1.98719 cal mol⁻¹ K⁻¹ = 8.31441 J mol⁻¹ K⁻¹

T_c = temperature of coalescence

$$k_C = \frac{\pi \Delta \nu}{\sqrt{2}} \quad (2)$$

In reactions that proceed without electronic excitation and one pathway, κ could be assumed as close to unity, thus equation 3 was obtained for $\kappa = 1$.

$$\Delta G^\ddagger = 19.14 \bullet T_c \left[10.319 + \log \frac{T_c}{K} \right] \text{ J mol}^{-1} \quad (3)$$

Cis-isomer- the isopropyl absorbance was used in the calculations.

$$T_c = 298\text{K}$$

$\Delta \nu = 68.0$ Hz, from isopropyl methyl groups of *cis*-isomer

$$k_C = \frac{\pi \Delta \nu}{\sqrt{2}} = 2.22 \Delta \nu = 150.96 \text{ s}^{-1}$$

$$\begin{aligned} \Delta G^\ddagger &= 19.14 \bullet T_c \left[10.319 + \log \frac{T_c}{K} \right] \text{ J mol}^{-1} \\ &= 5703.72(10.32 + 0.29535) \text{ J/mol} \\ &= 5703.72(10.615) \text{ J/mol} \\ &= 60,547 \text{ J/mol} \\ &= 60.5 \text{ kJ/mol} \end{aligned}$$

Trans-isomer- the isopropyl absorbance was used in the calculations.

$$T_C = 298\text{K}$$

$\Delta\nu = 22.4$ Hz, from isopropyl methyl groups of *trans*-isomer

$$k_C = \frac{\pi\Delta\nu}{\sqrt{2}} = 2.22 \Delta\nu = 49.728 \text{ s}^{-1}$$

$$\begin{aligned}\Delta G^\ddagger &= 5703.72(10.32 + 5.9926) \text{ J/mol} \\ &= 5703.72(16.3126) \text{ J/mol} \\ &= 93,042.5014 \text{ J/mol} \\ &= 93.0 \text{ kJ/mol}\end{aligned}$$

Method B: Complete line analysis-absorbance on the 4-position of pyridine was used.

Bruker's software TopSpin was used for complete line analysis. Eyring equation was rearranged equation 4).

$$RT \left(\ln \frac{h}{K_B} + \ln \frac{k}{T} \right) = -\Delta G^\ddagger \quad (4)$$

k/s	Temp	8.3144xT	ln(h/K _B)	ln(rate/T)	8.3144xT(-23.76+ln(rate/T))	(-ΔG [‡]) kJ/mol
3.793	240	1995.456	-23.76	-4.14748166	-55688.15172	-55.7
2.972	250	2078.6	-23.76	-4.43222579	-58600.36053	-58.6
2.571	250	2078.6	-23.76	-4.57716599	-58901.63323	-58.9
5.062	275	2286.46	-23.76	-3.99500944	-63460.71887	-63.5
3.748	275	2286.46	-23.76	-4.29554873	-64147.88996	-64.1
61.877	298	2477.6912	-23.76	-1.57194494	-62764.73706	-62.8
Average						-60.6

The rate was given by complete line analysis. The rate was applied to the Eyring equation giving

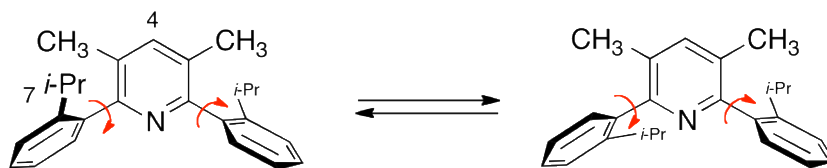
ΔG^\ddagger for each ¹H NMR taken at various temperatures. These averaged to ΔG^\ddagger of 60.6 kJ/mol.

TopSpin could not distinguish between the isopropyl groups on the *cis*- and *trans*-isomer as at the coalescence temperature there was overlap of all the isopropyl groups, which includes isopropyl signals from the *cis*-isomer, *trans*-isomer, and two isomers from the rotations of the

isopropyl groups. The margin of error is uncertain as TopSpin program was unable to distinguish the overlap of the isopropyl groups near the coalescence temperature between the isopropyl rotational and *cis*- and *trans*-isomers.

Cis-trans isomerization

Method A-approximation



$$T_C = 298\text{K}$$

$\Delta\nu = 15.6\text{ Hz}$, from hydrogen singlet on C-4

$$k_C = \frac{\pi\Delta\nu}{\sqrt{2}} = 2.22 \Delta\nu = 34.632\text{ s}^{-1}$$

$$k = \kappa \frac{k_B T_c}{h} e^{-\Delta G^\ddagger / RT_c}$$

$$\Delta G^\ddagger = 19.14 \cdot T_c \left[10.018 + \log \frac{T_c}{K} \right] \text{ J mol}^{-1}$$

$$\begin{aligned} &= 5,703.72 [10.018 + \log 8.6048] \text{ J mol}^{-1} \\ &= 5,703.72 [10.018 + 0.934739] \text{ J mol}^{-1} \\ &= 62,471.4 \text{ J mol}^{-1} \\ &= 62.5 \text{ kJ mol}^{-1} \end{aligned}$$

Or 64.2 kJ mol^{-1} if transmission coefficient is 1.

Or 65.9 kJ mol^{-1} if transmission coefficient is 2.

$$\Delta G^\ddagger = 19.14 \cdot T_c [10.62 + \log(T_c / k_C)] \text{ J mol}^{-1}$$

Method B-complete line analysis

Rate by line analysis

k/s	Temp, K	8.3144xT	ln(h/KB)	ln(rate/T)	$\frac{8.3144xT(-23.76+\ln(\text{rate}/T))}{23.76+\ln(\text{rate}/T)}$	(-ΔG‡), kJ/mol
0.464	240	1995.456	-23.76	-6.24851	-59880.7	-59.9
1.178	250	2078.60	-23.76	-5.35764	-60523.9	-60.5
0.935	250	2078.60	-23.76	-5.58867	-61004.1	-61.0
5.048	275	2286.46	-23.76	-3.99778	-63467.1	-63.5
5.072	275	2286.46	-23.76	-3.99304	-63456.2	-63.5
41.543	298	2477.69	-23.76	-1.97036	-63751.9	-63.8
Average						-62.0

Rate divided in half from complete line analysis

(k/s)/2	Temp, K	8.3144xT	ln(h/KB)	ln(rate/T)	$\frac{8.3144xT(-23.76+\ln(\text{rate}/T))}{23.76+\ln(\text{rate}/T)}$	(-ΔG‡), kJ/mol
0.232	240	1995.456	-23.76	-6.94166	-61263.8	-61.3
0.589	250	2078.60	-23.76	-6.05079	-61964.7	-62.0
0.4675	250	2078.60	-23.76	-6.28182	-62444.9	-62.4
2.524	275	2286.46	-23.76	-4.69093	-65051.9	-65.1
2.536	275	2286.46	-23.76	-4.68618	-65041.1	-65.0
20.7715	298	2477.69	-23.76	-2.66351	-65469.3	-65.5
Average						-63.5

Cis- versus trans-isomer

$K_{eq} = [I]/[II]$ at 240K integration show trans:cis ratio 2.75:1

$$\begin{aligned}\Delta G_o &= -RT \ln K_{eq} \\ &= -RT \ln 2.76 \\ &= -8.3144 \cdot 240 \times \ln 2.76 \\ &= -1995.46 \times 1.015 \text{ J/mol} \\ &= -2025.84 \text{ J/mol} \\ &= -2.0 \text{ kJ/mol}\end{aligned}$$

Trans-isomer is 2.0 kJ/mol more stable.

Or

$$\begin{aligned}\Delta G_o &= -1995.46 \times \ln(1.0/2.75) \\ &= -1995.46 \times -1.0116 \\ &= 2.0 \text{ kJ/mol}\end{aligned}$$

Cis-isomer E_a is 2.0 kJ/mol less stable.

3,5-Dimethyl-2,6-di(2-methylphenyl)pyridine

Method A- estimate, using hydrogen on the 4-position of pyridine

$$T_c = 270\text{K}$$

$$\Delta\nu = 10.8\text{ Hz}$$

$$k_c = \frac{\pi\Delta\nu}{\sqrt{2}} = 2.22 \Delta\nu = 24.0\text{ s}^{-1}$$

$$\begin{aligned}\Delta G^\ddagger &= 19.14 \cdot T_c \left[10.319 + \log \frac{T_c}{K} \right] \text{ J mol}^{-1} \\ &= 5263.5(10.32 + 1.05) \text{ J/mol} \\ &= 5263.5(12.63) \text{ J/mol} \\ &= 66478.0 \text{ J/mol} \\ &= 66.5 \text{ kJ/mol}\end{aligned}$$

This is the minimal estimated ΔG^\ddagger as the instrument could not go lower in temperature to find the maximum $\Delta\nu$.

Method B- complete line analysis – hydrogen on the 4-position of pyridine was used

k/s	Temp, K	8.3144xT	ln(h/KB)	ln(rate/T)	$\frac{8.3144 \times T(-23.76 + \ln(\text{rate}/T))}{23.76 + \ln(\text{rate}/T)}$	(-ΔG‡)
13.694	240	1995.456	-23.76	-2.864	-53126.38	-53.13
26.63	250	2078.6	-23.76	-2.239	-54042.40	-54.04
44.697	270	2244.888	-23.76	-1.799	-57376.00	-57.38
Average						-54.85

Rate halved

(k/s)2	Temp	8.3144xT	ln(h/KB)	ln(rate/T)	$\frac{8.3144 \times T(-23.76 + \ln(\text{rate}/T))}{23.76 + \ln(\text{rate}/T)}$	(-ΔG‡)
6.847	240	1995.456	-23.76	-3.557	-54509.53	-54.51
13.315	250	2078.6	-23.76	-2.933	-55483.18	-55.48
22.3485	270	2244.888	-23.76	-2.492	-58932.04	-58.93
Average						-56.31

3,5-Dimethyl-2,6-Di(4-methylnaphthyl-1-yl)pyridine

Method A- Using the 4-methyl on naphthyl absorbance.

$$T_c = 275\text{K}$$

$$\Delta\nu = 6.80\text{ Hz}$$

$$k_c = \frac{\pi\Delta\nu}{\sqrt{2}} = 2.22 \Delta\nu = 15.1\text{ s}^{-1}$$

$$\begin{aligned}\Delta G^\ddagger &= 19.14 \cdot T_c \left[10.319 + \log \frac{T_c}{K} \right] \text{ J mol}^{-1} \\ &= 5263.5(10.32 + 1.26) \text{ J/mol} \\ &= 5263.5(11.58) \text{ J/mol} \\ &= 60,953.2 \text{ J/mol} \\ &= 60.9 \text{ kJ/mol}\end{aligned}$$

This is the minimal estimated ΔG^\ddagger as the instrument could not go lower in temperature to find the maximum $\Delta\nu$.

Method B- complete line analysis- using 4-methyl on the naphthyl

k/s	Temp	8.3144xT	ln(h/KB)	ln(rate/T)	$\frac{8.3144xT(-23.76+\ln(\text{rate}/T))}{-}$	(- ΔG^\ddagger)
1.4796	240	1995.5	-23.76	-5.08887	-57566.6	-57.6
0.738	250	2078.6	-23.76	-5.82527	-61495.9	-61.5
4.3464	250	2078.6	-23.76	-4.05211	-57810.3	-57.8
25.4301	275	2286.5	-23.76	-2.38084	-59770.0	-59.8
49.4173	275	2286.5	-23.76	-1.71647	-58250.9	-58.3
average						-59.0

Rate halved

(k/s)/2	Temp	8.3144xT	ln(h/KB)	ln(rate/T)	$\frac{8.3144xT(-23.76+\ln(\text{rate}/T))}{-}$	(- ΔG^\ddagger)
0.7398	240	1995.5	-23.76	-5.78201	-58949.8	-58.9
0.369	250	2078.6	-23.76	-6.51842	-62936.7	-62.9
2.1732	250	2078.6	-23.76	-4.74526	-59251.0	-59.3
12.7151	275	2286.5	-23.76	-3.07398	-61354.8	-61.4
24.7087	275	2286.5	-23.76	-2.40962	-59835.8	-59.8
average						-60.5

Method B- complete line analysis- using H on the 8-position of the naphthyl ring

k/s	Temp	8.3144xT	ln(h/KB)	ln(rate/T)	$\frac{8.3144xT(-}{23.76+ln(rate/T)}$	(-ΔG‡)
3.793	240	1995.5	-23.76	-4.14748	-55688.2	-55.7
2.972	250	2078.6	-23.76	-4.43223	-58600.4	-58.6
2.571	250	2078.6	-23.76	-4.57717	-58901.6	-58.9
5.062	275	2286.5	-23.76	-3.99501	-63460.7	-63.5
3.748	275	2286.5	-23.76	-4.29555	-64147.9	-64.1
61.877	298	2477.7	-23.76	-1.57194	-62764.7	-62.8
					average	-60.6

Rate halved

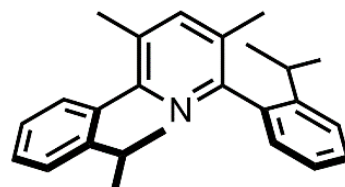
(k/s)/2	Temp	8.3144xT	ln(h/KB)	ln(rate/T)	$\frac{8.3144xT(-}{23.76+ln(rate/T)}$	(-ΔG‡)
1.8965	240	1995.5	-23.76	-4.84063	-57071.3	-57.1
1.486	250	2078.6	-23.76	-5.12537	-60041.1	-60.0
1.2855	250	2078.6	-23.76	-5.27031	-60342.4	-60.3
2.5310	275	2286.5	-23.76	-4.68816	-65045.6	-65.0
1.8740	275	2286.5	-23.76	-4.9887	-65732.7	-65.7
30.9385	298	2477.7	-23.76	-2.26509	-64482.1	-64.5
					average	-62.1

APPENDIX D: SELECTED SPECTRA

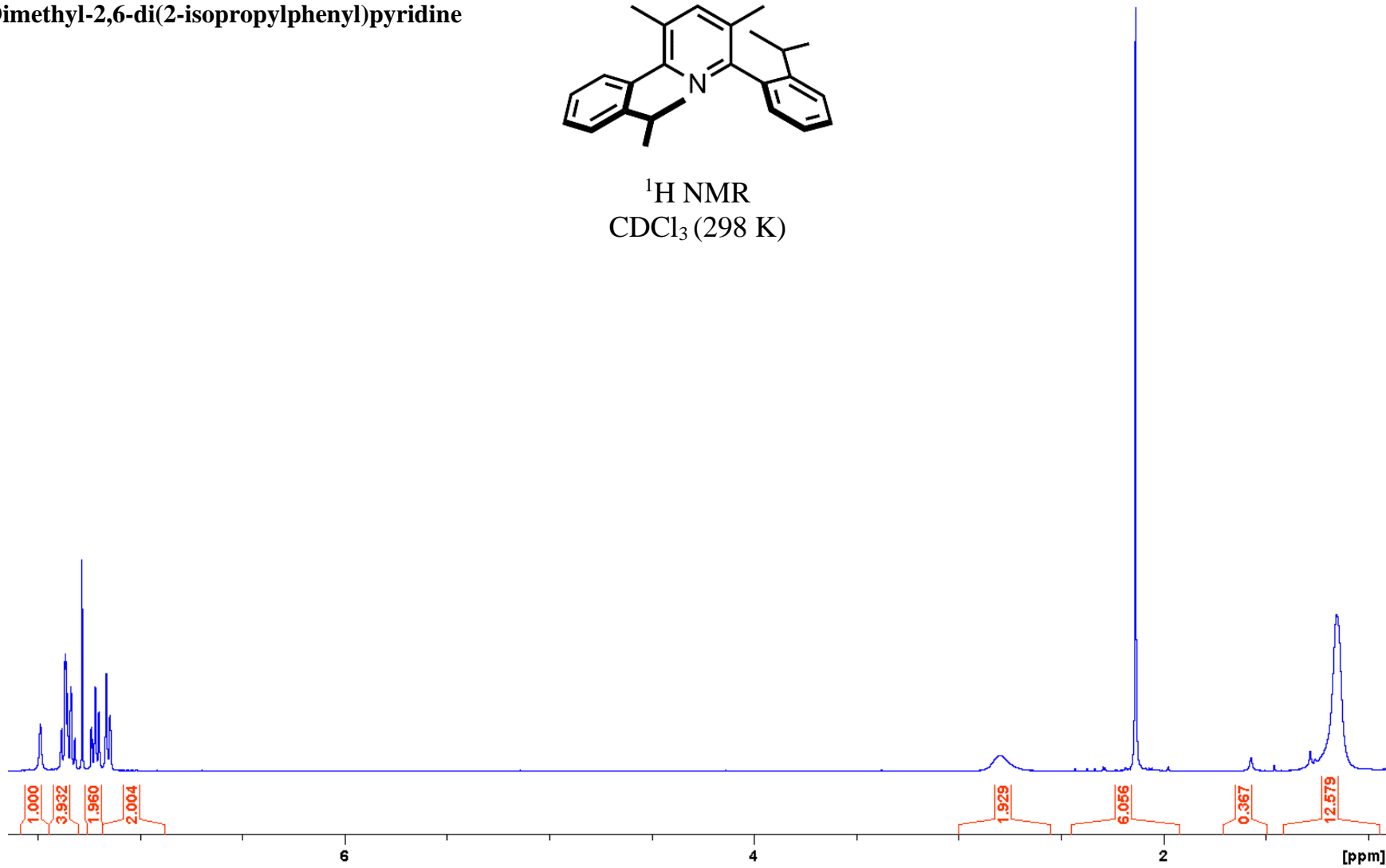
Compound	Page
3,5-Dimethyl-2,6-di(2-isopropylphenyl)pyridine.....	185
2-bromo-6-(2-isopropylphenyl)-3,5-dimethylpyridine.....	195
3,5-Dimethyl-2,6-di(2-methylphenyl)pyridine.....	202
2-bromo-3,5-dimethyl-6-(<i>o</i> -tolyl)pyridine.....	211
3,5-Dimethyl-2,6-di(3-methylphenyl)pyridine.....	218
2-bromo-3,5-dimethyl-6-(<i>m</i> -tolyl)pyridine.....	225
3,5-Dimethyl-2,6-Di(4-methylnaphthyl-1-yl)pyridine	229
2-bromo-3,5-dimethyl-6-(4-methylnaphthalen-1-yl)pyridine.....	238
1,3,5-Dimethyl-2,6-Di(4-methylnaphthyl-1-yl)pyridinium iodide.....	245
1,3,5-Trimethyl-2,6-di-(2-methylphenyl)pyridinium iodide.....	253
1,3,5-trimethyl-2,6-di-(3-methylphenyl)pyridinium iodide.....	261

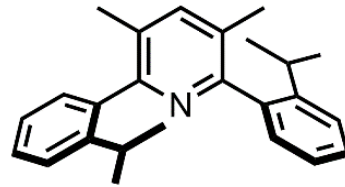
Appendix D includes ^{13}C NMR, ^1H NMR, IR spectra and MS spectrometry data.

3,5-Dimethyl-2,6-di(2-isopropylphenyl)pyridine

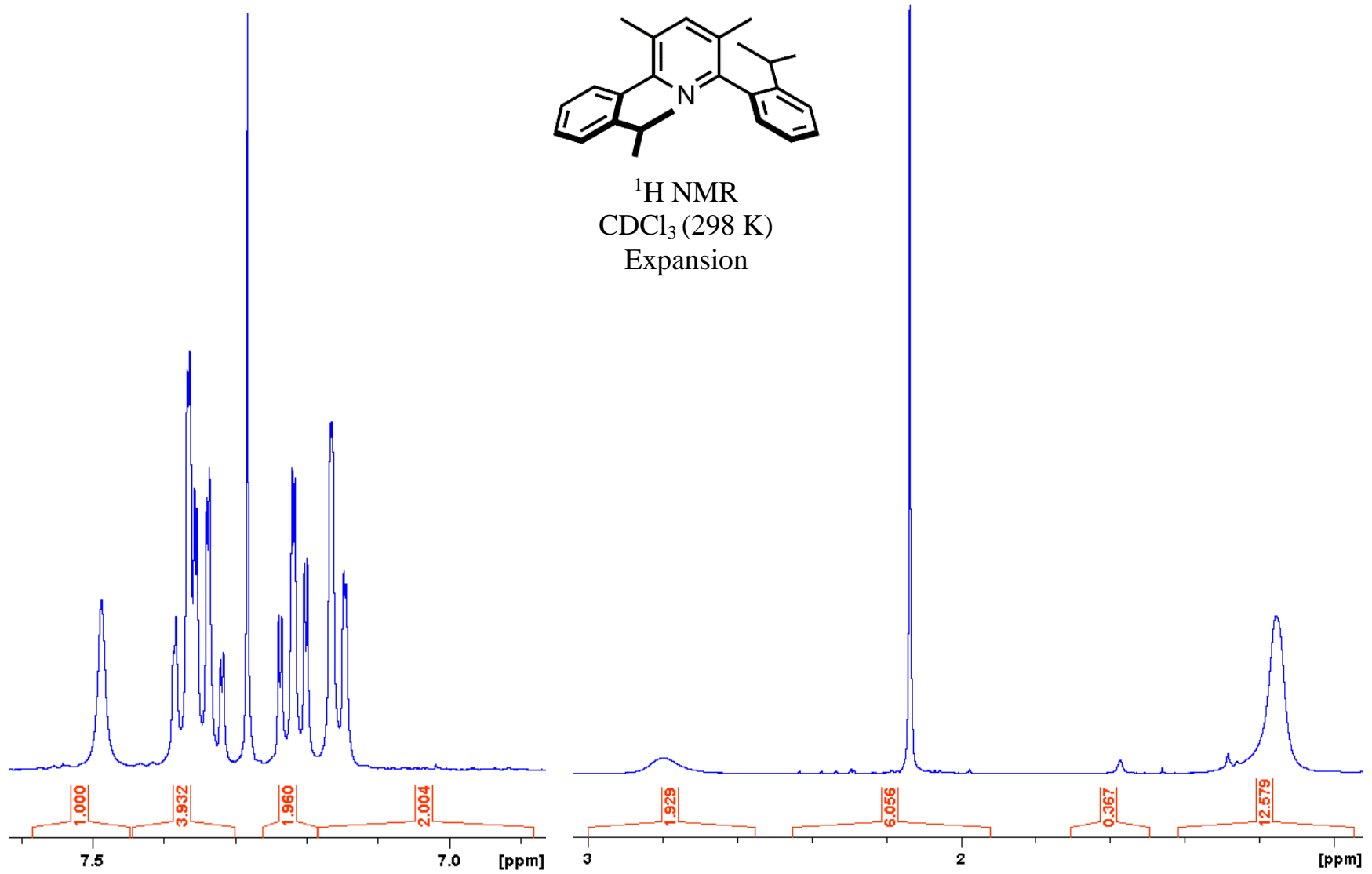


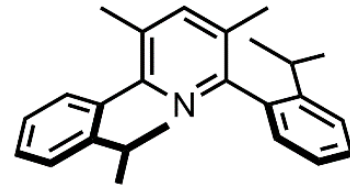
^1H NMR
 CDCl_3 (298 K)



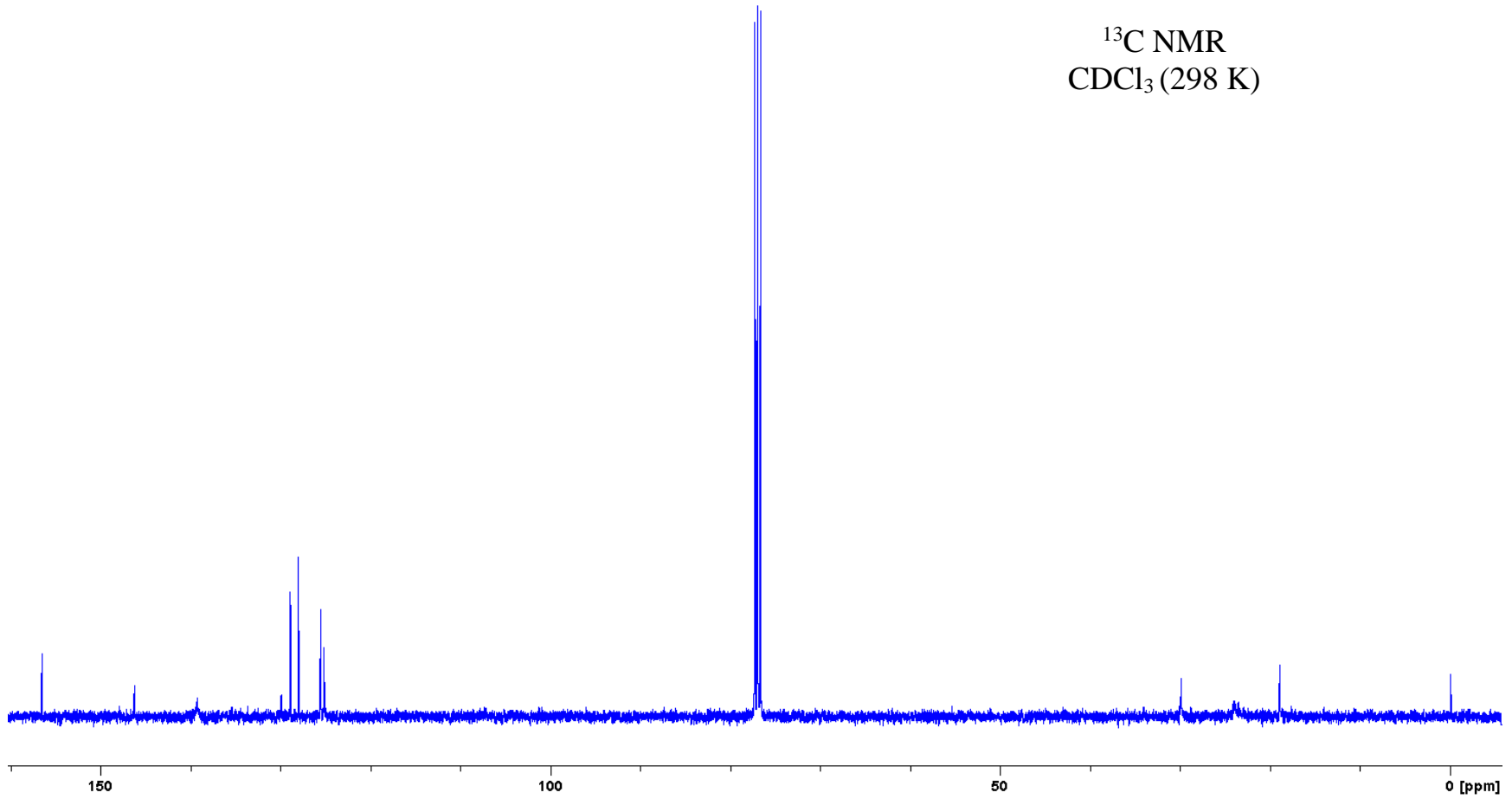


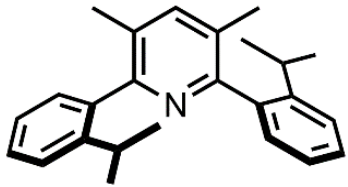
^1H NMR
 CDCl_3 (298 K)
Expansion



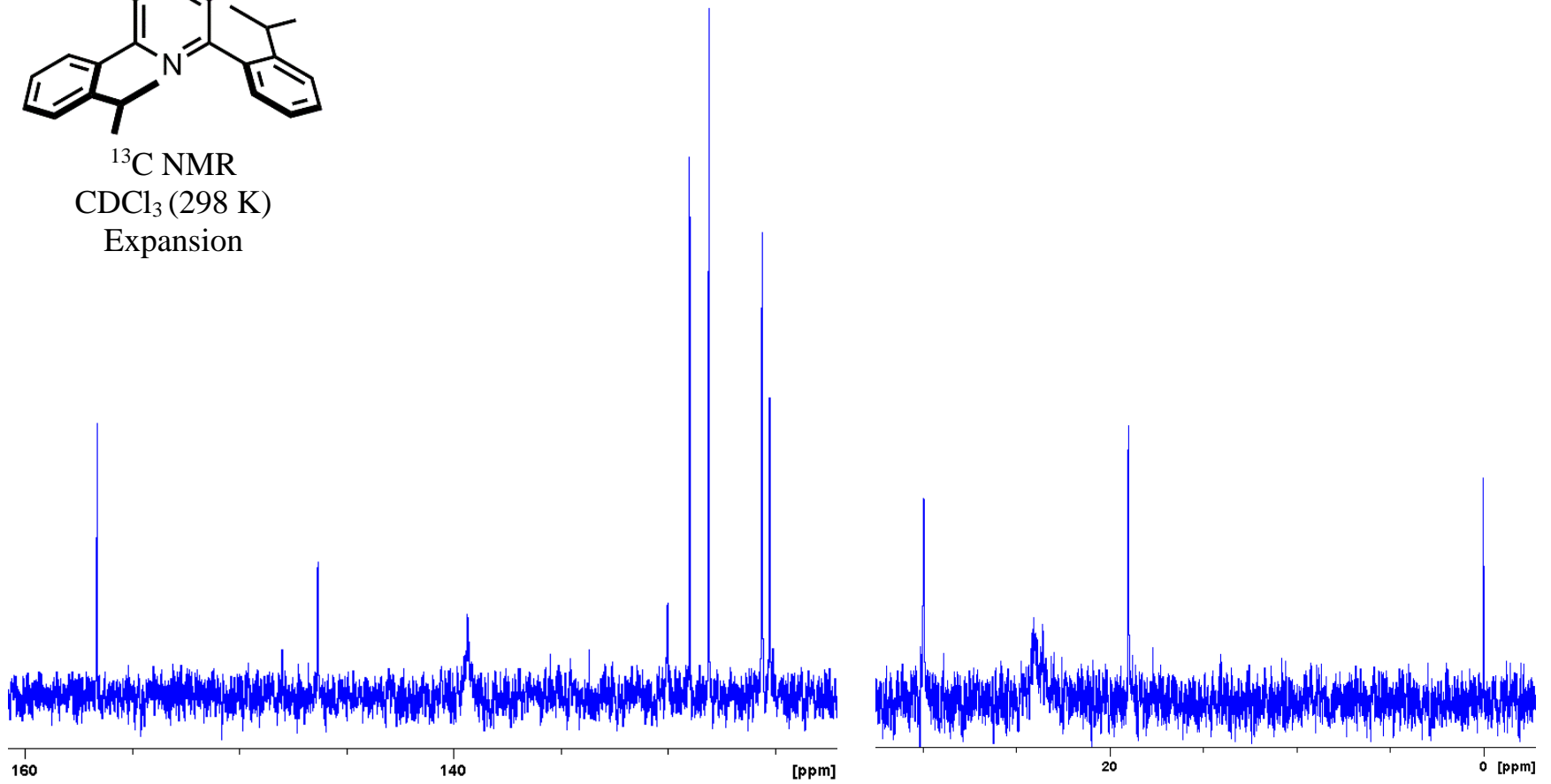


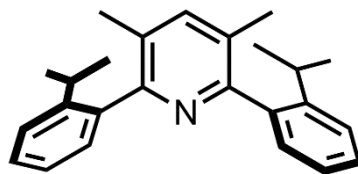
^{13}C NMR
 CDCl_3 (298 K)



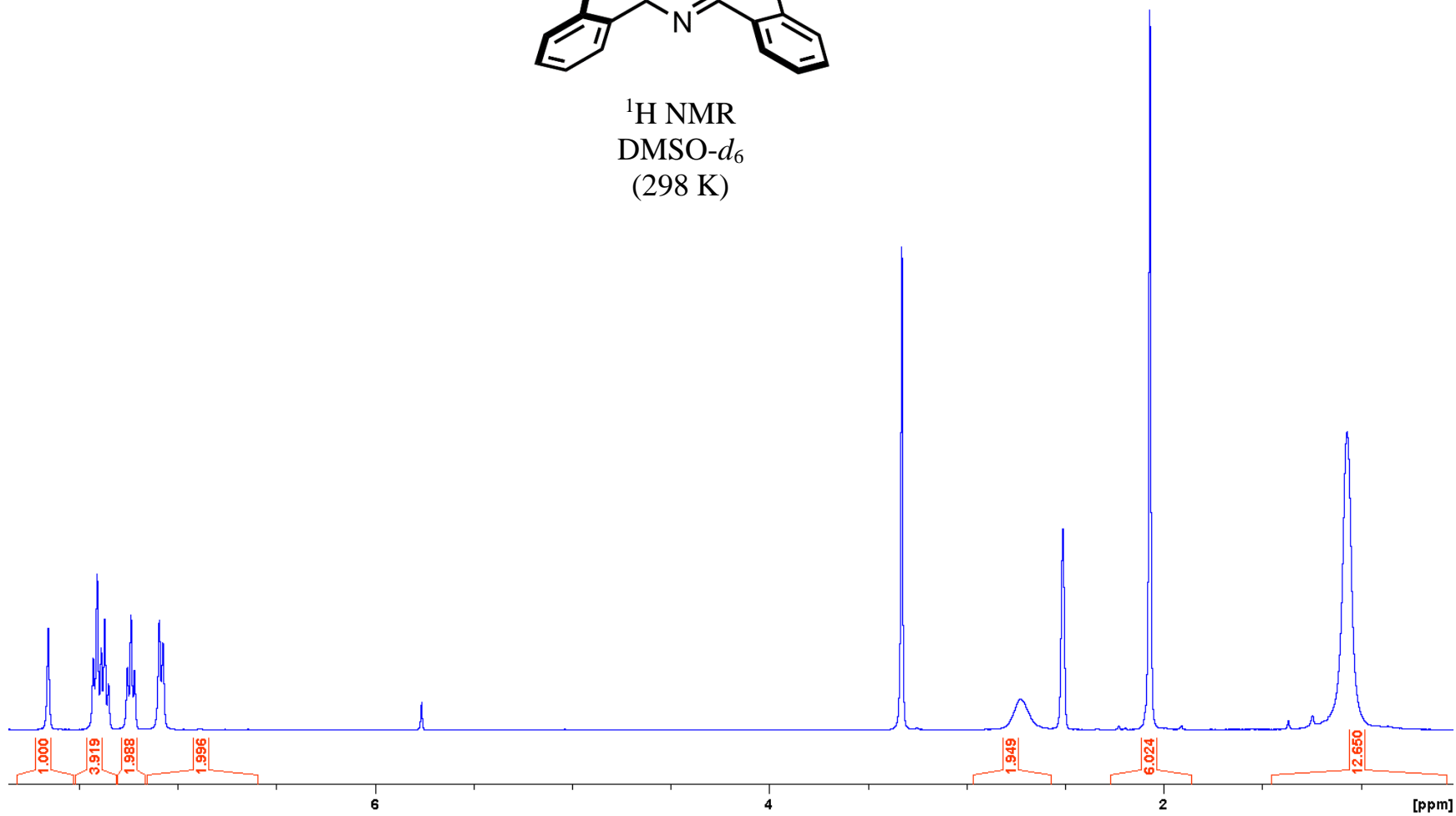


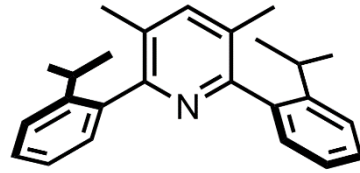
^{13}C NMR
 CDCl_3 (298 K)
Expansion



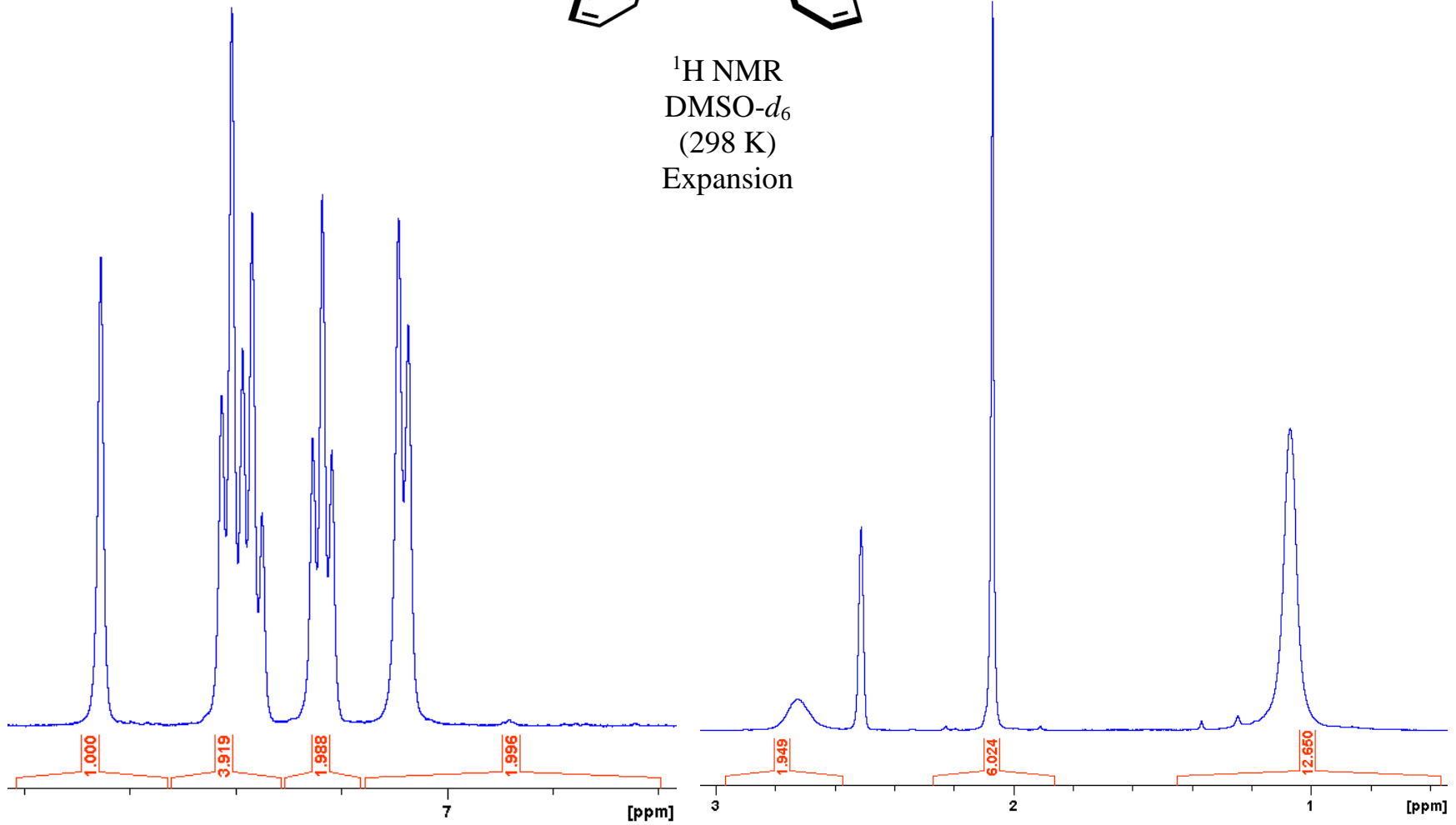


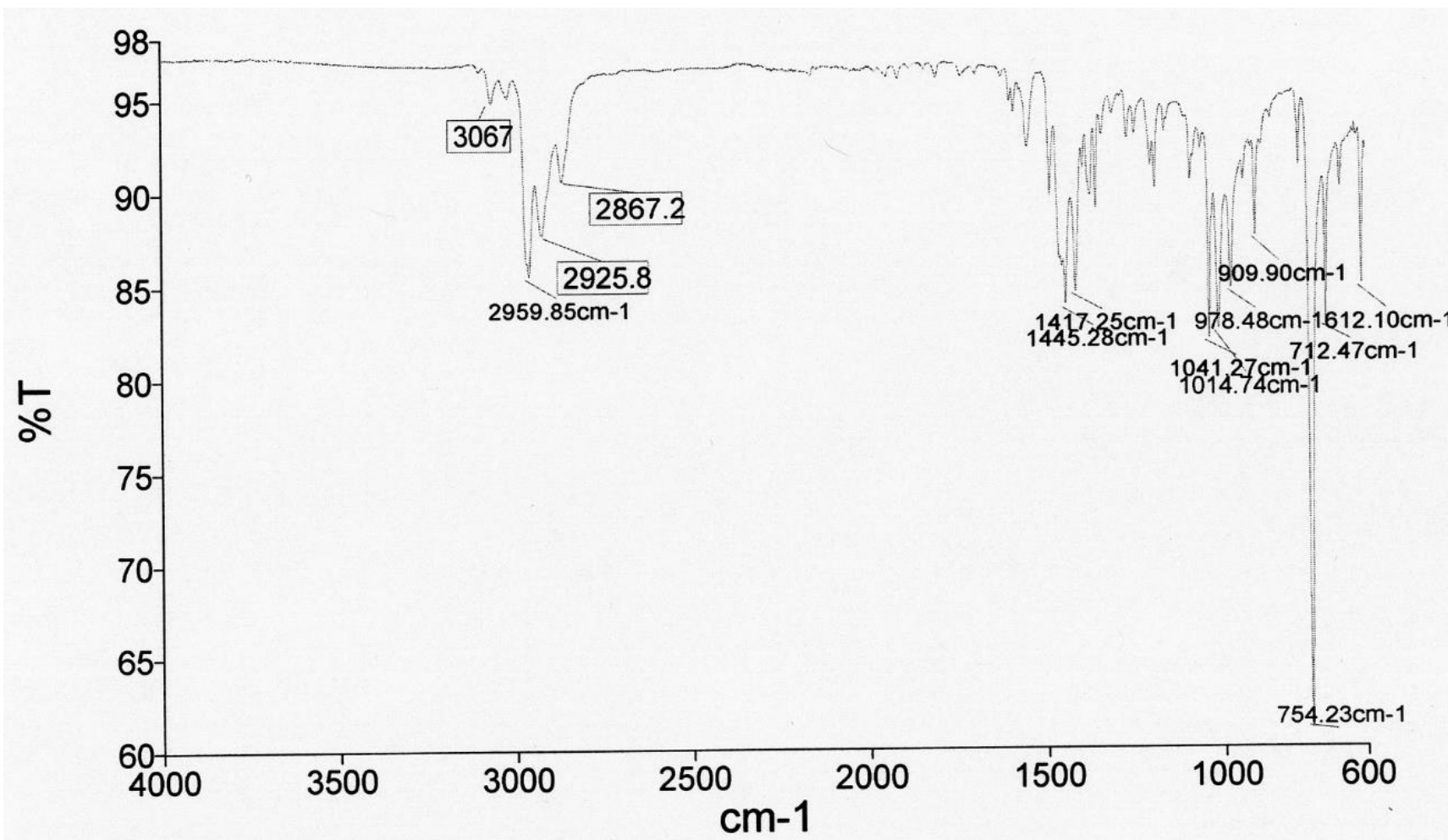
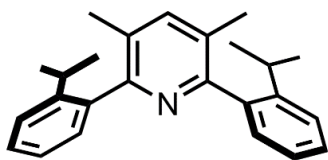
^1H NMR
DMSO- d_6
(298 K)

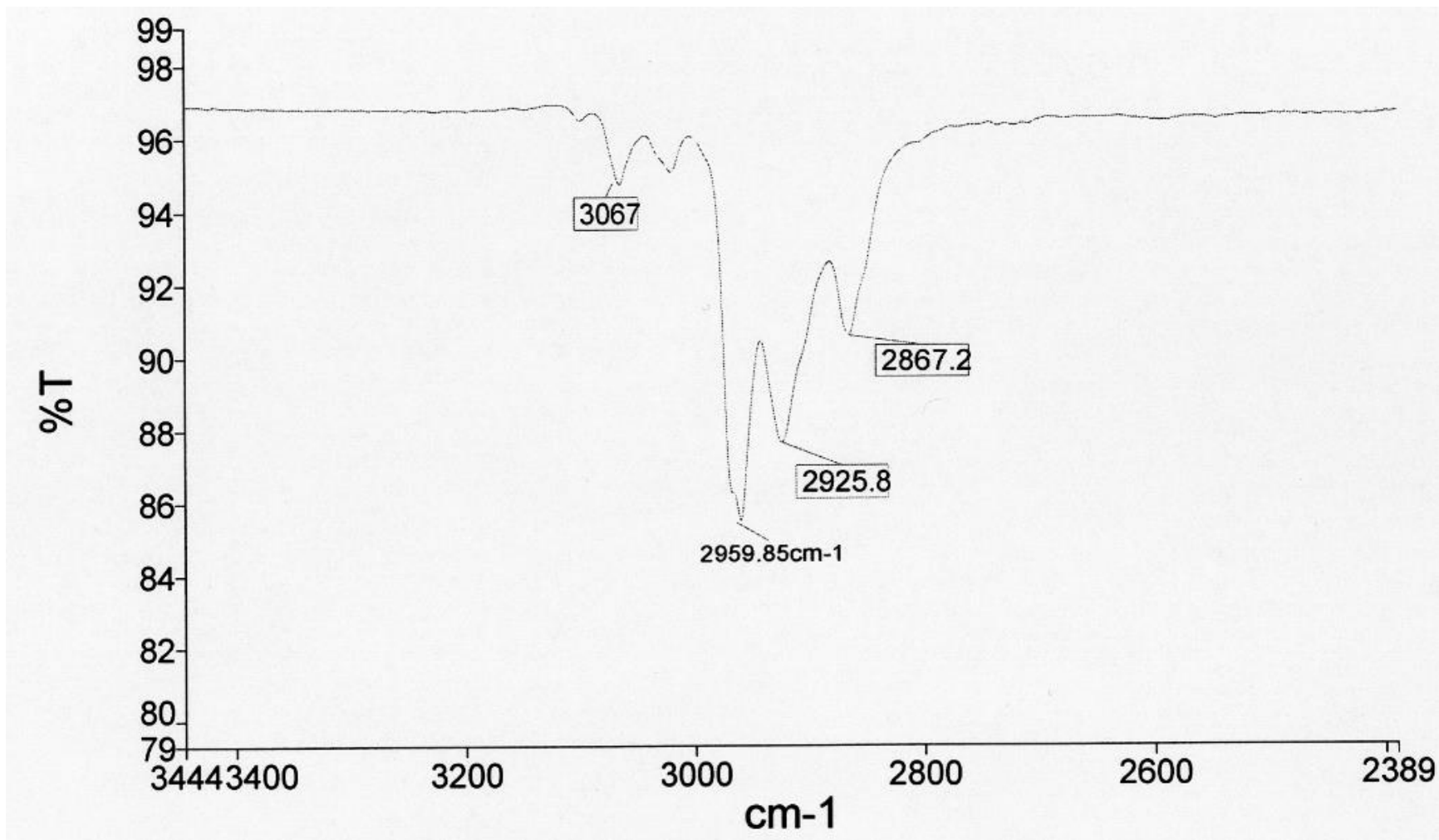
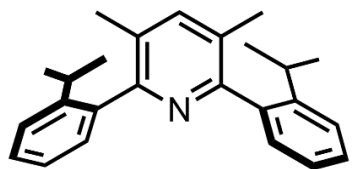


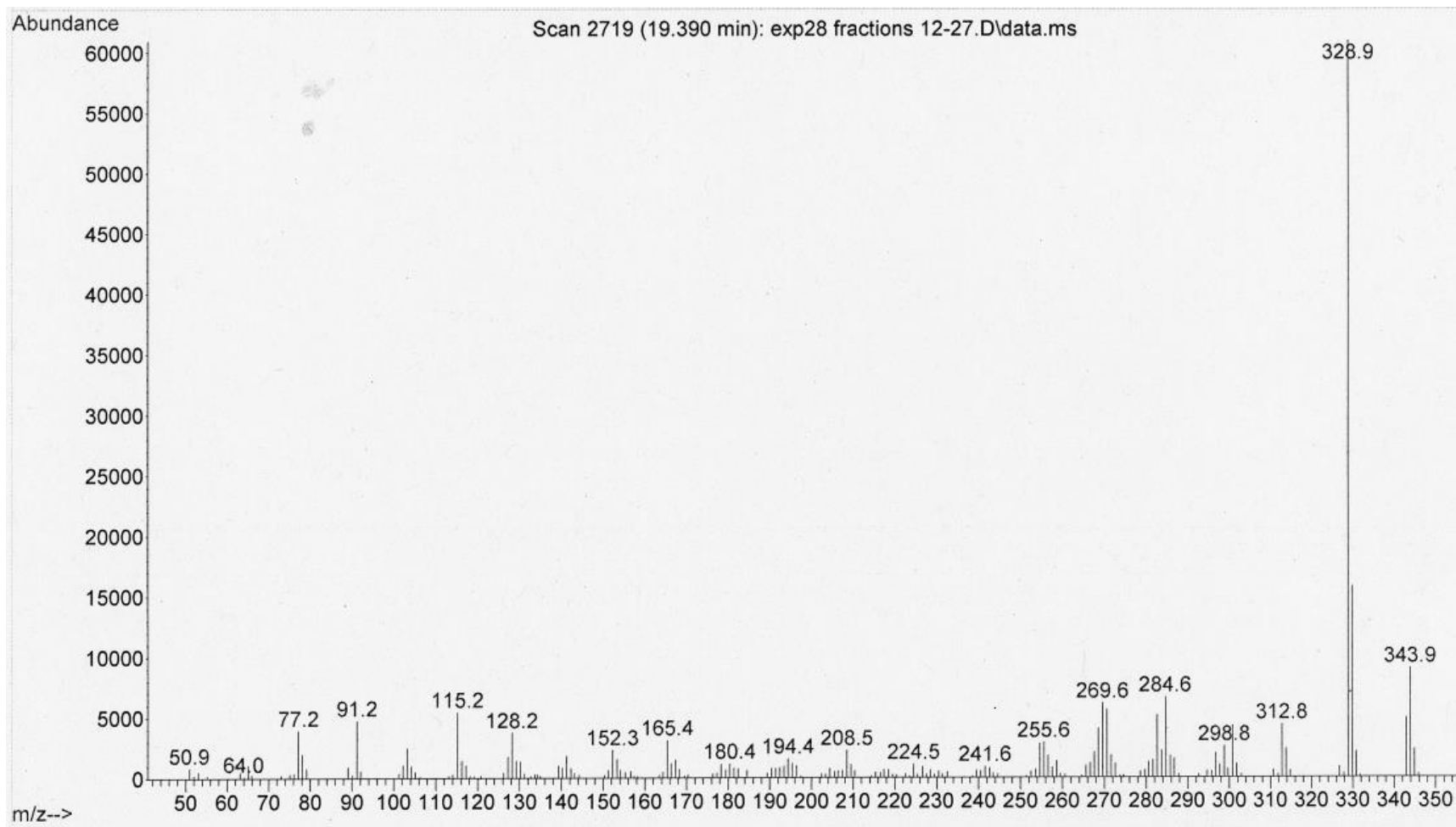
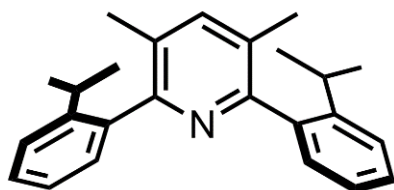


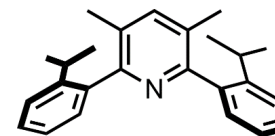
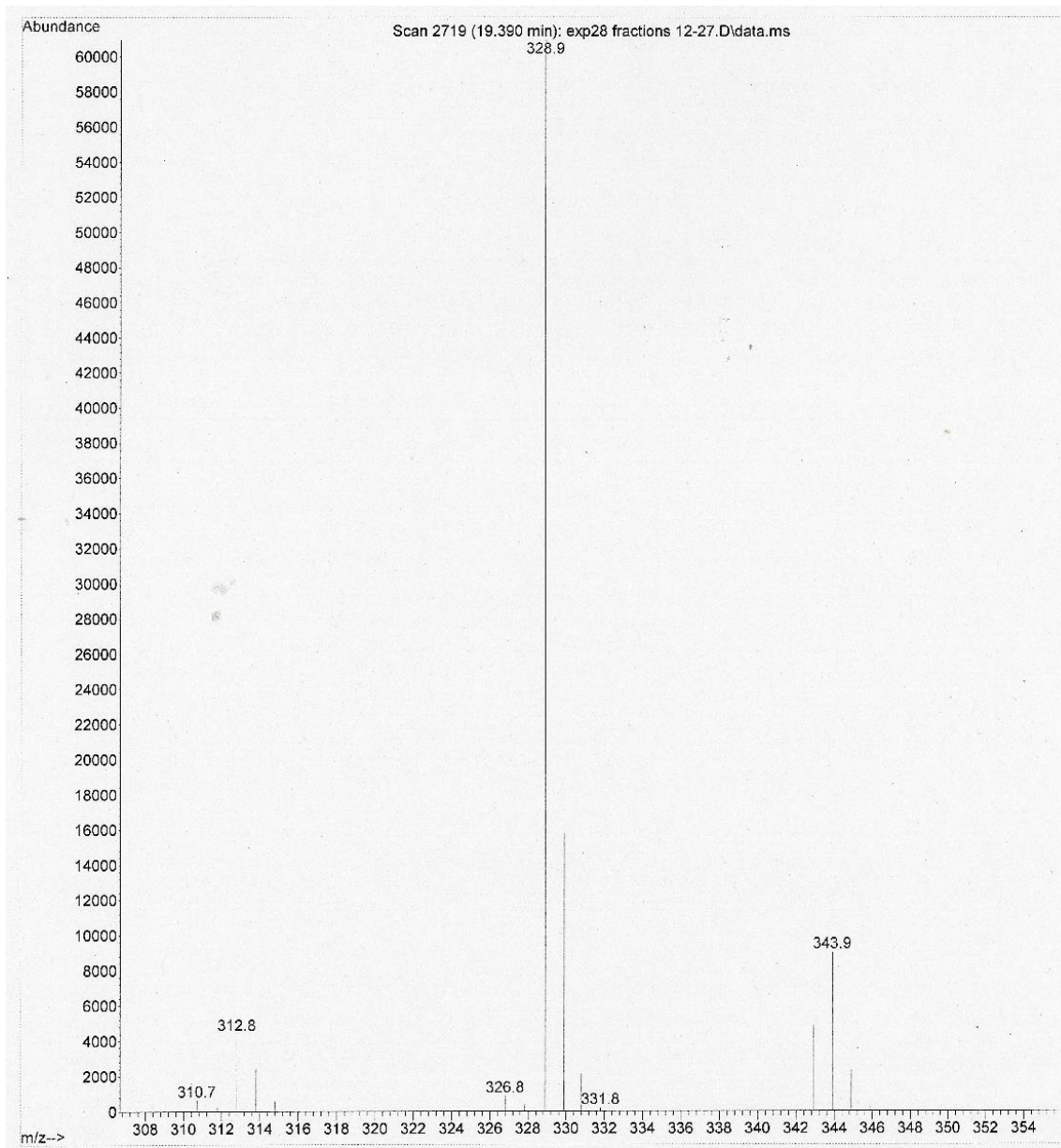
^1H NMR
DMSO- d_6
(298 K)
Expansion



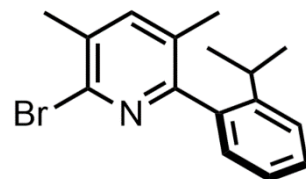




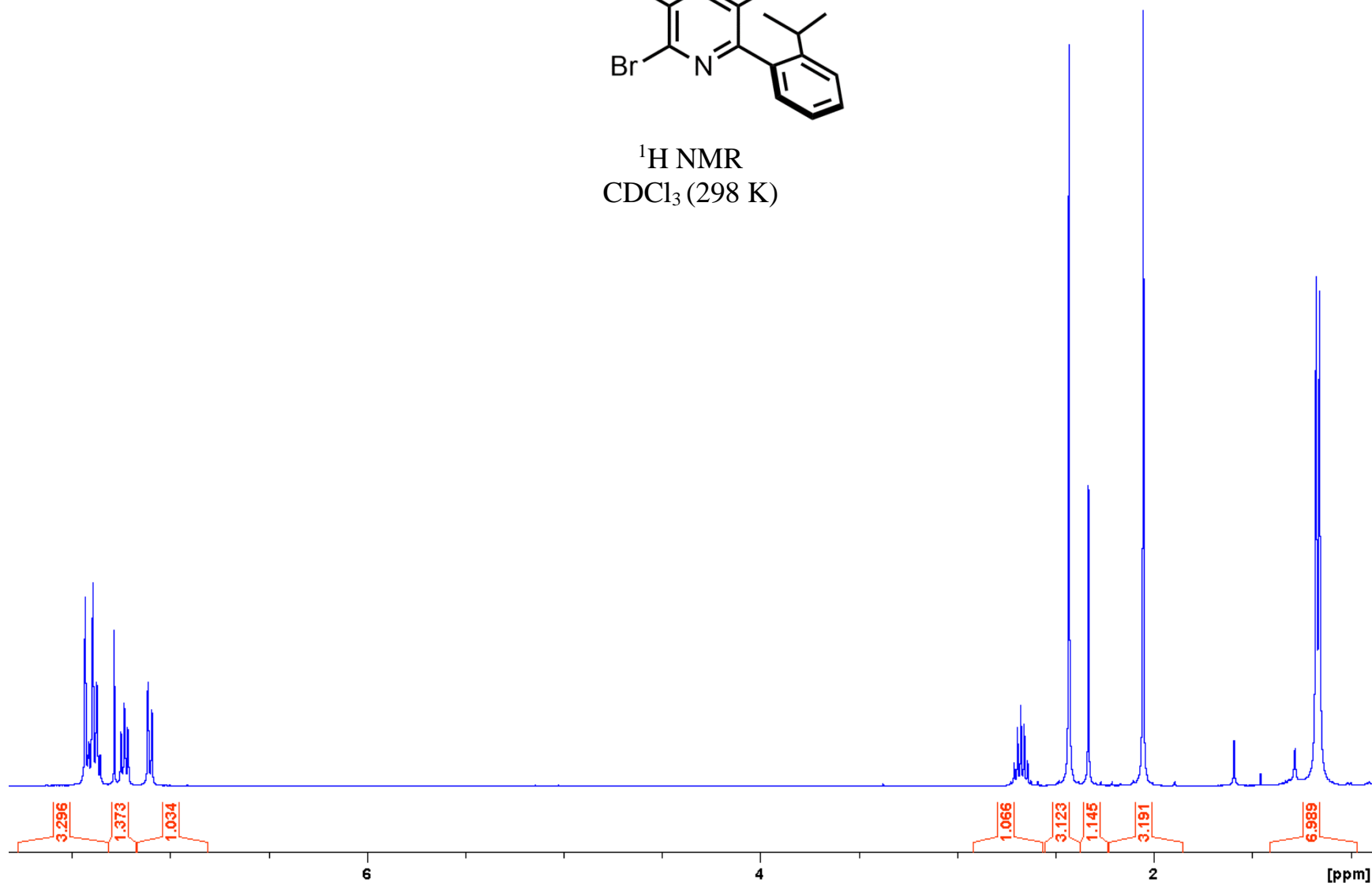


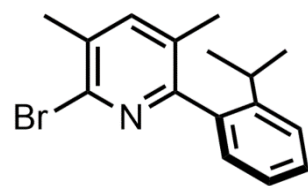


2-bromo-6-(2-isopropylphenyl)-3,5-dimethylpyridine

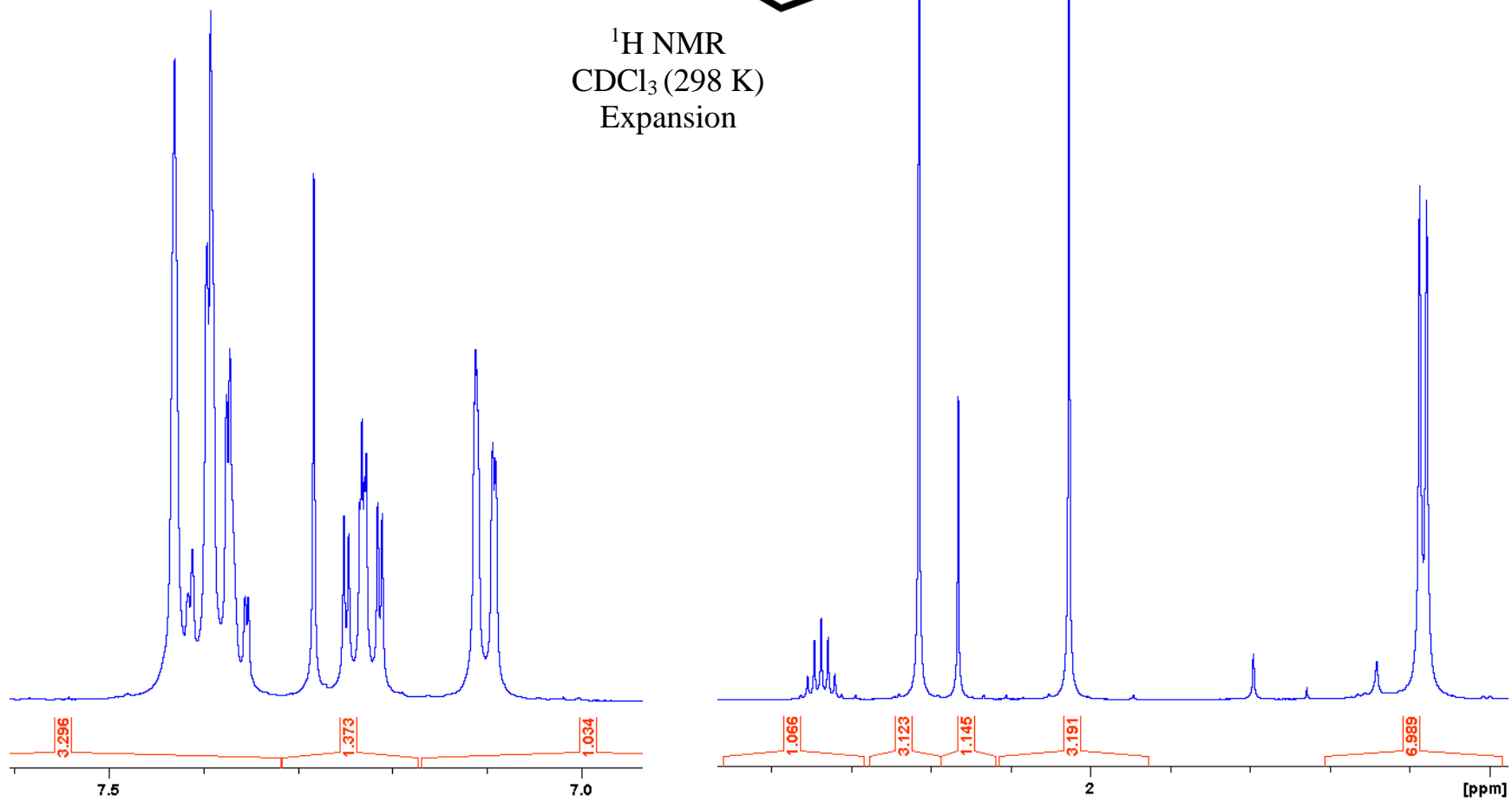


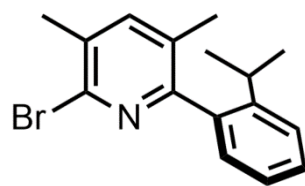
^1H NMR
 CDCl_3 (298 K)



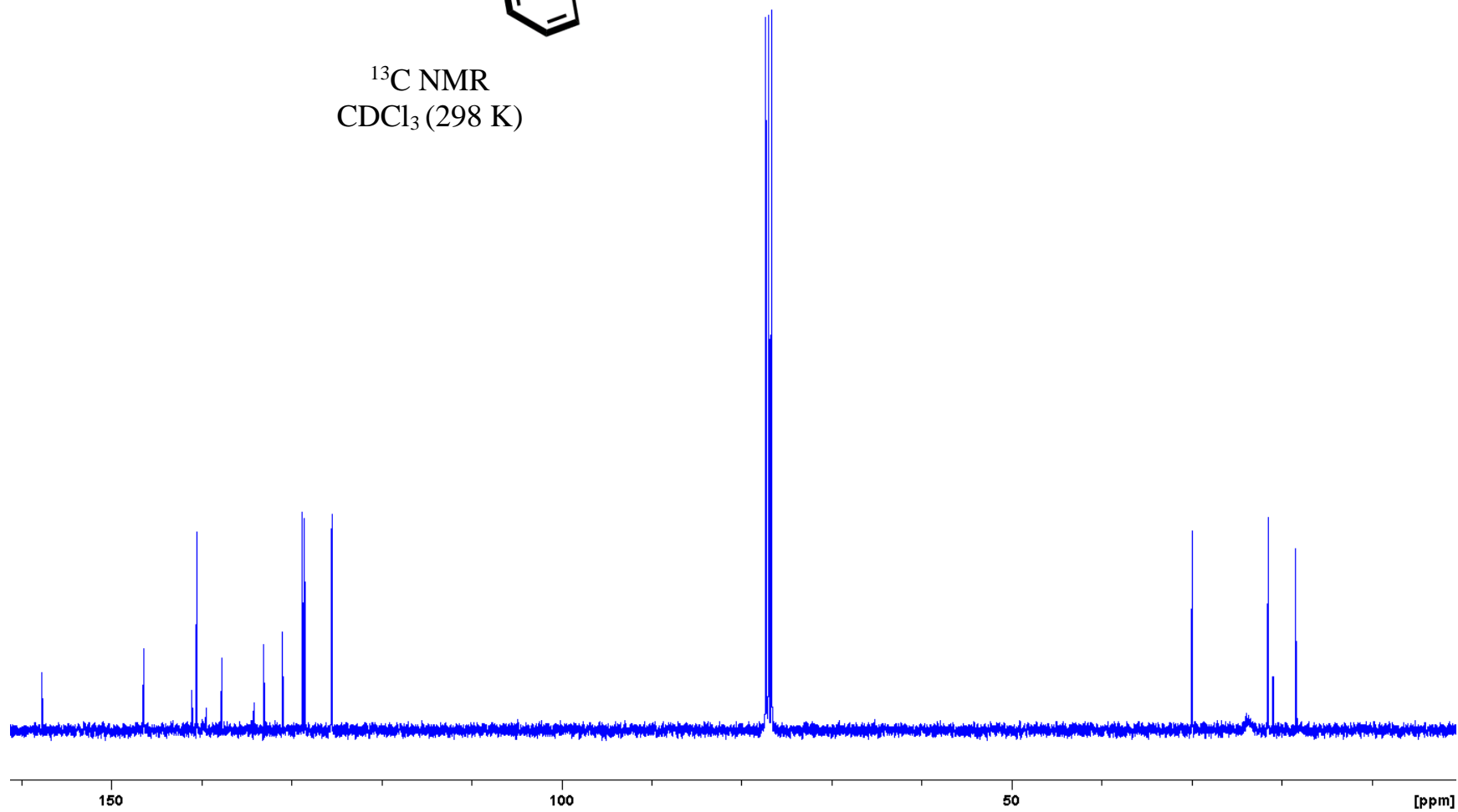


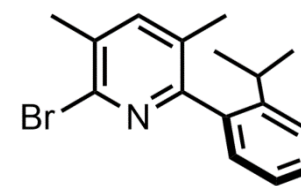
^1H NMR
 CDCl_3 (298 K)
Expansion



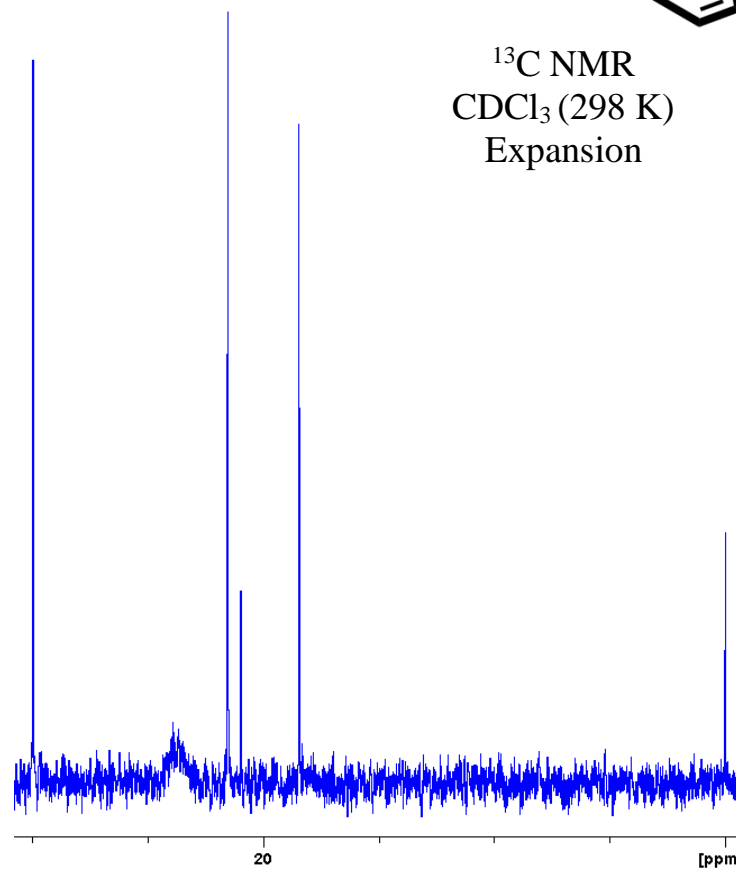
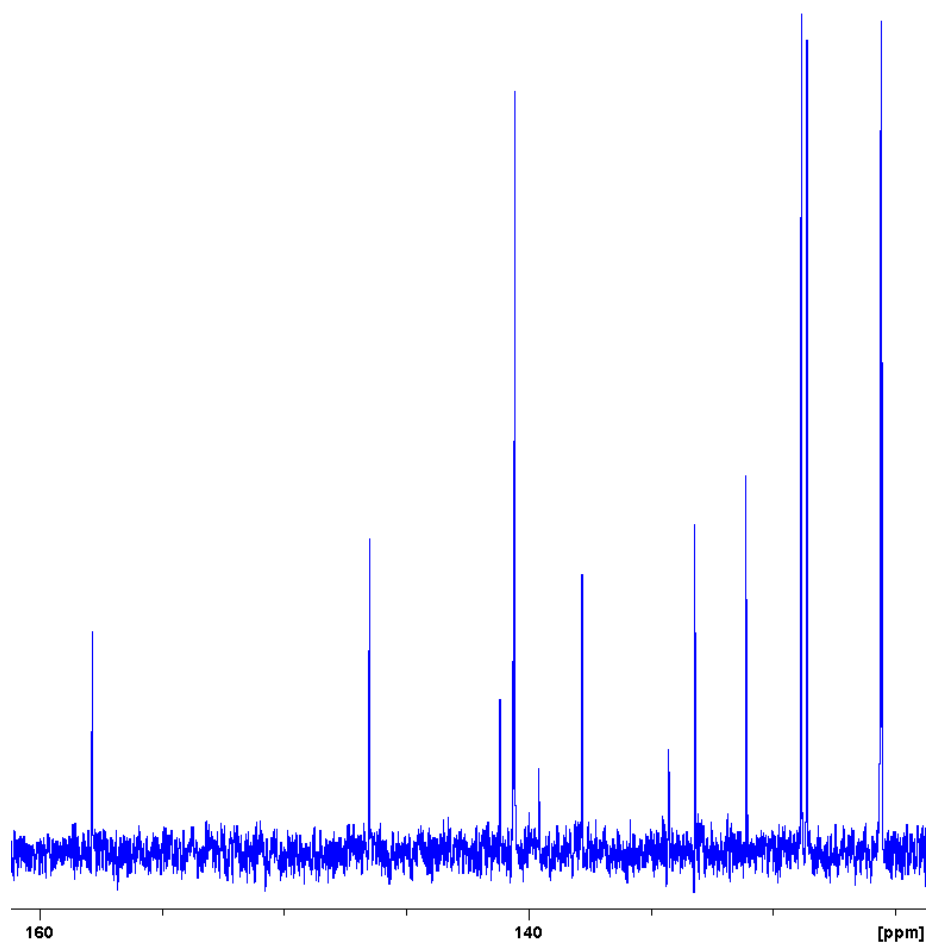


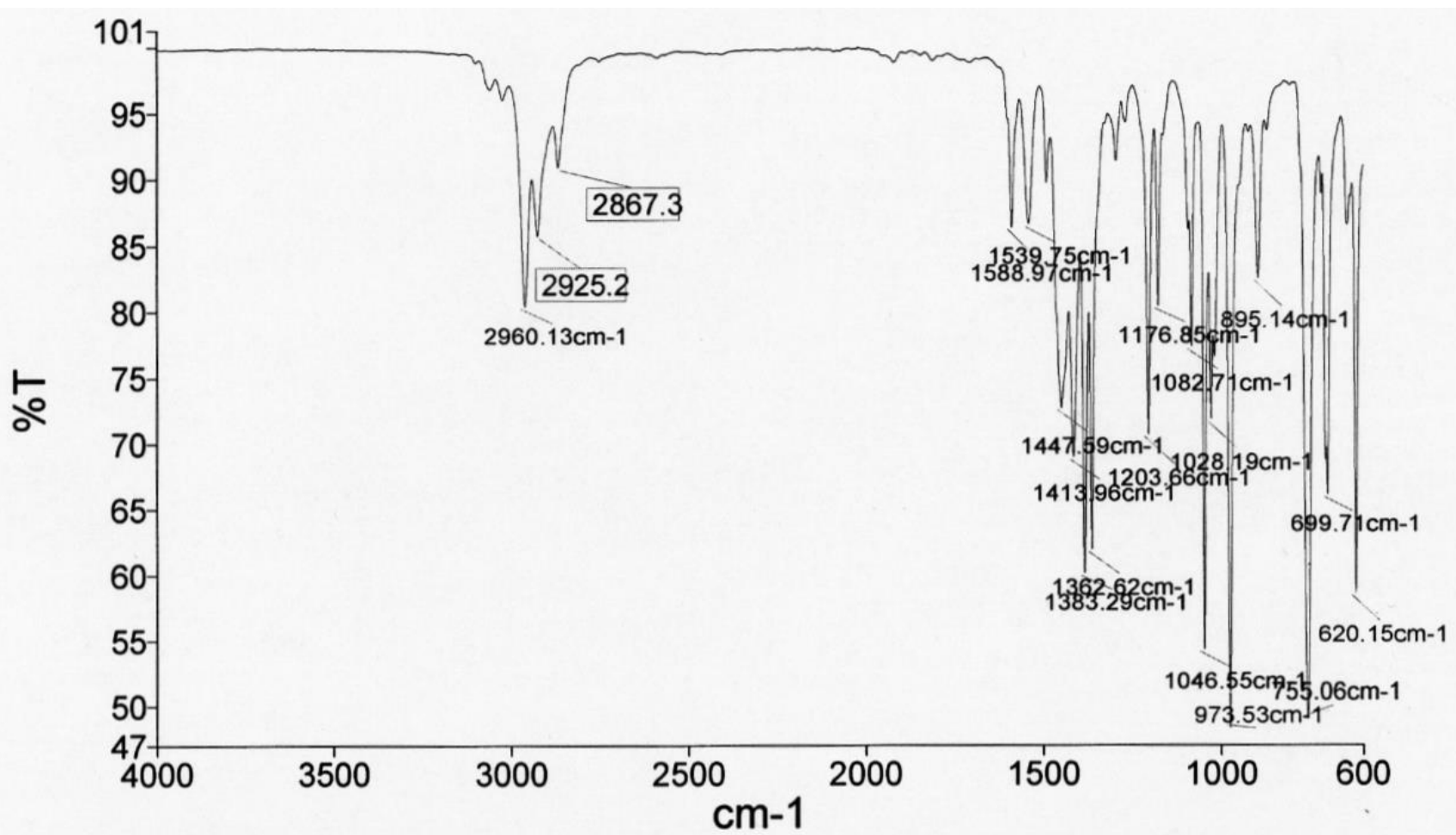
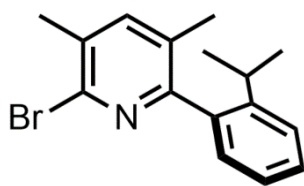
^{13}C NMR
 CDCl_3 (298 K)

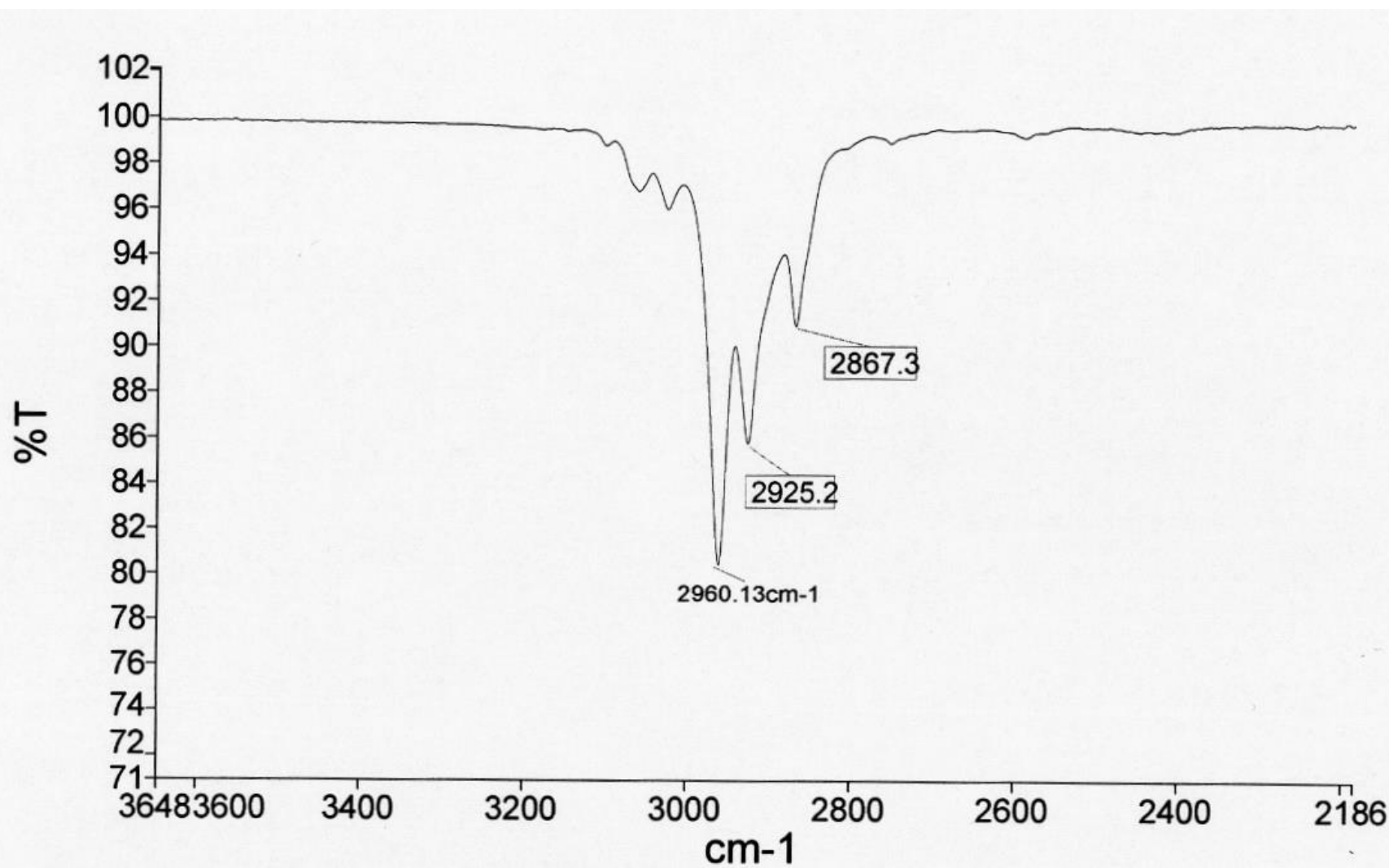
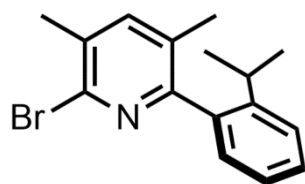


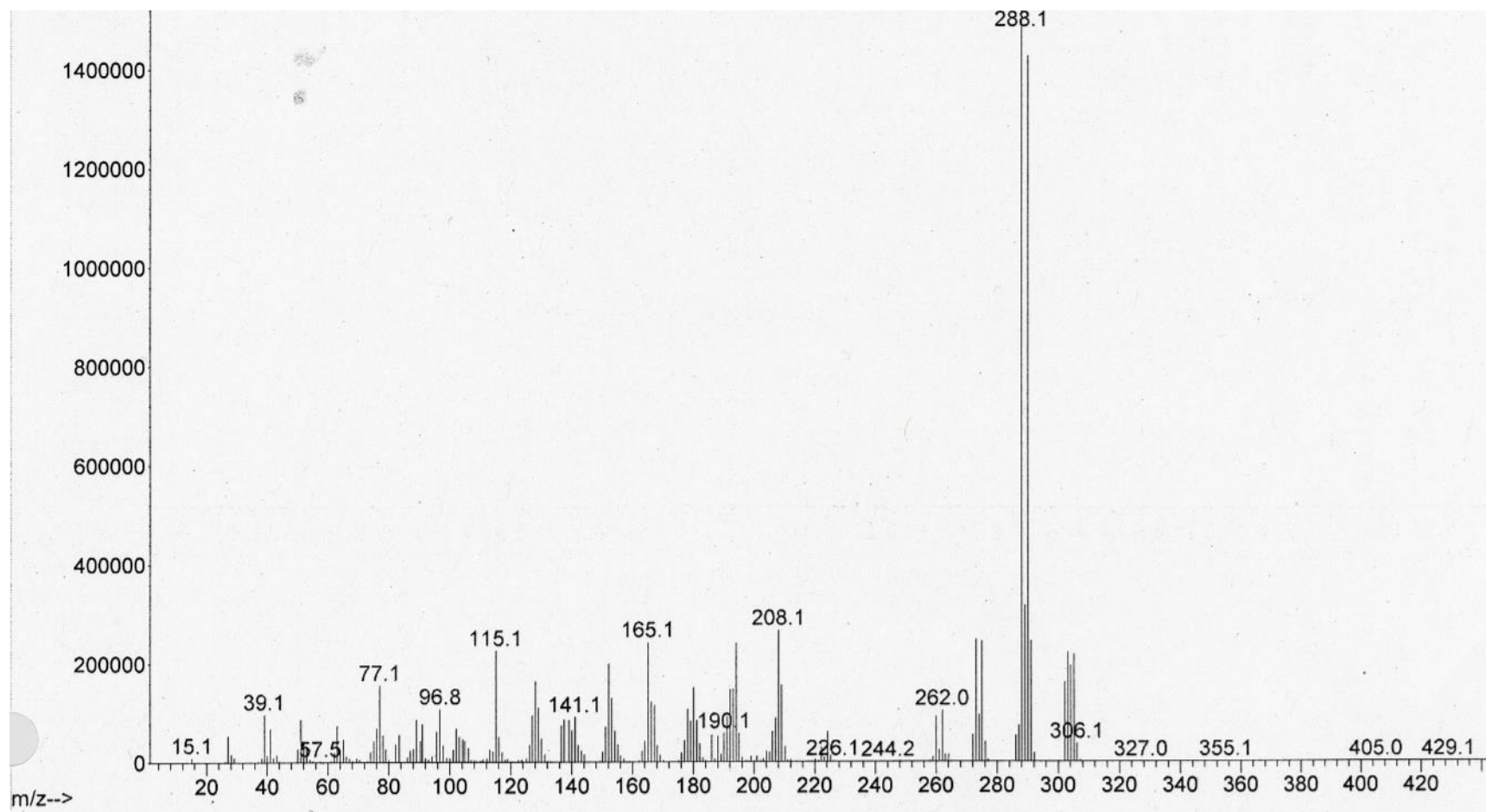
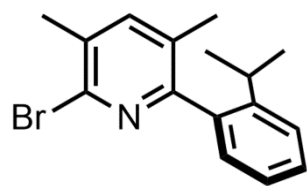


^{13}C NMR
 CDCl_3 (298 K)
Expansion

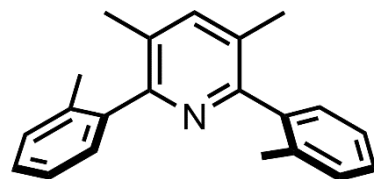




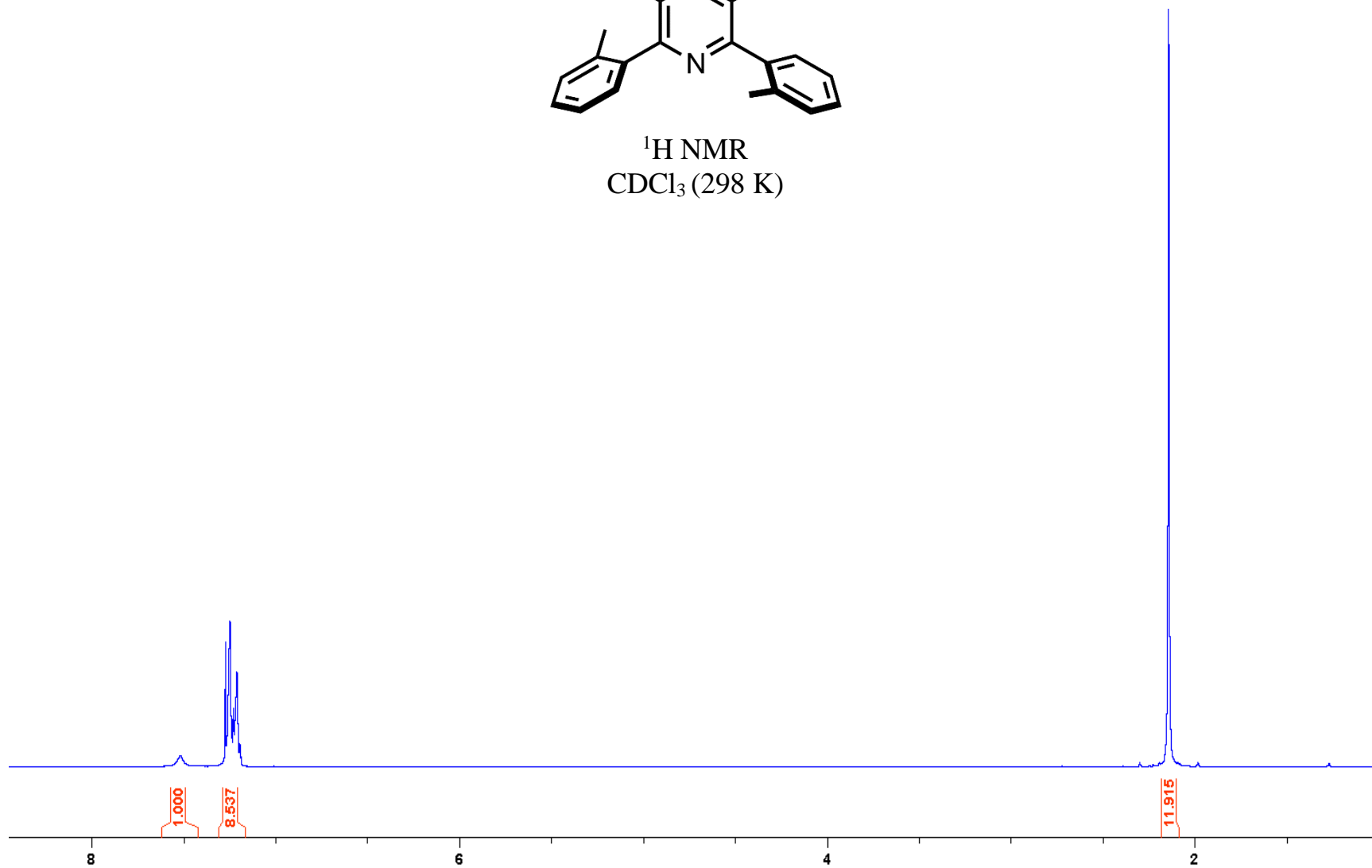


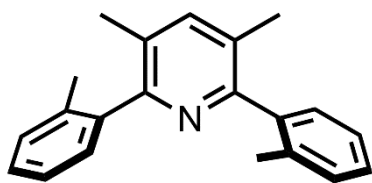


3,5-Dimethyl-2,6-di(2-methylphenyl)pyridine

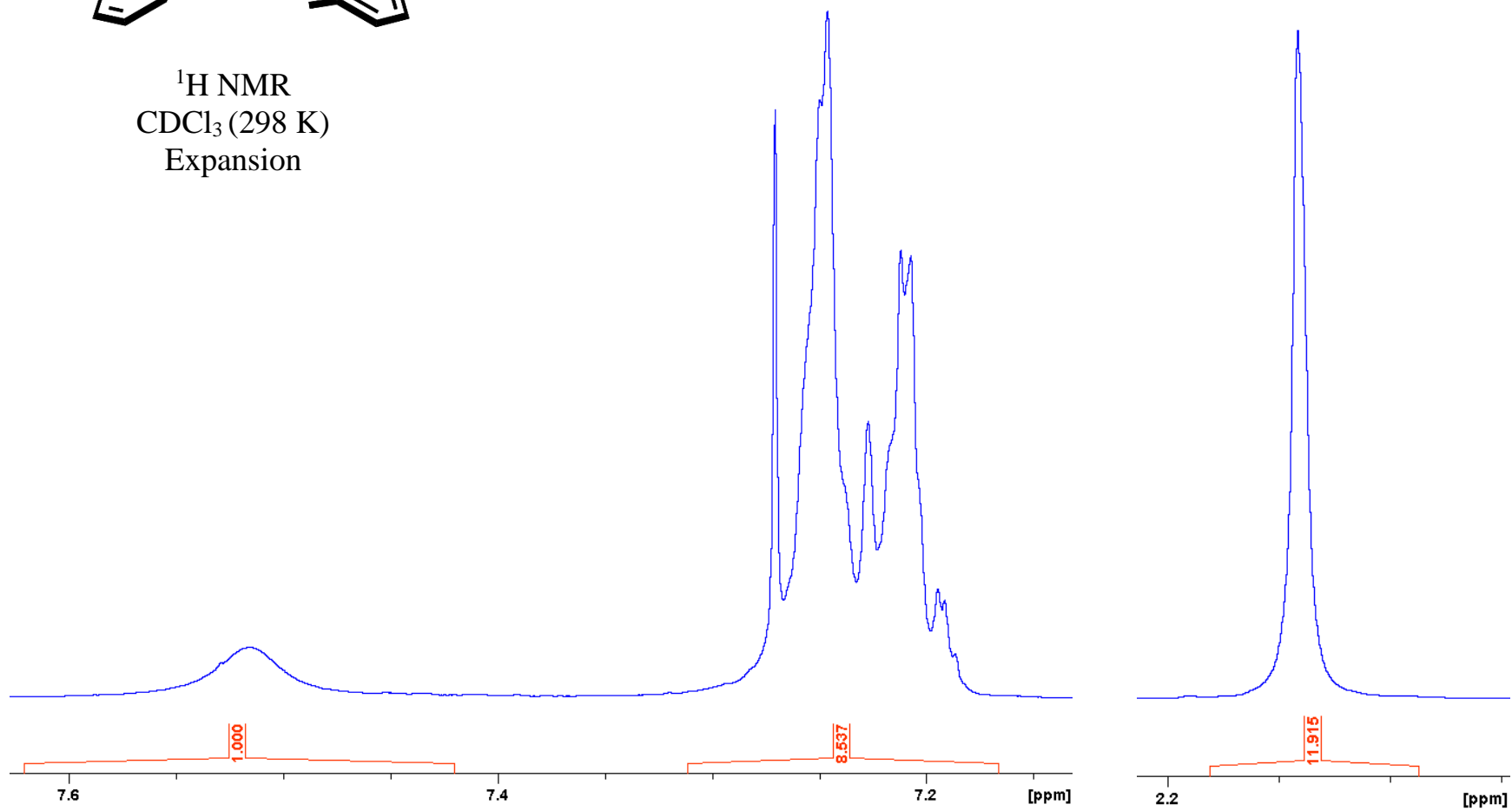


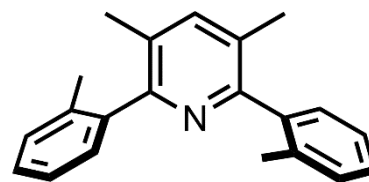
$^1\text{H NMR}$
 CDCl_3 (298 K)



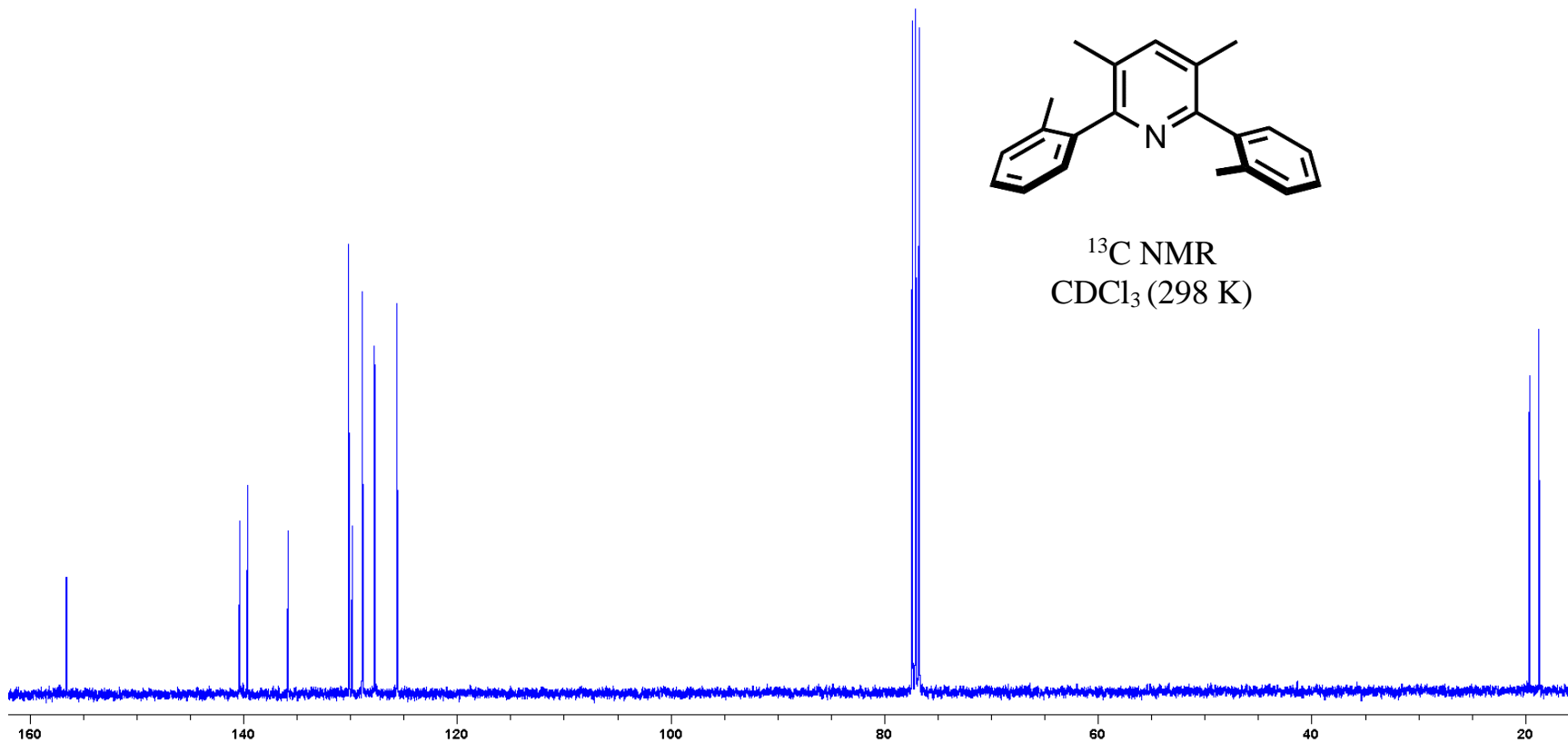


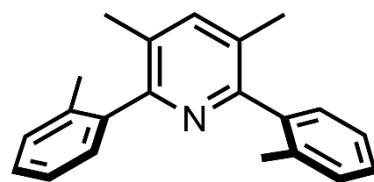
^1H NMR
 CDCl_3 (298 K)
Expansion



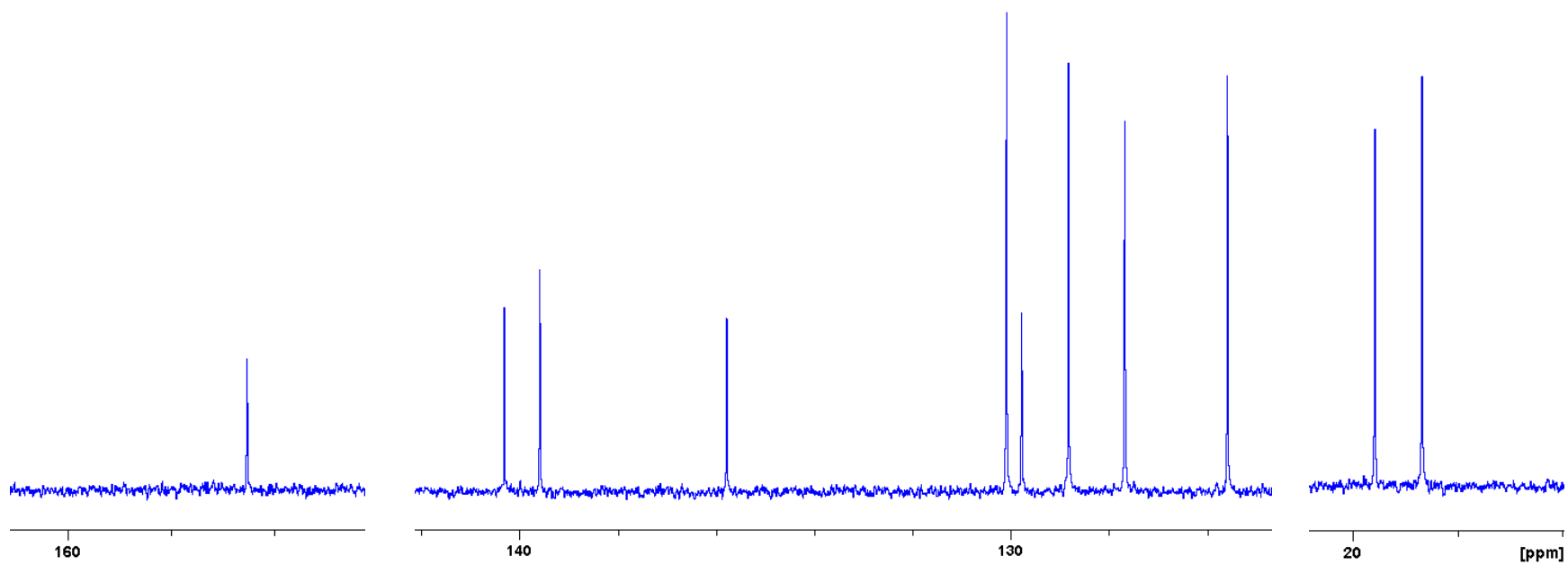


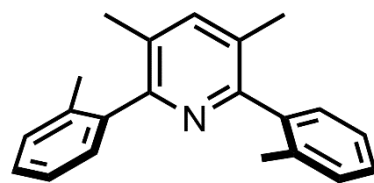
^{13}C NMR
 CDCl_3 (298 K)



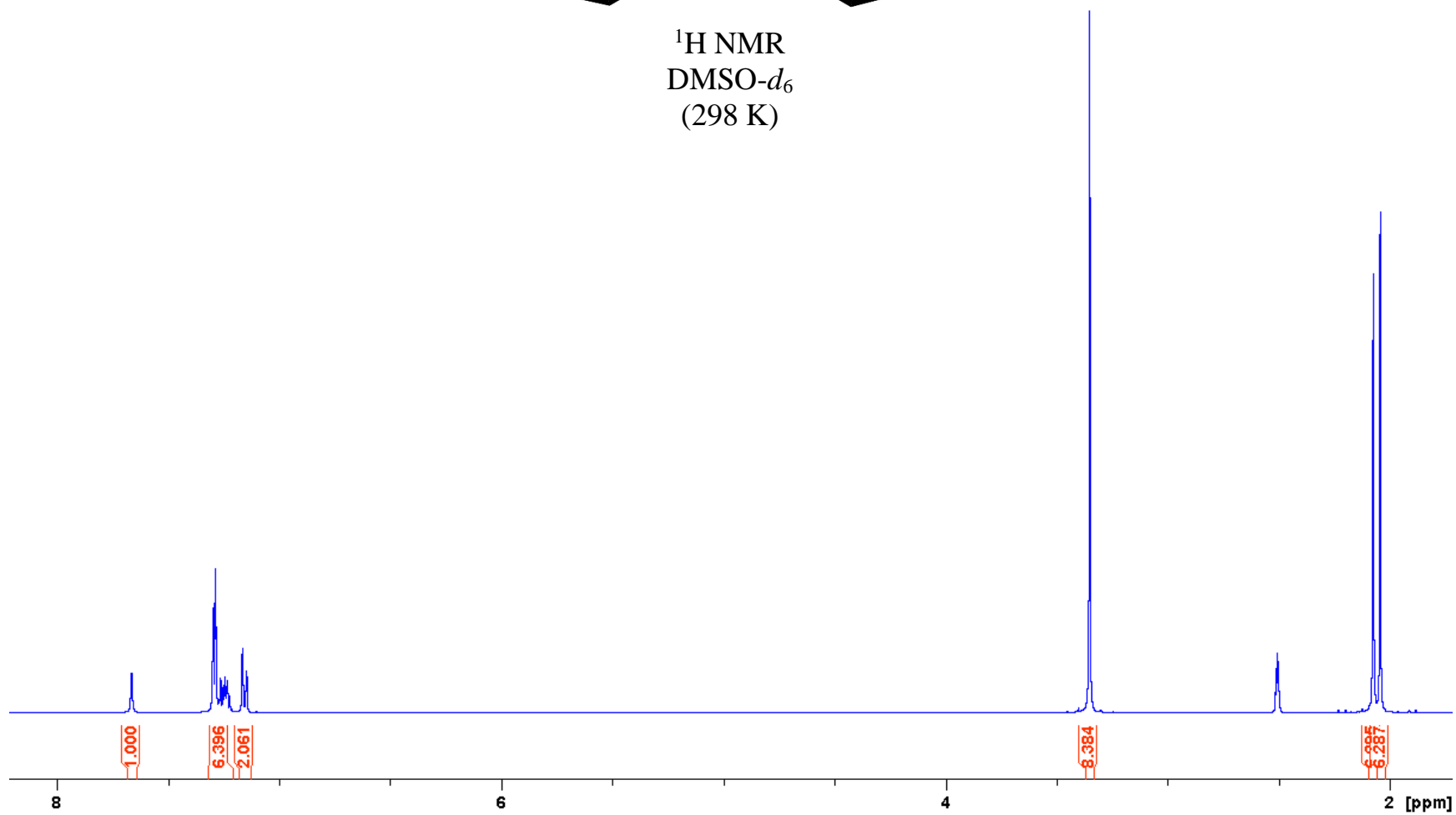


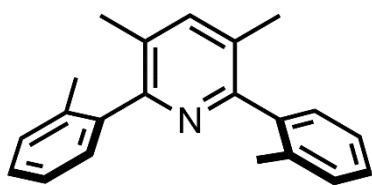
^{13}C NMR
 CDCl_3 (298 K)
Expansion



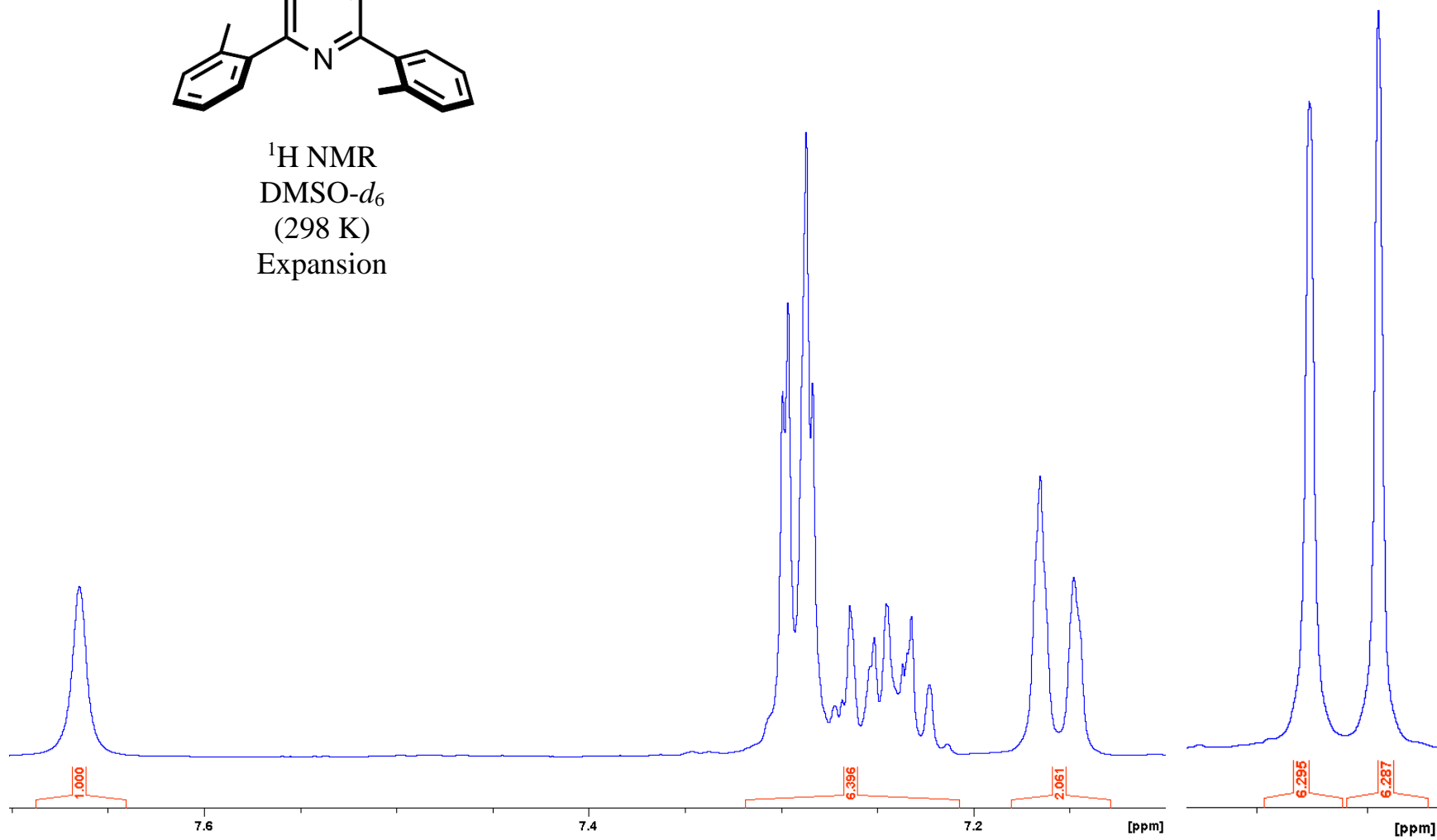


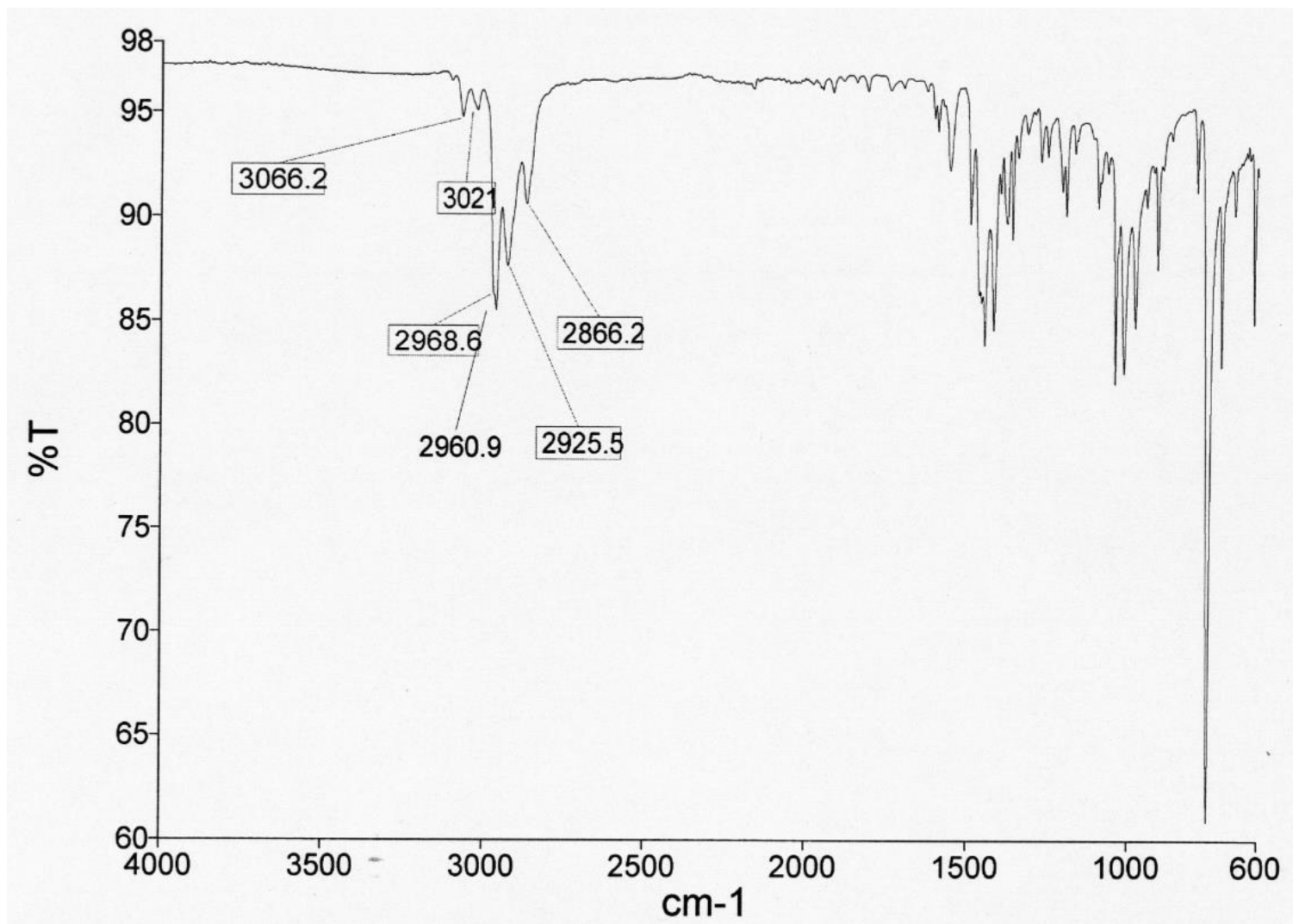
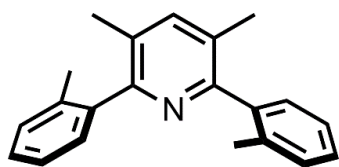
^1H NMR
DMSO- d_6
(298 K)

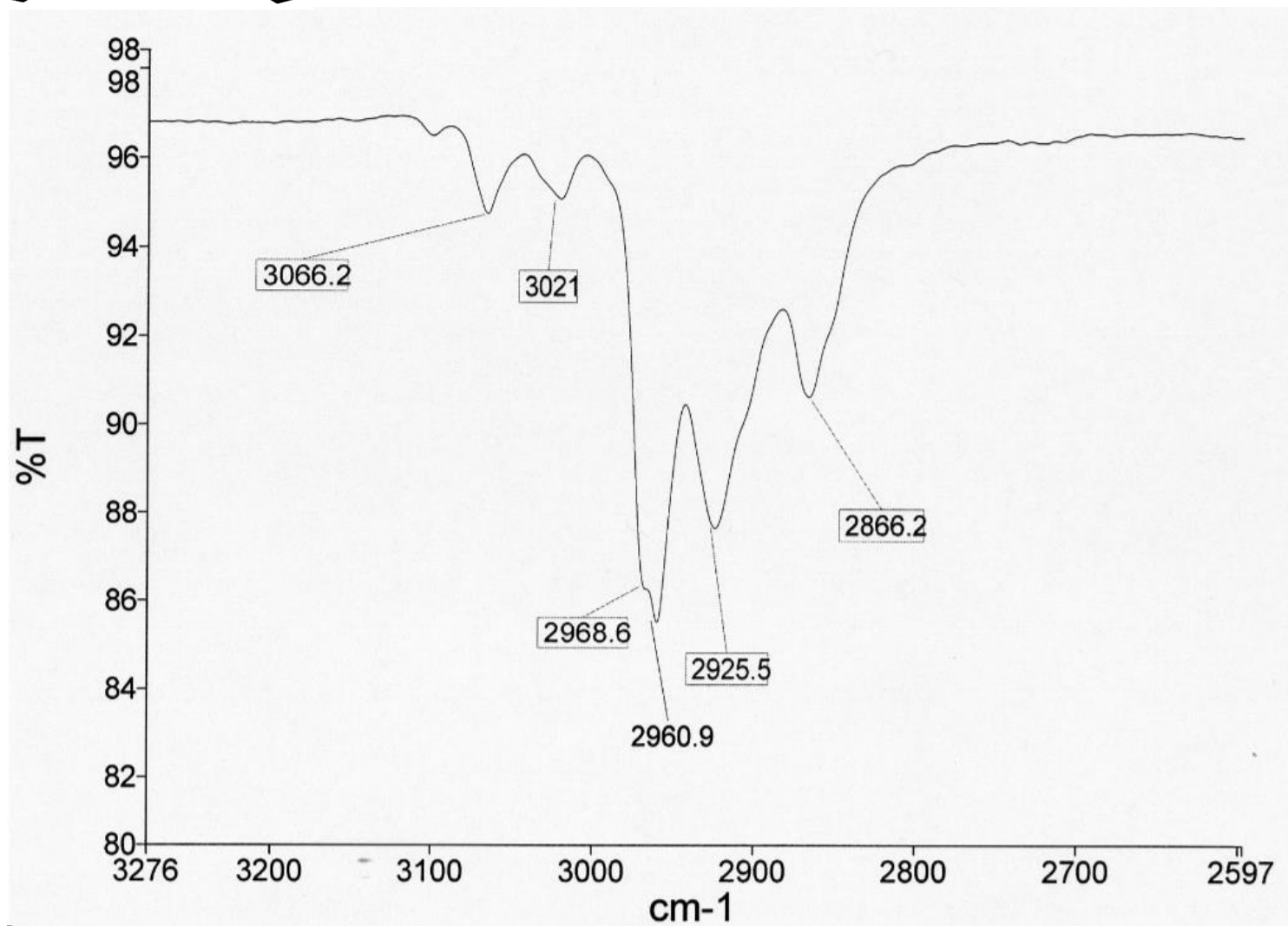
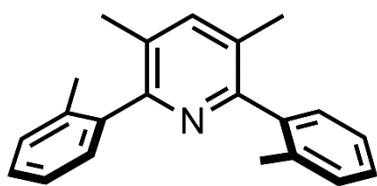


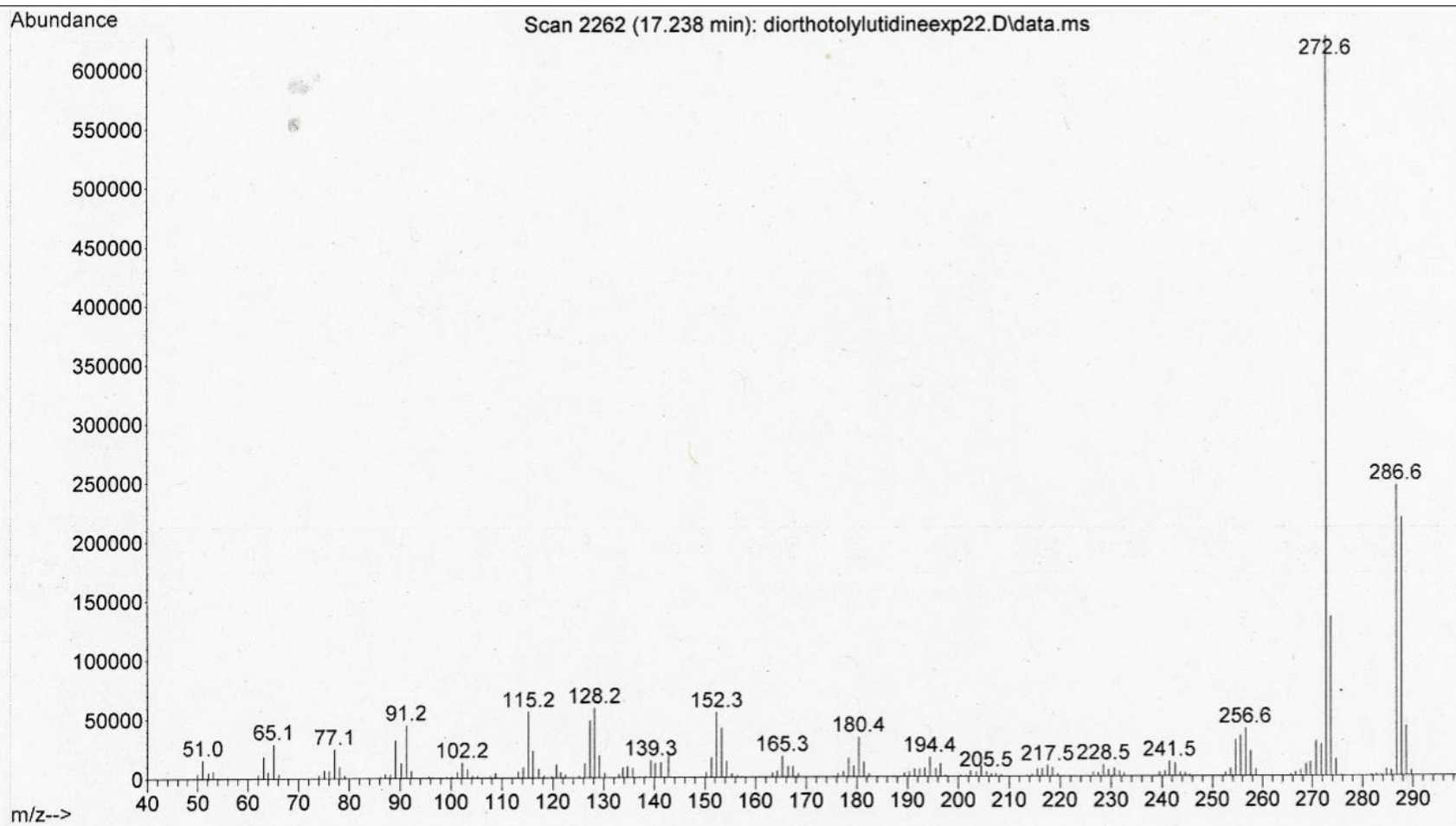
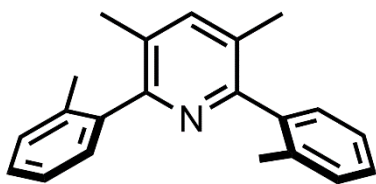


^1H NMR
DMSO- d_6
(298 K)
Expansion

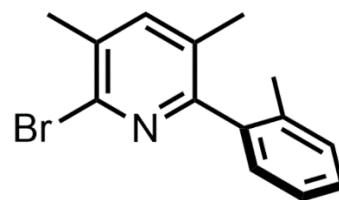




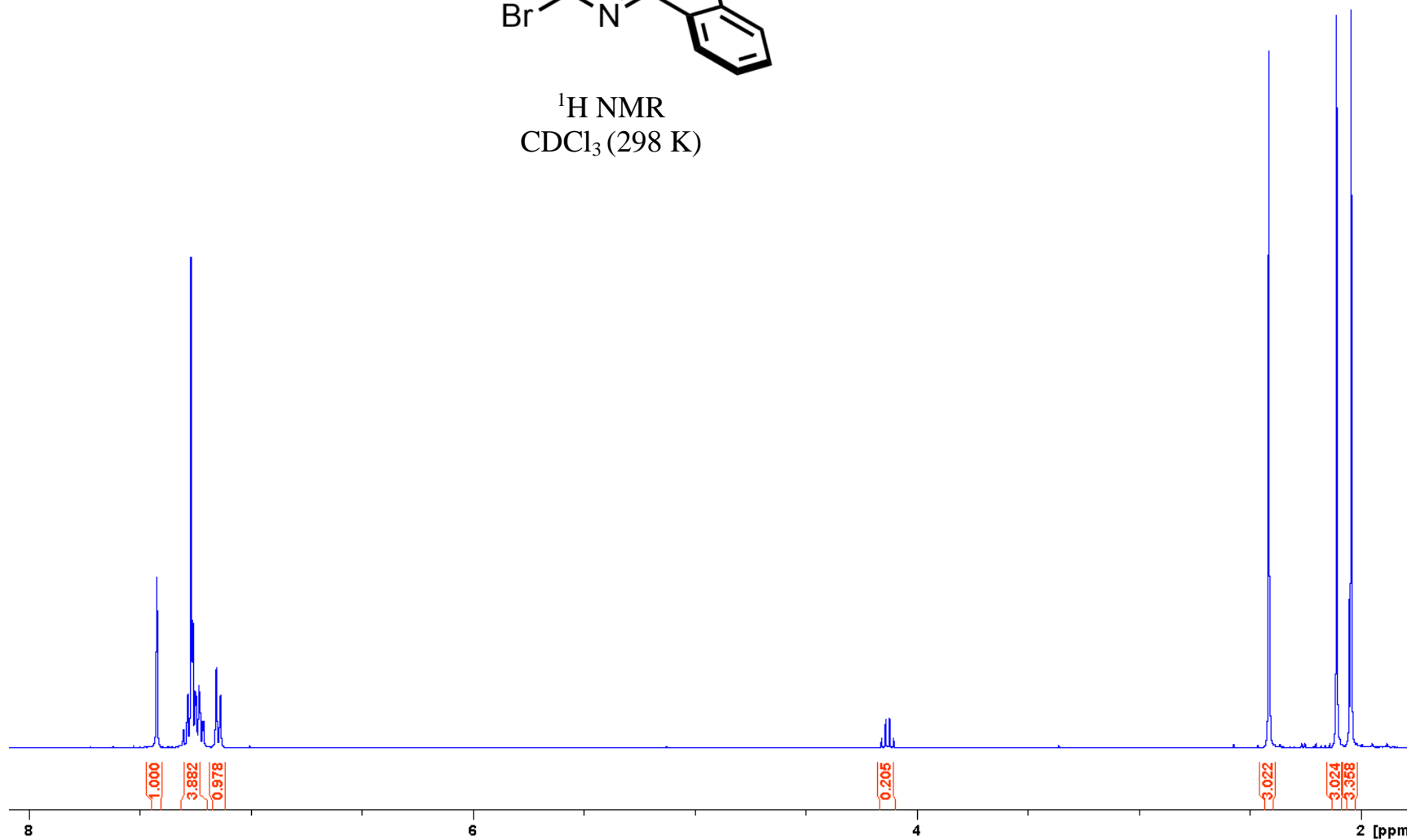


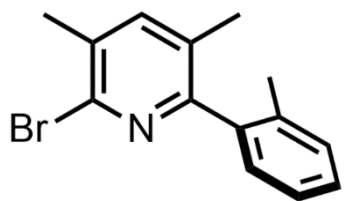


2-bromo-3,5-dimethyl-6-(*o*-tolyl)pyridine

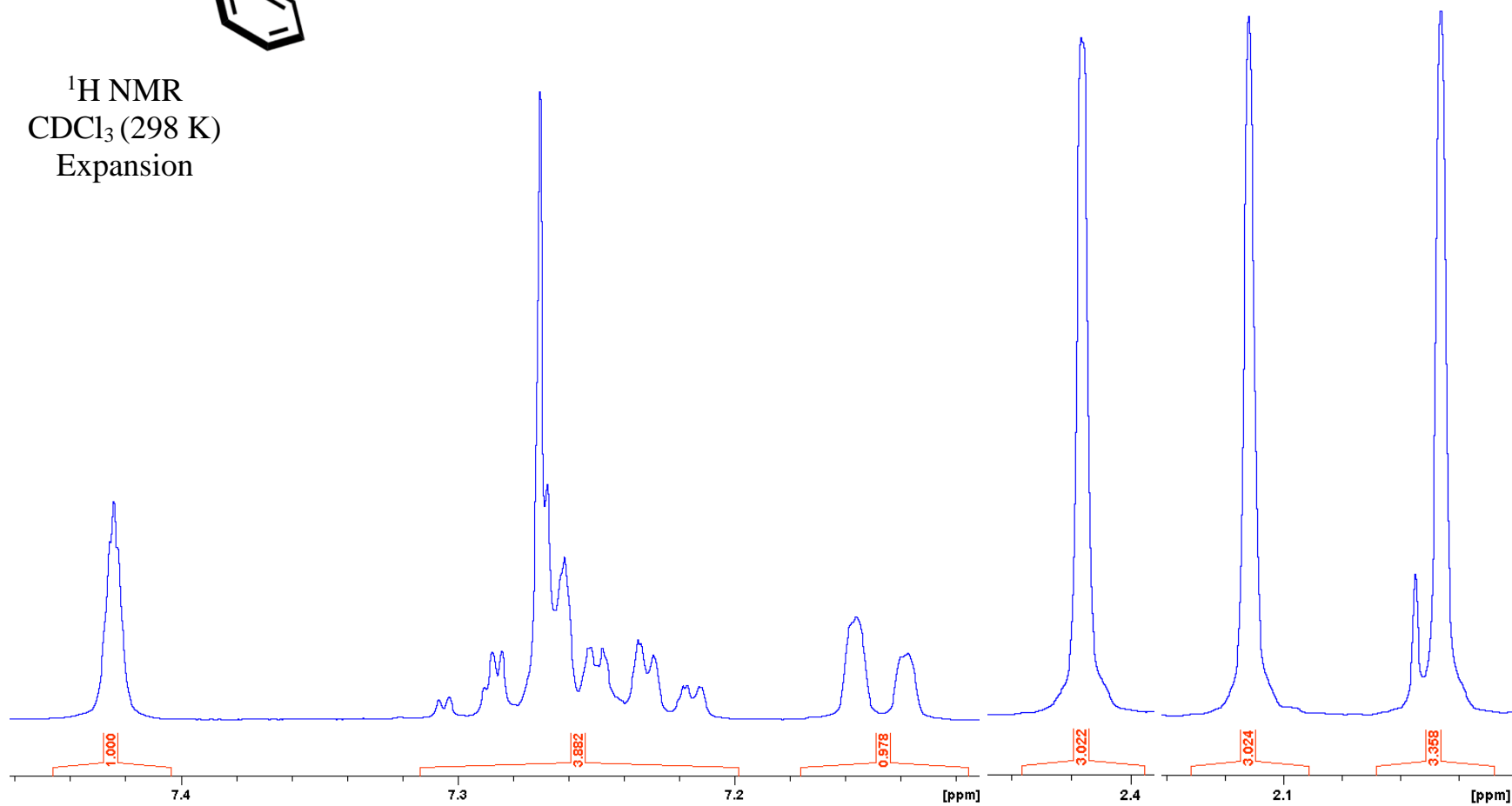


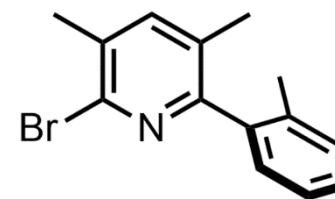
^1H NMR
 CDCl_3 (298 K)



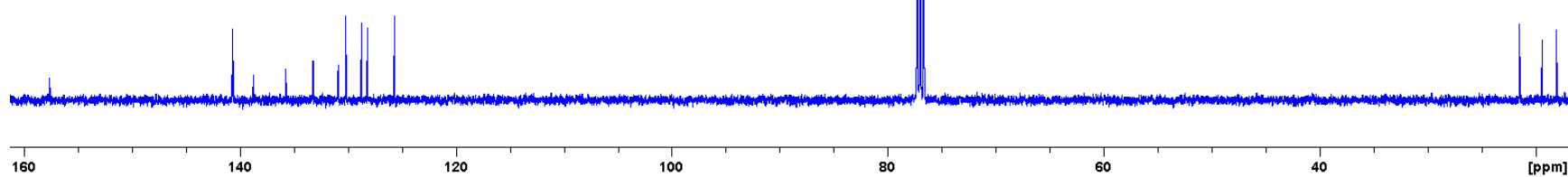


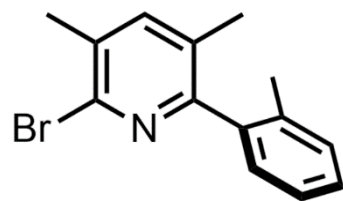
^1H NMR
 CDCl_3 (298 K)
Expansion



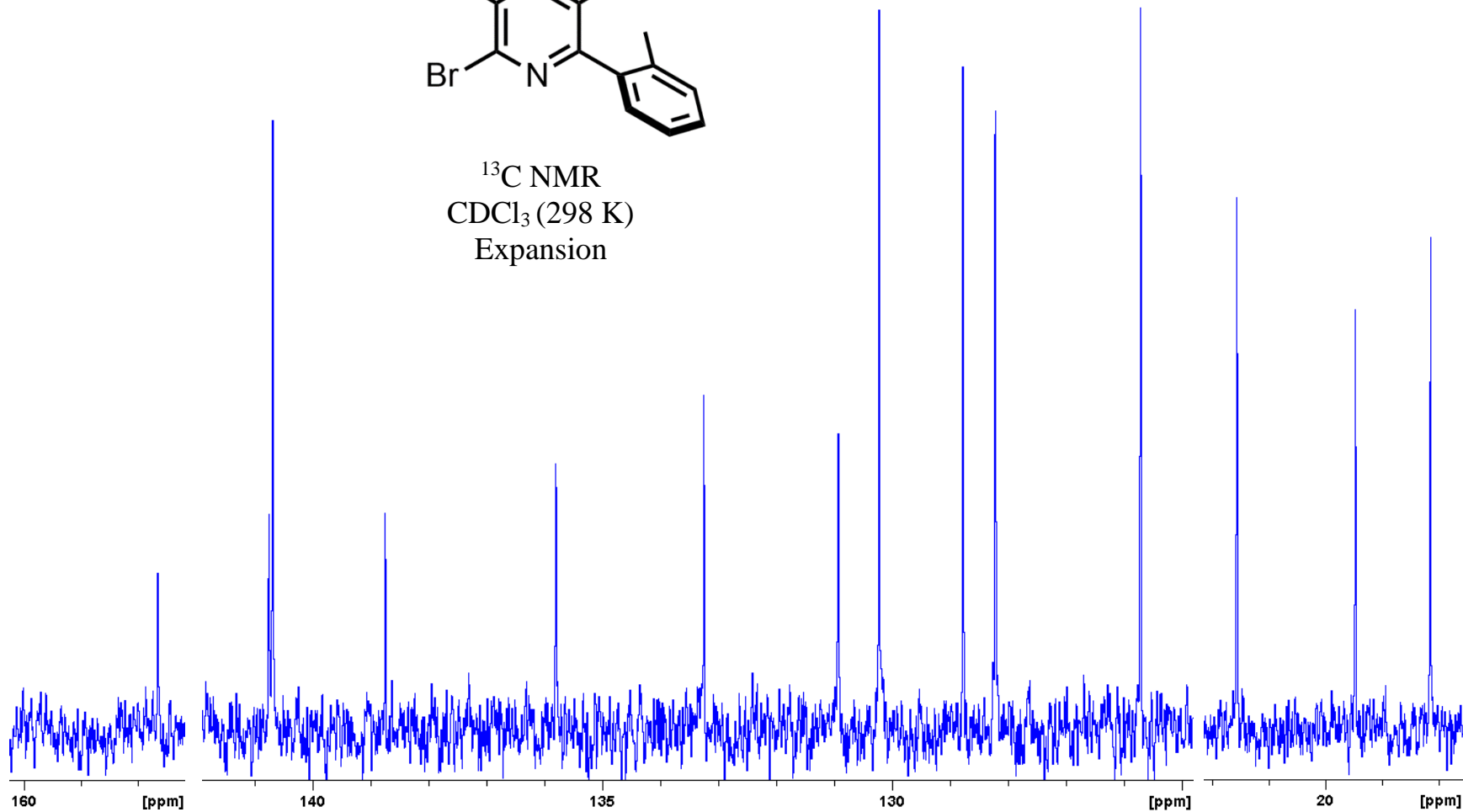


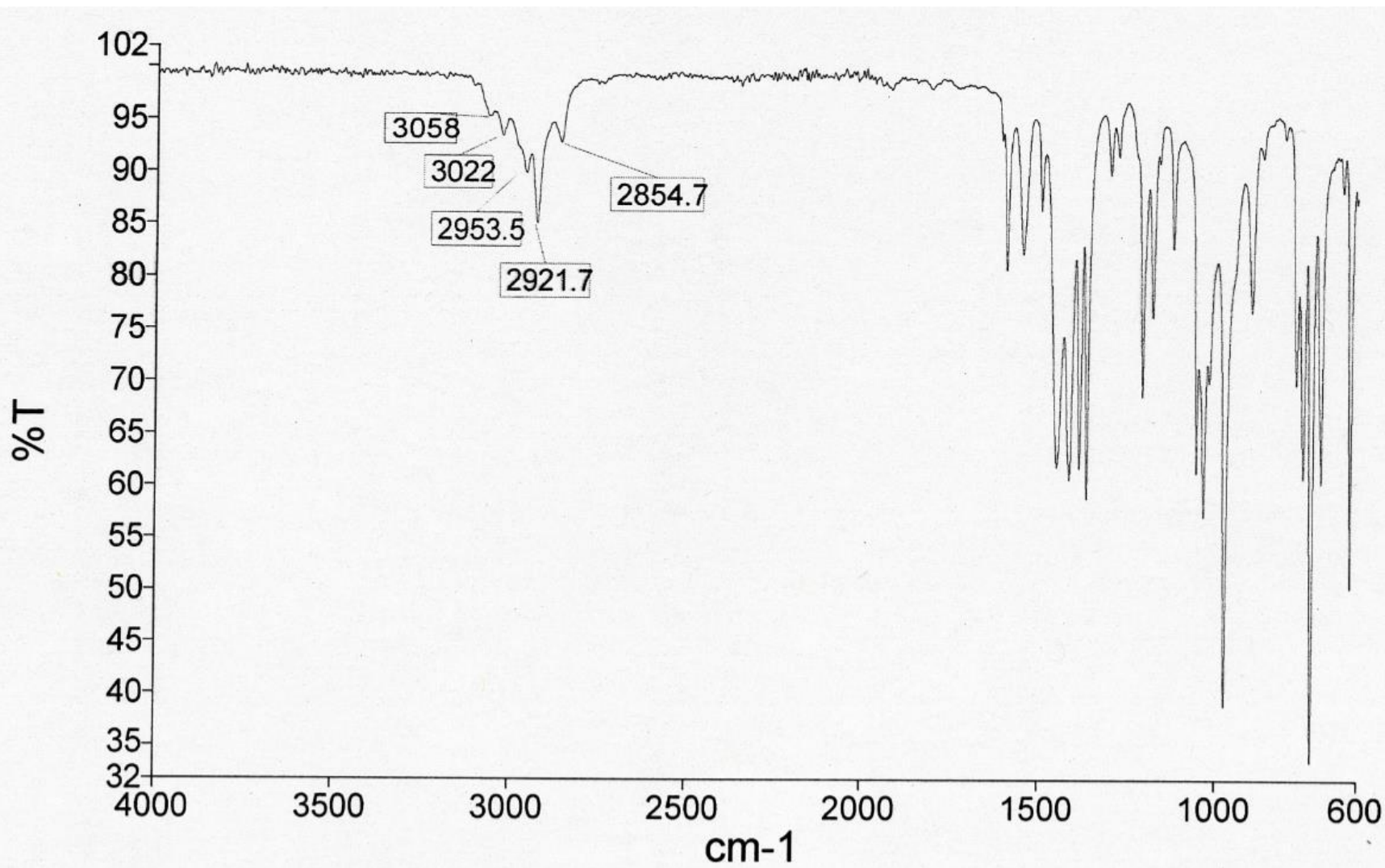
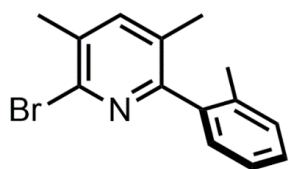
^{13}C NMR
 CDCl_3 (298 K)

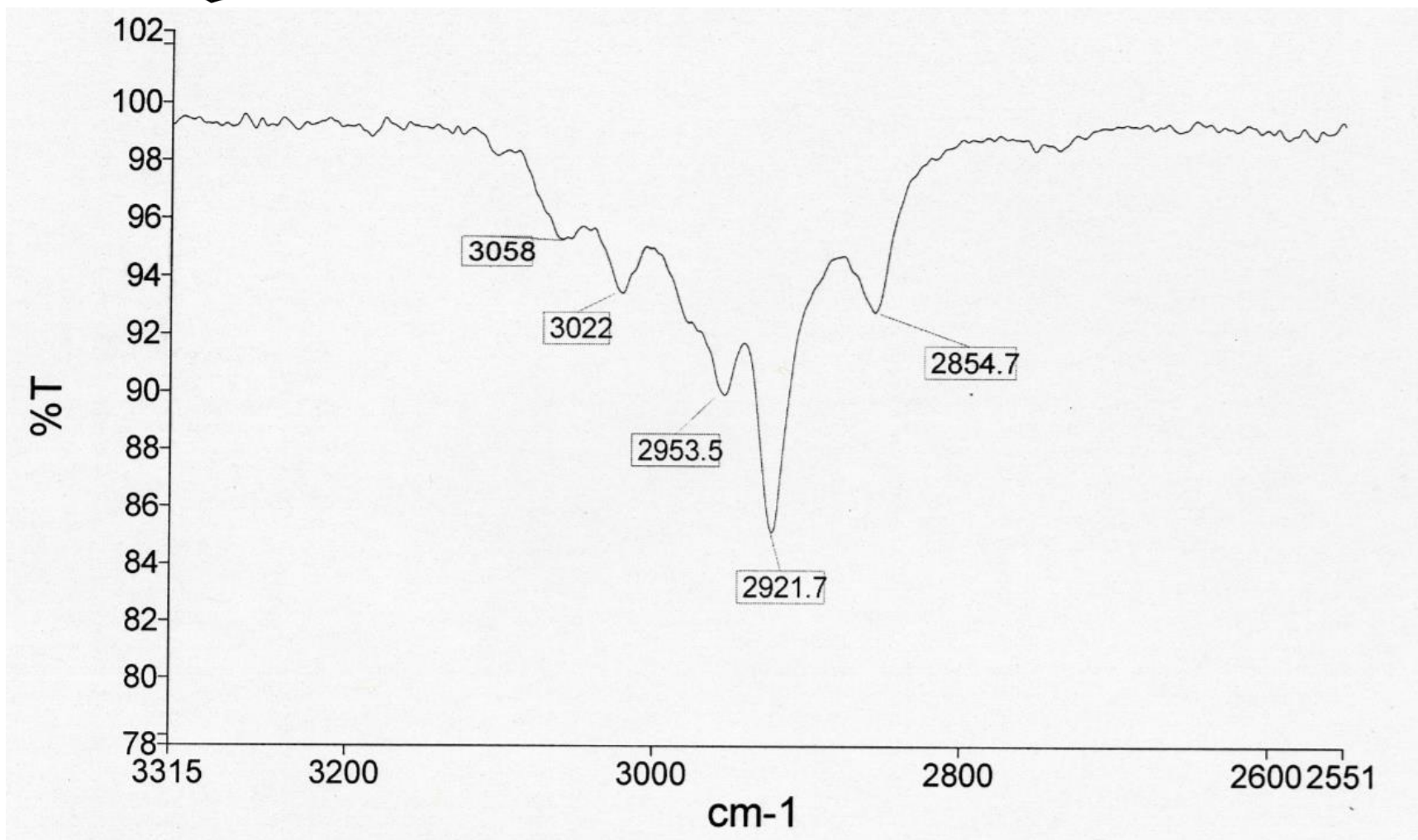
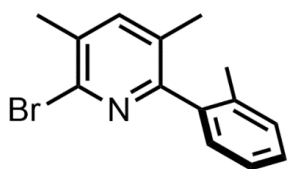


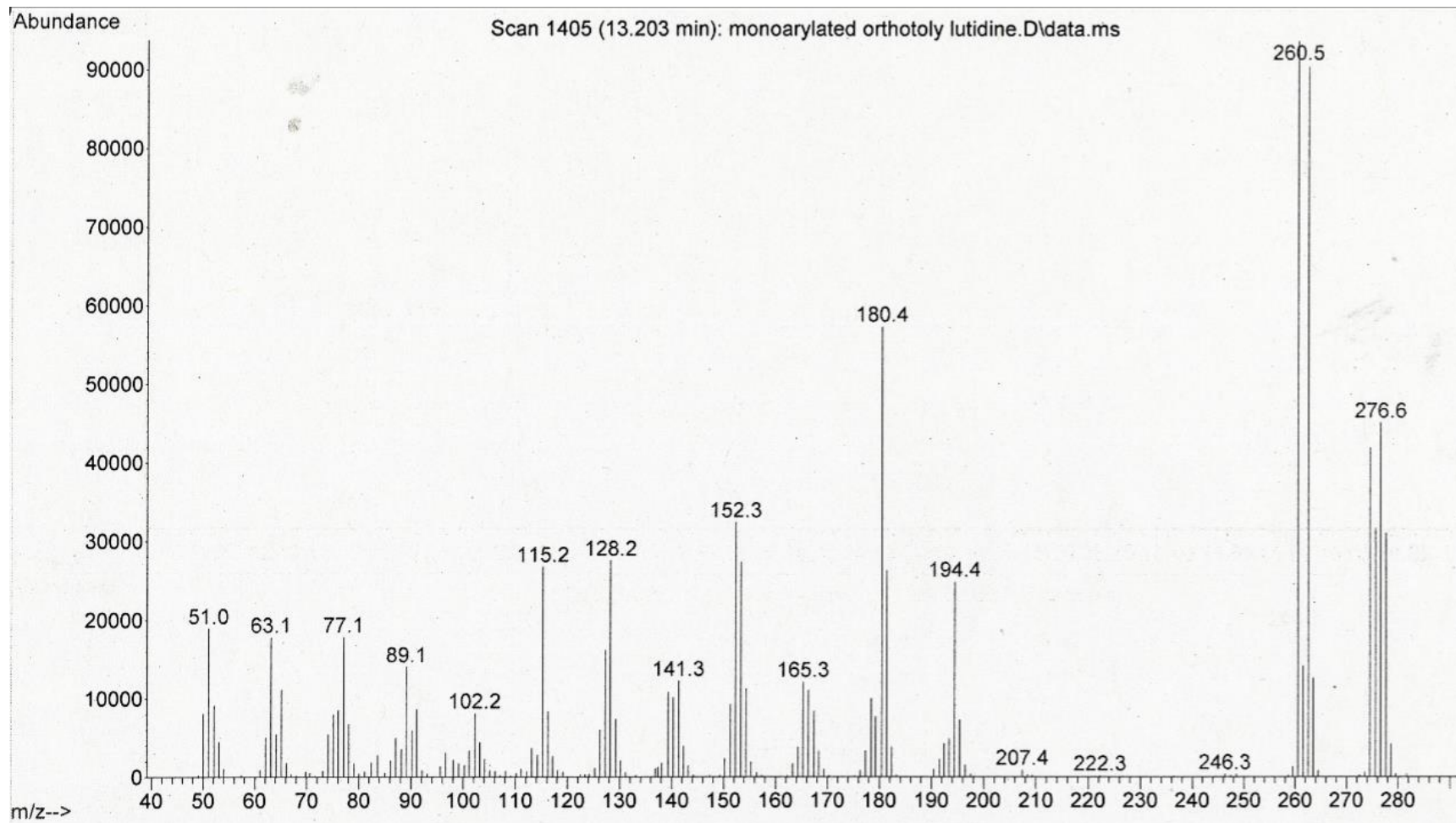
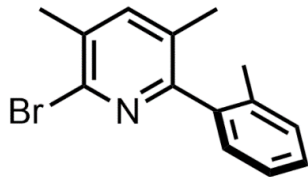


^{13}C NMR
 CDCl_3 (298 K)
Expansion

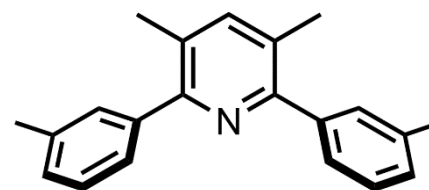




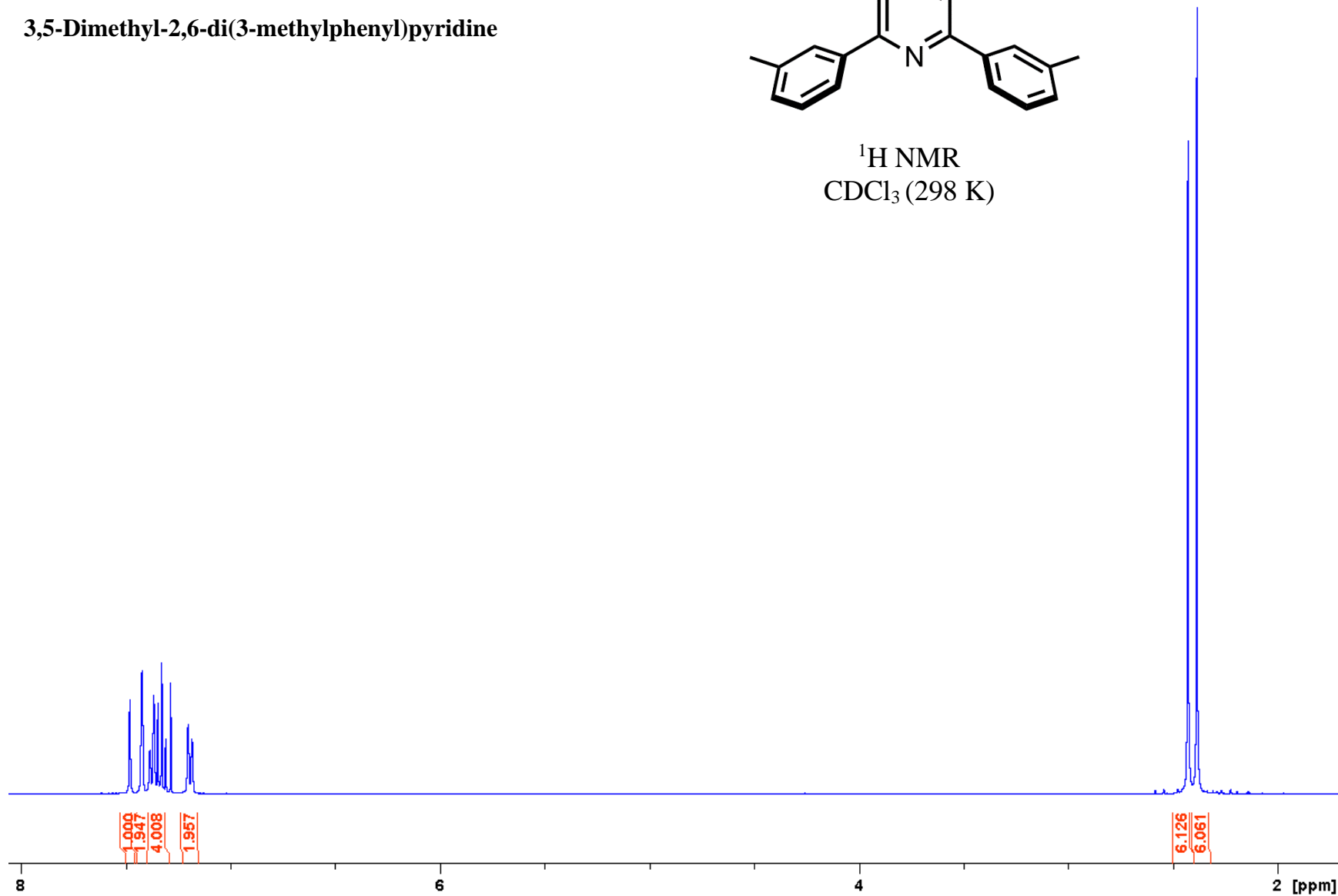


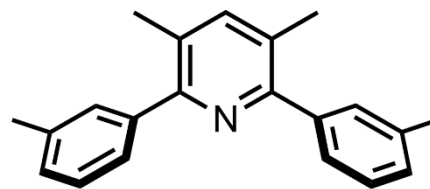


3,5-Dimethyl-2,6-di(3-methylphenyl)pyridine

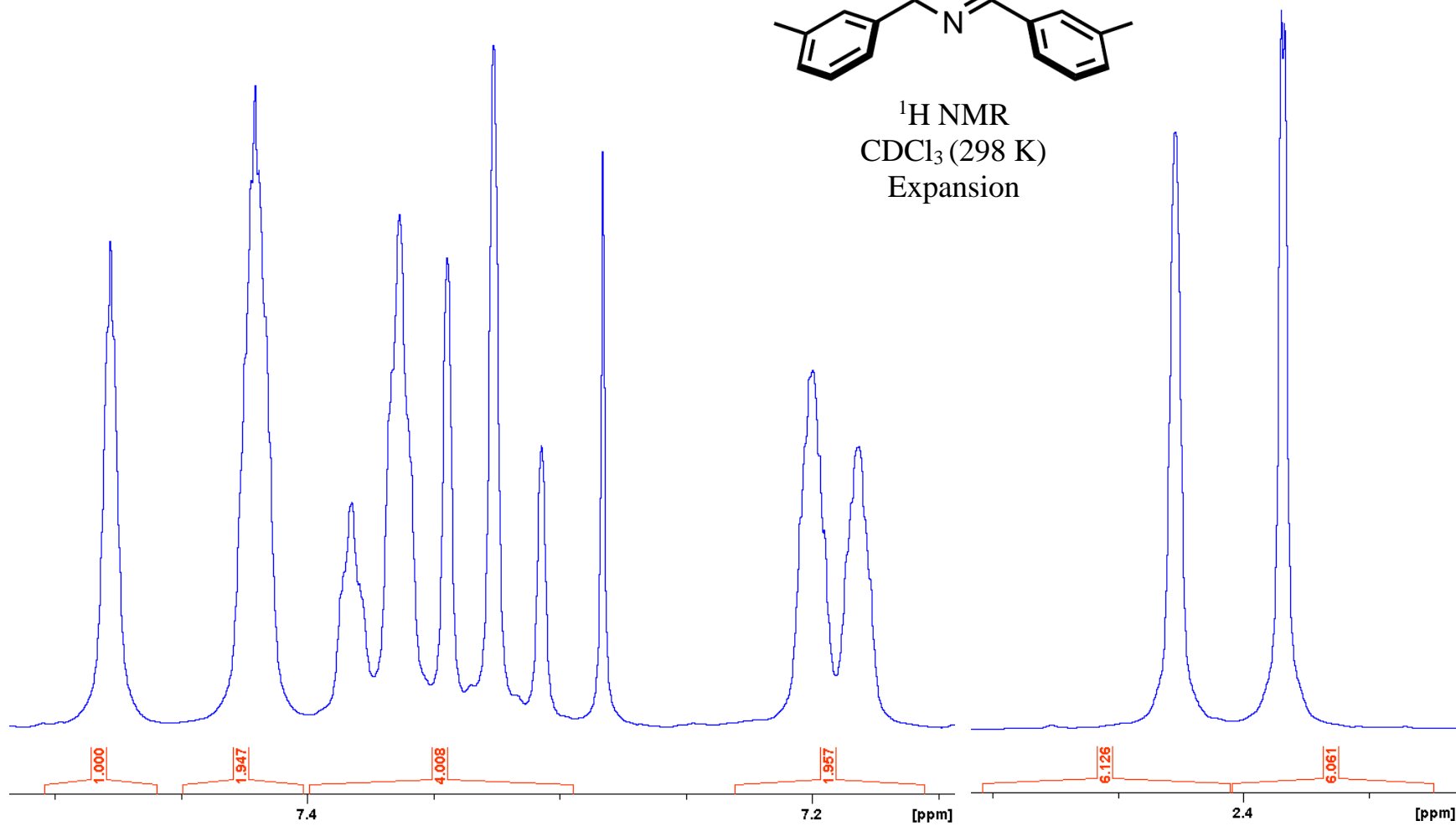


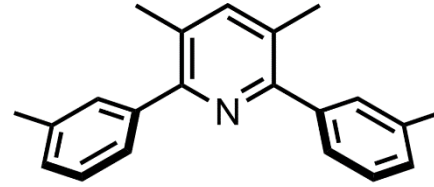
¹H NMR
CDCl₃ (298 K)



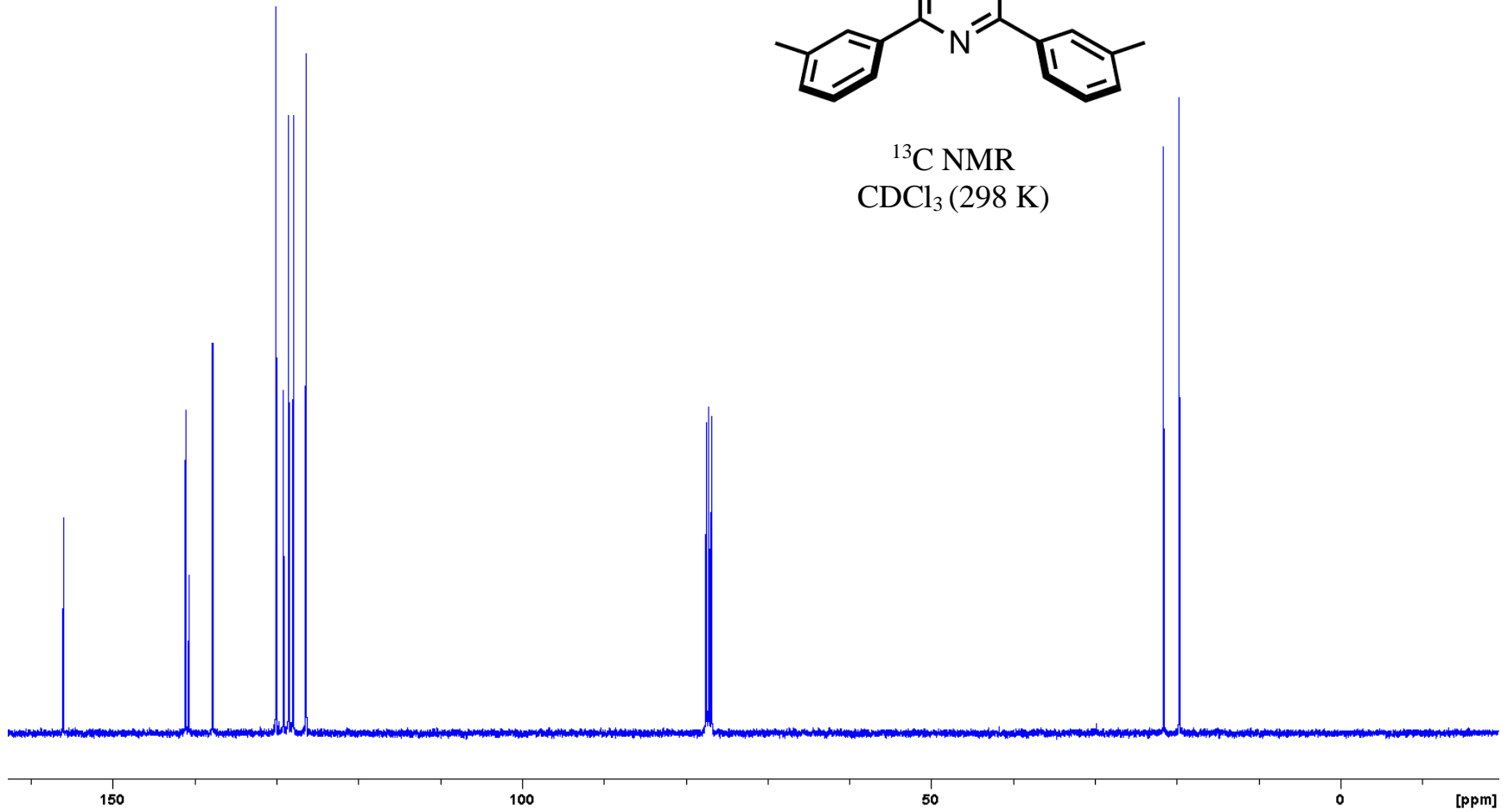


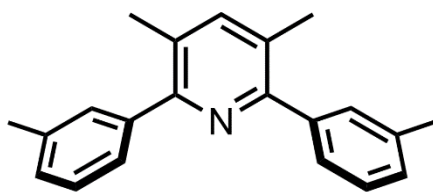
^1H NMR
 CDCl_3 (298 K)
Expansion



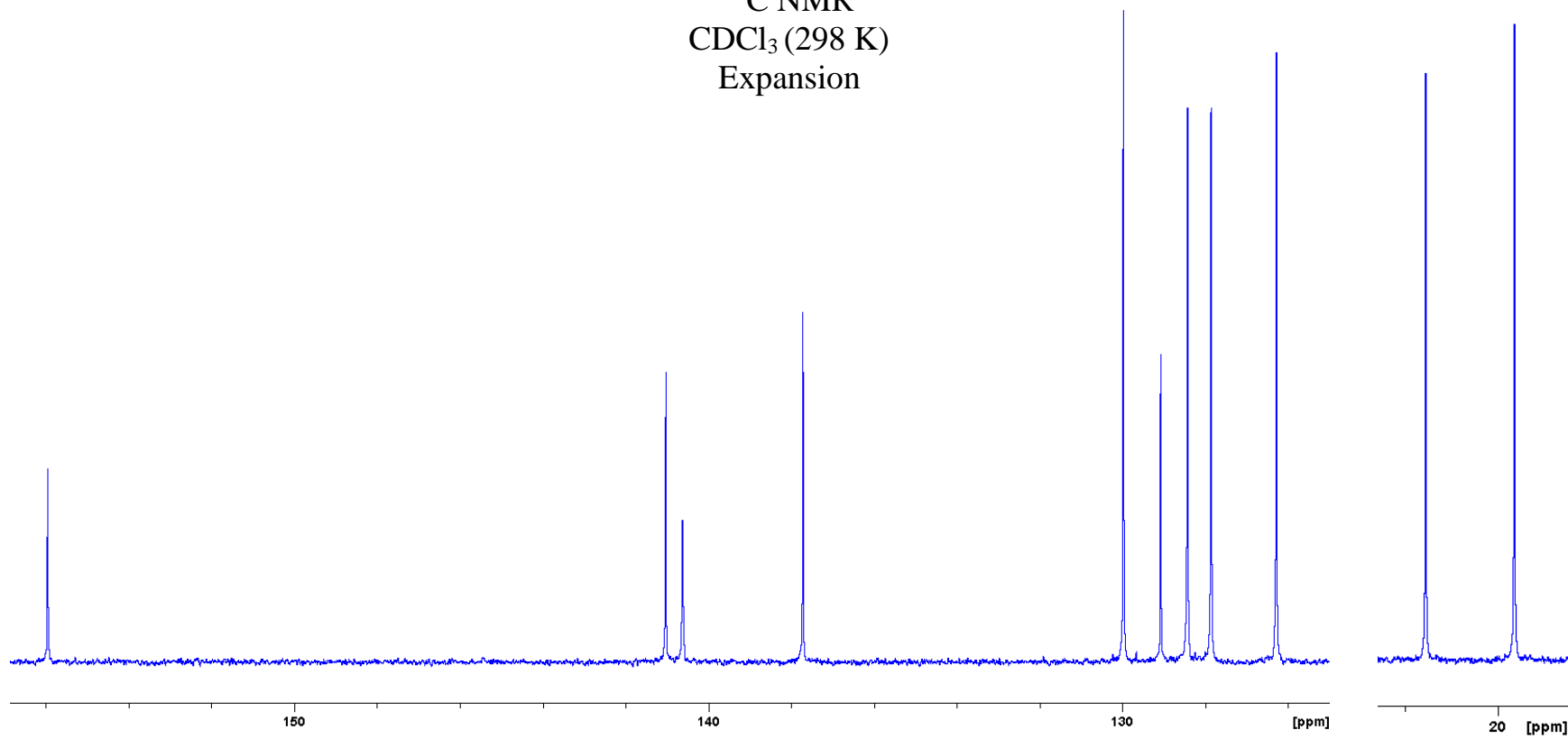


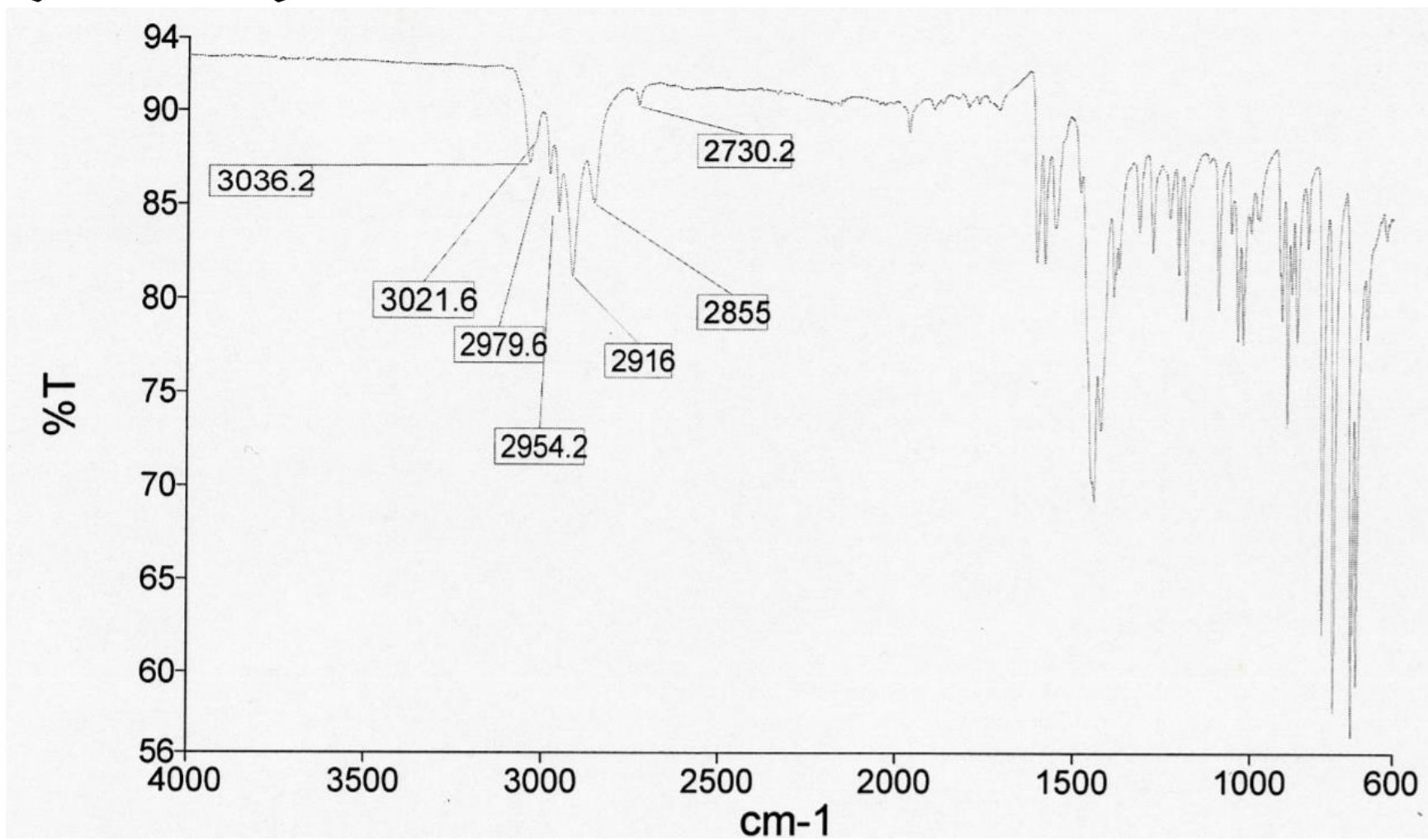
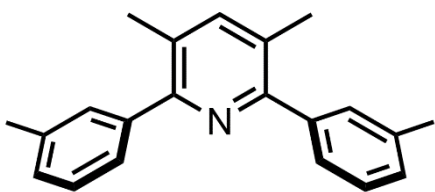
^{13}C NMR
 CDCl_3 (298 K)

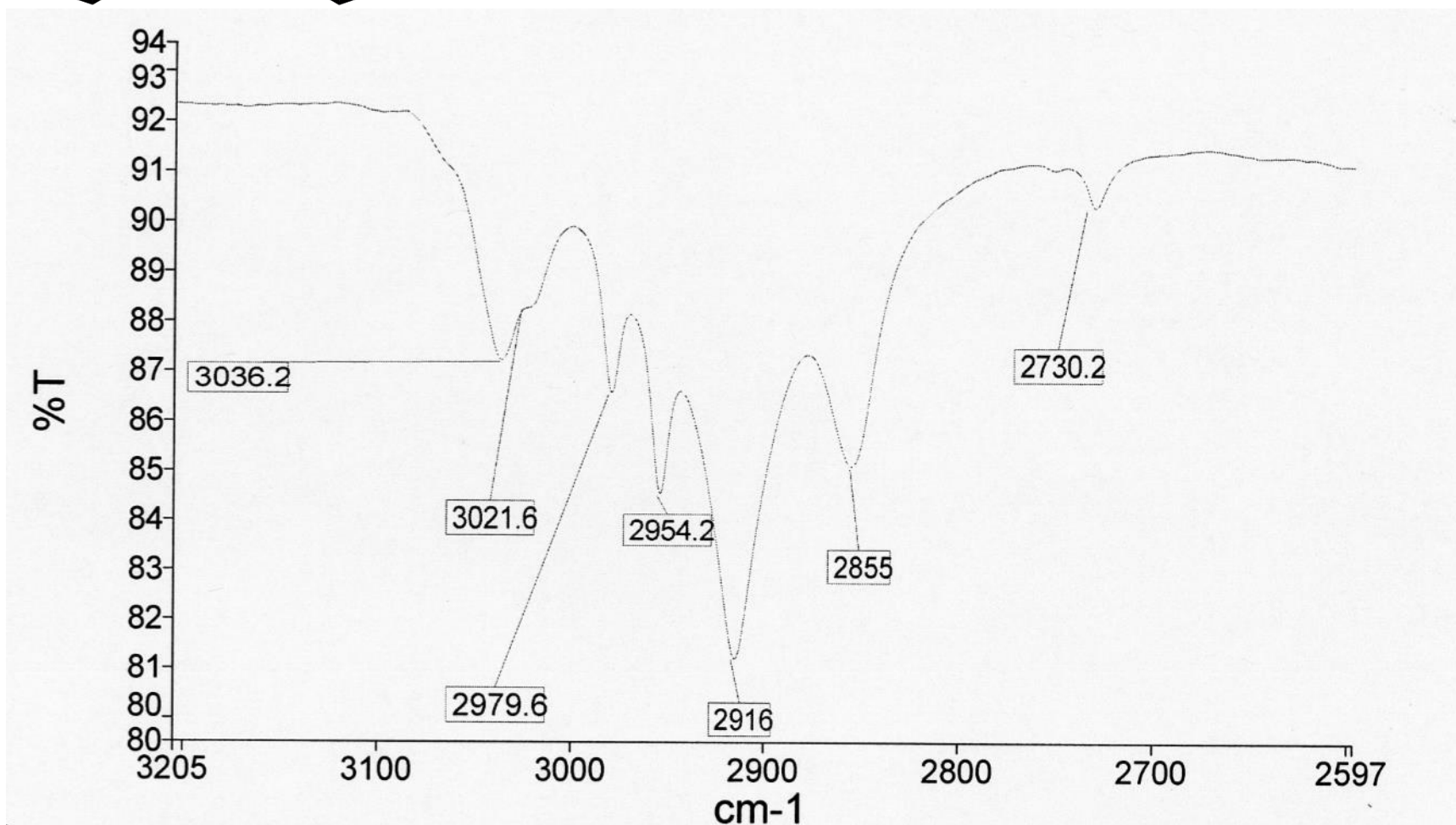
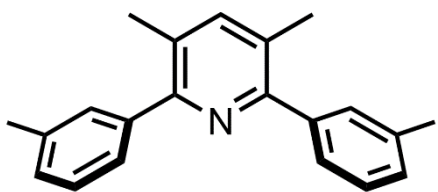


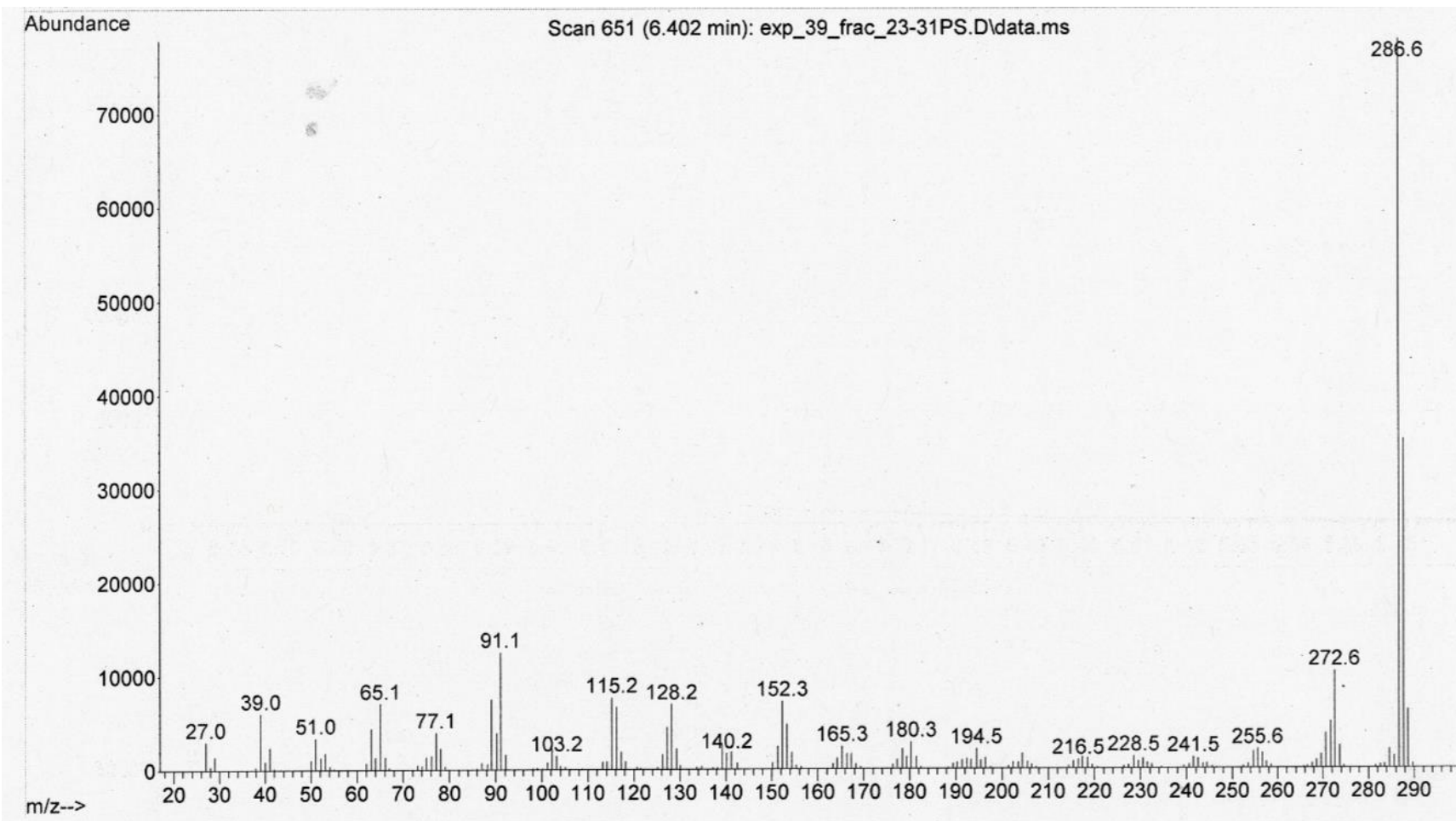
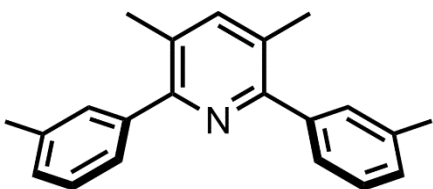


^{13}C NMR
 CDCl_3 (298 K)
Expansion

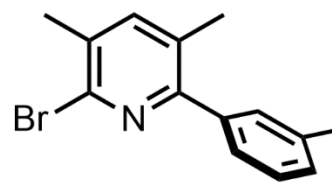




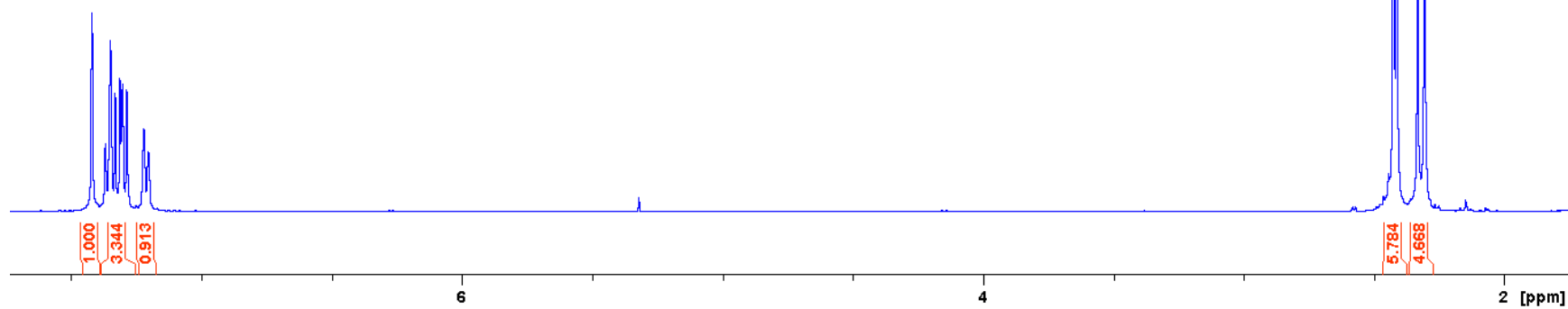


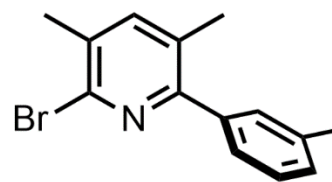


2-bromo-3,5-dimethyl-6-(*m*-tolyl)pyridine

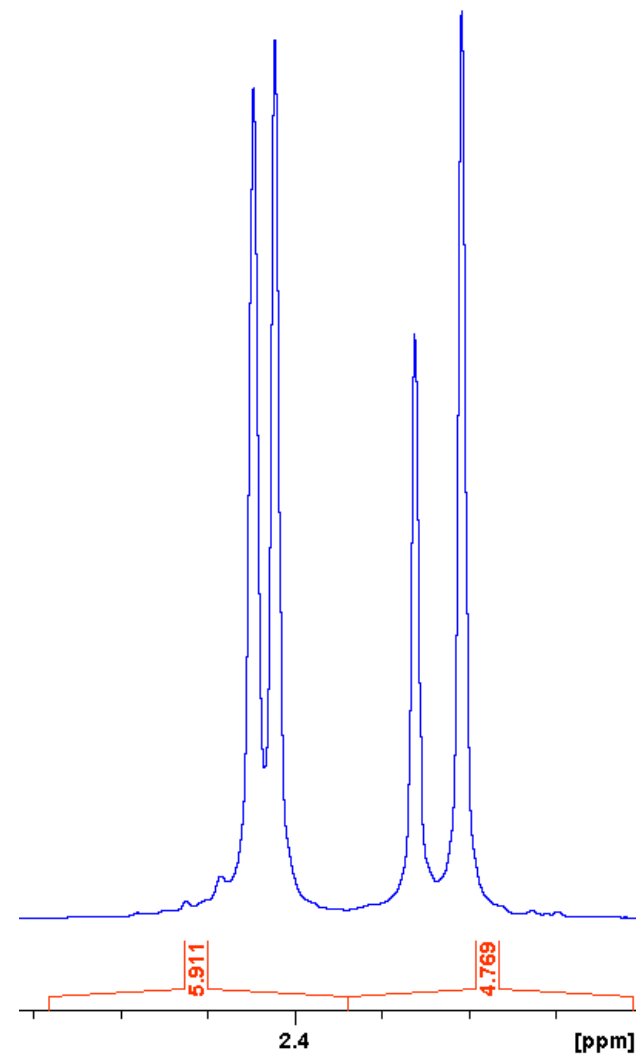
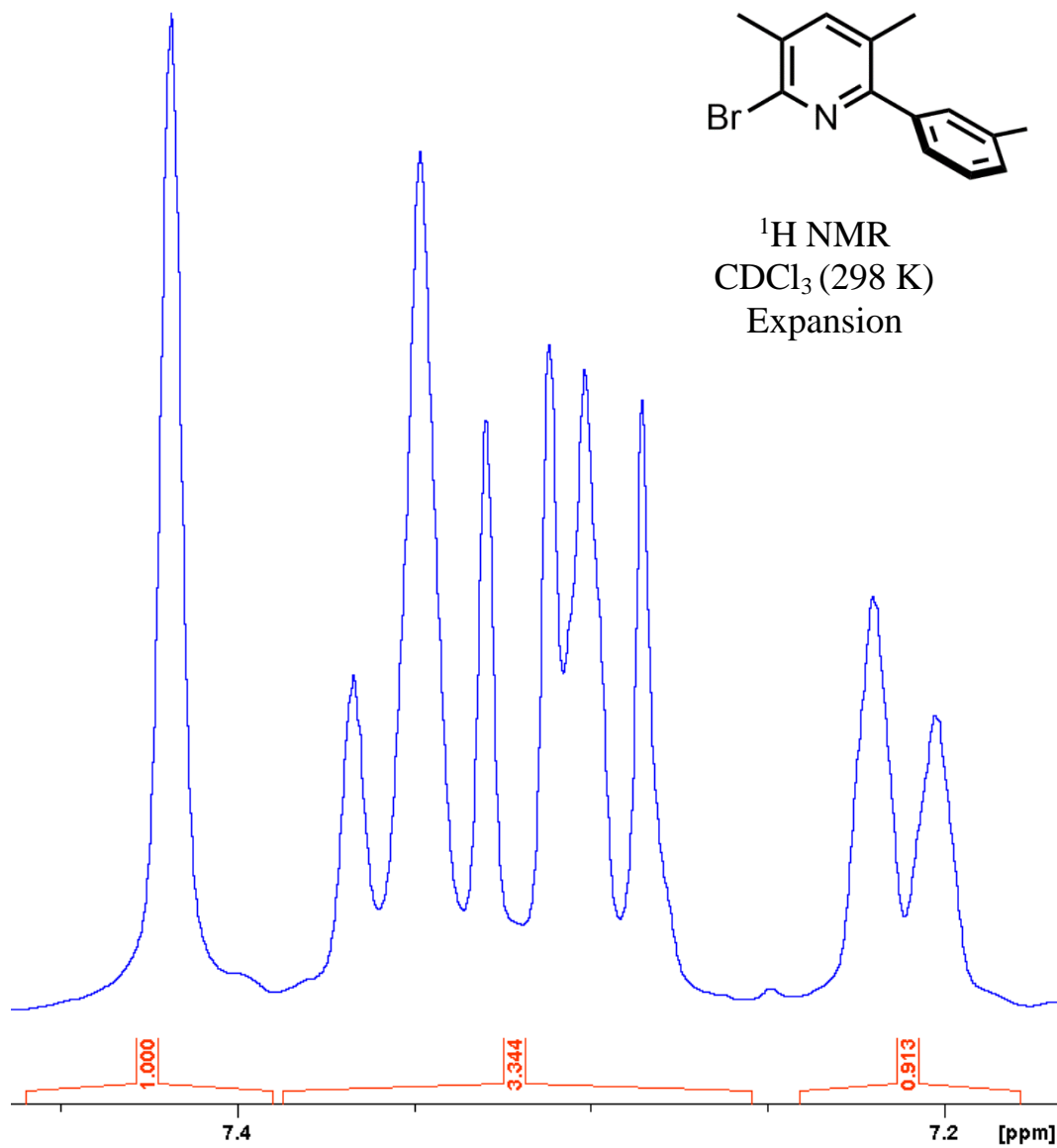


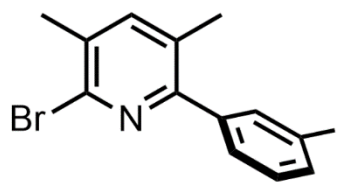
^1H NMR
 CDCl_3 (298 K)



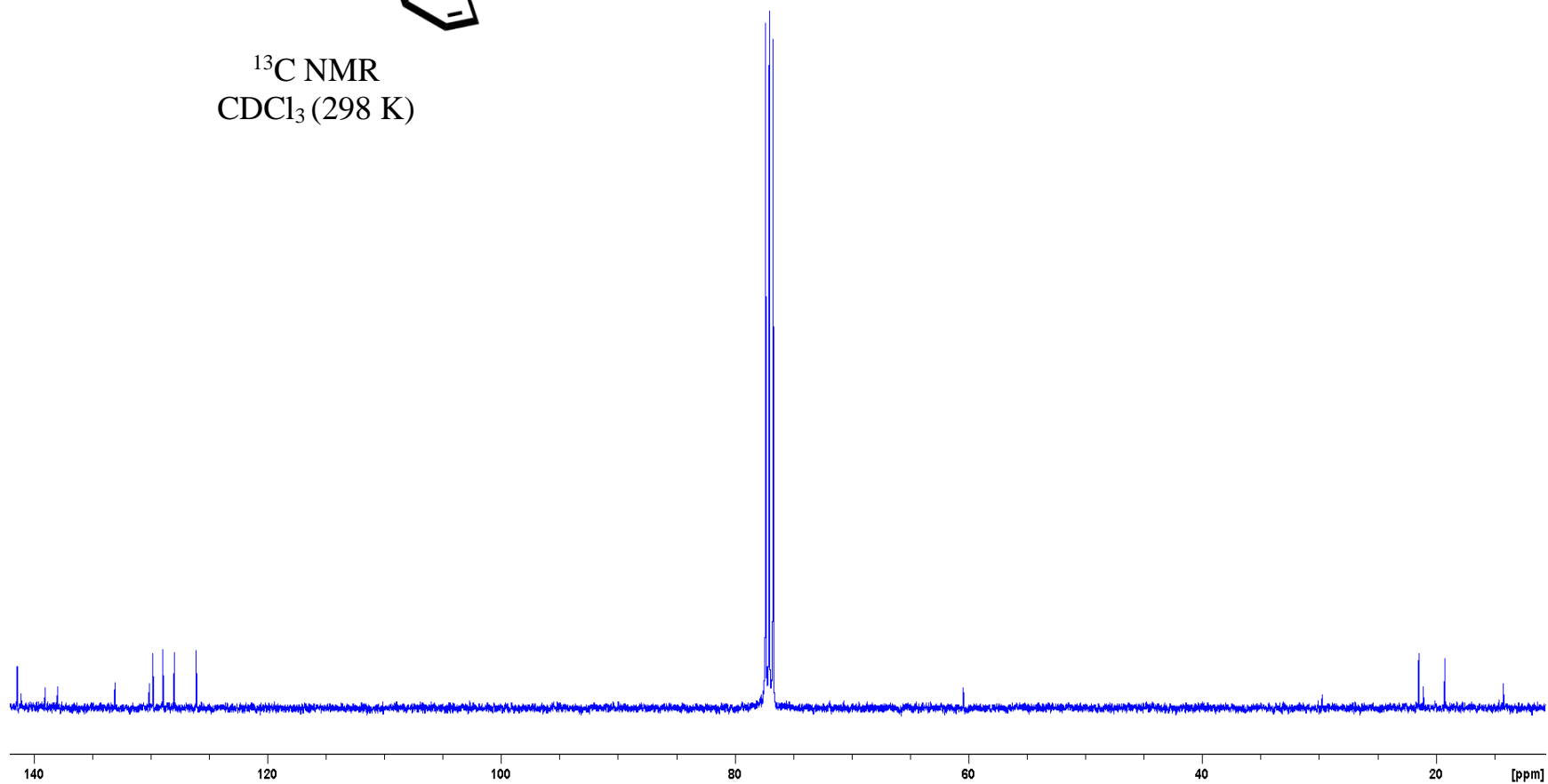


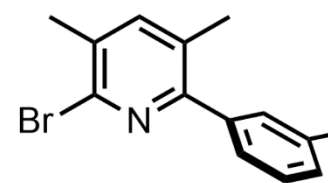
^1H NMR
 CDCl_3 (298 K)
Expansion



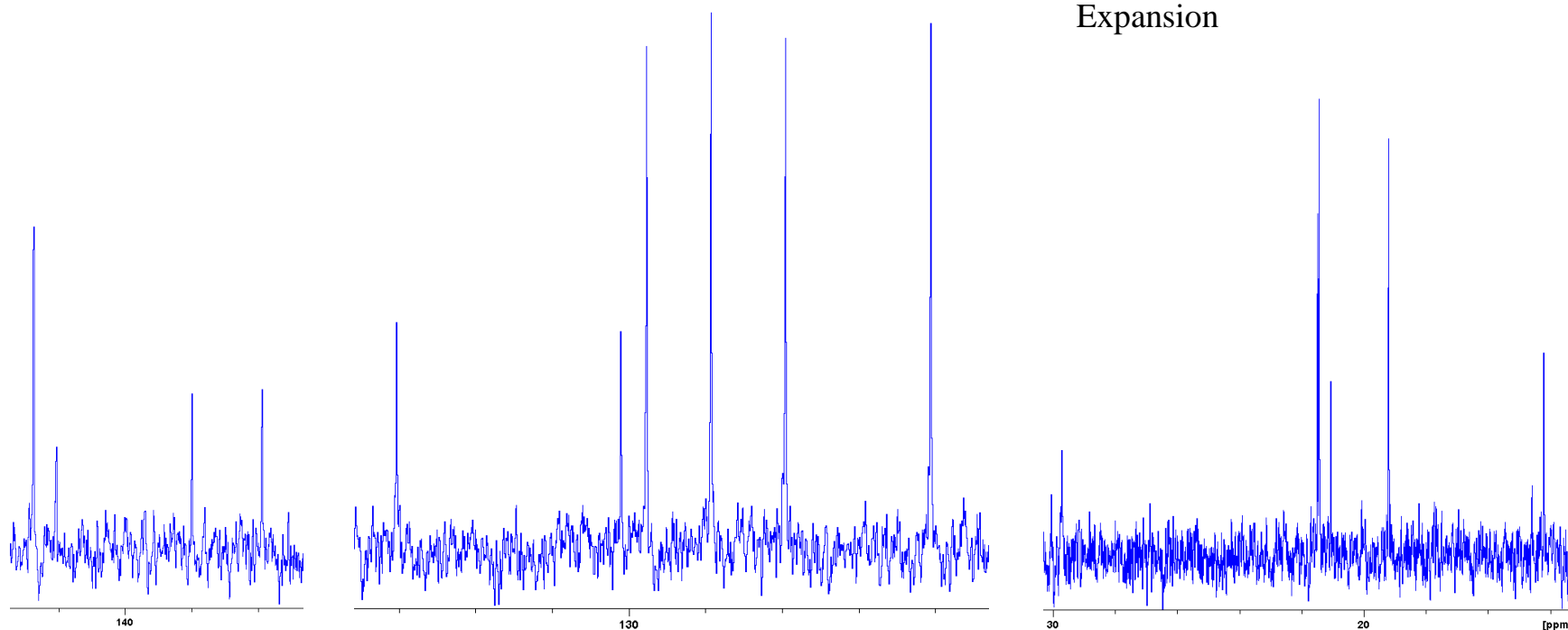


^{13}C NMR
 CDCl_3 (298 K)

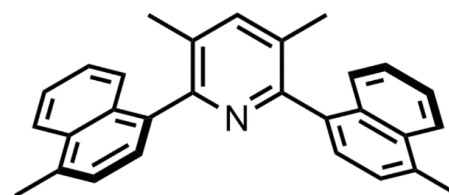




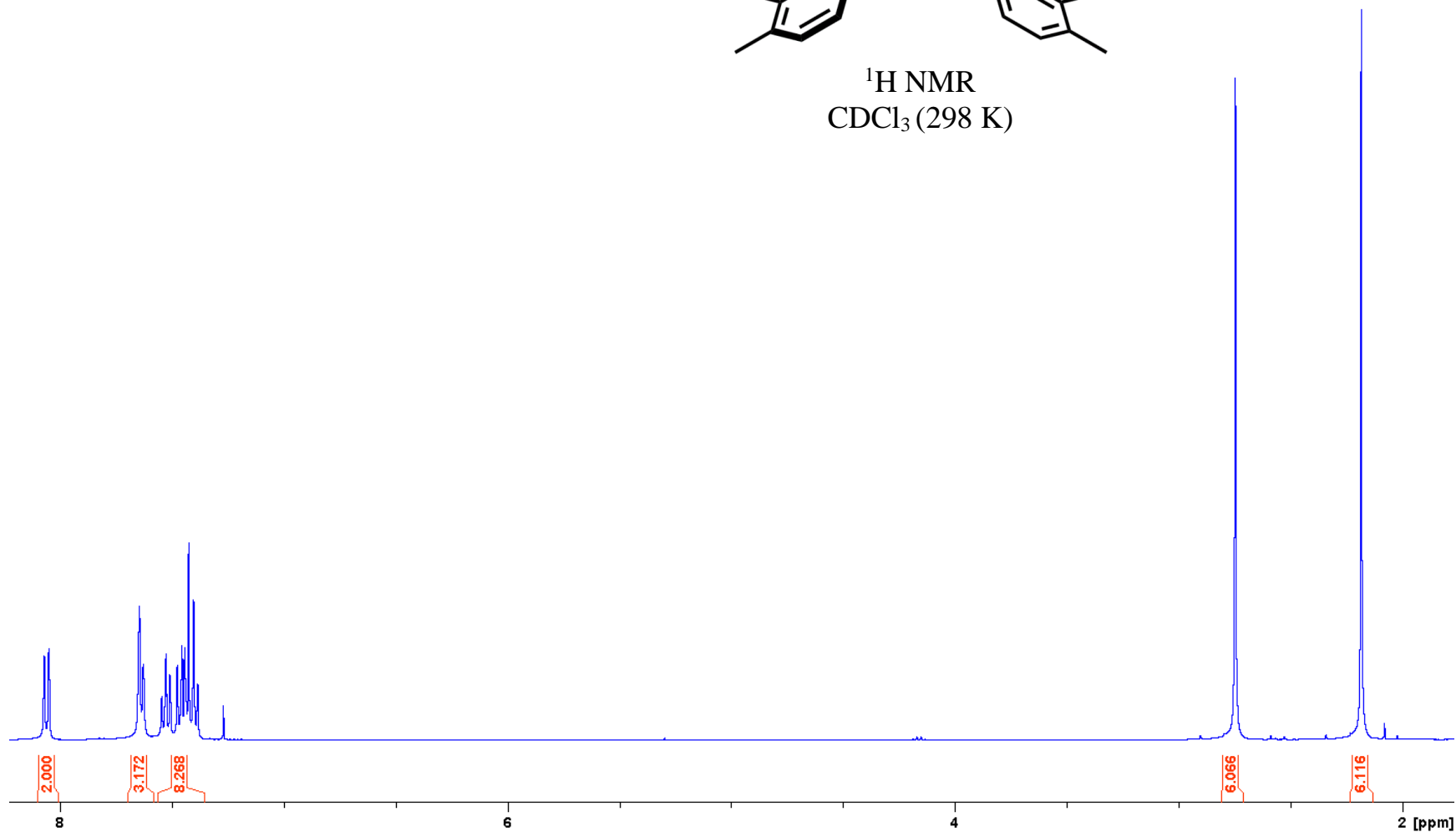
^{13}C NMR
CDCl₃ (298 K)
Expansion

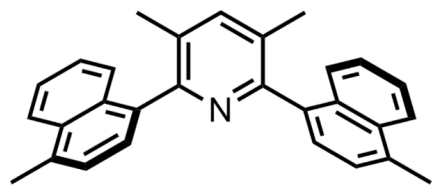


3,5-Dimethyl-2,6-Di(4-methylnaphthyl-1-yl)pyridine

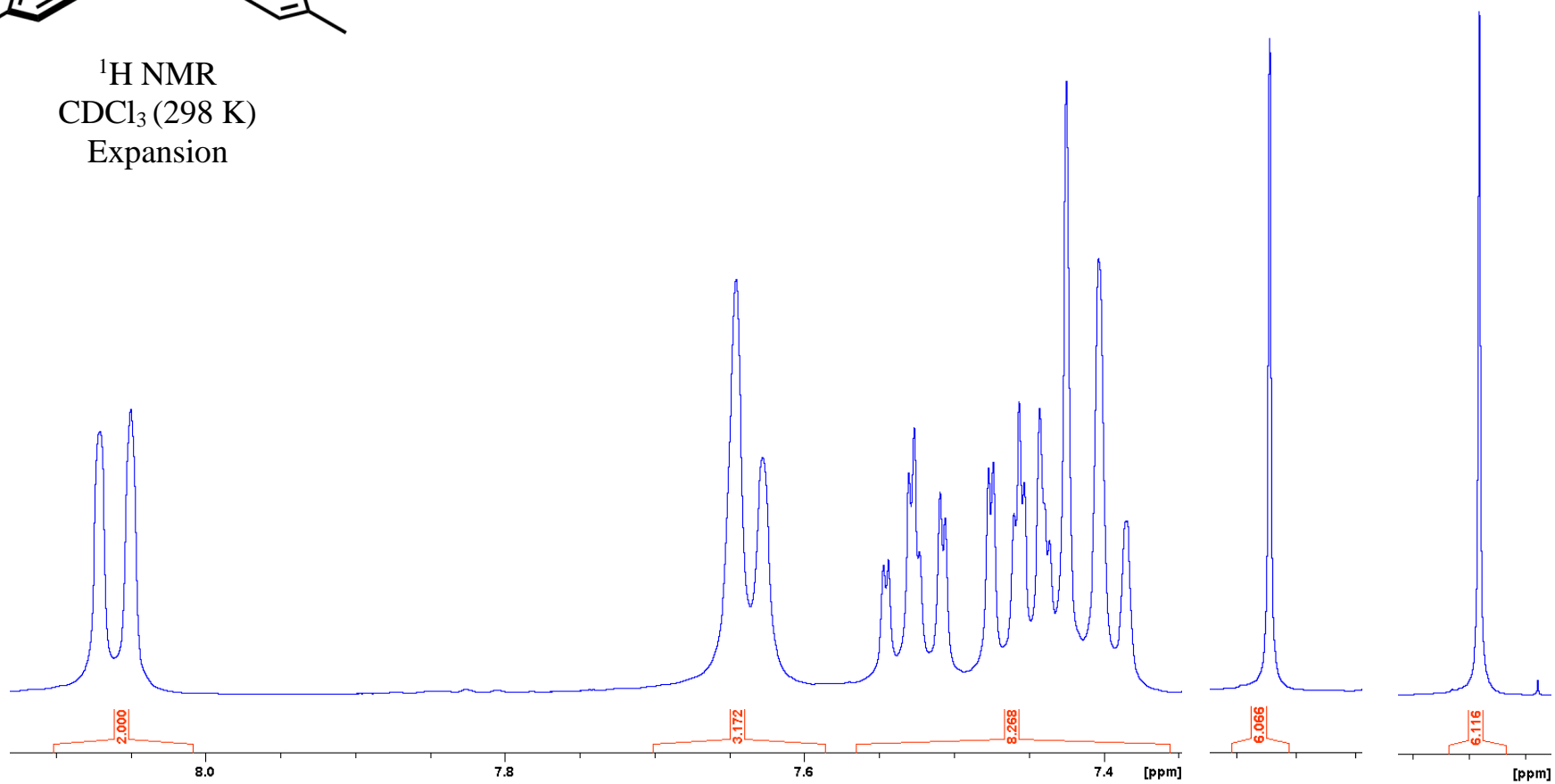


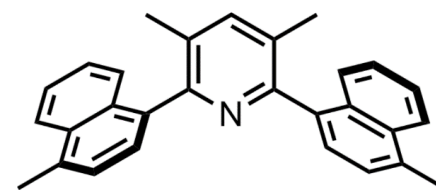
¹H NMR
CDCl₃ (298 K)



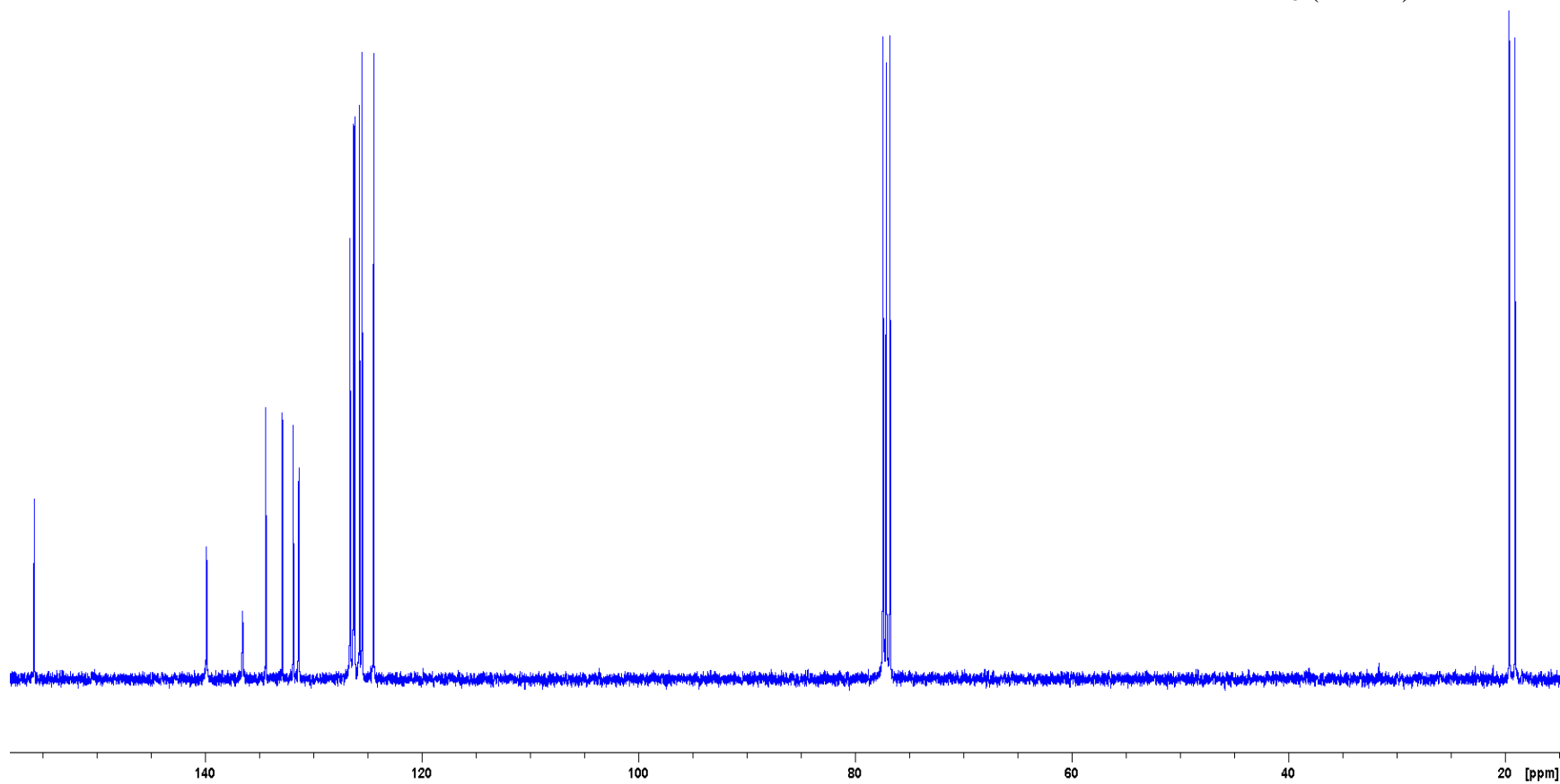


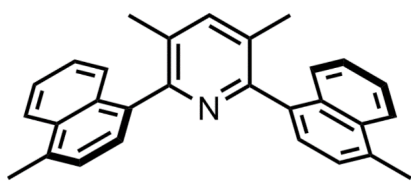
^1H NMR
 CDCl_3 (298 K)
Expansion



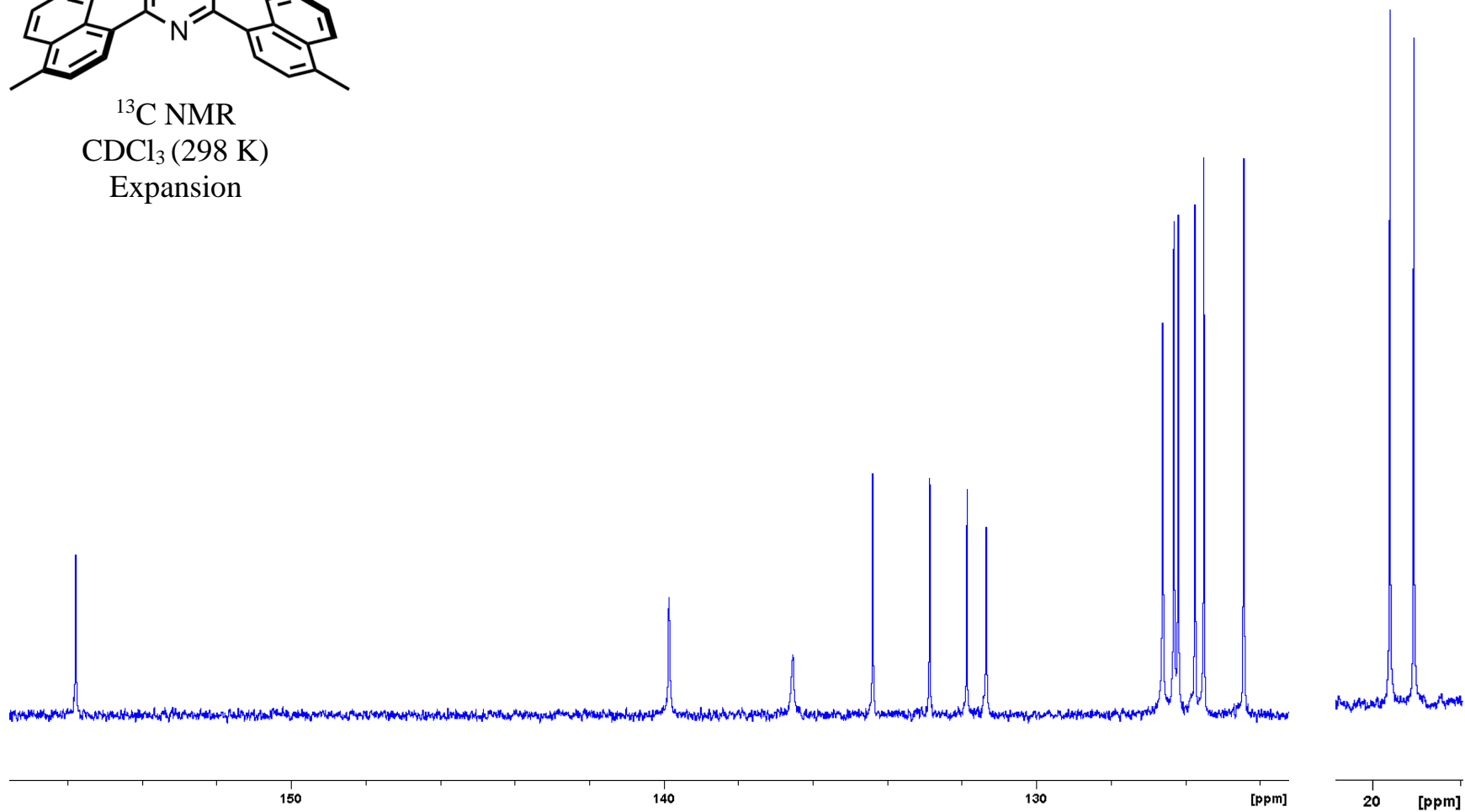


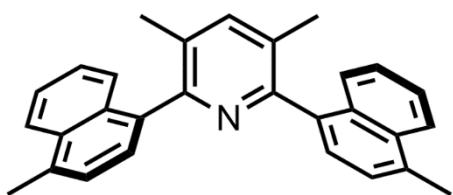
^{13}C NMR
 CDCl_3 (298 K)



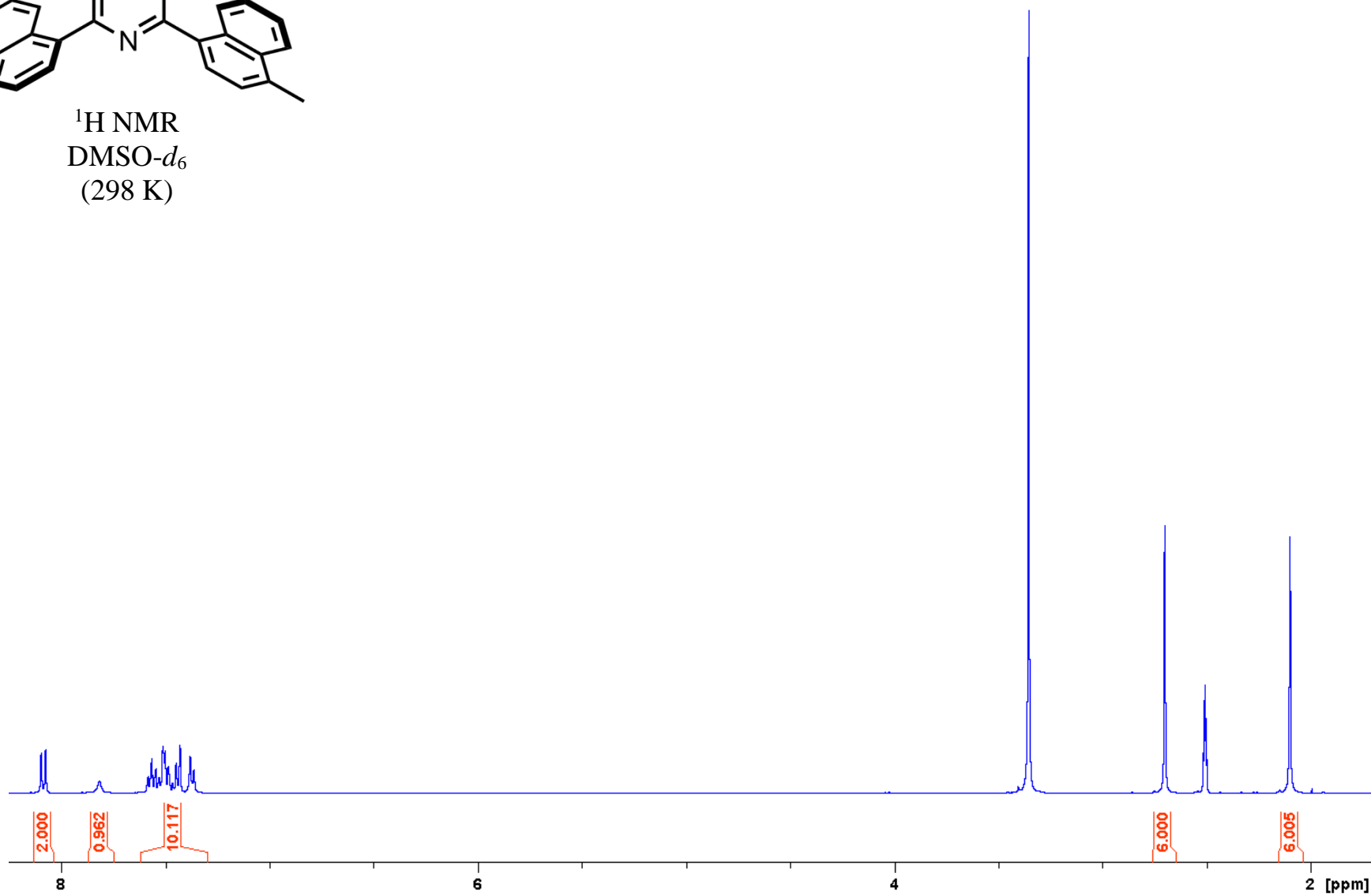


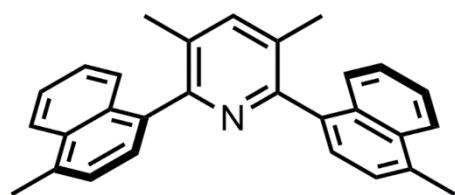
^{13}C NMR
 CDCl_3 (298 K)
Expansion



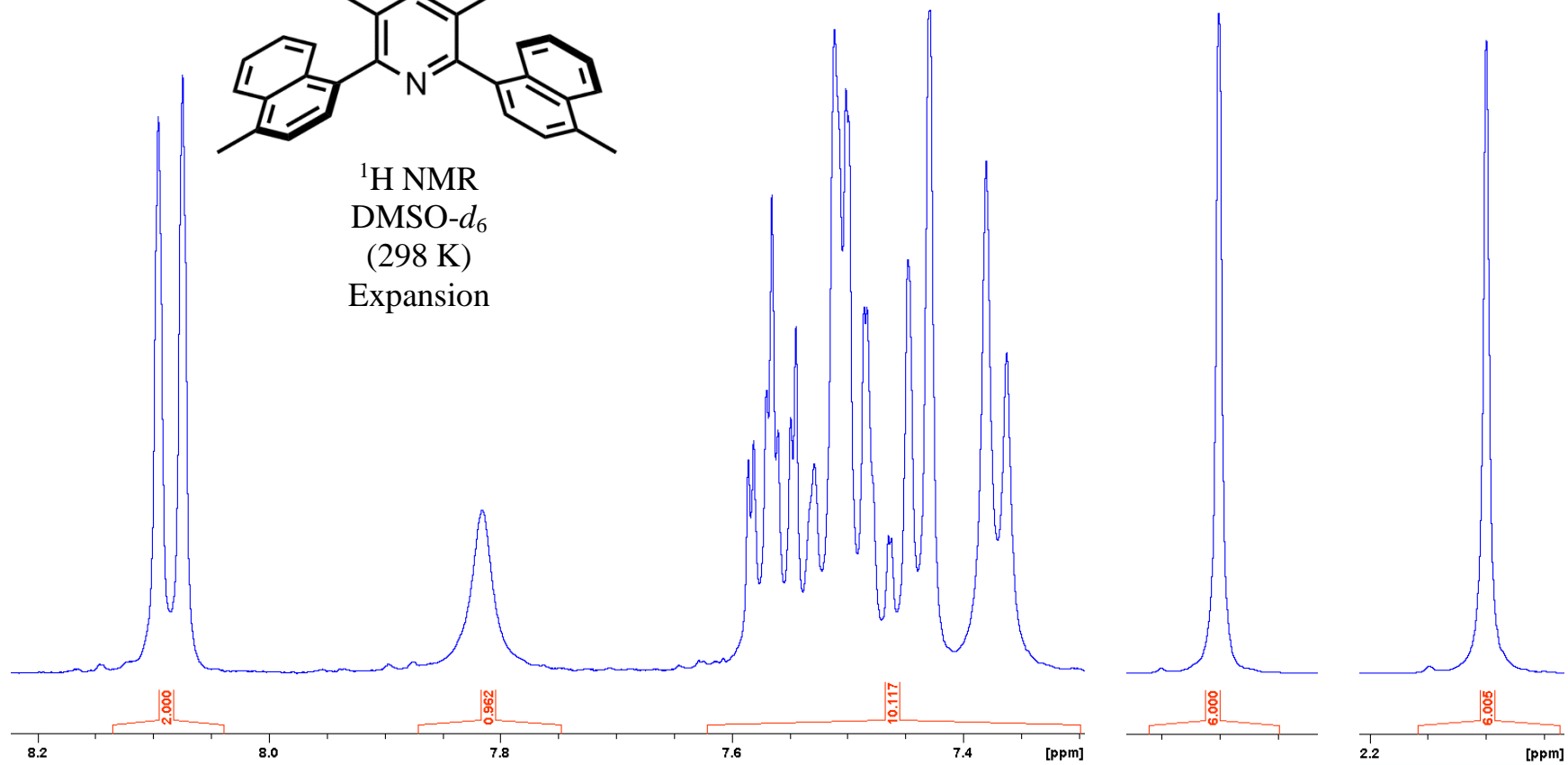


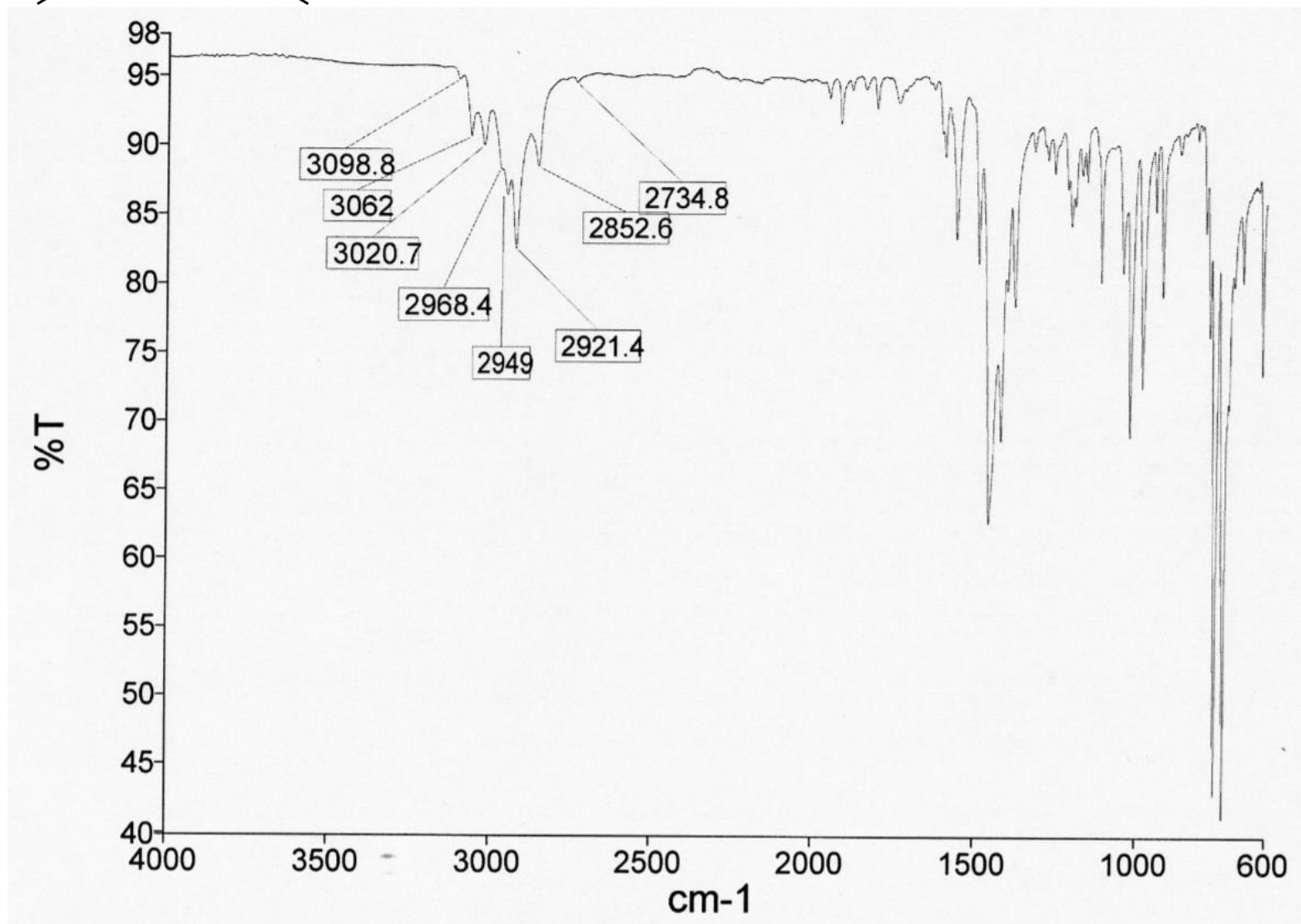
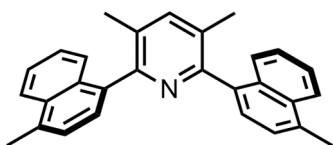
^1H NMR
DMSO- d_6
(298 K)

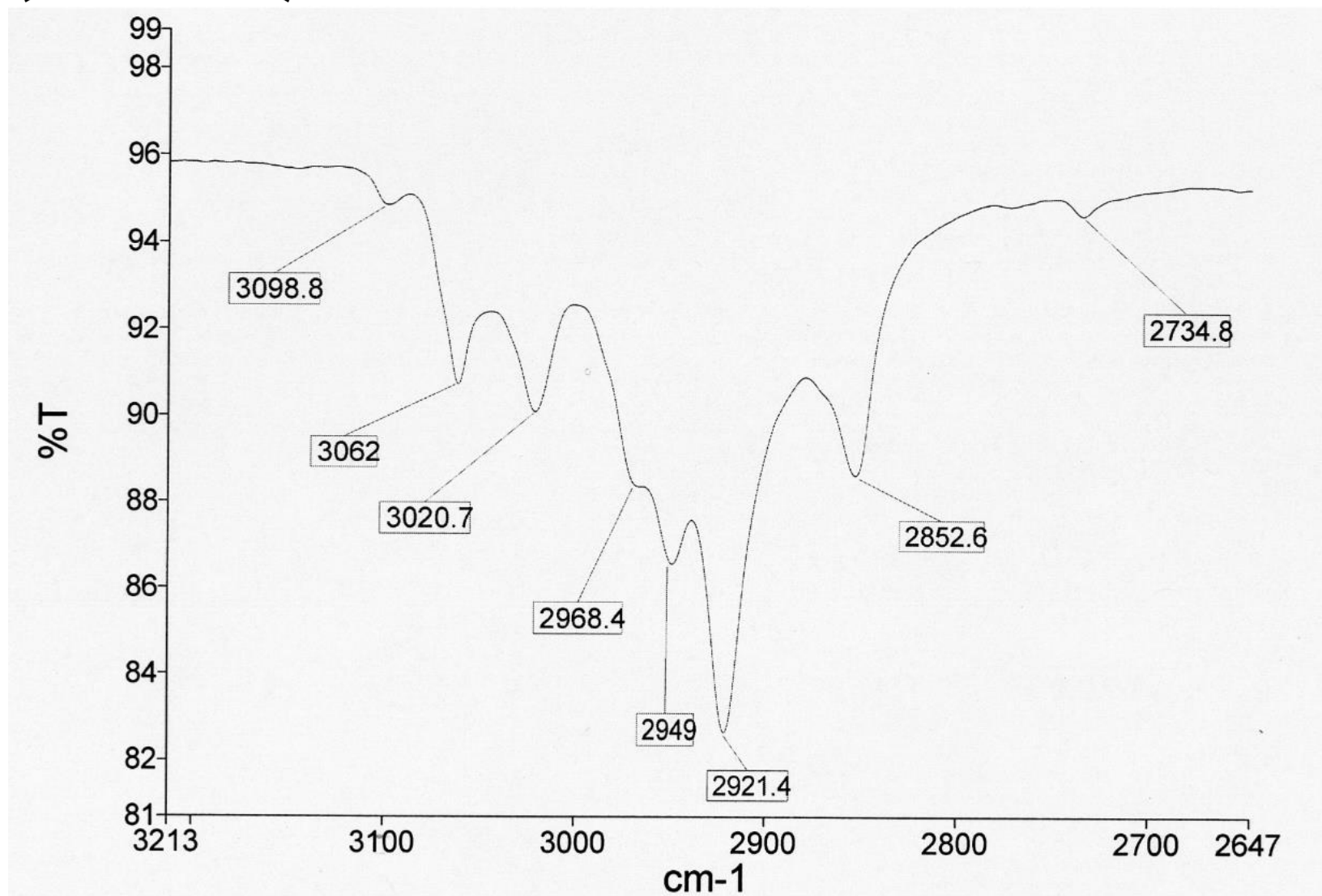
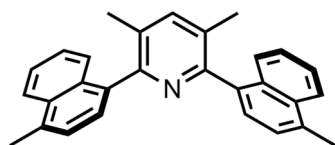


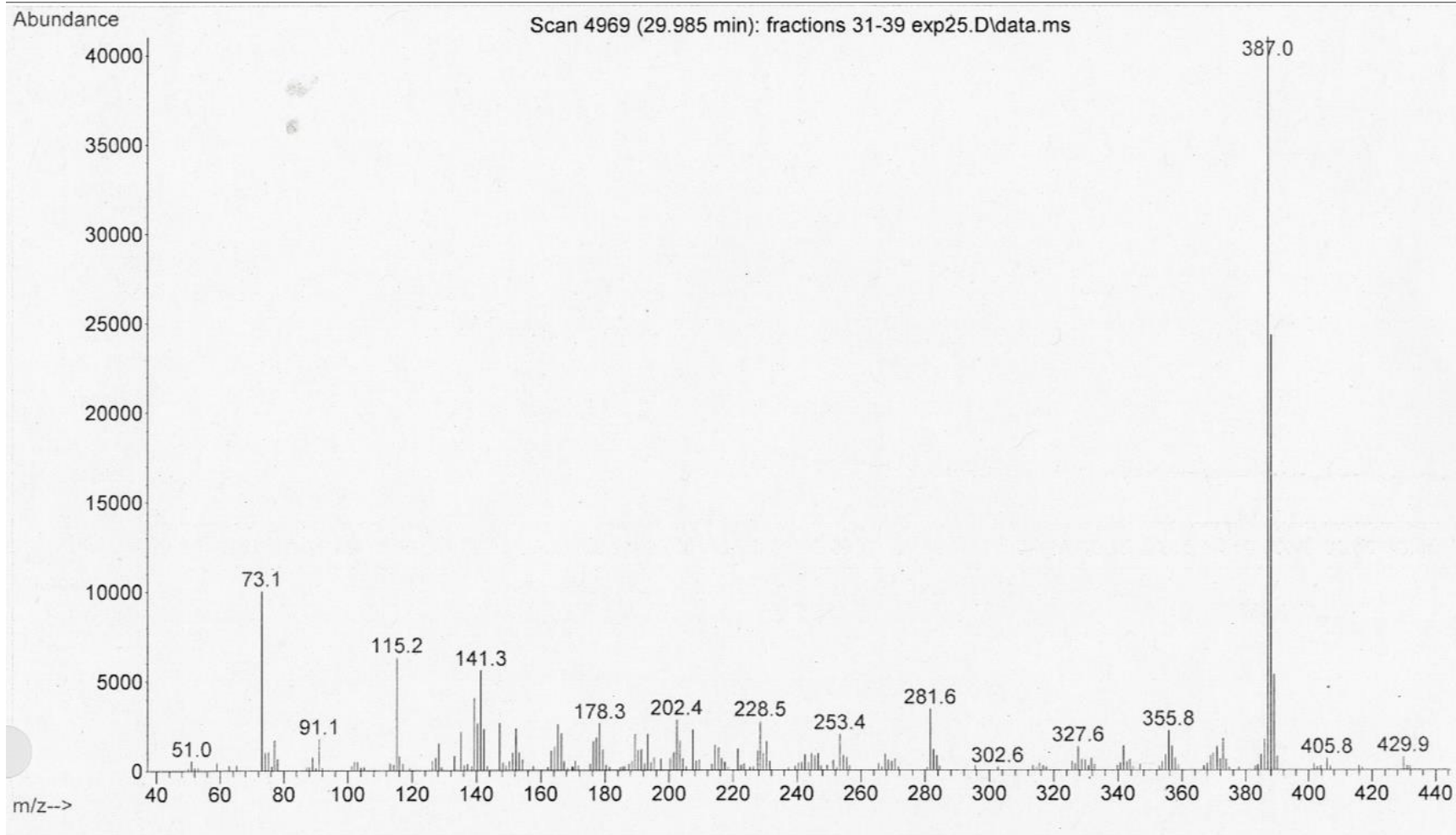
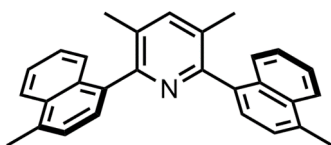


^1H NMR
DMSO- d_6
(298 K)
Expansion

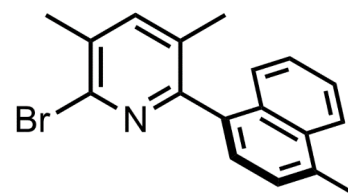




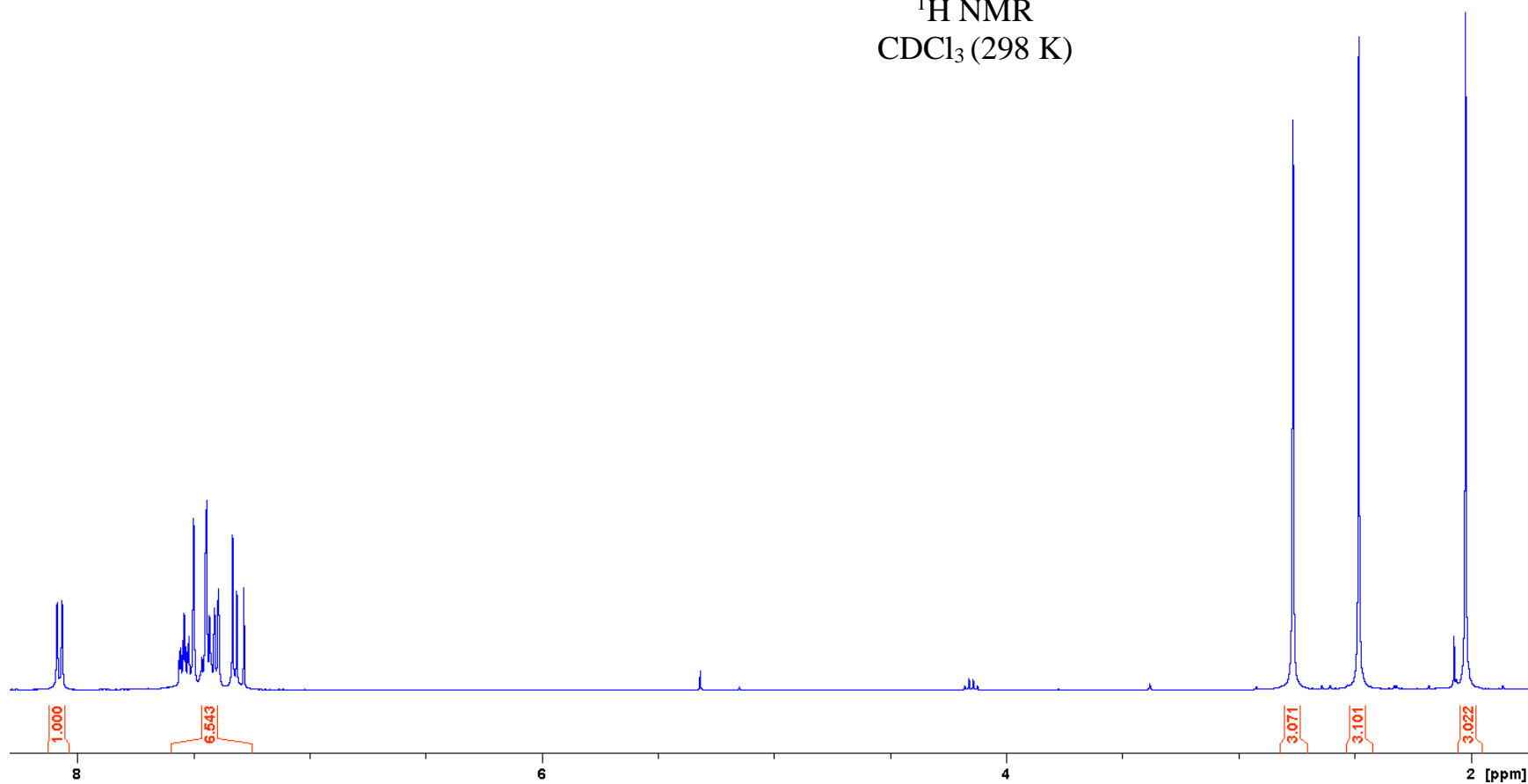


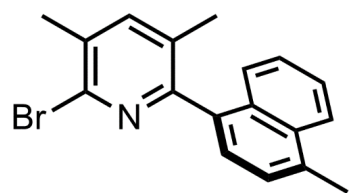


2-bromo-3,5-dimethyl-6-(4-methylnaphthalen-1-yl)pyridine

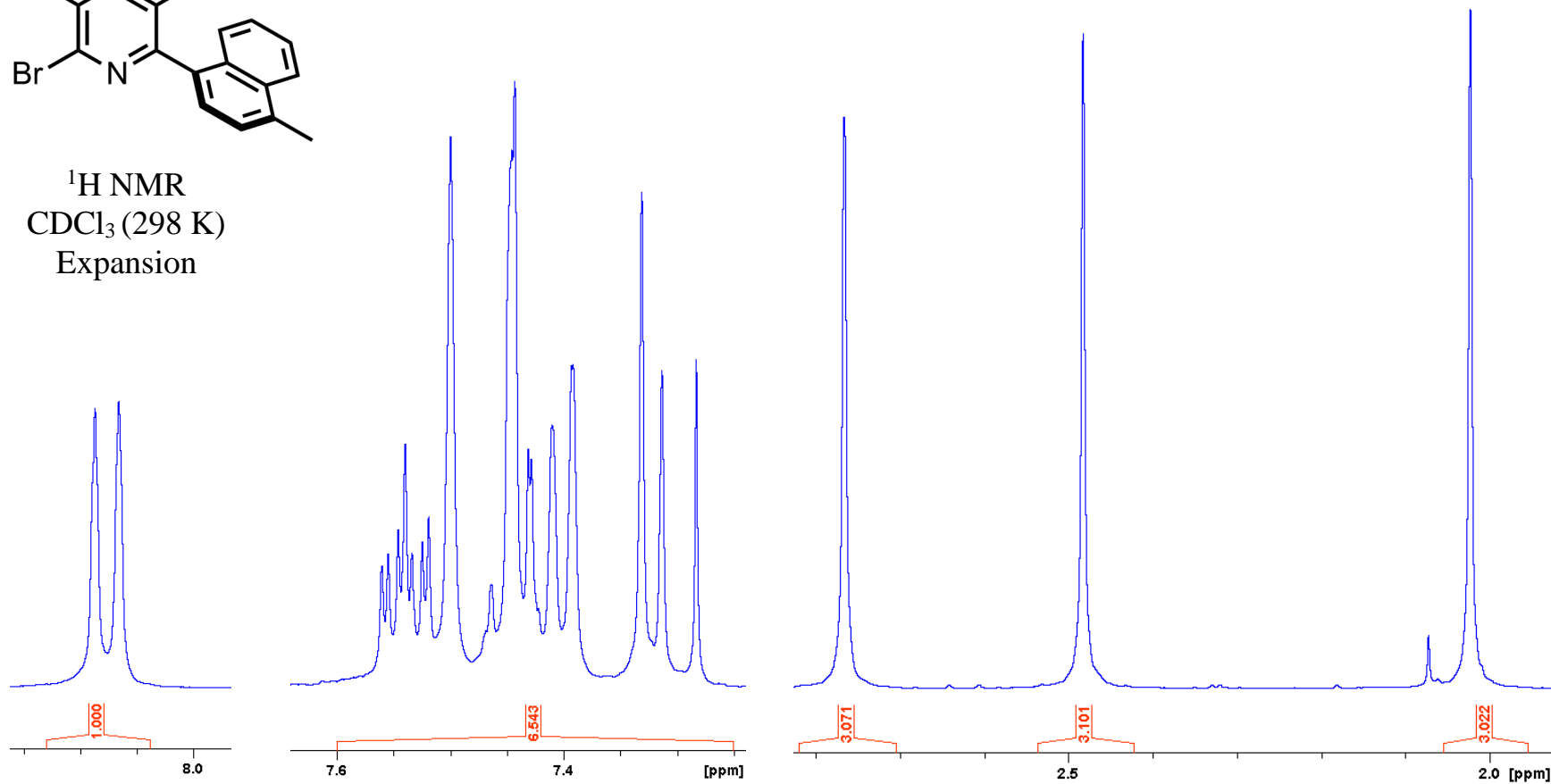


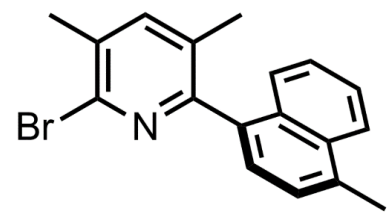
$^1\text{H NMR}$
 CDCl_3 (298 K)



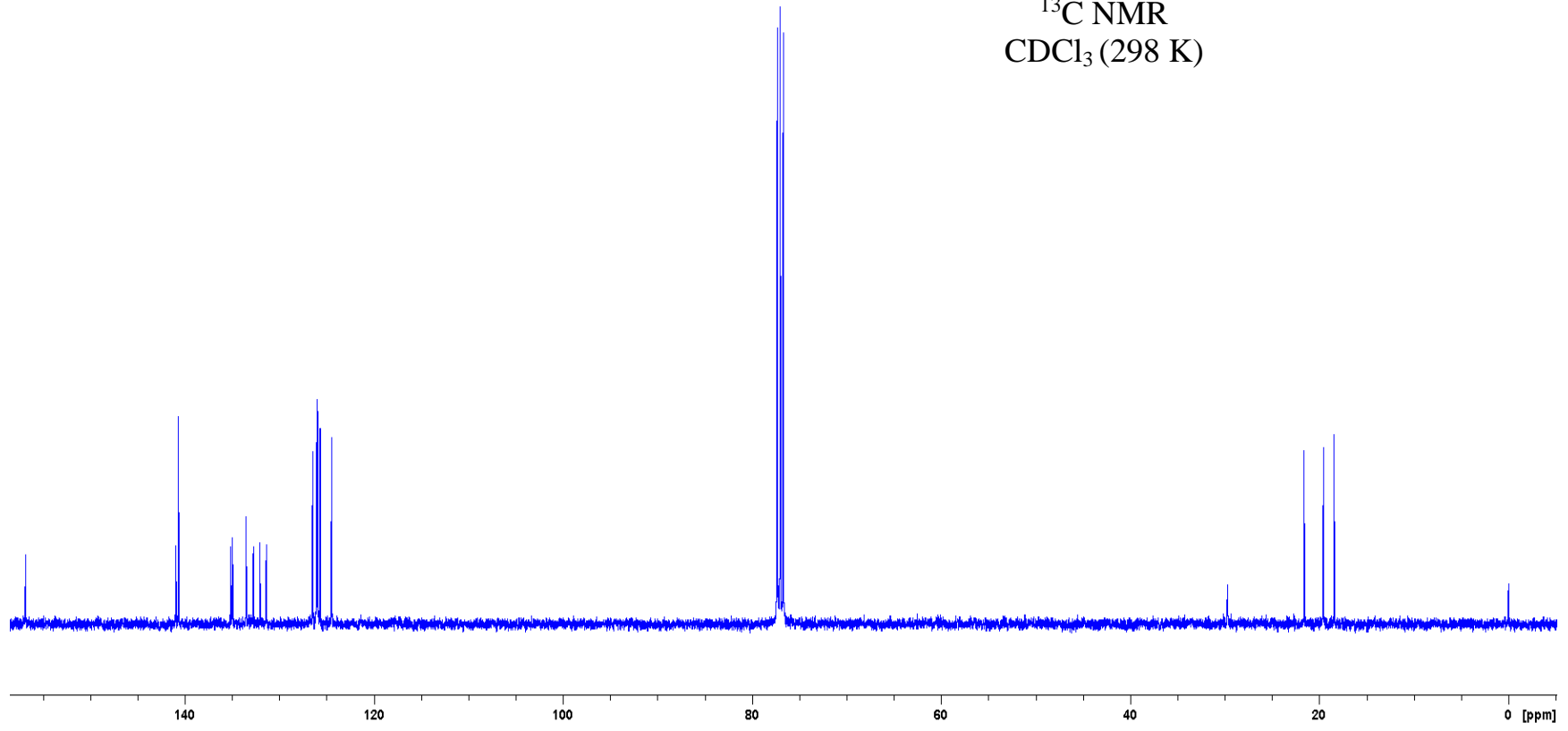


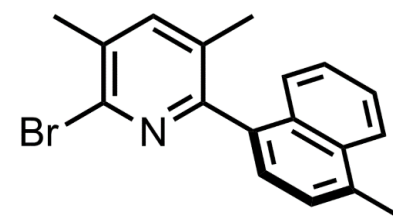
^1H NMR
 CDCl_3 (298 K)
Expansion



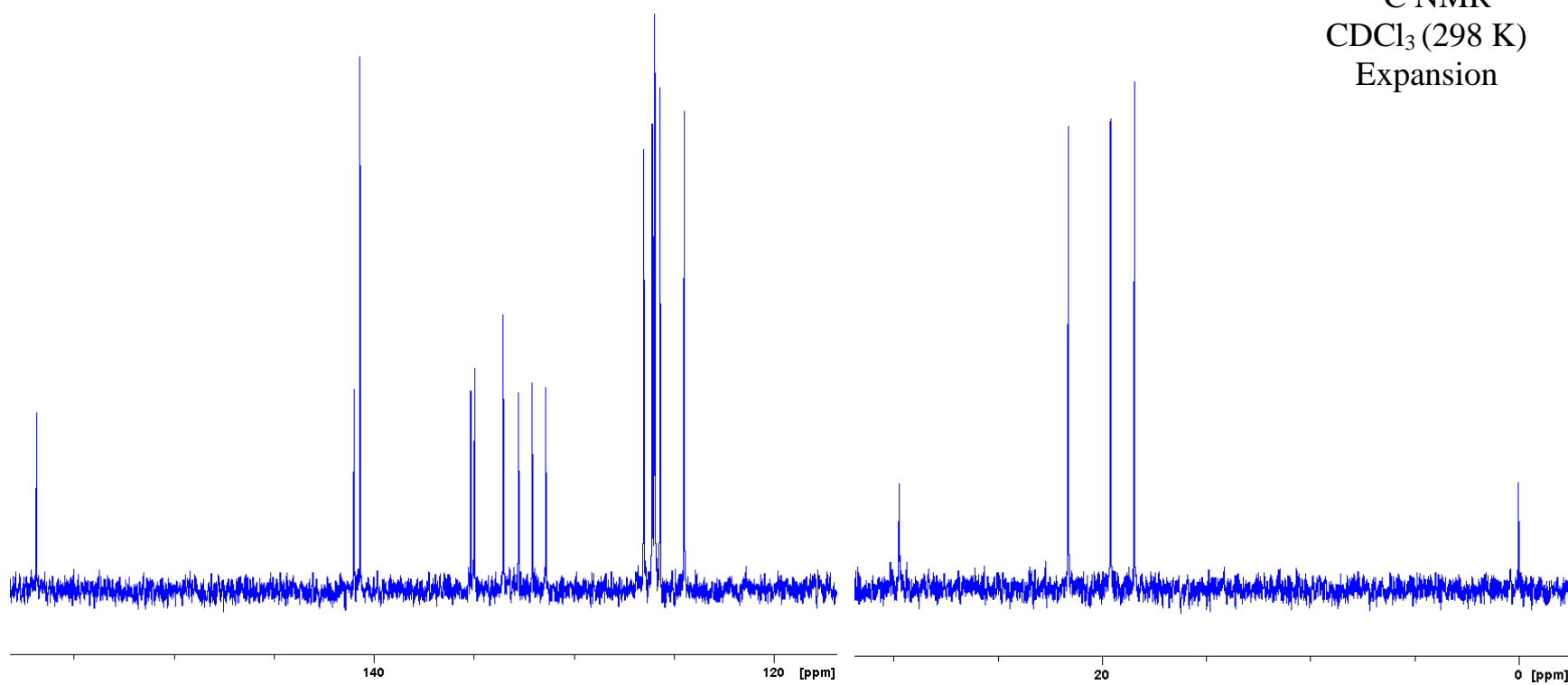


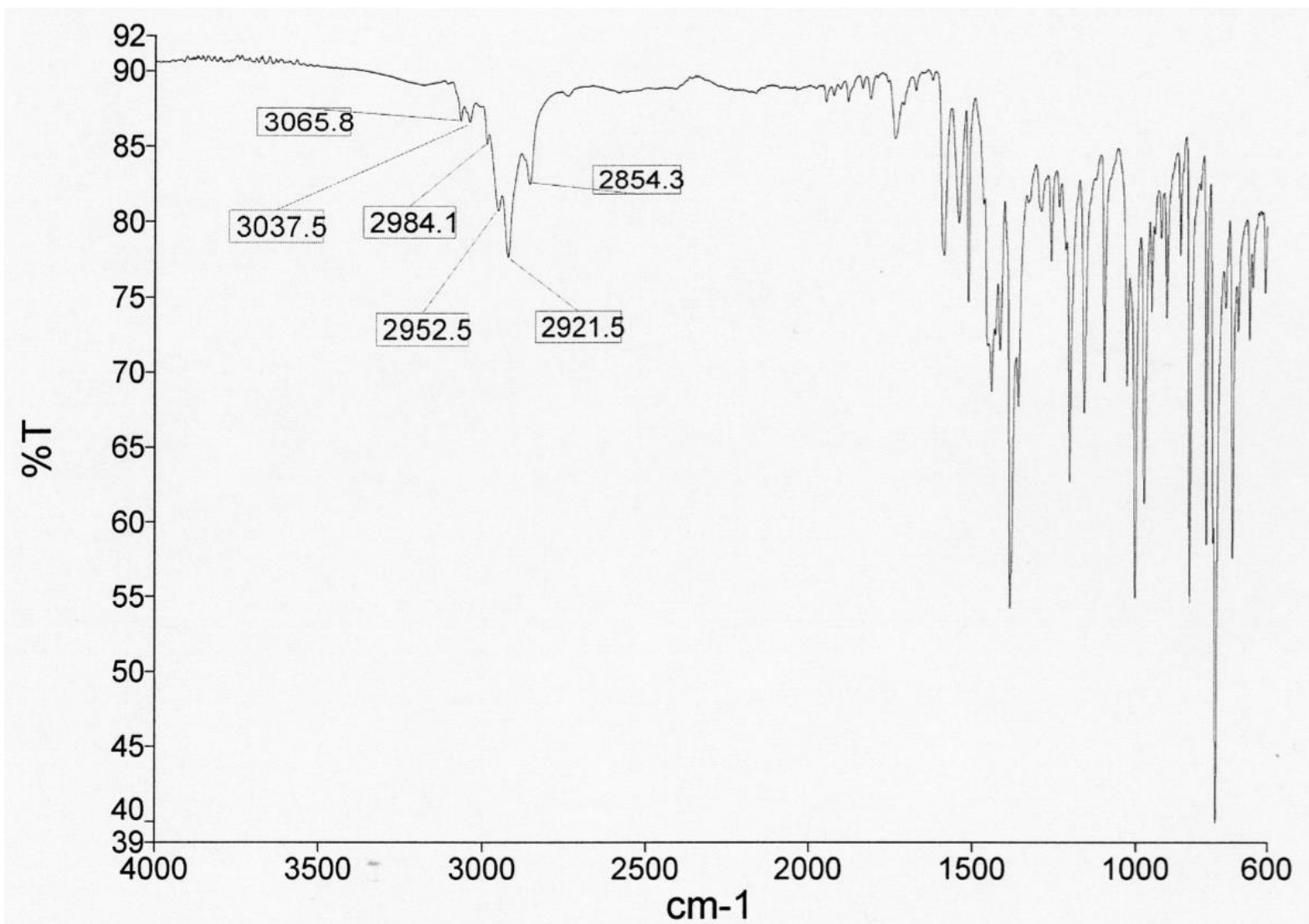
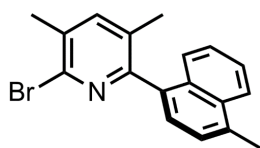
^{13}C NMR
 CDCl_3 (298 K)

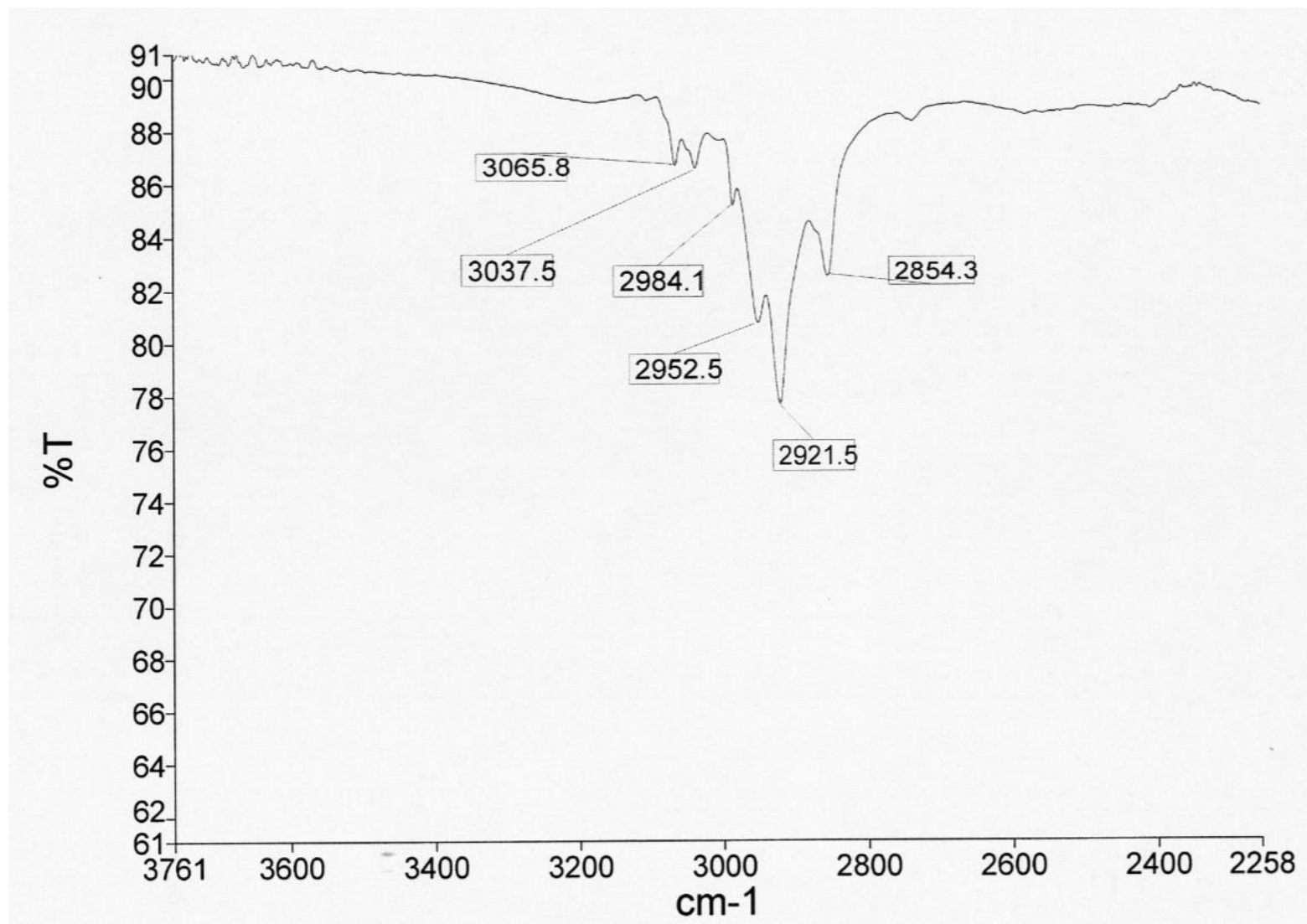
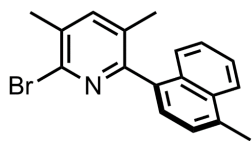


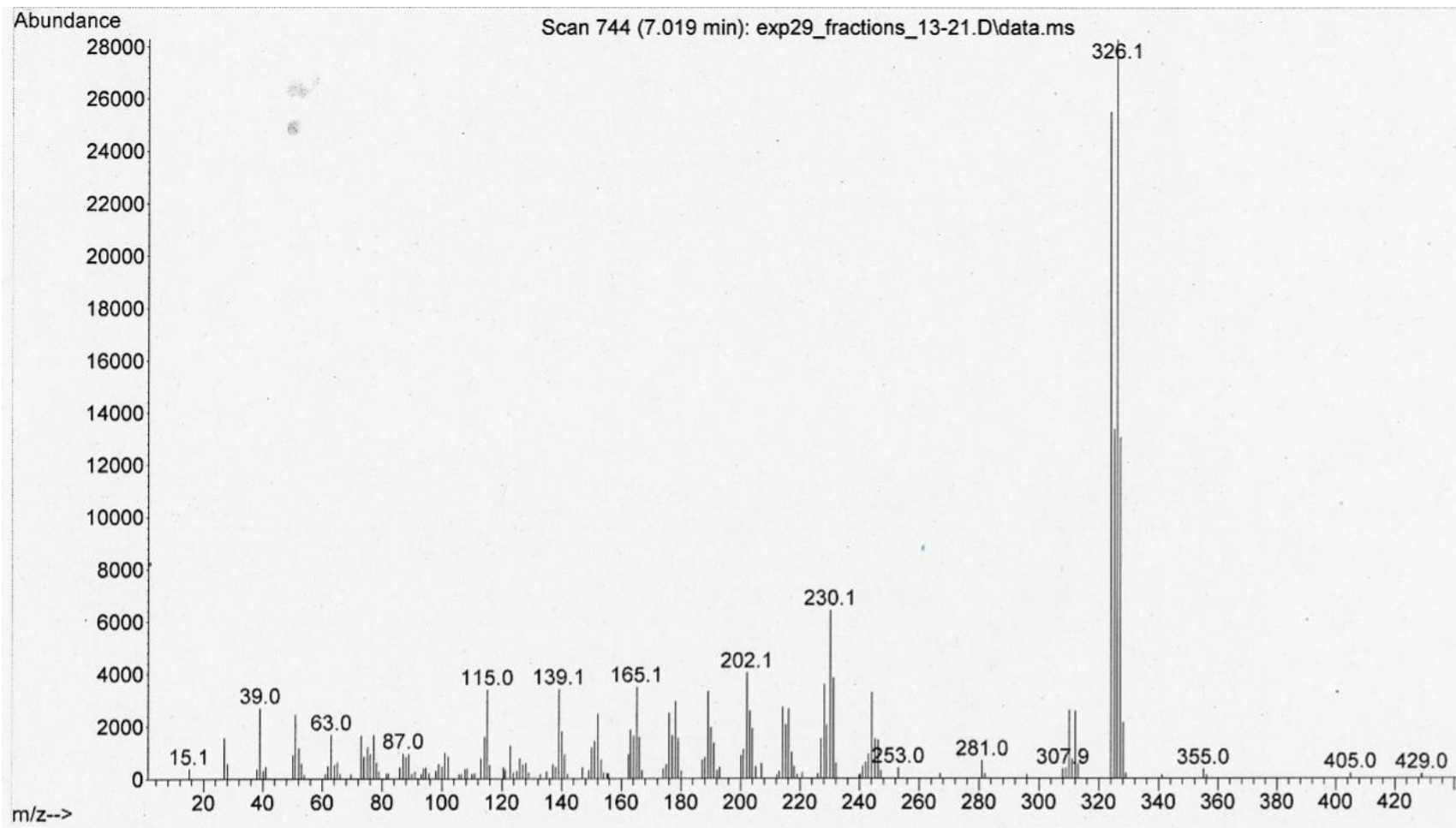
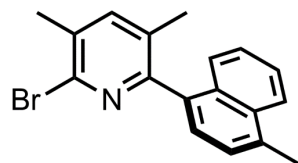


^{13}C NMR
 CDCl_3 (298 K)
Expansion

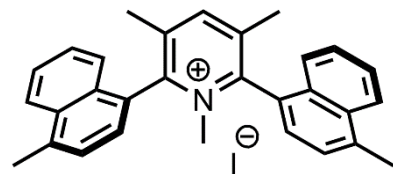




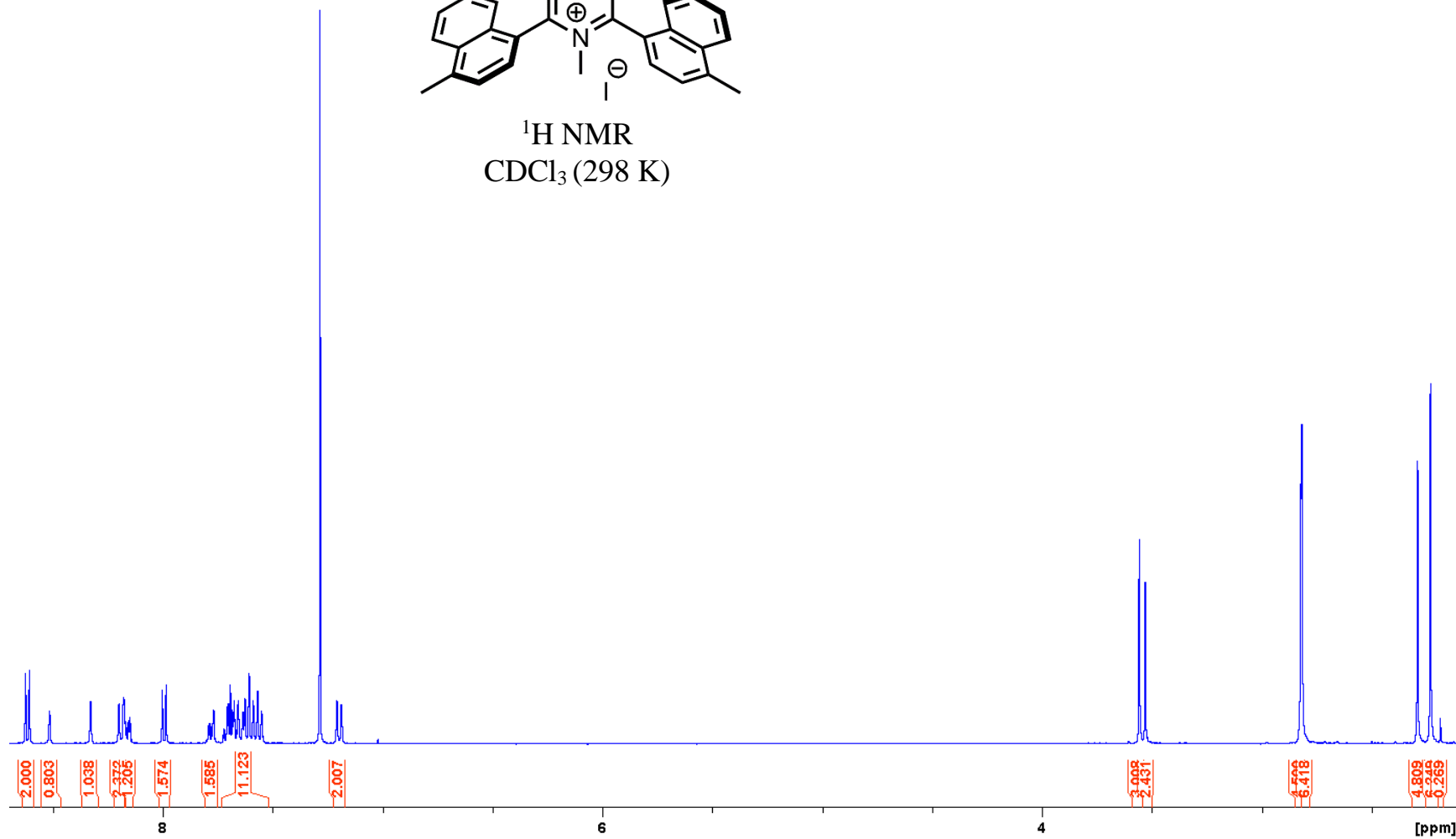


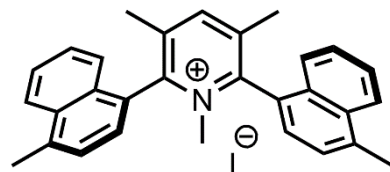


1,3,5-Dimethyl-2,6-Di(4-methylnaphthyl-1-yl)pyridinium

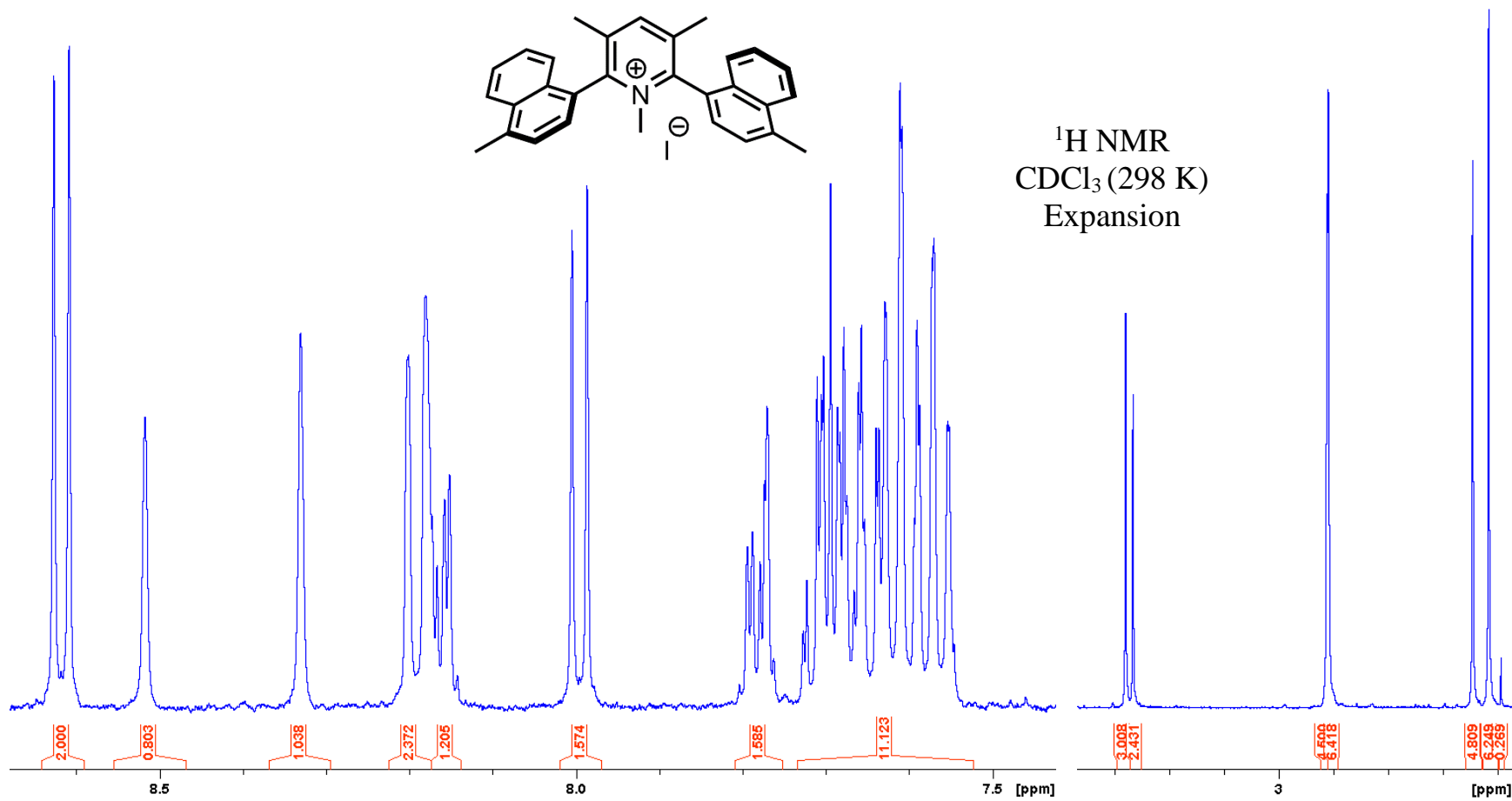


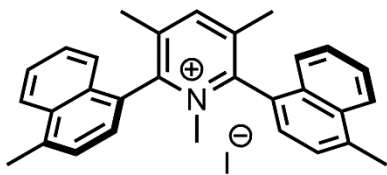
$^1\text{H NMR}$
 CDCl_3 (298 K)



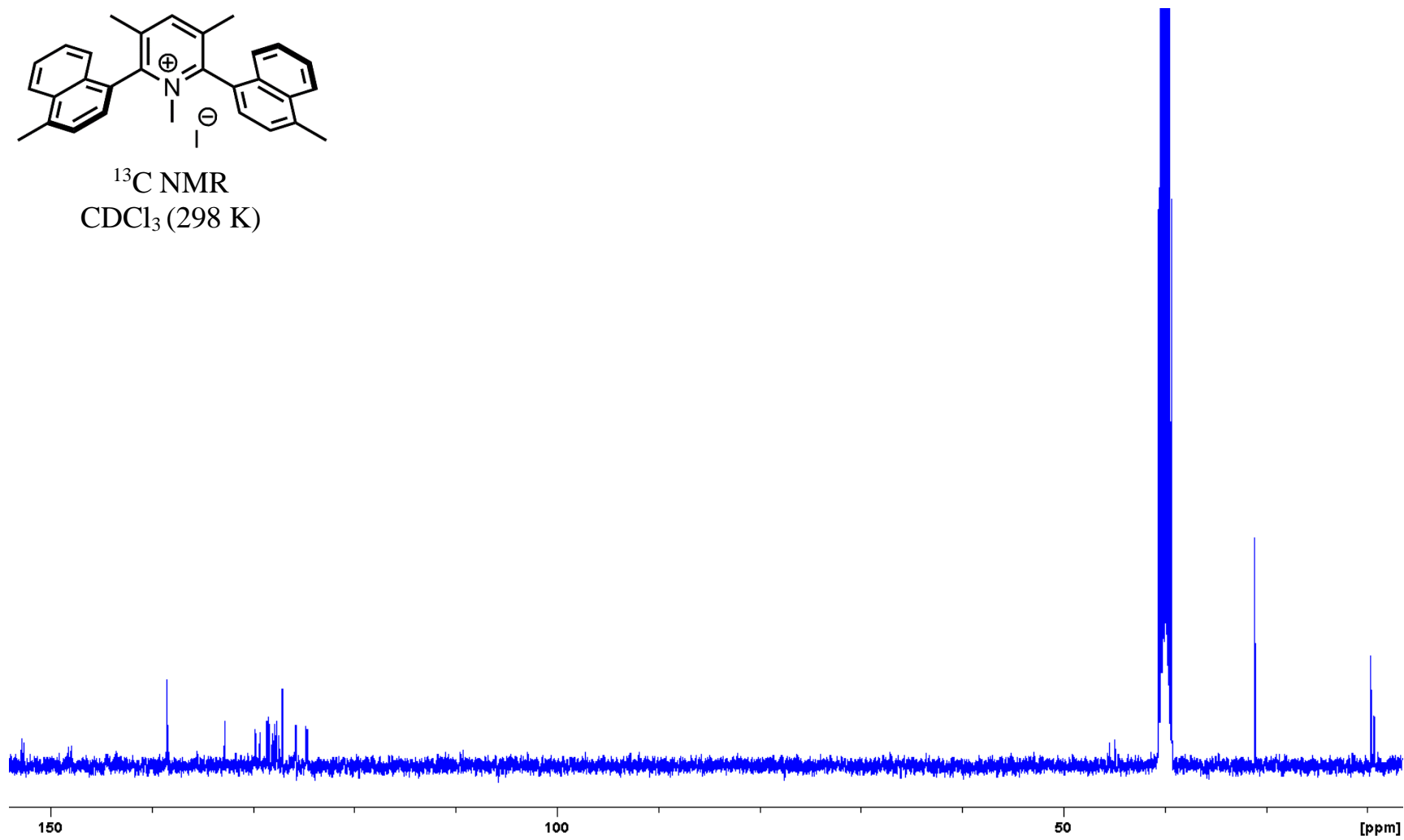


$^1\text{H NMR}$
 CDCl_3 (298 K)
Expansion

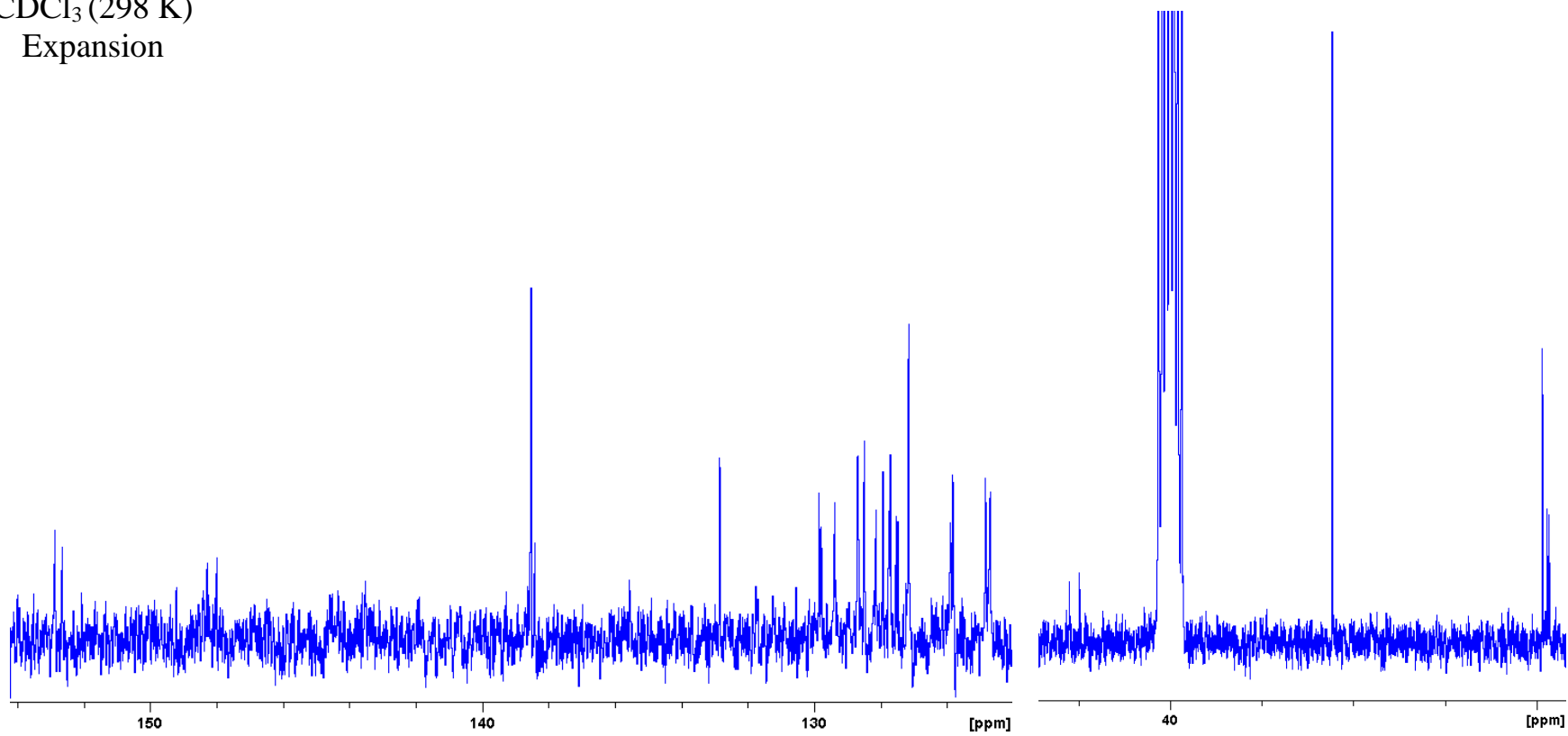
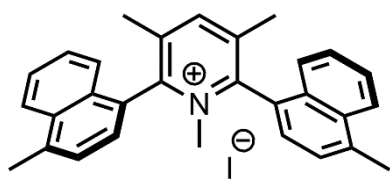


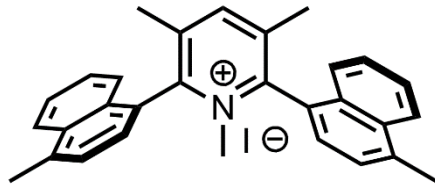


^{13}C NMR
 CDCl_3 (298 K)

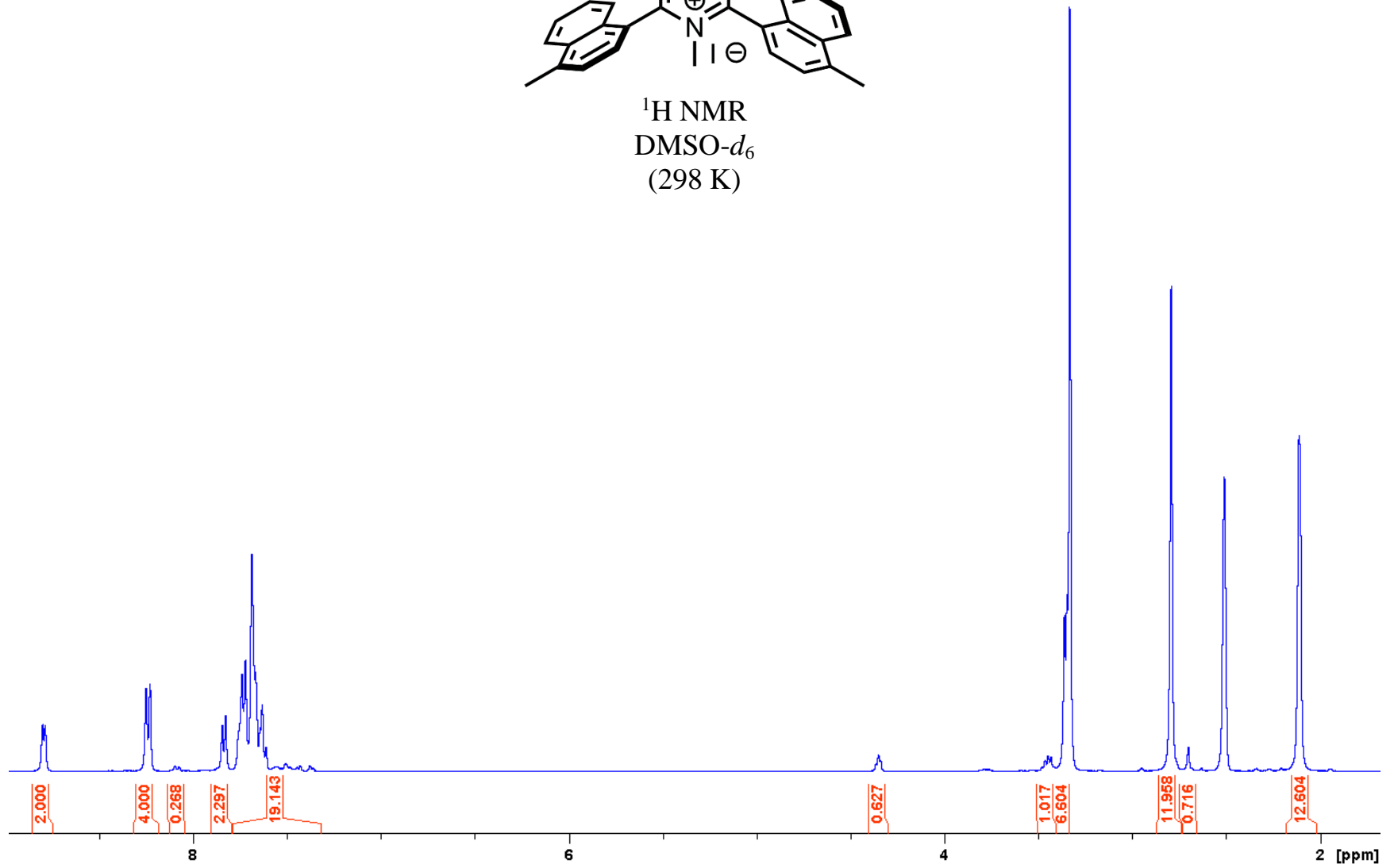


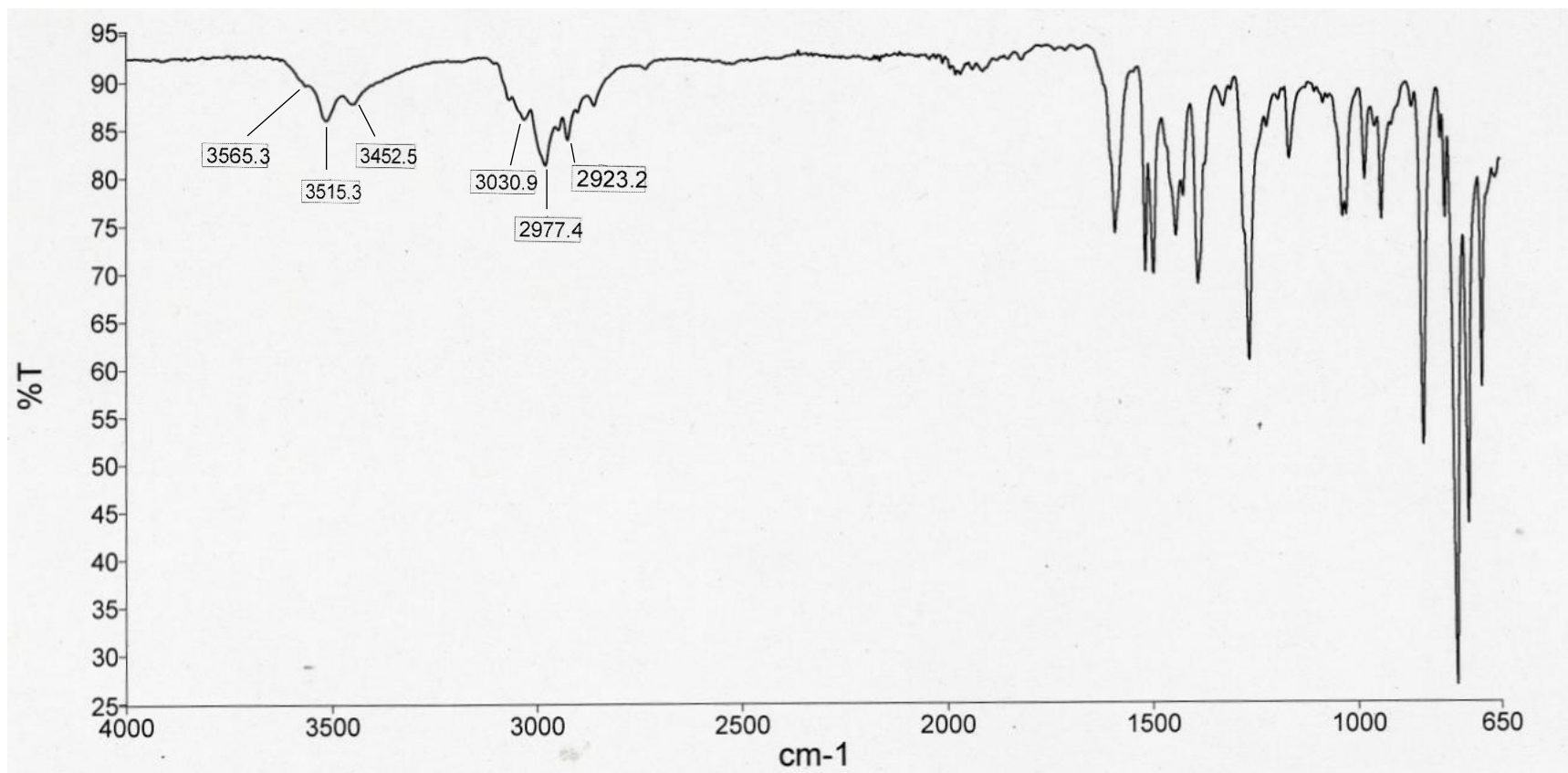
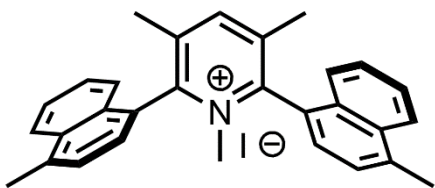
^{13}C NMR
 CDCl_3 (298 K)
Expansion

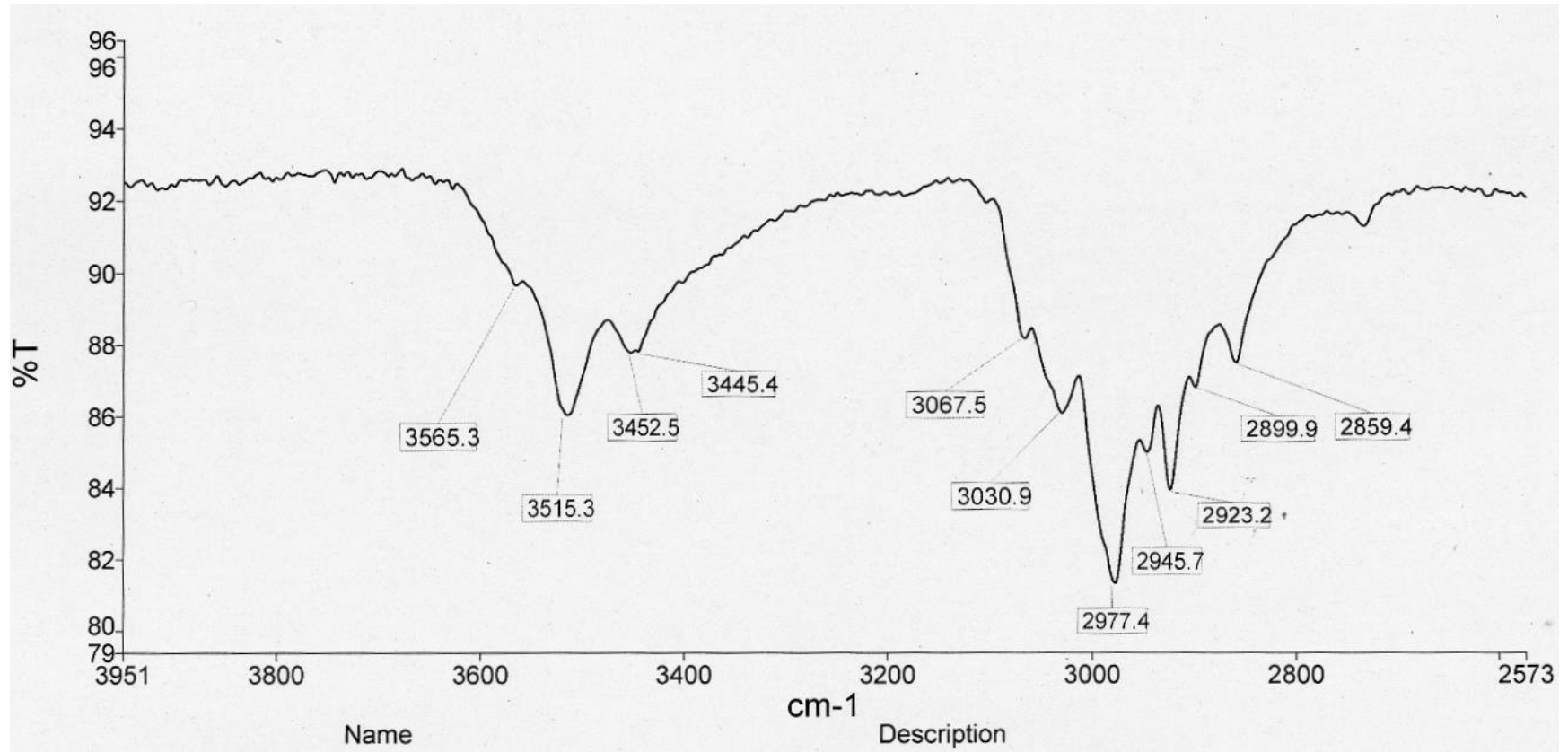
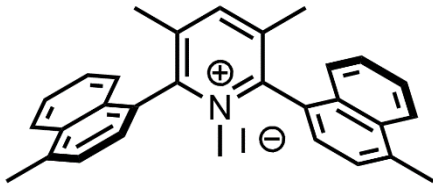


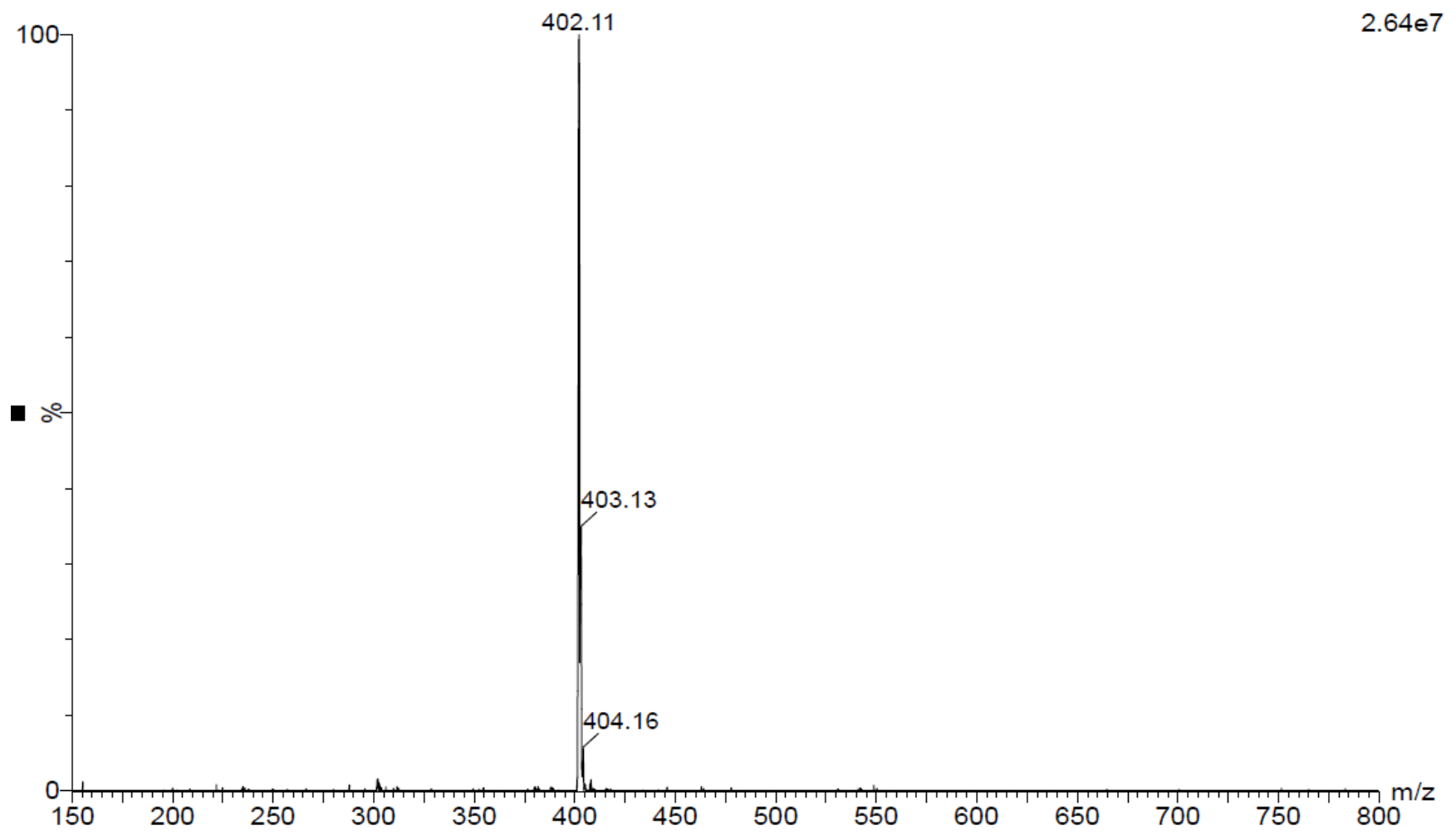
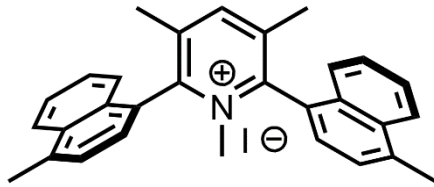


^1H NMR
DMSO- d_6
(298 K)

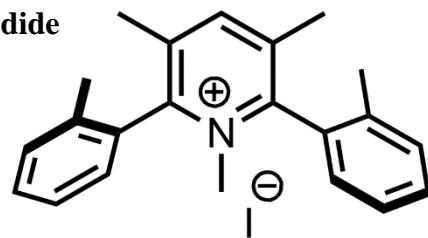




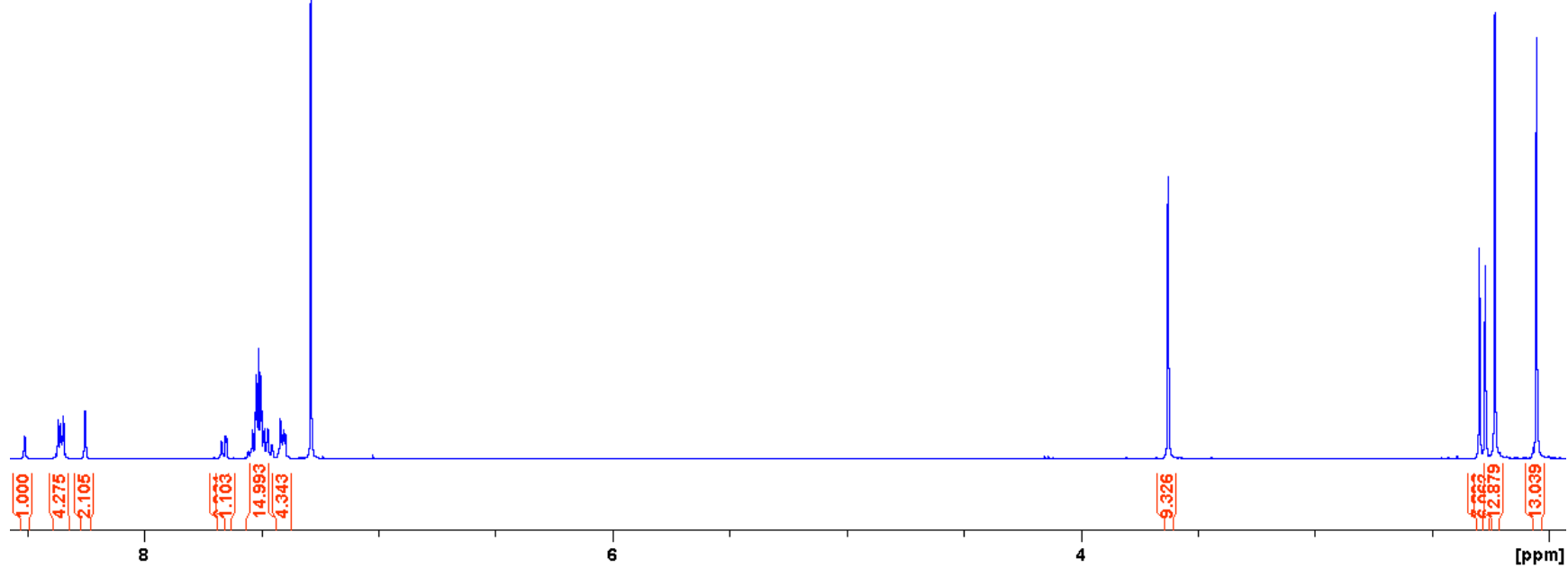


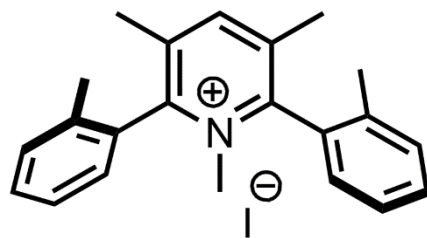


1,3,5-Trimethyl-2,6-di-(2-methylphenyl)pyridinium iodide

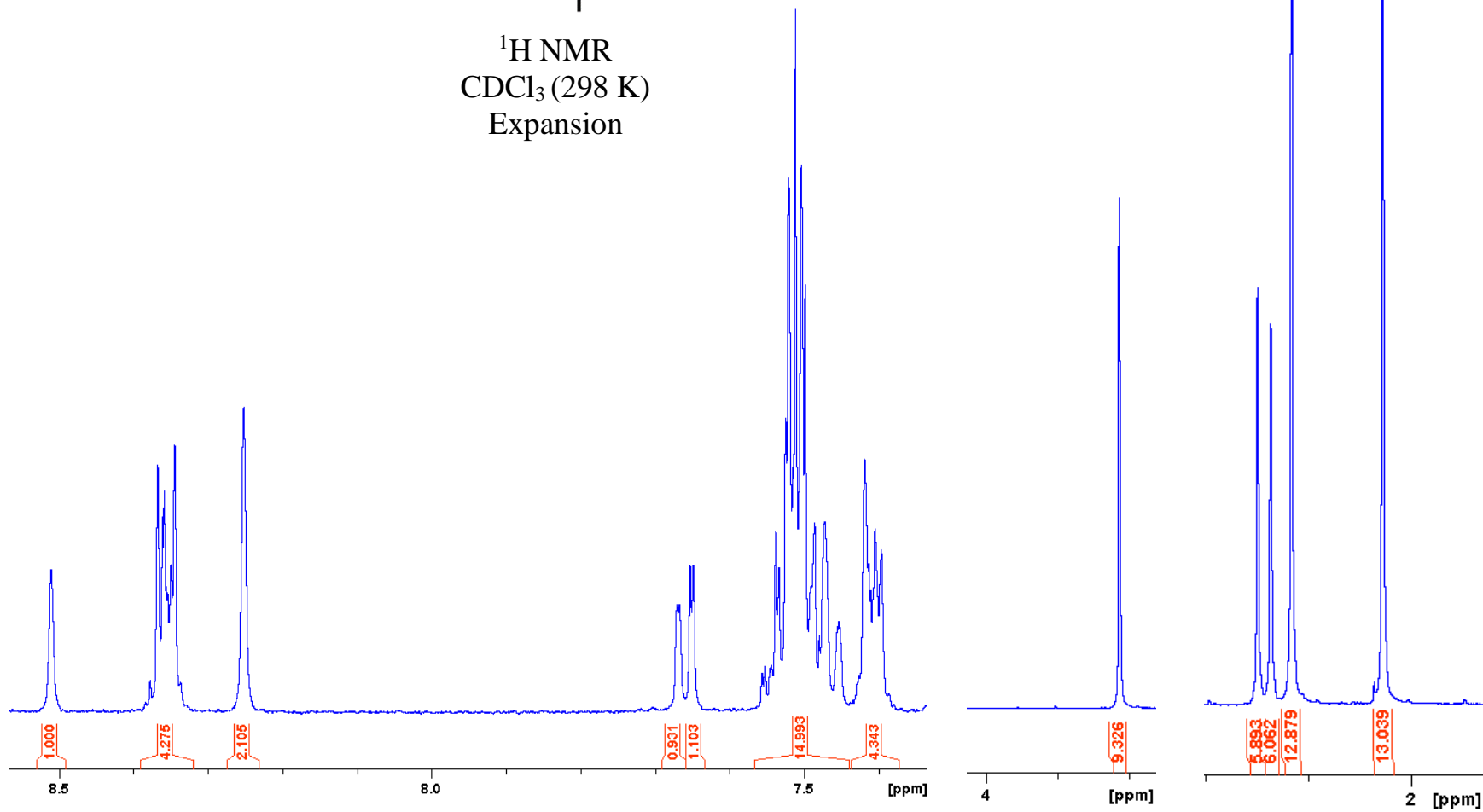


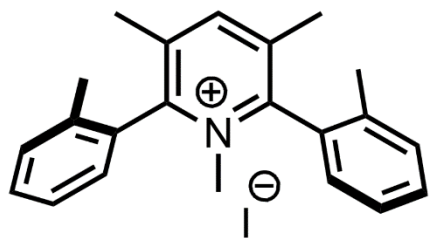
$^1\text{H NMR}$
 CDCl_3 (298 K)



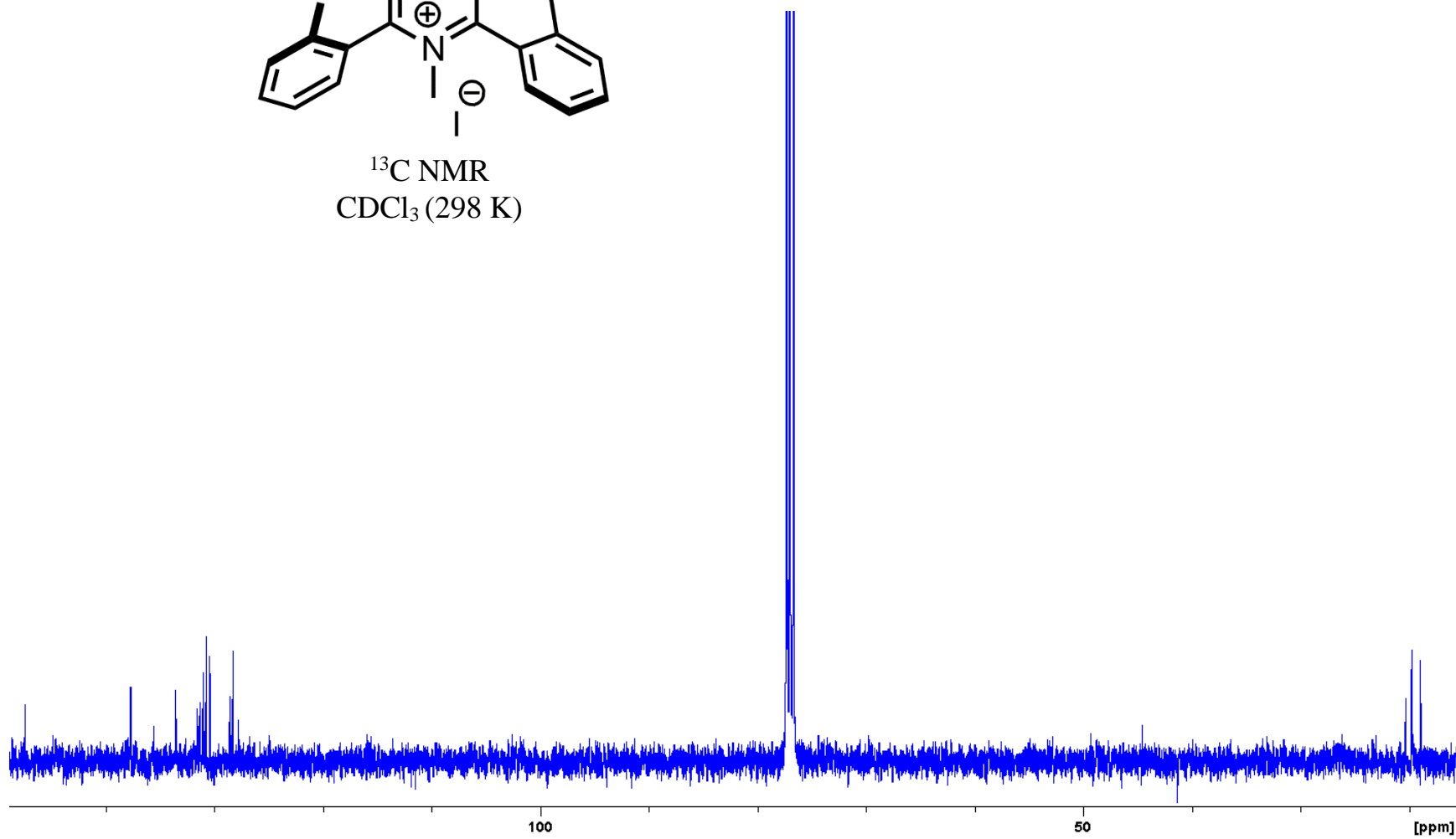


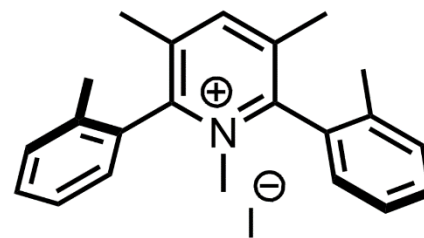
^1H NMR
 CDCl_3 (298 K)
Expansion



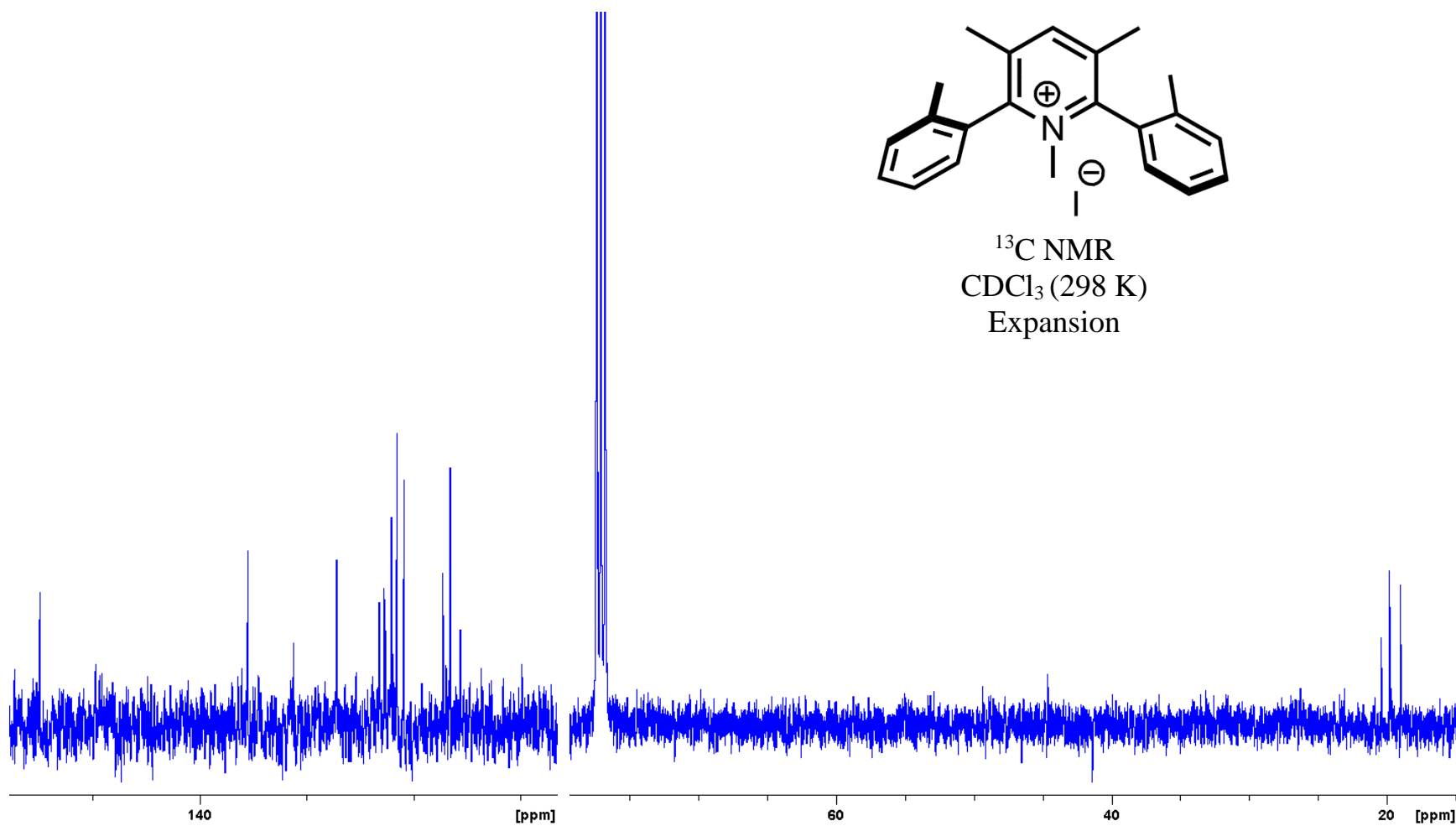


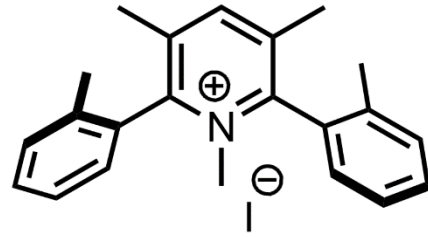
^{13}C NMR
CDCl₃ (298 K)



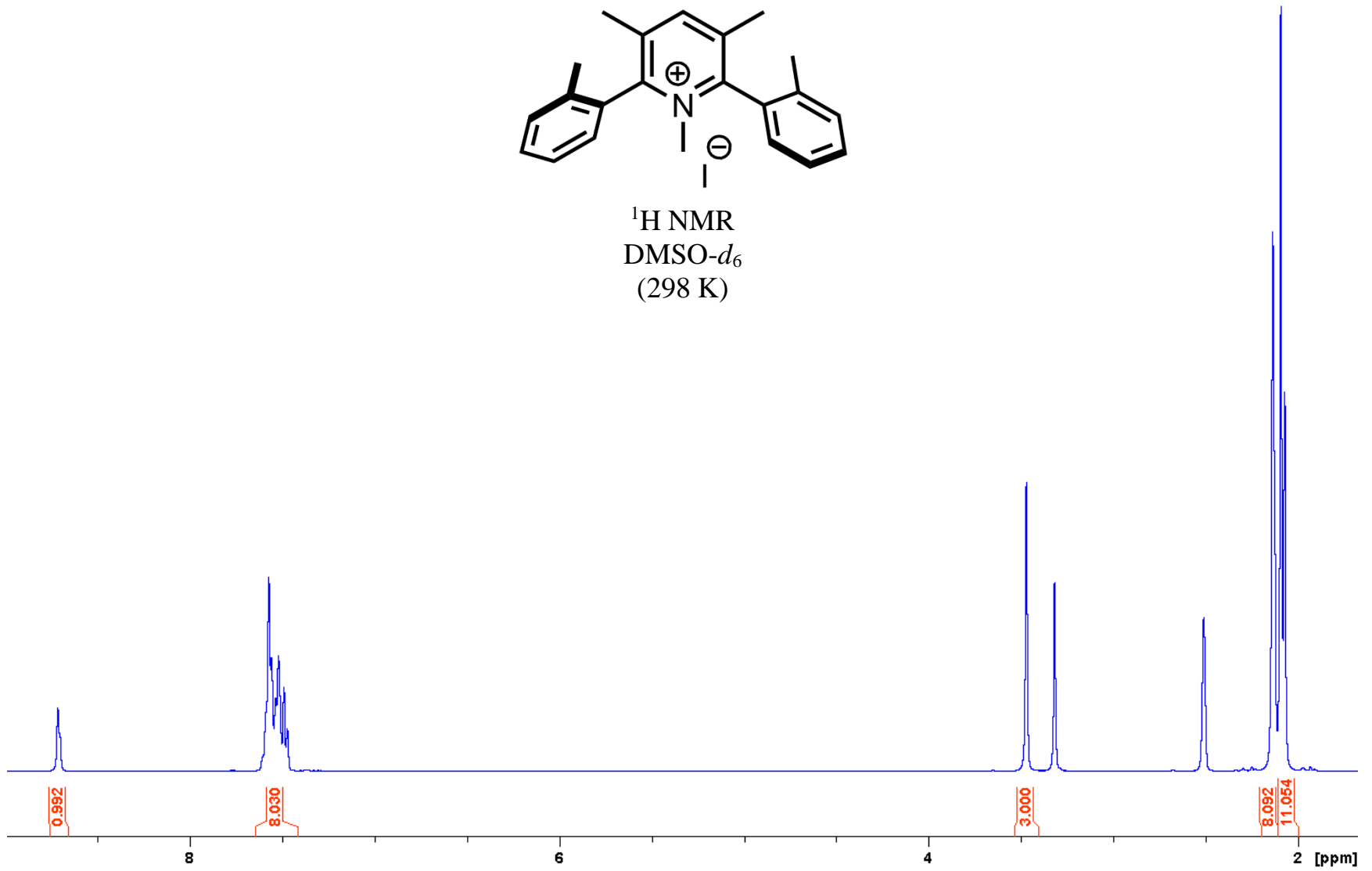


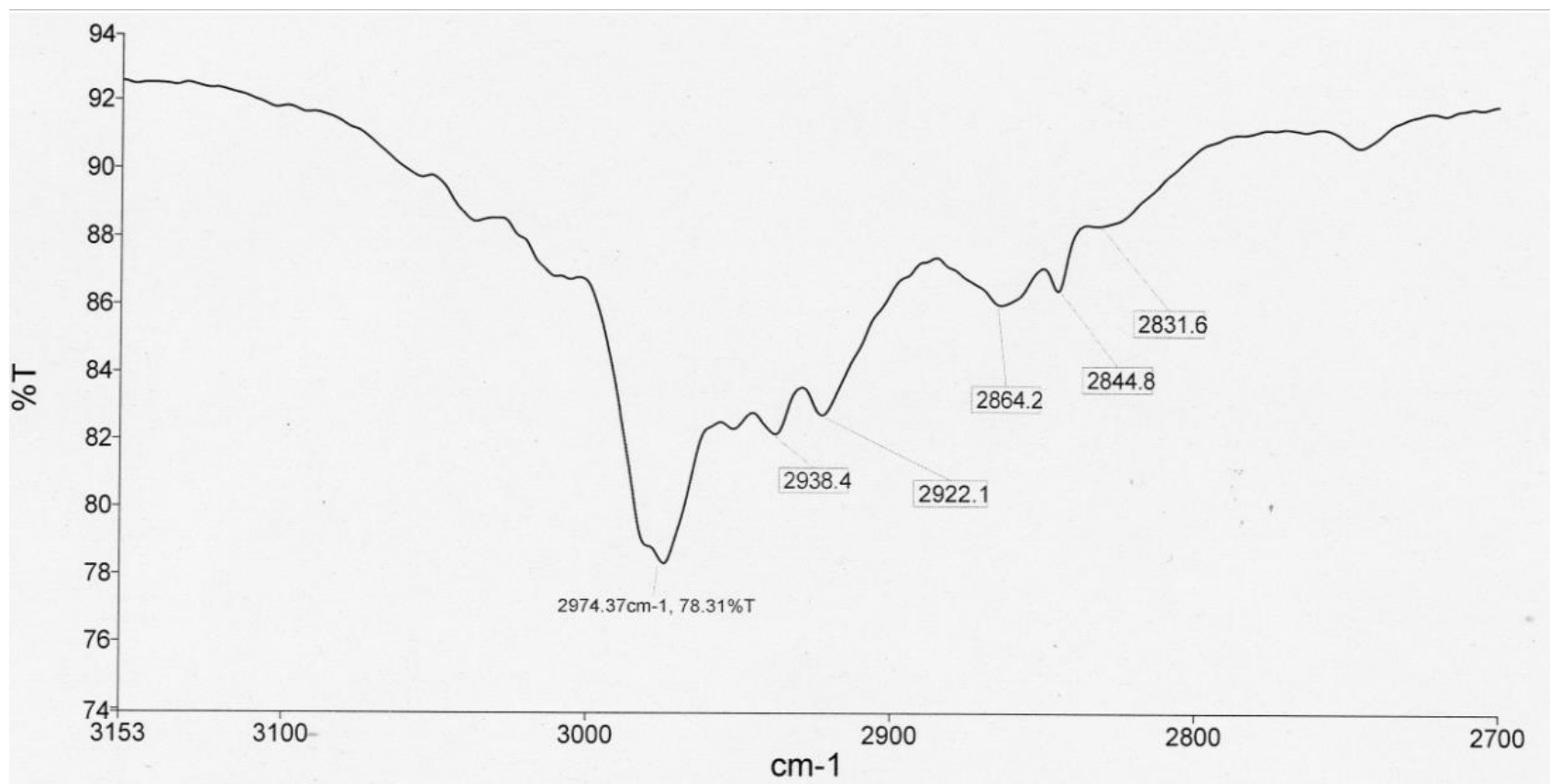
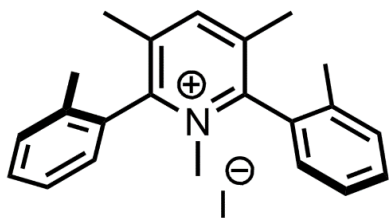
^{13}C NMR
CDCl₃ (298 K)
Expansion

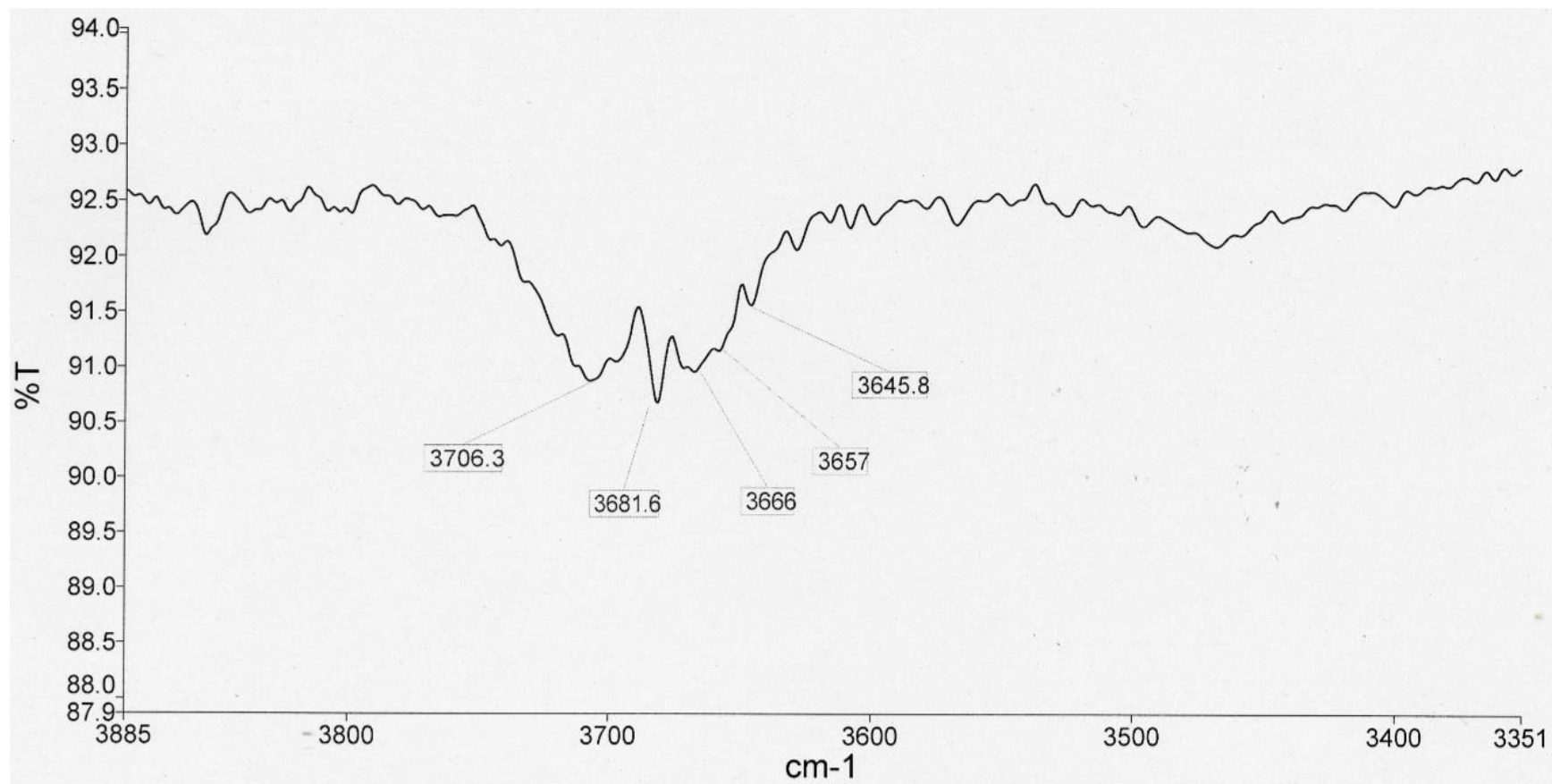
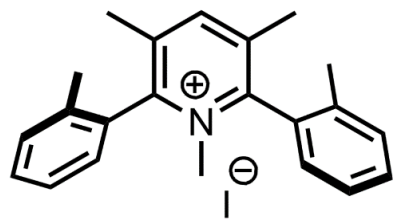


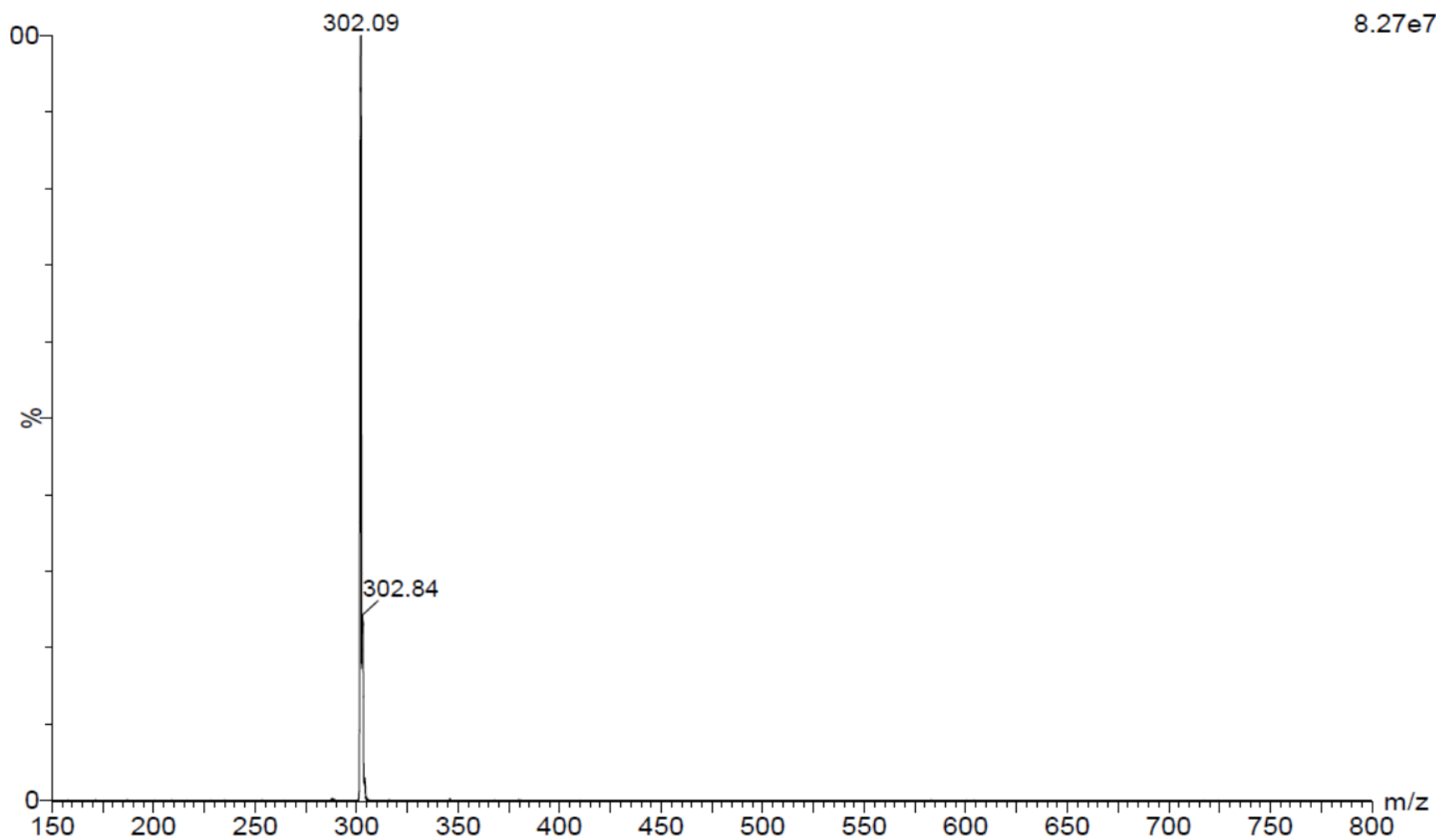


^1H NMR
DMSO- d_6
(298 K)

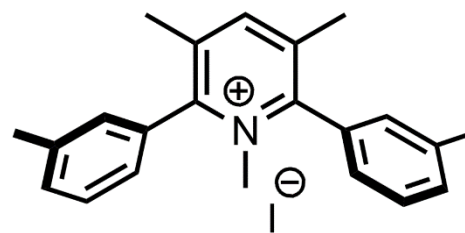




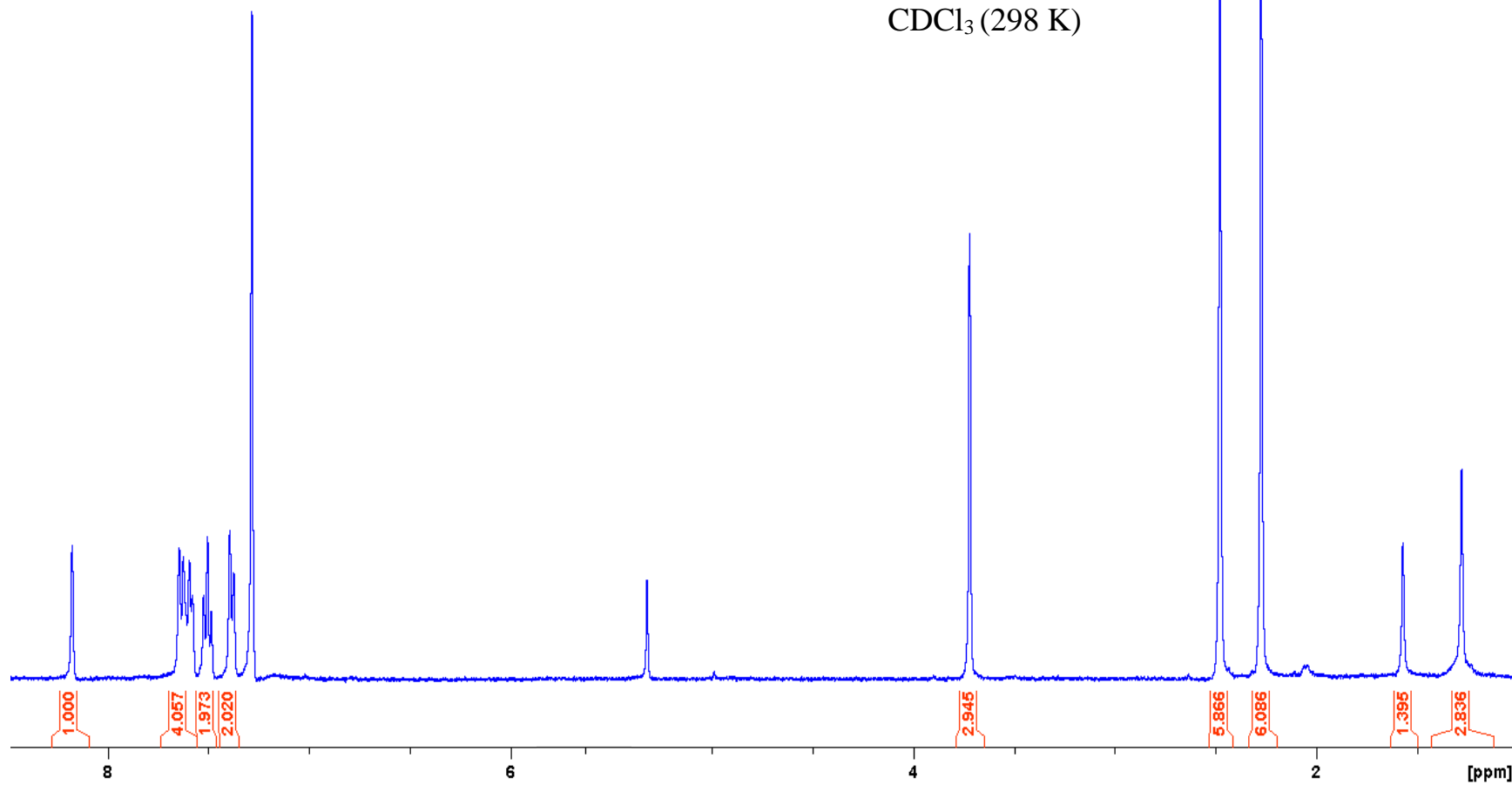


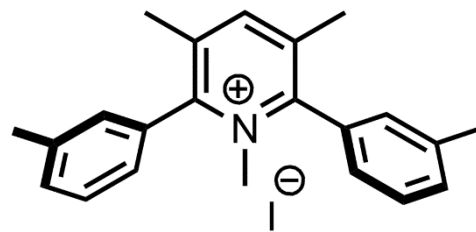


1,3,5-trimethyl-2,6-di-(3-methylphenyl)pyridinium iodide

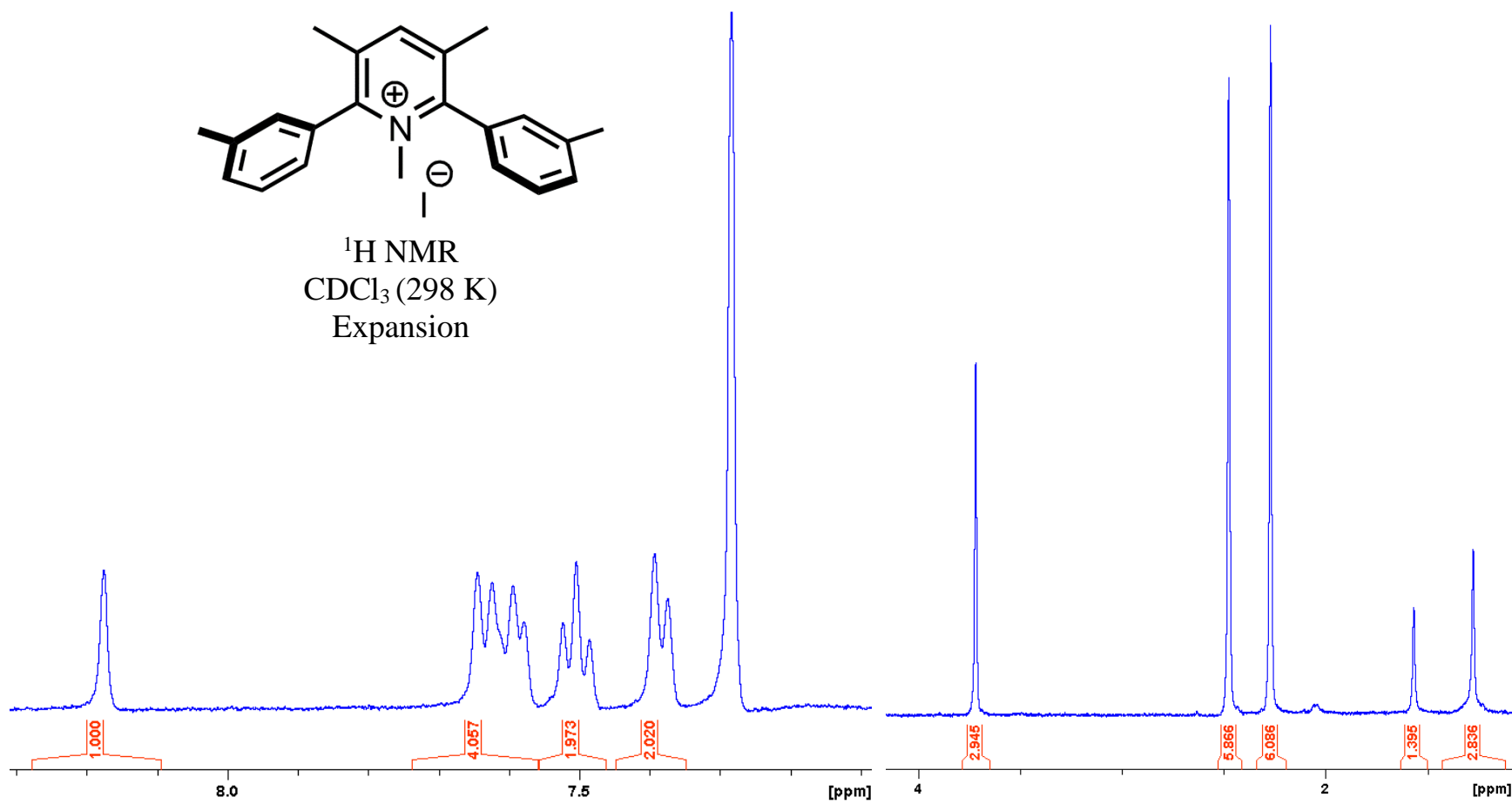


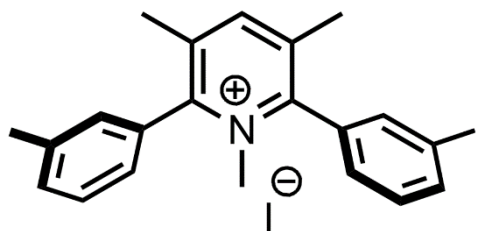
¹H NMR
CDCl₃ (298 K)



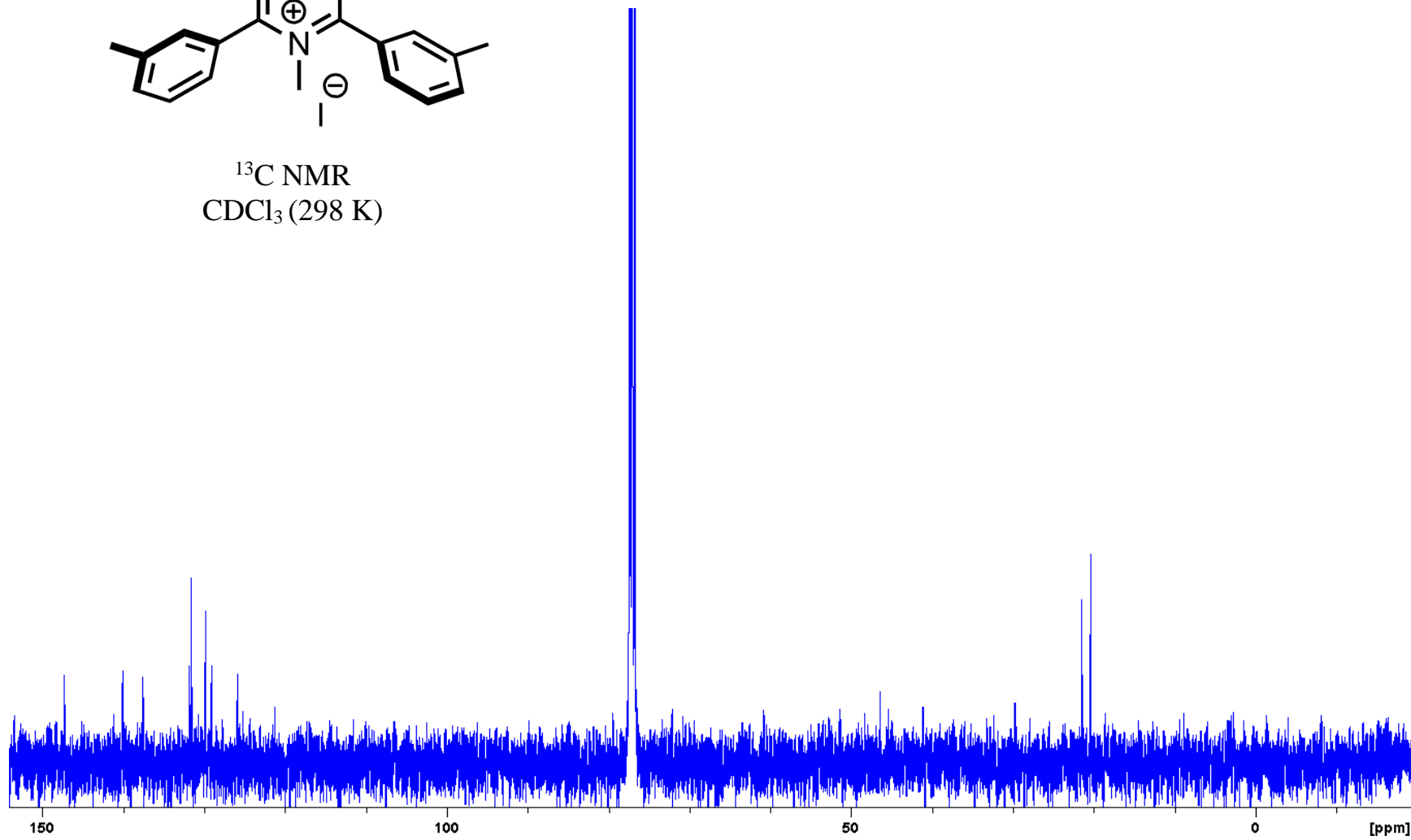


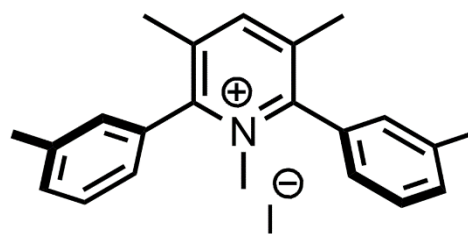
^1H NMR
 CDCl_3 (298 K)
Expansion



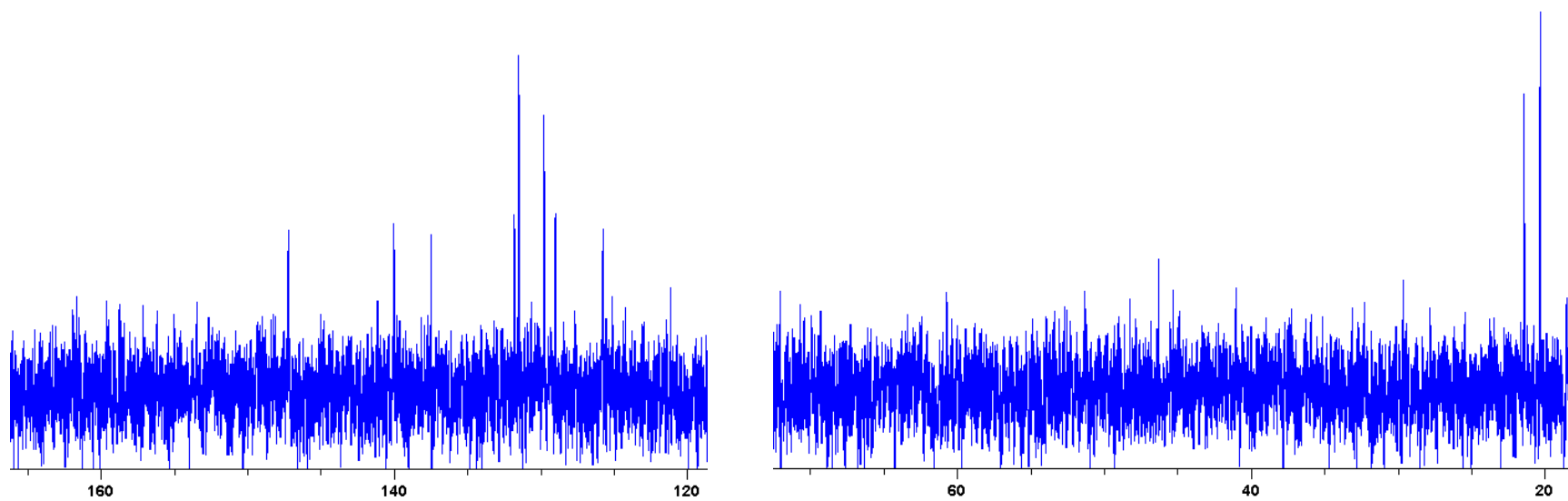


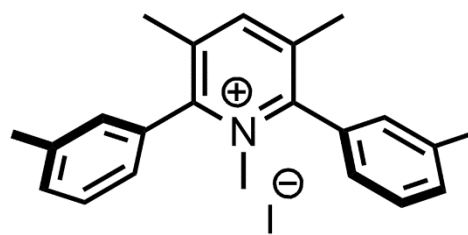
¹³C NMR
CDCl₃ (298 K)





^{13}C NMR
 CDCl_3 (298 K)
Expansion





¹H NMR
DMSO-*d*₆
(298 K)

